CRANFIELD INSTITUTE OF TECHNOLOGY

DEPARTMENT OF FLUID ENGINEERING AND INSTRUMENTATION

Ph.D THESIS

Academic Year 1985-6

K. D. SPENDEL

On non-invasive ultrasonic flowmeasurement

Supervisor: J. Hemp

November 1985

SUMMARY

This thesis is concerned with non-invasive ultrasonic flow measurement, using the transit time principle.

The errors associated with the transit-time flowmeter are investigated and a design of flowmeter is suggested. A theoretical and experimental study of the transmission of sound through pipe walls is carried out where it is shown that advantage can be taken of the excitation of Lamb modes. A design of transducer arrangement is made from the results of the work.

A solution to the difficult problem of measuring very small times is provided in the form of a novel vernier timing system. The benefits and disadvantages of this timing system are discussed along with the design aspects of other electronic circuits required in the construction of the flowmeter. The flowmeter has been built and tested in the laboratory and is shown to be highly repeatable and accurate. The results of testing the flowmeter compare favourably with tests conducted on a commercial instrument.

Improvements to the design and construction and suggestions for further work are given.

LIST OF CONTENTS

LIST OF FIGURES

NOTATION

v	=	flow velocity
C	=	speed of sound in the fluid
ℓ	=	path length
α	=	angle the transducer beam makes with the normal
α	=	attenuation constant
Θ	=	angle the beam makes in the fluid with the pipe
Δt	=	time difference between upstream and downstream pulses
$T_{12,21}$	=	time in one direction
Q	=	volume flowrate
D	=	external pipe diameter
d	=	pipe wall thickness
C_p	=	speed of sound in perspex
ω	=	radian frequency
Z	=	characteristic impedance
$T_{1,2}$	=	oscillator periods
δt	=	difference in the oscillator periods
$f_{1,2}$	=	oscillator frequencies
$N_{1,2}, Y, R$	=	Number of pulses in counter
nS	=	nano seconds
C_L	=	Lamb wave velocity
C_1	=	longitudinal wave velocity
C_2	=	shear wave velocity
$\xi K \beta \gamma \Omega \Sigma \alpha$	=	wavenumbers (subscripts p=plates, f=fluid, s=solid)
b	=	plate thickness
$\underline{U}$	=	displacement vector
$\underline{\Phi}$	=	scalar potential
$\underline{H}$	=	vector potential
$\underline{\tau}$	=	stress
ρ	=	density (subscript p=plate, f=fluid, s=solid)
Z	=	acoustic impedence
λ	=	wavelength

CHAPTER 1 INTRODUCTION AND LITERATURE REVIEWS

1.1 Introduction

The relatively recent introduction of completely external flowmetering, using ultrasonics, offers the ultimate promise to users of flowmeters. The technique is non-invasive does not require expensive pipe modifications or costly shutdown upon installation and offers no resistance to flow. Added to this is the case of easy maintenance (again, without shutdown) and low cost with increasing pipe size. Alas, the instrument is not yet accurate enough to compete with accepted flowmeters such as electromagnetic and differential pressure devices, to name but two.

The Department of Fluid Engineering and Instrumentation (DFEI) has had a long standing interest in flowmetering as a user and designer and has a reputation for expertise in electromagnetic flowmetering. It was decided that a complementary Investigation into Clamp-on ultrasonic transit-time flowmeters would expand the DFEI's expertise.

The choice of approach to studying clamp-on flowmeters was considered and it was decided to adopt an overall approach and to construct, from basic principles, a complete flowmeter and to investigate its inherent weaknesses. This approach was adopted in preference to studying one particular area (eg, transmission of sound through plates) as it was felt that a better appreciation of the flowmeters overall capabilities and limitations would follow.

It should be emphasised that the instrument under consideration is a transit time (or contrapropagating) instrument and not one of the other varieties as mentioned for example by Lynnworth (1). Indeed it is felt that the reluctance of users encountered in accepting any ultrasonic flowmeter is due largely to the overselling of the first generation of ultrasonic flowmeters, particularly the doppler version.

There is little difference in principle between the clamp-on transit time flowmeter and the spool piece flowmeter (i.e. a pipe section flowmeter) and initial investigations did not separate the two.

The clamp-on transit time flowmeter can be sectioned into three pieces, the transduction process, the physics of transmission and the timing of small intervals (the order of times to be measured will be discussed in chapter 2 but suffice it to say that accuracy levels of better than 1×10^{-9} seconds are required).

It was decided to search through the literature on several topics using the databases Compendex and Inspec and others (Derwent database for patents, etc). An initial search was conducted covering the past 8-12 years. The search profile was then put onto an SDI file (Selective Dissemination of Information) which was kept permanently up to date. Search profiles were set up for the timing, flowmetering, transmission of sound through plates and transduction.

When a paper of interest was discovered a search was made of the authors' references and of the author as a cited reference. Selected papers were reproduced.

In addition to the technical searches, two further searches were conducted on patents and grants which it was felt would identify fellow workers in the field of interest. However, the grant search provided little information since it was mostly USA based; this search will not be discussed further. The patent search shows that significant interest exists in ultrasonic flowmetering and that no comparable system to the one presented in this thesis exists.

A review of the papers is given in four sections,

1.1.1 Ultrasonic flowmetering
1.1.2 Transmission of sound through plates
1.1.3 Time interval measurement
1.1.4 Transduction

In section 1.2 an outline of the thesis material is given.

1.1.1 Ultrasonic flowmetering

This review covers briefly the transit-time ultrasonic flowmeter in its clamp-on and insertion (spool piece) form and is intended as a guide to the main problems encountered in the design of a flowmeter and the attempts to solve the problems.

The review considers the historical background and present day problems associated with ultrasonic transit time flowmeters. The advantages of a transit time flowmeter are that;

(i) there is little or no obstruction to flow
(ii) it has no moving parts
(iii) it is applicable to all clean fluids and (slightly) particulate fluids
(iv) it is a low cost competitve device, even more so at the larger pipe sizes since the instrument cost, is approximately independent of pipe size
(v) it is easily maintained

In addition the clamp on flowmeter has;

(vi) portability
(vii) no requirement for system shut down upon installation

The principle of operation of a transit time flowmeter is best described by reference to figure 1.1 where two transducers are placed in the flow but could just as easily be placed obliquely across the pipe, the only requirement is that a component of the flow velocity is in a direct line between the transducers.

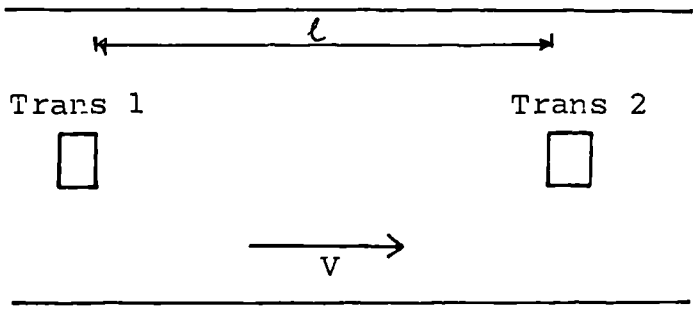

FIG 1.1
A Transit-Time Ultrasonic Flowmeter

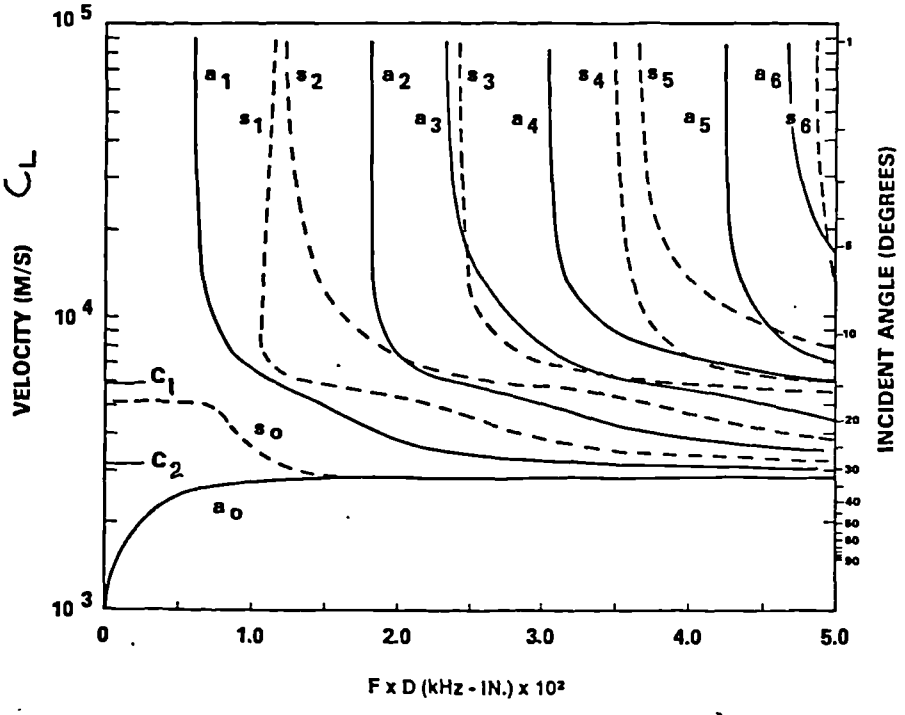

FIG 1.2
Dispersion diagram for steel plate in vaccuo
(taken from Madigosky & Fiorito- see text)

The equations for the times taken for the sound to travel from one transducer to the other are given by

$$T_{12} = \frac{\ell}{C+V} \qquad T_{21} = \frac{\ell}{C-V}$$

1.1

and thus for $V \ll C$, $\Delta t \approx \frac{2\ell V}{C^2}$, and v is seen to be directly proportional to Δt. The path length ℓ is very often known in spool piece instruments but is slightly more difficult to predict in clamp on instruments. The speed of sound C, presents a problem since for any arbitrary fluid it is unknown and further, it varies with temperature. For an accurate instrument C should be tracked.

A further factor of importance is the velocity profile effect (or Reynolds number effect). In the above equations V has been assumed to be uniform over the pipe section but in reality this is not the case. This effect will be discussed shortly.

Excellent reviews on transit time flowmeters are given by Lynnworth (2), who concentrates on the non-electronic aspects, Sanderson and Hemp (3), who concentrate more on the electronics and McShane (4).

The origin of the present transit time flowmeters probably stems from Ruttens (5), patent of 1928 in which a flowmeter was designed with a central transmitter and transducers up and down stream. The velocity could then be computed from the preceeding equations.

Significant developments in sonar and underwater ultrasonics during the war provided a sound footing for the development of flowmeters after the war. According to Del Grasso and Spurlock (6), Gray (1945), Sproule (1946) and Kalmus (1952), suggested various methods of in line flowmeters. Del Grasso and Spurlock produced the first feasibility study into the possibility of flow measurement from outside of the pipe and their suggested flowmeter (machined, parallel faces to accomodate the transducers) is, probably, the forerunner of todays clamp on flowmeters. Their system used pulsed carrier transmission and detection of the beat envelope.

Early flowmeters, in the late 50's and early 60's required valve amplifiers and as a consequence were very bulky and not really portable. In the medical field Farral(7) developed a flowmeter for use on blood flows as low as 1cm/sec and in sections of tubing only 6mm diameter. Even by today's standards (and the enormous advantages afforded by present electronics) the problem is quite acute.

The dependance upon C, noted earlier was of importance and Fischbacher (8) designed an instrument using an optimum value of transducer angle to reduce this dependance.

With the advent of the transistor (late 50's early 60's) and integrated circuit (late 60's), the size of the flowmeter electronics has decreased whilst at the same time the measuring capability has been improved dramatically. Consequently the emphasis of design changed from that of improving the electronic timing aspects to one of consideration of other factors such as transmission aspects etc.

A variety of flowmeter configurations exist today all offering claimed improvements over others. Lynnworth (9) identifies several means of mounting the transducers and includes clamp-on versions and spool piece versions with and without transducer windows.

The error associated with the change in velocity profile can be shown (Baker and Thompson (10)) to be significantly reduced by the use of two paths off the diametrical chord. In a patent (11), Westinghouse propose a multibeam system with a predetermined weighting factor for each path programmed into the system. The four beam strap-on version is claimed to have a resultant error of 0.1% for a Reynolds number change of 10^4-10^7 (12).

Other methods of compensating for the velocity profile induced error have been suggested and a patent by Lynnworth (13) proposes the use of a rectilinear cell in which a volume of fluid is interrogated, bi-directionally and obliquely. Drost (14) in the medical field proposes a pair of transducers completely enclosing a thin walled vessel of any arbitrary shape and claims, for an experimental model, an accuracy of the order of 10%.

Using the flow tube as an acoustic waveguide has been proposed to eliminate the velocity profile error by Lechner (15) and others (16),(17),(18) and (19). The limitation with this technique would appear to be the low frequency required to excite the fundamental mode. It may, therefore, be better suited at the present time to lower sound speed fluids and smaller pipe sections such as in gas flow measurement.

It will be shown later in the thesis and is shown by Lynnworth (20) that the mounting and positioning of the transducers is very important. Baumoel's patent (21) shows a scheme for rigidily mounting the transducers and this is apparently the method used in one commercial instrument of which the author has had extensive experience and confirms its excellent mechanical repeatability.

The tracking of C, as mentioned previously is not difficult in direct insertion flowmeters (see e.g. Sanderson (22)) but is, in the case where there is substantial media between the transducer and fluid. It will be shown in this thesis that provided the block material is well known and characterised then the time delay for non-fluid parts can be removed such that the resulting time measured is a measure of C. The method of measuring a time in the block material is discussed by Kalinoski and Vignos (23) in a patent, in which a small path is maintained in the block and the time sound takes to travel this path is measured.

Nowadays, flowmeters have accuracies of the order of 1% (insertion type) and for clamp-on flowmeters accuracy of around 1% plus an offset which relies on other factors such as pipe thickness error etc,. Removal and reapplication of clamp-on flowmeters adds a further 1% error to the overall error.

A significant error possible with ultrasonic flowmeters is the zero drift, which adds a considerable error at low flows. An improvement in zero stability may be achieved by reciprocal action of the transducers as discussed by Hemp (24) and a scheme for its implementation is shown by Sanderson (22).

Errors and the associated loss mechanism in flowmeters are discussed by Brumer (25) and Lynnworth (9) and application considerations for clamp-on flowmeters are described by Schmidt (26) who also presents some test results.

Special applications for ultrasonic flowmeters include the design and use of a clamp-on model for cryogenic liquids and water which is claimed to have an accuracy of better than 1% (27).

The use of ultrasonic flowmeters in oil and gas lines is widely reported in the literature, Dell and Erickson (28) who report their use as leak detectors and Munk (29) describes the use of a single beam system in a 60cm pipe providing an uncertainty level of $\pm$2%. Pedersen etal (30), describe a gas flowmeter for the pipe angle of 30-90cm and claim an accuracy of $\pm$.45% over an integration period of 1 hour. Battye etal (31), discuss a flowmeter system for a 60cm pipe, monitoring refrigerated hydrocarbon for custody transfer purposes. The combination of a flowmeter with a densitometer and a time interval measurement system provide a mass flowmeter and one such meter is described by Lynnworth and Pedersen (32).

With the evolution of the microprocessor age and improved signal processing capabilities the ultrasonic flowmeter must decrease in size and carry on board significant compensation. It is possible for the majority of the electronics to be reduced to single chip size and this coupled with low cost at large pipe sizes should ensure a secure future.

1.1.2 The transmission of sound through plates

The transmission and reflection of sound through and from plates is an extremely complicated affair. Rayleigh (33) and Lamb (34) were the first to study the modes of vibration of elastic plates; Rayleigh studying shear-stress-free plates. They found that natural (or free) modes of vibration existed.

A free mode of vibration of a plate is defined as a mode of vibration that can exist with finite amplitude without external excitation. The classical characteristic equation is (taken from Graff (35)) for a free, infinite, isotropic elastic plate;-

$$\frac{\tan \beta b}{\tan \alpha b} + \left\{ \frac{4 \alpha \beta \xi^2}{(\xi^2 - \beta^2)^2} \right\}^{\pm 1} = 0 \qquad 1.2$$

+1=symmetric

-1=antisymmetric

where

$$\alpha^2 = \frac{\omega^2}{C_1^2} - \xi^2 \qquad \beta^2 = \frac{\omega^2}{C_2^2} - \xi^2$$

and C_1, C_2 are the longitudinal and shear wave speeds in the plate, ξ is the wave number $\frac{\omega}{C_L}$, ω is the radian frequency, C_L is the Lamb wave velocity.

Solutions of this transcendental equation for ξ and hence C_L (1.2) are real, imaginary or complex. The real solutions correspond to an infinite set of non-lossy propagating modes of finite phase velocity and the imaginary set of solutions correspond to all points in the plate having the same phase. Complex solutions exist and are discussed by Sherwood (36) and Lyon (37).

The real solutions are often displayed on a dispersion diagram, as shown in figure 1.2 which is taken from Madigosky and Fiorito (38). It can be seen that the axes are marked in terms of phase velocity (or trace velocity) against frequency thickness product (in this case khz-in $x10^2$).

The modes are coded with a letter and a subscript number and this corresponds to the symmetric (S) or antisymmetric (A) family of modes and the subscript number is the modal number. The form of the S or A wave is as depicted in figure 1.3 and shows the resulting motion on the plate surfaces. Particles on the surface undergo elliptical orbits (Viktorov(39)).

Two modes, the So and Ao mode approach the Rayleigh velocity of a half space in vaccuo in the high F x D limit. All other modes approach, from above, the bulk shear velocity in the plate. The So and Ao mode exist for all values of F x D whilst all the other modes have low frequency cut offs. These cut offs correspond to the plate being an integral number of the half wavelengths (shear or longitudinal), and are given by ,

$$\left.\begin{aligned} \frac{2FD}{C_1} &= 1\ 3\ 5 \\ \frac{FD}{C_2} &= 1\ 2\ 3 \end{aligned}\right\} \quad \text{for symmetric waves} \qquad 1.3a$$

$$\left.\begin{aligned} \frac{FD}{C_1} &= 1\ 2\ 3 \\ \frac{2FD}{C_2} &= 1\ 3\ 5 \end{aligned}\right\} \quad \text{for antisymmetric waves} \qquad 1.3b$$

These, then, are the natural vibrating modes of a freeplate, the so called Lamb waves. There are very strong similarities between Rayleigh and Lamb waves and this is seen by the fact that increasing the frequency thickness causes the Ao and So mode to combine and tend towards the Rayleigh/velocity. Similarities between Rayleigh and Lamb modes are discussed in (40).

If one now considers the plate to be immersed in a fluid and searches for free modes one finds that an equation similar to (1.2) exists but now includes a term to account for the effects of the fluid. This equation is (taken from Viktorov with suitable changes to the nomenclature);-

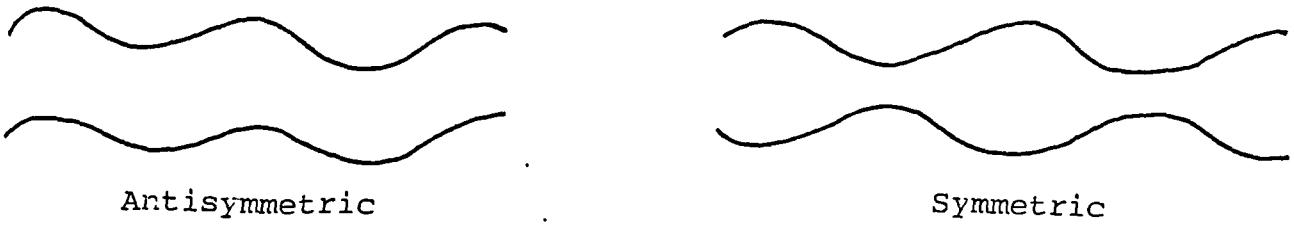

FIG 1.3
The form of Lamb modes (or waves)

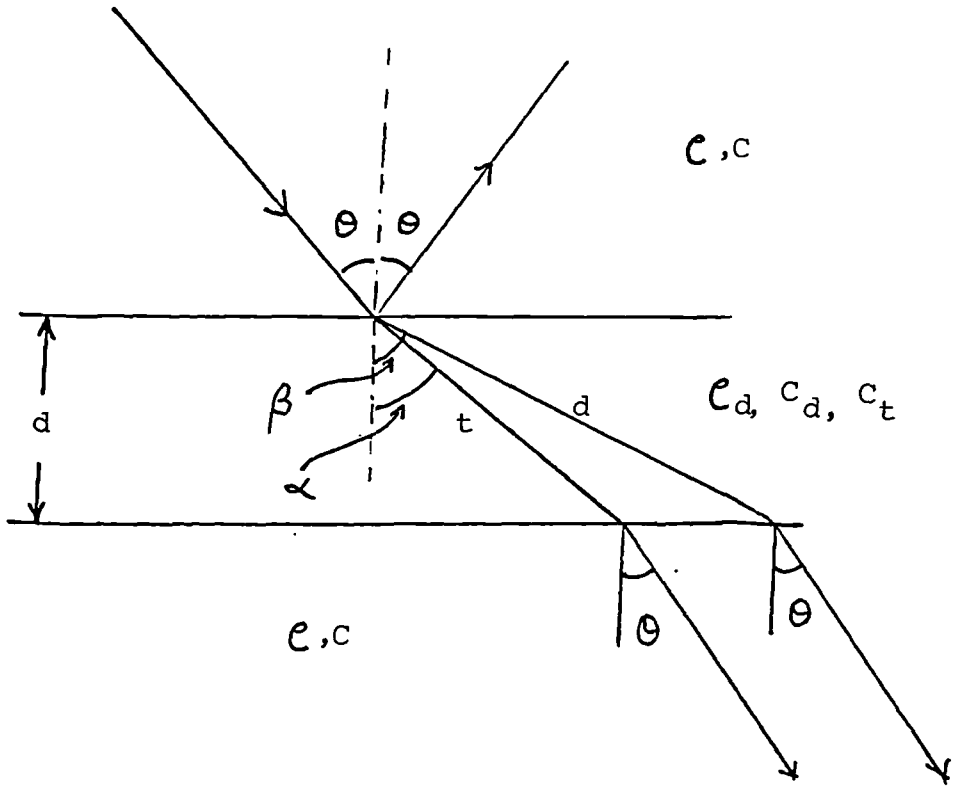

FIG 1.4
The model used by F.M.U.

for symmetric modes,

$$\frac{\left(2\xi^2-\left(\frac{\omega}{c_2}\right)^2\right)^2}{\tan\sqrt{\left(\frac{\omega}{c_1}\right)^2-\xi^2}\,b}+\frac{4\xi^2\sqrt{\left(\frac{\omega}{c_1}\right)^2-\xi^2}\sqrt{\left(\frac{\omega}{c_2}\right)^2-\xi^2}}{\tan\sqrt{\left(\frac{\omega}{c_2}\right)^2-\xi^2}\,b}=-\frac{\rho_L}{\rho_f}\frac{\sqrt{\left(\frac{\omega}{c_1}\right)^2-\xi^2}\left(\frac{\omega}{c_2}\right)^4}{\sqrt{\left(\frac{\omega}{c_{1f}}\right)^2-\xi^2}} \quad 1.4a$$

and for antisymmetric modes,

$$\left(2\xi^2-\left(\frac{\omega}{c_2}\right)^2\right)\tan\sqrt{\left(\frac{\omega}{c_1}\right)^2-\xi^2}\,b+4\xi^2\sqrt{\left(\frac{\omega}{c_1}\right)^2-\xi^2}\sqrt{\left(\frac{\omega}{c_2}\right)^2-\xi^2}\tan\sqrt{\left(\frac{\omega}{c_2}\right)^2-\xi^2}\,b \quad 1.4b$$
$$=\frac{-\rho_L\sqrt{\left(\frac{\omega}{c_1}\right)^2-\xi^2}\left(\frac{\omega}{c_2}\right)^4}{\rho_f\sqrt{\left(\frac{\omega}{c_{1f}}\right)^2-\xi^2}}$$

The physically admissable solutions of interests are now complex with the magnitude of the imaginary parts being related to the fluid loading. The real part of the solution is very close to the solutions of free modes in a vacuum providing the loading is light and this can be seen by reducing $\frac{\rho_L}{\rho_f}$ in the RHS of 1.4 which causes the term to vanish in the limit of $\rho_L \to 0$. Plona (41) suggests that a change of 1% occurs in the dispersion curves for the case of vacuum and water loading on a brass plate. For the case of this thesis, where attention is focussed on water steel plates the loading should therefore cause less effect on the dispersion curves.

Analysing the fluid/plate/fluid case shows that inhomogeneous waves exist in the fluid (i.e. waves with planes of constant phase and amplitude at right angles), and decaying waves along the plate. Once again the real part of the solution can be plotted on a dispersion diagram and can be found in the literature (see e.g: Freedman (42) who credits Sides with the computer work). These waves are termed Leaky Lamb waves.

Intuitively one would feel that if an incident wave could be directed so as to excite the free modes then advantage could be taken of the natural frequency, as in any vibration system.

On the dispersion diagram, for a fluid loaded plate, a new label can be attached to the trace velocity axis and this is the Lamb angle and is the angle at which an incident sound wave projection, matches that of the phase (or trace) velocity of a Lamb mode. The angle is said to coincide, or to be a coincidence angle. This coincidence was, see Schoch (43), first found by Cremer (44), who used elementary bending theory and was extended by Gotz (45) to other modes and thicker plates.

Reissner (46) is credited by Freedman (loc cit) as being the first to produce an exact equation for the transmission of sound through plates but did not explain the complicated form of the transmission curve.

Schoch(loc cit) considered the transmission through plates and linked this to the free modes in a plate. He then proceeded to find, through the use of trace velocities, the conditions of total transmission. He found that the total transmission points were grouped around the dispersion curves. However both he and Brekhovskikh (47) point out that there are positions on the curves at which total transmission does not exist. Both authors provide experimental confirmation. Note that there is a transposition of 'figures' in Brekhovskikh's book (page 77 and 78).

Schoch also observed that for bounded beams incident at the Lamb angles non specular reflection and transmission occurred. This has been extended slightly by the work of Plona (loc cit), Plona, Pitts and Mayer (48) and Plona, Behravesh and Mayer (49). The displacement in the beam being partly due to the build up and re-radiation of the Lamb wave.

Freedman and Swinerd (50), (51) present the internal field of an insonified elastic plate excited by an incident wave with particular attention being paid to the regions around the Lamb angles. Attention is focused on plates of thickness 0.55 and 2.5 shear wavelengths thick. These thicknesses correspond to intersection of 3 and 9 Lamb modes respectively. The displacement fields show the gradual build up of

the Lamb waves peaking at the intersected angles, and producing normal displacements in excess of 100 times the amplitude of the incident wave. This has also been the experience of the author and will be presented in chapter 4. Also identified in Freedman and Swinerd are transmission minima where the non-insonified surface shows virtually no normal displacement.

A more physical interpretation of the internal mechanism producing the form of the transmission curves is given by Fiorito and Uberall (52) for a fluid layer embedded in another fluid and by Fiorito, Madigosky and Uberall (53) for a solid plate (admitting shear stress) in a fluid medium. In the case of Fiorito and Uberall the solutions for total transmission are found to be identically equal to the free modes of a plate (shear-stress-free). In Fiorito, Madigosky and Uberall the conditions for total transmission are not the same as the free modes nor as the loaded leaky modes as described earlier.

FMU rewrite Schoch's equations as:

$$T = i\tau\left(\frac{1}{C_s - i\tau} + \frac{1}{C_a + i\tau}\right) \qquad 1.5$$

and

$$R = \frac{C_s C_a - \tau^2}{C_s + C_a}\left(\frac{1}{C_s - i\tau} + \frac{1}{C_a + i\tau}\right) \qquad 1.6$$

The model for this analysis is given in figure 1.4
and τ is the angle dependent impedence ratio, of the fluid to the plate

$$\tau = \frac{\rho_f C_f}{\cos\theta} \cdot \frac{\cos\alpha}{\rho_p C_p} \qquad 1.7$$

and

$$\begin{Bmatrix} C_s \\ C_a \end{Bmatrix} = \cos^2 2\beta \begin{Bmatrix} \cot\delta \\ \tan\delta \end{Bmatrix} + r^2 \sin 2\alpha \sin 2\beta \begin{Bmatrix} \cot\epsilon \\ \tan\epsilon \end{Bmatrix} \qquad 1.8$$

with $\delta = \frac{\omega d}{2C_p} \cos\alpha$

$$\epsilon = \frac{\omega d}{2C_t} \cos\beta$$

$$r = \frac{C_t}{C_p}$$

$$k = \frac{\omega}{C}$$

Inspection of 1.5 and 1.6 show that a resonance behaviour could be expected when the real parts of the denominators vanish i.e: $C_s = o$ or $C_a = o$ (which are, in fact, the free mode solutions).

FMU consider two variables $x = kd$ and $y = \sin\Theta$ and expand C_s and C_a as functions of x or y around resonance and develop new series expressions for T and R which show that the total transmittivity is made up from contributions from all modes.

Computational work in all three angular regions, presented by FMU, show excellent agreement. Their method has the advantage of working in the real domain without the need for complex root searches as in Pitts etal (40).

Freedman in two papers (42) and (54) clarifies some properties and provides support and minor extensions to FMU's work. Freedman also points out that erroneous results can be produced and provides an example of this for the case where only one mode is intersected, such as past the critical angle where only the S_o and A_o mode are intersected (with $y = \Lambda\omega\theta$ as the variable of interest). Freedman and Swinerd (55) examine in detail the internal and external fields along the S_o and A_o branches.

The inclusion of absorption coefficients into the wave equation, thus making it complex, reveal dramatic changes in the transmission characteristics, particularly around abruptly changing regions of maxima and minima. Resonance formalism is once again used to provide the analysis (38).

The use of Lamb waves, therefore, appear to offer the promise of high transmission and have found wide use in other disciplines such as NDT (see Viktorov). Mode conversion of a Lamb wave into a longitudinal wave in a fluid is calculated to be 100% efficient and to have a narrow angular width of $1-2^{o}$ (56). The reconversion process is found to be only 80% efficient due to reradiation of the incident beam (by the same authors). Virtually no energy is lost in transmitting Lamb waves along an air/plate arrangement and this facility is used to advantage in hostile arrangements (57).

The attenuation of Lamb waves in the presence of a fluid has been calculated by Watkins etal (58) and experimental verification is given for one particular case.

The reflection coefficient of plane waves, in a fluid, incident on a layered half space is given by Bogy and Gradcewski (59), and is studied for several cases. Approximations are made to produce simpler models, (in terms of frequency thickness) and these are compared to known results. A further paper by Bogy & Gradcewski (60) studies the non-specular reflection of bounded beams and by controlling the material parameters they produce reflection curves for various intermediate values between water/solid/water and water/solid/solid showing the evolution of the curves.

1.1.3 Time interval measurement

In Chapter Two the three basic methods of measuring the time of flight of the ultrasonic pulse will be discussed. Sanderson and Hemp (3) and others (2) (4) discuss the relative merits of each method.

At an early stage in the project, it was decided to choose a time interval measurement system, and all effort was therefore, concentrated on surveying the literature with a time interval profile as mentioned previously. It was decided therefore to consider firstly counting techniques, and these are described fully in the literature (61), (62) and (63) and in manufacturers application notes (64), (65) and (66).

The measurement problem is one of measuring a time difference to the order of 0.5-1nS resolution. This would require a counter, used in the standard mode, of 2GHz and is thus out of the question when regarding cost. Present generation counters at 500 MHz possess inherent difficulties in layout etc, and techniques have, therefore, aimed at expanding the time interval to be measured and a review of subnanosecond time interval measurement techniques is given by Porat (67), who compares the various methods available and tabulates the relative stabilities and linearities.

A difficulty encountered in any counting system is the trade-off between the counter size, time of response and range of time measurement. Counter systems exist with the capability of measuring in the picosecond region (Swapp (68) and Furko (69)) but are expensive and difficult to build since they usually require precise circuit layout and noise-free environments. It was felt that such systems would be unsuitable for industrial environments.

The search was, therefore, constrained to one of looking for systems with the measurement capability of nanoseconds and 100's of picoseconds and a suitable range, (or perhaps with minor modifications an extended range). The range would be, for a 100mm pipe, approximately 1μS at 10m/s velocity. A further consideration was the ability of the system to interface to a microprocessor.

Bunn etal (70) have produced a 12.5nS counter system that uses a Z80 microprocessor. Their system uses a 80MHz crystal oscillator and a ring counter and the output is given directly in 8 bit digital form. Their claimed range is 410μS.

The possibility of using multiphase clocks has been raised by Dhawan (71) and by Legrele and Lugol (72). In these systems use is made of a clock signal and the clock signal plus delay to represent various phases of the clock. This is simple to see in the case of a clock signal and its complement as shown in figure 1.5. In this case two codes exist, either 1.0 or 0.1 and this effectively doubles the clock frequency usually at the expense of a counter. Dhawan uses a 7 phase clock system and claims a resolutin of 2.5nS. Legrele and Lugol use a 32 bit code to obtain a resolution of 1nS (with a 125MHz gated oscillator). Race conditions do exist and must be considered.

Digital and analog systems have been designed with relatively high resolution by Hudor (73) (resolution approximately 15nS) and by Reinmuller (74) (resolution approximately 6nS). Both systems require significant analog circuitry, although Reinmuller's time-interval system is computer controlled. Evgrafov and Kartsenovs (75) digitiser has a claimed resolution of 1nS and a range of 0-1μsec. Their system works on the capacitor charging method whereby the time interval is expanded and then high frequency pulses are counted within the expanded interval.

Voronov etal (76) rely on averaging to produce a resolution of 2nS. However, it is not clear from their paper if they fulfil the conditions necessary for an unbaised time interval average as mentioned in (77) and (78).

Two other systems, almost totally digital, have been mentioned by Demyanchuk etal (79) and Kovrigin (80). Kovrigin uses a clock of 100MHz and a form of digital interpolation. Demyanchuk's system claims an accuracy of 2nS but cannot measure below 4nS interval. This system appears to be essentially a Vernier timing system in which the fractional part of a signal is recirculated until a coincidence is detected.

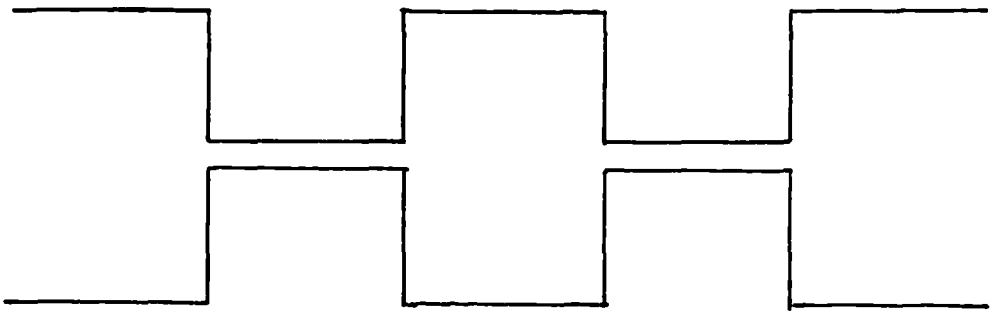

FIG 1.5
The use of multiphase clocks to expand a time interval

Vernier timing systems are well described in the literature (Porat, Kindlmann and Sunderland (81)) and consist of two oscillators, two counters and a detector. The two oscillators are separated by a small period or frequency difference of approximately 0.5-1%. The operation is then that the slow oscillator is started first, by the start pulse and the fast oscillator is started by the stop pulse. Slowly the fast oscillator catches up with the slow oscillator and a detector detects when a coincidence is made and stops the counters counting the two pulse trains. The time interval is then related to the counts in the counter by:

$$\Delta t = (N_2 - N_1) T_2 + N_1 \delta t$$

$$\delta t = T_1 - T_2 \qquad 1.9$$

Of the methods described by Porat, this one was felt to fullfil the main requirements of a flowmeter timing system, such as single shot resolution (0.5-1nS), low frequency oscillators (40MHz), thus minimal special requirements and direct digital/microprocessor application.

Kahane (82) uses a Vernier system to measure laser wavelength and obtains accuracies around 8 nanoseconds using inexpensive MECL-10K logic and Intersil 7226A counter chips.

Further back intime (late 60's early 70's), Barton and King (83) built two VTID (Vernier time interval digitisers) using commercial logic modules and inexpensive integrated circuits MECL II. MECL II is now obsolete. Barton and King confirmed the linearity of the system over five ranges of channel width δt (from 16.6pS - 182pS), but a drawback to their system was the substantial warm up period required.

Bowman and Whitehead (84) have designed a Vernier system using MECL III with a charmed resolution of 50pS provided sufficient time is allowed for warm up. The range of the system is limited to 12nS.

Karpov (85) in an approach aimed at overcoming the range difficulty, combines a Vernier system with a successive counting system. His resolution appears to be around 3nS but would be better using present integrated circuits since his (Russian) circuits appear to be slower.

The main difficulty with Vernier sytems is the detection of two coincident pulses and a typical method employed is to use a comparator. A paper describing the use of an AM685 comparator has been delivered by Bowman and Whitehead (86) and their experiment appears to confirm resolutions of the order of 50pS. This however, appears to be a limiting value since other values of channel widths (18pS and 30 pS) are biased and the reason given is the frequency locking of the two oscillators.

It was therefore decided to build a Vernier system, in outline form, similar to Barton and Kings. Although the MECL II logic used was obsolete copies of various data sheets were available from the manufacturer's reference libraries. A suitable comparable choice of logic was found to be fast (Fairchild Advanced Schottky logic). It was decided to relax the specifications of the system to around 0.5 nS or so. This was felt to be a region below which other factors would come into play, such as velocity profile effects and transmission through the wall effects etc. It was felt that nothing could be gained at this stage in pursuing a high resolution system (of 50pS level say). Adopting this requirement of 0.5nS period difference, would mean that the size of counter employed could be reduced and as mentioned earlier the system response is faster, of this method over a pure counting technique which would require averaging to produce the desired accuracy.

A crucial part of the system, as mentioned previously is the detector circuitry and a signficant amount of time was spent considering this aspect. In the end a novel, simple detector was found to be a pair of D-type flip flops configured in a certain manner. There is a synchronisation difficulty in using flip flops if the two inputs are from different time frames. Stoll (87), Chaney etal (88) and

Veendrick (89) cover the factors of importance when using the flip flops, since this particular problem of synchronisation is of paramount importance to the computer industry.

1.1.4 Piezoelectric transducers

Ultrasonic waves can be generated by a variety of methods see (90), (91). In the main it would appear that piezoelectric transducers cover the majority of requirements for generators and for the flowmeter discussed in this thesis the generator is a piezoelectric ceramic transducer operating in a thickness mode. Natural crystals such as quartz possess true piezoelectricity (pressure electricity) but for the man made ceramics the piezoelectric effect is due to the ferroelectric properties and this topic and the construction of piezoelectric ceramics is discussed in manufacturer's literature such as (92), (93).

The transient behaviour of a piezoelectric ceramic has been studied by Filipcynski (94) who produced, via Laplace transform techniques, an equivalent model of a Quartz transducer and showed that the external wave was comprised of elastic disturbances propagated from the boundaries and reflected at each boundary according to the well established phenomena.

Redwood (95), (96), (97) and (98) conducted a systematic analysis of the piezoelectric transducer, in the early sixties. Using the one directional equations which are (95)

$$T = cS - hD \qquad 1.10$$

$$E = -hS + \frac{D}{\epsilon} \qquad 1.11$$

where
- T = stress
- S = strain
- D = electric flux density
- E = electric field
- h = piezoelectric constant
- ϵ = permittity
- c = elastic constant

and solving the wave equation by Laplace techniques Redwood provides equations that can be used to produce an equivalent circuit as given by Mason (99). It can be seen that when h = o (i.e: no piezoelectricity) the equations reduce to the normal equations for non-piezoelectric material. Mason's equivalent circuit can be used for transient and continuous wave operation. Interesting features of the circuit show a negative capacitance and a transmission line, a necessary requirement to allow for the time of elastic disturbances to traverse the material. For simple boundary conditions, Redwood produces solutions which explicitly show the delay of the responses as emanating from within the material. If the media and ceramic are acoustically matched the resulting response to a delta function is a pair of pulses, one from the front face and one from the back face a delay of $\frac{x}{v}$ later, where x is the ceramic thickness and v is the propagation speed of waves in the material. This then is the minimum response possible with a transducer.

Therefore, either an exact equivalent circuit, as given by Mason, or the fundamental equations 1.10 must be used to provide the exact resulting ultrasonic pulse from a voltage input. Redwood shows, however, that an approximate analysis can be made by ignoring the negative capacitance; and by constructing an electrical analog circuit, the response of a transducer to either voltage or force input, can be viewed on a scope. An approximate determination of the parameters (about $\pm$ 10%) of the equivalent RLC network around resonance is provided in (98). The RLC equivalent circuit will be discussed shortly.

Further extension of the transient behaviour to mechanically free boundaries is given in Stuetzer (100) who shows that for short circuit operation the response finally approaches a sinusoid superimposed with delta functions. Stuetzer also provides (101) a method of determining the parameters, to within a few percent, of a piezoelectric transducer. Zhang etal (102) provide full analytic solutions for the internal stress field within any general transducer operating in the thickness mode and which is excited by a delta voltage source, with or without

internal resistance. An interesting feature of this paper is the "acoustic-electrical regeneration" which occurs because the changing thickness modifies the electric field which modifies the displacement which in turn modifies the field and so on. Zhang etal show that this effect is the origin of the negative capacitance in Mason model.

The RLC circuit, mentioned previously is a circuit valid around an isolated resonance where the components can be considered independent of frequency (approximately) and where the RLC branch is known as the motional arm and is related to the mechanical properties of the ceramic (103). This branch is in parallel with the normal capacitance of a plate capacitor C_o, which is $\epsilon_o \epsilon_R \frac{A}{D}$. This circuit has a low impedance at the RLC resonant frequency (fs) and a high impedance at a parallel resonant frequency (fp) where the RLC branch tunes with C_o. When loaded by acoustic media the frequency of operation lies between fs and fp and this is discussed in (104). Co can be tuned out by an inductor, at the series resonant frequency or the frequency of operation and this yields an improvement in the response.

Using Laplace methods and basing themselves on Redwoods work, Hayward etal (105) have developed a systems feedback model of the piezoelectric transducer valid for any arbitrary loading. They claim that the system model produced yields greater clarity in the understanding of the secondary piezoelectric effect; experimental verification of the model is given. Hayward (106) analyses the transducer impedance using the system feedback approach, for a variety of mechanical load conditions.

A disadvantage of using Laplace techniques to analyse the transducer is that their application is only valid over a limited number of input conditions for which transforms exist. The analysis of a piezoelectric transducer using $\mathcal{Z}$ transform technique is presented by Challis and Harrison (107) and Hayward and Jackson (108). Experimental confirmation shows that the technique is applicable and accurate and would appear to offer computational advantages.

Martin and Sigelmann (109) and Sigelmann and Caprihan (110) have developed design methods using an equivalent Thevenin circuit for the transducer, either as a transmitter or receiver. This is achieved by reducing the three port network of the transducer (transducer with backing, loading and electrical connection) to a two port network and then finding the Thevenin equivalent circuit. Computer simulation is found to agree closely with the experimental results and a design method is proposed.

The use of short-pulse (hence wideband width) ultrasound transducers is desirable in many applications (medical imaging, NDT etc) and is often achieved by backing the transducer so that no signal is returned to the transducer, i.e: the backing is highly attenuative and is often a tungsten powder/araldite mixture. However although the theory of transduction is well known there is a practical difficulty in the manufacture of transducers to fulfil the expected theoretical performance and the design and construction of probes is very much an art form.

The design and construction of wideband transducers is covered by Low and Jones (111) Sayers and Tait (112) and Foster and Hunt (113) who discuss the backing and bonding of transducers; and by Belleval and Lecuru (114) and Sung (115) who consider multilayer transducers (front face loading). Broadening the bandwidth of transducers has been achieved by using PVF2 film (116), a piezoelectric plastic and by using electrical transmission lines (117) to delay the return signal. Winter etal (118) and Brown and Weight (119) discuss the driving of transducers with complex waveforms to produce the required response.

Factors that influence the design of probes are discussed by Smith and Awojobi (120) and Kervel and Thijssen (121) and an extended model of the transducer is given by Silk (122). The performance and quality control of probes is discussed by Hall (123) and a review of recent advances in ultrasonic NDT is given by Bond and Punjani (124). A practical approach to the choice of transducer is given in Krautkramer (125).

The radiated field, its structure and its measurement is the subject of papers by Weight (126), Walton and Chivers (127), Chivers and Aindow (128) and Lewin and Chivers (129).

It is important to relate the main features of the theoretical model to the practical application (e.g: tuning out C_o). Matching the system can be important (see Krautkramer) and is achieved by inserting a reactive network between driving source and transducer so that the driving source sees a matched impedance at the frequency of operation (but this changes slightly as a function of loading). Matching over a range of frequencies is more difficult but see for example (130).

1.2. Outline of the Thesis

In Chapter two, the principle of the ultrasonic transit time flowmeter is explained and the various methods used for measuring the small time differences Δt are discussed. It is shown that in all practical systems there is a dependency on C, the speed of sound in the fluid and that for an instrument to be accurate the value of C should be tracked. Further more it is shown that C is a function of temperature and that this needs to be considered when operating the instrument. A model of a clamp on ultrasonic flowmeter is investigated with respect to the likely errors and a temperature coefficient is found to be 0.044%/ °C

A general specification for the instrument to be designed, is drawn up and includes consideration of the following points:

(i) The instrument design should be simple and use proprietary electronics. The instrument should be designed with a marketable view and we should therefore consider factors such as custom logic, single power supplies etc. It should be constructed with microprocessor compatibility.

The instrument should have a high speed of response (for transient or turbulence measurements).

(ii) The instrument should be designed to be flexible but to cover the largest market sector. Initial investigations suggest that pipe sections of 50-150mm covered the majority of cases and the flowrates were to be considered to be between 0.5 m/s and 10m/s. The fluids are often water based (thus C≈1500 m/s) but also gases and oils were to be considered. With the aforementioned considerations an overall design of instrument emerges. It is shown that the biggest errors are associated with velocity profile effects and, for the clamp on flowmeter, the unknown internal diameter. A smaller error is produced from the change in C due to temperature change for example, (providing, of course, that C is approximately known to start with). Compensation of velocity profile effects is discussed and a method of measuring C from outside of the pipe is presented with an error analysis.

Chapter three covers the electronic aspects of the flowmeter design and begins by discussing the problems encountered in any high speed design. Factors such as layout, decoupling, reflections and noise are shown to be important considerations in the design.

The first prototype flowmeter used transducers from a local manufacturer and it was not until late into the project that it was discovered how poorly matched to each other, the transducers were, in fact it was discovered that each transudcer had several unharmonic modes. These transducers were discarded and a new pair were purchased with considerably improved characteristics. The factors that need to be considered in the selection of the transducers are discussed and it is concluded that lead metaniobate transducers are, presently the most suitable.

The timing of short time intervals can be achieved in many ways, as discussed in the literature search and in Chapter 2. For the case of the flowrate, where turbulence spreads the timing and where an average flowmeter is required, a frequency (sing-around) or phase comparison system, with its inherent averaging, provides an elegant solution.

Similarly a direct timing system can be employed and its results averaged providing the conditions for unbiased averaging are considered (see 78). In some applications, however, it is felt that a single shot device may be more useful and that for the prototype instrument the design should be based upon that approach. It can be seen that a single shot device has a fast response time. The requirement was set initially at 0.5-1nS resolution on a one shot basis.

A suitable method, which is considered to be simple, easily constructed and accurate is a Vernier timing system. This system employs two very closely matched oscillators, differing in period by a small time difference; two counters and a detector. The principle of operation is discussed in detail in Chapter 3 but in essence requires that the oscillator output pulses are counted until there is a coincidence of pulses, at which point the detector stops the oscillators and counters. The time difference is related to the count in the counters.

Presented in Chapter three is a simple cheap implementation of the Vernier timing system using a novel detector. Conservative claims of the accuracy is shown to be of the order of 2nS, which is considered to be the limit of the measuring apparatus available. The instrument is shown to be highly repeatable and reliable.

An analysis of the errors in a Vernier timing system is considered and is found to consist of two parts, one, normally associated with time interval measurement and related to the period to be measured and one associated with the difference in period of the two oscillators. Auxilliary equipment was required for the testing of the systems, notably a suitable time delay unit and this equipment is discussed in detail. It is shown that drift tests on the timing system do not exceed the accuracy specifications set.

The other circuitry necessary to provide the remaining functions, the receiving and processing circuitry, and the control and firing circuitry is discussed in detail. The receiving and processing circuit consists of a low noise preamplifier which feeds a fast comparator, the output of which is a time marker used as a start pulse for one of the oscillators.

The firing of transducers can be achieved in a variety of ways; capacitor discharge, avalanche transistor methods, inductor discharge, SCR or Rf excitation (see (131) (132)). For the level of signals required in flowmetering it was found that a suitable novel device was a line driver and this was incorporated into the circuit. It is necessary to excite the transducers with a fast falling edge so the frequency transform contains enough energy in the high frequency range. For the system designed a variable pulse can be produced between 0-30v with a falling edge of 8-10nS duration.

The control circuitry presented contains extra circuits, whose function in a commerical model would be carried out by a microprocessor. The designed circuitry is hardwired synchronisation circuitry and controls all of the resetting, general timing and control necessary for the flowmeter to perform repetitively. This circuit is designed using standard components.

Circuit diagrams for all circuits are given.

The theory of the transmission of sound is covered in Chapter 4. The starting point is the development of a program to plot the Ao and So modes for a free plate equation 1.2 operating in the region $C_{phase} < C_{shear}$ since these modes are related to the angles of maximum transmission as discussed previously. The advantage of the So and Ao modes is that they offer the steepest angle into the fluid, thus reducing the stringent requirement of the timing system, and as pointed out by (57) the Ao mode is very wide compared to the other modes.

The emphasis then shifts to one of defining a model suitable for use in clamp-on flowmeters and theoretical development is undertaken of two infinite models depicting the two surface conditions, i.e: a wedge/plate/fluid and a fluid/plate/wedge. Using the standard methods of analysis (47) the equations of the two models are developed into a matrix representation and are then coded into a computer program. Included in the program is an energy balance equation which forms a partial check on the numerical work.

A search of the literature provided no comparative work with which the solutions could be checked and it was found necessary to consider reducing the models to the case of fluid/plate/fluid for which there is comparative work to check solutions. Even so it was still not precisely clear that the comparisons were favourable and it was found useful to develop a new model, fluid/plate/fluid and to compare first, the solutions of the reduced models against this new model and to then compare the solutions of it against that of other authors. The results of this work are presented and it is shown that the models would appear to be reliable.

Finally in Chapter four the peaks of the transmission curves are compared for a fluid/plate/fluid case against the free models of a dispersion curve and it is shown that maximum transmission peaks are grouped around the dispersion curves as was discussed previously in 1.2. This comparison is shown for two materials, steel and brass.

To provide a test facility for the prototype instrument it was necessary to construct a static rig. This would also be used to provide actual transmission curves for comparison with the theoretical curves. An earlier static rig had shown that the form of the actual curves had transmission peaks, but that the rig model was unreliable and unrepeatable.

In Chapter five the results of the experimental work carried out on the static rig are presented. It is shown that the rig has reasonable repeatability but that the specially designed transducer blocks (designed to rotate) had errors associated with the interfaces and the coupling medium.

Temperature and attenuation effects in the rig are discussed and results of testing are presented. Correction factors for the attenuation in the transducer blocks is considered and two sets of actual transmission curves are presented representing the case of a practical model with attenuation, and with the correction factor employed, the equivalent response of a non-attenuative material. The

actual curves are considered and compared against the theoretical curves. It is shown that rough agreement exists but that there is an offset in the peaks. Typical industrial pipe sections are used for comparison purposes.

The proposed method of determining C from outside of the pipe is given in Chapter 2 and in Chapter 5 experimental verification is attempted. It is shown that the measurement of C is consistent but heavily dependent on accurate positioning of the blocks and accurate measurement of other factors such as the speed of sound in perspex etc.

The effect of clamping/reclamping and experiments on the differential drift are presented. It is shown that over a short period there is a no effect from clamping/reclamping. Effects of zero crossing and temperature on the differential delay are considered and test results are produced.

The testing of the prototype instrument is carried out in Chapter six and to form an assessment of the relative accuracy of the prototype instrument it was found useful to test two commercial instruments, a spool piece instrument and a clamp on instrument. The clamp on instrument had the facility of being switched into an external mode (whereby the zero and top flowrate were set) and an internal mode (which was the factory setting).

Both instruments were set up according to the manufacturers suggestions and tested. The results of testing the instruments in a variety of positions is presented and it is shown that the spool piece instrument has an accuracy of $\pm$2% whilst the clamp on instrument is shown to have a linearity (external mode) within $\pm$2% but (in internal mode) on offset of approximately 7%.

The results of testing the protyotype instrument one presented and are shown to be comparable or better than the commerical clamp on in internal mode, a figure of around 4-5% being claimed. Discussion of the procedure adopted and method of analysis is covered in detail. Measurement of required parameters is also detailed.

The measurement of C from outside of the pipe is carried out for four positions and is shown to be remarkably consistent, corrections for varying pulse forms is considered and applied.

The final chapter, Chapter Seven provides conclusions drawn from the work and suggestions for the next stage of research and development of a marketable instrument.

CHAPTER 2 THE PRINCIPLE OF OPERATION OF THE TRANSIT-TIME ULTRASONIC FLOWMETER

2.1 Introduction

Of the many ultrasonic flowmeters available, the advantages of the transit-time types, mentioned in chapter 1, establish their position as leaders in the group. The two types of transit time flowmeter, the clamp-on type or the spool piece instrument have many similarities, with the spool piece instrument having inherently higher accuracy. Nevertheless there are many occasions where a clamp-on instrument will suffice.

In this chapter the basic principle underlying the operation of the instrument is discussed and the methods used in measuring the very small times (order of nanoseconds) are also covered . The difficulties in realising ideal systems are discussed and a specification for a clamp-on instrument is made.

The Department of Fluid Engineering and Instrumentation has a long standing interest in flow measurement and in particular flow metering. Previous work in the department had laid a foundation for this work. It was felt that a full understanding of the intricacies of ultrasonic flowmetering would only be gained by constructing, from scratch, a meter. Operational problems would also provide a better understanding of the user end.

A choice of systems was therefore made in accordance with the specification and it was decided to thoroughly investigate one particular model. This was to be the leading edge system.

The sources of errors are therefore of importance and an attempt is made to cover all the factors that influence the prediction of flowrate.

Finally, proposed methods of compensating for the errors are put forward and discussed in some detail. It is hoped that as a result, higher accuracy instruments can be produced.

2.2 The principle of operation of the transit-time ultrasonic flowmeter.

The principle of operation of the transit-time ultrasonic flowmeter (TTUSFM) can best be described by reference to figure 2.1. Depicted in figure 2.1 are the two cases of interest; in 2.1(a) the clamp-on flowmeter and in 2.1(b) the spool piece instrument.

The clamp-on instrument consists of two transducers, mounted in blocks (or wedges) which are mechanically clamped onto the pipe. The blocks can be permanently fixed (with araldite for example) or temporarily fixed (with some non-setting coupling compound).

The spool piece instrument consists of a section of pipe which has cavities built in to house the transducers. The transducers may or may not (the open cavity type) have a window of material in front of them.

Ultrasound is transmitted from transducer 1 and is detected by transducer 2. The procedure is reversed and transducer 2 transmits the ultrasound whilst transducer 1 detects the ultrasound. For a single-beam system the ultrasound traverses the diametrical chord but in a two beam system is displaced to approximately the R/2 position.

In the following argument the velocity is considered uniform throughout the pipe section.

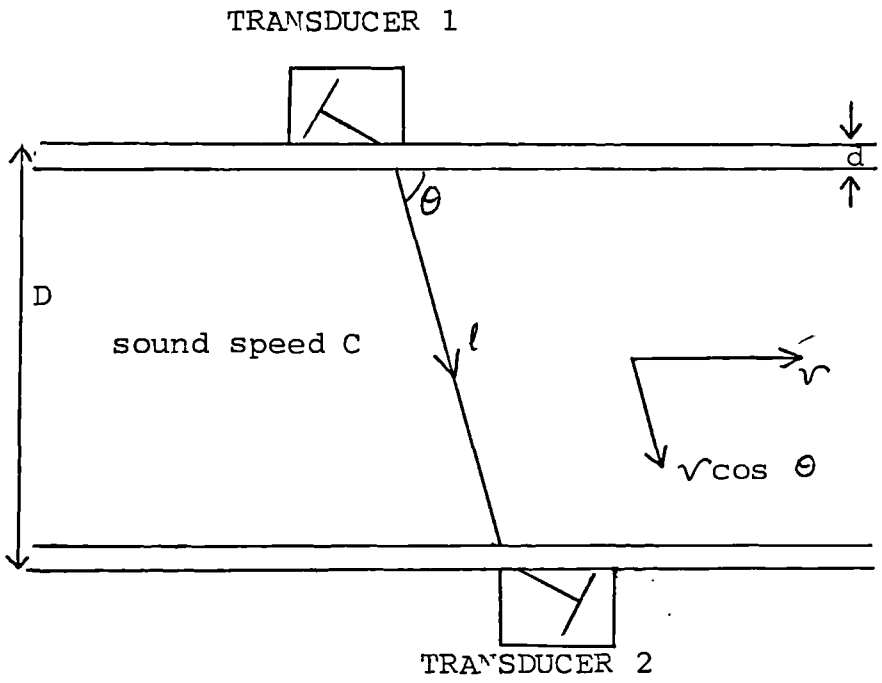

(a)

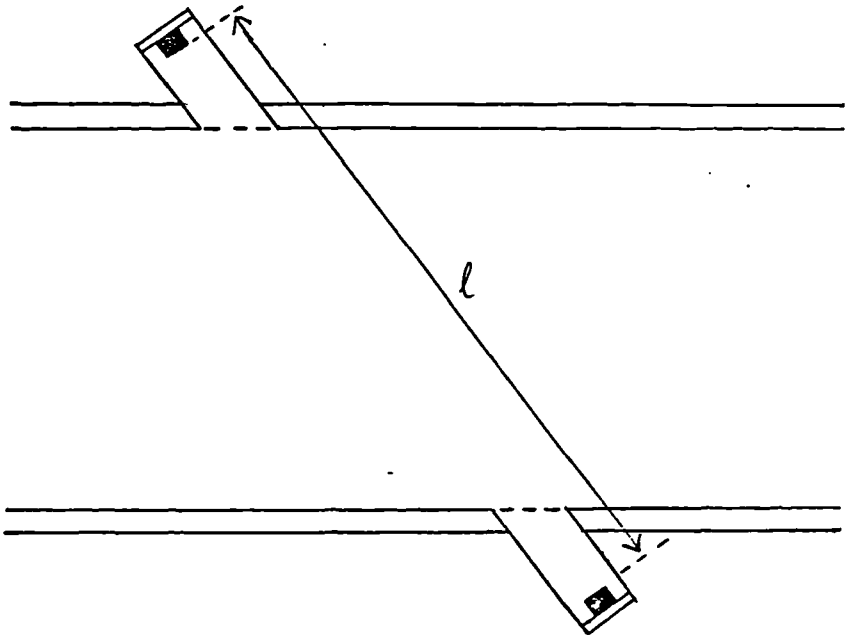

(b)

FIG 2.1
Two types of Transit Time Flowmeter (a) Clamp-on (b) Spool piece

The time of flight of the ultrasound, in the fluid only is given by:-

$$T_{12} = \frac{\ell}{C + v\cos\Theta} = \frac{\ell}{C}\left(1 - \frac{v}{C}\cos\Theta\right) \qquad 2.1$$

for the time from transducer 1 to transducer 2 and by:-

$$T_{21} = \frac{\ell}{C - v\cos\Theta} = \frac{\ell}{C}\left(1 + \frac{v}{C}\cos\Theta\right) \qquad 2.2$$

for the time from transducer 2 to transducer 1.

In both cases terms of higher order in $\frac{v}{C}$ have been ignored and this is perfectly acceptable in liquids where v is of the order of 10 m/s and C, is of the order of 1500 m/s but not in the case of gases where $\frac{v}{C}$ can be of the order of $1/3$.

The difference between T_{12} and T_{21} is Δt and is given by

$$\Delta t = T_{21} - T_{12} = \frac{2\ell v\cos\Theta}{C^2} \qquad 2.3$$

This equation shows that v is related to Δt through ℓ, Θ and C.

The dependence upon C can be eliminated by considering that the speed is given by the distance divided by the time, ie:-

$$C = \frac{2\ell}{T_{12} + T_{21}} \qquad 2.4$$

and thus,

$$\frac{\Delta t}{(T_{12} + T_{21})^2} = \frac{v \cos\Theta}{2\ell} \qquad 2.5$$

hence,

$$v = K_1 \frac{\Delta t}{(T_{12}+T_{21})^2} \qquad 2.6$$

Alternatively the product $T_{21}\ T_{12}$ can be computed, which to lowest order is,

$$T_{12}\, T_{21} = \frac{\ell^2}{C^2} \qquad 2.7$$

then,

$$\frac{\Delta t}{T_{12}\, T_{21}} = \frac{2v \cos\Theta}{\ell} \qquad 2.8$$

and hence,

$$V = \frac{K_2 \Delta t}{T_{12} T_{21}} \qquad 2.9$$

In either case the dependence upon C has been eliminated and for the case of spool-piece flow meters where ℓ and θ are both known, these methods of compensating for C are employed.

The volumetric flowrate is usually the required quantity and thus the velocity is required to be multiplied by the area resulting in, for 2.6 and 2.9.

$$Q = \frac{K_{11} \Delta t}{(T_1 + T_2)^2} \qquad 2.10$$

where

$$K_{11} = \frac{K_1 \pi (D-2d)^2}{4}$$

and

$$Q = \frac{K_{22} \Delta t}{T_{12} T_{21}} \qquad 2.11$$

where

$$K_{22} = \frac{K_2 \pi (D-2d)^2}{4}$$

For the case of the clamp-on flowmeter where neither ℓ nor Θ are known, the dependence upon C cannot be simply eliminated and the flowrate Q is given by

$$Q = \frac{\pi C^2 (D-2d) \Delta t}{8 \cot \Theta} \qquad 2.12$$

Θ can be eliminated through recourse to Snell's law ($\frac{Cp}{\sin \alpha} = \frac{C}{\sin \Theta}$) and then,

$$Q = \frac{\pi (D-2d) C Cp \Delta t \sqrt{1 - (\frac{C}{Cp} \sin \alpha)^2}}{8 \sin \alpha} \qquad 2.13$$

and thus

$$Q = K \Delta t \qquad 2.14$$

Here, Cp = the speed of sound in the block material, and
α = the angle of the transducer wrt normal.

Clearly, the problem of constructing an accurate flowmeter relies upon accurately knowing the values of (D-2d), α, C and Cp and of being able to accurately measure Δt, T_{12} and T_{21}. These accuracies providing the limit to the overall accuracy of the instrument. Furthermore it is important to know how the constants vary (particularly with temperature) and how this will affect the sensitivity of the instrument.

It is instructive at this point to consider the magnitudes of the times that are required.

From a commercial point of view it would appear that the pipe sizes of most interest, in industrial situations, (process industries etc,) range from 50mm to 150mm with a peak demand for 75-100mm sections. Because we are primarily concerned with the design of a commercial instrument a choice of section of 100mm would seem sensible.

For similar reasons to the above let us assume the fluid to be water, then for a beam crossing a 100mm section at 45° the times are

$$\Delta t = 88 \times 10^{-9} \text{ secs}/_{M/S}$$

and

$$T_{12} \sim T_{21} = 94 \times 10^{-6} \text{ secs}$$

where C has been taken as 1500m/s

It can be seen, therefore, that measurement of v to better than 1% requires measurement of Δt to better than $.88 \times 10^{-9}$ seconds and that this time of Δt is comparable to the fastest, presently available logic, the Emitter Coupled logic family (ECL).

2.2.1 Methods used in measuring Δt.

There are three basic modes of operation used for the measurement of Δt and numerous variations of each.
The modes of operation are:

(i) the leading edge system
(ii) the phase comparison system
(iii) the frequency (sing-around) system

All of the above systems are essentially time interval measuring systems which measure between time markers and carry out some form of averaging.

There would appear to be no significant advantage in choosing one system over the other particularly when one considers that turbulence spreads the time and averaging would be required to reduce its effect. The overall accuracy is therefore a function of statistical methods and must be traded off against the response time required.

2.2.1.1 The Leading Edge System

In this system the transducers are used as transmitters/receivers. The transducers can be fired either simultaneously or individually and the equations governing this mode of operation are those previously given.

Firing the transducers simultaneously requires two identical electronic paths, if differential delays are to be eliminated. The transducers are firstly configured as transmitters and are then fired simultaneously, the acoustic pulses passing over each other in the fluid. The control circuitry the switches the transducers to the receive mode and the pulses are received separated by the time difference Δt. Measurement of the time in one direction is usually sufficient to allow prediction of the sound speed velocity.

The differential delays, mentioned previously, can lead to significant errors at low flows since the times of the delays are comparable with the times of low flowrates.

In the individual mode of firing, one transducer is used as a transmitter and the other transducer is used as a receiver. The pulse is transmitted and received and a timing measurement made. The roles of the transducers are then reversed and another pulse launched and received. A second timing measurement is taken. This method is sufficient to yield Δt, T_{12} and T_{21}. In this system one electronic path can be utilised and thus the differential delay can be eliminated. However, there is a difficulty in measuring relatively long times accurately.

There would appear to be two main advantages of the simultaneous method of firing the transducers. One advantage is that the pulses effectively traverse the same volume of fluid and thus any distortion in the flow affects both pulses equally. The other advantage is the inherently faster response time.

2.2.1.2 The Phase Comparison System

If the transducers are used in a continuous or quasi-continuous system then the phase difference between upstream and downstream signals is given by

$$\Delta\phi = 2\pi f \Delta t = \frac{4\pi f v (D-2d) \cot\theta}{C^2} \qquad 2.15$$

The advantage of this system is that increasing f increases the phase difference to be measured and this eases the electronic problem. However, there are practical limitations upon f which depend upon the fluid, for example the attenuation in fluid increases as the square of the frequency f.

Various techniques have been utilised to improve this method, the chief one being heterodyning (mixing) the received signals with a local oscillator. Because mixing the signals maintains phase relationships the problem of timing is eased by mixing at a frequency very near to that of the signal itself.

A problem exists with this method when $\Delta\phi > 2\pi$ since the phase difference is a multi-valued function. Careful consideration of flowmeter applications is therefore essential in using this method to ensure that $\Delta\phi$ does not fall outside of limits.

It can be seen from equation 2.15 that $\Delta\phi$ is also subject to a C dependency and compensation is still required for this method as in the time interval method.

2.2.1.3 The Frequency (sing around) system

In this method of operation one transducer is configured as a transmitter and the other as a receiver. A pulse is transmitted and received and the received pulse retriggers the transmitter, thus a frequency train is set up. The roles of the transmitter and receiver are reversed and the procedure is carried out in the reverse direction. The difference in frequency is a measure of the velocity, since

$$F_1 = \frac{1}{T_1} = \frac{C + V\cos\Theta}{\ell} \qquad 2.16$$

and

$$F_2 = \frac{1}{T_2} = \frac{C - V\cos\Theta}{\ell} \qquad 2.17$$

then

$$\Delta f = F_1 - F_2 = \frac{2V\cos\Theta}{\ell} \qquad 2.18$$

This elegant method, which comprises of all the measuring electronics in one feedback loop is seen to be independent of C, but once again a problem exists in that Δf is of the order of 1000 times smaller than F_1 and F_2 and hence a long response time is required, the response time depending upon the resolution required. (For example, using the previous example of 100mm pipe with water as a fluid the ratio $\frac{\Delta f}{F} \simeq \frac{10}{10000}$ per m/s).

Earlier models of the sing around system suffered from a major drawback in that if the signal was lost (say from a particle blocking the beam) then the frequency would cease. This particular problem seems to have been overcome by the 'electronic flywheel' approach in which two

identical pulses are generated, with one going through the fluid and the other being delayed by the last acceptable value. In this way if the fluid pulse is blocked then the internal pulse maintains the oscillation. For references on this technique, see Sanderson (22).

2.2.2 Realisation of practical systems

In all practical systems the above methods suffer from delays in the electronic paths and in the non-fluid paths. The differential delays in the electronic paths are of the same order of time as that of low flowrates and this clearly presents a problem.

In the leading edge system the equation governing the time Δt is modified to

$$\Delta t = \frac{2(D-2d)\cot\theta\, v}{c^2} + \tau_1 \qquad 2.19$$

where τ_1, is made up from differential delays in the electronic paths for simultaneous firing systems and multiplexing delays in both systems (simultaneous firing and individual firing systems). The delay τ_1, can be subtracted if known but it is also a function of temperature and this does lead to a residual problem.

In the phase comparison system the equation becomes modified to

$$\Delta\phi = \frac{4\pi f(D-2d)\cot\theta\, v}{c^2} + \phi_\tau \qquad 2.20$$

where ϕ_τ is made up of different phase/frequency characteristics of the transducers and electronic circuits. Once again a value for ϕ_τ can be subtracted but it is usually a function of temperature.

In the frequency system the equations becomes

$$F = \frac{1}{T+\tau} = \frac{c \pm v\cos\Theta}{\ell + \tau(c \pm v\cos\Theta)} \qquad 2.21$$

and

$$\Delta f = \frac{2\ell v\cos\Theta + ((c^2 - v^2\cos^2\Theta)\tau_2 - \tau_1)}{[\ell + (c - v\cos\Theta)\tau_2][\ell + (c + v\cos\Theta)\tau_1)]} \qquad 2.22$$

where τ_2 and τ_1 are made up from the delays in non fluid paths in both directions. Even if $\tau_1 = \tau_2$ the system has a dependency upon C and this has to be compensated for electronically as with the other systems.

In a clamp-on system the main part of the delay is associated with the wedge.

Factors that influence the choice of a system are for example the echoes produced. In a time or quasi-continuous phase-comparison system the echoes can be allowed time to settle down. In the frequency system this is usually achieved by inserting a long enough delay, but this further aggravates the measurement of Δf. This problem is less severe in clamp-on systems where the interfaces deflect some of the incident and reflected energy.

A further consideration is the response time/resolution and this has been pointed out in the previous sections. The leading edge system would appear to have an advantage here in that individual measurements can be recorded. This may be important in, for example, the study of transient flow.

2.3 The specification chosen for the design of a clamp-on ultrasonic flowmeter.

It will be recalled from chapter 1 that the objectives of this thesis were to provide a foundation and working model of a clamp-on flowmeter suitable for commercialisation.

The choice of system had to be based, therefore, on typical industrial requirements, but with sufficient flexibility for specialised work (for example on a consultancy basis).

The considerations put forward were:-

(i) pipe sizes 50-150mm
(ii) mostly water based liquids
(iii) possibility of dirty liquids, particulate flow
(iv) speed of response
(v) transient flow and turbulence measurement
(vi) use commercially available electronics
(vii) significant digital content with inclusion of microprocessor technology

From these considerations it was decided to thoroughly investigate a leading edge system which had a simultaneous mode of firing, using digital counting techniques. The pipe size chosen was 100mm.

2.4 The sources of errors in transit-time ultrasonic flowmeters.

2.4.1 The sources of errors in predicting the flowrate Q.

In the assessment of errors it is convenient to separate those errors that produce a change in calibration from those errors that produce an offset.

Since

$$\varphi = K\Delta t \qquad 2.23$$

then a change in K (δK) and Δt ($\delta \Delta t$) means

$$\delta\varphi = \delta K \Delta t + \delta \Delta t K \qquad 2.24$$

(ignoring second order effects).

Thus the error is made up from a calibration error $\delta K \Delta t$ and an offset error $\delta \Delta t K$

The error δK can arise in two ways, firstly by an incorrect measurement of one of the constants that make up K. Secondly, if one of the constants changes (say due to temperature) and is not compensated for then an error will exist.

Errors in Δt are caused by incorrect measurement of Δt.

Consider the equation for Q, for a clamp-on flowmeter, equations 2.13.

$$\varphi = \frac{\pi (D-2d) C C_p \sqrt{1-\left(\frac{C}{C_p}\sin\alpha\right)^2}\ \Delta t}{8 \sin\alpha} \qquad 2.13$$

Inspection of 2.13 shows that of the constants, the ones that can change with temperature are C and Cp. Since α is under the manufacturers control and can be held to very tight tolerances.
The measurement of (D-2d) presents a problem. D-2d will not vary with temperature, since a typical expansion coefficient (β) is of the order

of 10^{-5} (Kaye and Laby) (133) and an estimate of change in diameter is

$$\delta(D-2d) = (D-2d)(\beta \Delta temp) \qquad 2.25$$

thus a change in temperature of 100°c would only cause a .1% change in (D-2d).

Therefore, of interest is the error in predicting Q when there is an error in (D-2d), C, Cp and α.

It can be seen directly that a percentage error in (D-2d) reflects directly as the same percentage error in Q.

To estimate the effect from errors in C, Cp and α it is necessary to compute $\frac{\partial \varphi}{\partial C}$, $\frac{\partial Q}{\partial Cp}$ and $\frac{\partial \varphi}{\partial \alpha}$ and to estimate the fractional change in Q ie $\frac{d\varphi}{\varphi}$

Therefore, differentiating 2.13, in terms of C and Cp

$$\frac{\partial \varphi}{\partial Cp} = \frac{\pi (D-2d) C}{8 \sin\alpha}\left[\frac{\sin^2\alpha}{\sqrt{1-\left(\frac{C}{Cp}\sin\alpha\right)^2}}\left(\frac{C}{Cp}\right)^2 + \sqrt{1-\left(\frac{C}{Cp}\sin\alpha\right)^2}\right]\Delta t \qquad 2.26$$

and

$$\frac{\partial \varphi}{\partial C} = \frac{\pi (D-2d) Cp}{8 \sin\alpha}\left[\frac{-\sin^2\alpha}{\sqrt{1-\left(\frac{C}{Cp}\sin\alpha\right)^2}}\left(\frac{C}{Cp}\right)^2 + \sqrt{1-\left(\frac{C}{Cp}\sin\alpha\right)^2}\right]\Delta t \qquad 2.27$$

If we assume that the change in C and Cp is brought about by temperature then one could compute the total differential

$$d\Phi = \frac{\partial \Phi}{\partial C_p} \cdot \frac{\partial C_p}{\partial temp}\, dtemp + \frac{\partial \Phi}{\partial C} \cdot \frac{\partial C}{\partial temp}\, dtemp \qquad 2.28$$

and obtain the fractional change $d\Phi/\Phi$ in the estimate of the flowrate. This would thus provide the temperature coefficient of the uncompensated instrument.

The temperature coefficients of water and perspex at 20°c are (taken from Kaye and Laby and Physical Acoustics Vol XIV),

$$\frac{\partial C}{\partial temp} = 3.09 \quad m/s/^{o}C$$

and

$$\frac{\partial C_p}{\partial temp} = -2 \quad m/s/^{o}C$$

Using values for C and Cp (from Kaye and Laby) and for α and D-2d as given below,

C	=	1500 m/s
Cp	=	2700 m/s
α	=	62^{o}
(D-2d)	=	.1 m.

the value of d Q can be found for a 1°c, temperature change, thus

$$d\Phi = \frac{\pi (D-2d)\Delta t}{8 \sin\alpha} \left\{ C \left[\frac{\sin^2\alpha}{\sqrt{1-\left(\frac{C}{C_p}\sin\alpha\right)^2}} \left(\frac{C}{C_p}\right)^2 + \sqrt{1-\left(\frac{C}{C_p}\sin\alpha\right)^2} \right] .-2. \right. \qquad 2.29$$

$$\left. + \left[\frac{-\sin^2\alpha}{\sqrt{1-\left(\frac{C}{C_p}\sin\alpha\right)^2}} \left(\frac{C}{C_p}\right)^2 + \sqrt{1-\left(\frac{C}{C_p}\sin\alpha\right)^2} \right] .3.09 \right\}$$

and inserting values,

$$d\Phi = -155.17\Delta t + 227.9\Delta t \qquad 2.30$$

A typical value for Q would be

$$\Phi = 156967\ \Delta t \qquad 2.31$$

and thus the percentage errors are

$$\frac{d\Phi}{\Phi} = -.098\%/^{\circ}C \quad \text{for changes in Cp} \qquad 2.32$$

$$\frac{d\Phi}{\Phi} = .145\%/^{\circ}C \quad \text{for changes in C} \qquad 2.33$$

$$\text{and } \frac{d\Phi}{\Phi} = .044\%/^{\circ}C \quad \text{for changes in both C and Cp} \qquad 2.34$$

It should be noted that the temperature coefficients are of opposite sign and one would therefore expect a partially compensating system. However, there are three possible scenarios.

(i) an ambient temperature rise:- then Cp would change but not C

(ii) a fluid temperature rise:- then C would change but not Cp

(iii) the system is in steady state:- then C and Cp change together with temperature

It is likely that most systems would consist of a wedge material with a negative temperature coefficient and thus there would be partial compensation in the steady state. In which case a 20°c rise in temperature would produce an error of approximately 1%.

Hence it now becomes clear why compensation methods are utilised, for if the system has been calibrated at one particular temperature and its application is at another different temperature, an error will exist. Within small movement about a value say $\pm 5^{o}C$, the error would be likewise small $\pm .2\%$.

Notwithstanding the earlier comments about the tight tolerancing of α, it is still desirable to compute the effect of a change in α. Even with a tightly toleranced α it may be that the blocks do not lie at the precise angle on the pipe due to paint layers for example, or non parallel walls.

Therefore, we require to find $\frac{d\Phi}{d\alpha}$ and $\frac{d\Phi}{\Phi}$

differentiating 2.13, wrt α,

$$\frac{d\Phi}{d\alpha} = \frac{-\pi(D-2d)CC_p\Delta t}{8}\left[\frac{\cos\alpha}{\sqrt{1-\left(\frac{c}{C_p}\sin\alpha\right)^2}}\left(\frac{C}{C_p}\right)^2+\frac{\sqrt{1-\left(\frac{c}{C_p}\sin\alpha\right)^2}\cos\alpha}{\sin^2\alpha}\right] \quad 2.35$$

and using the previously given values one can compute

$$\frac{d\Phi}{\Phi} = -1.18\ \%\ /_{per\ ^{o}}$$

Therefore to summarise it can be seen that the errors in predicting Q are made up from

(i) D-2d a percentage error in (D-2d) reflects as the same percentage error in Q.
(The likely error in (D-2d) is probably around 0.5% - 2% value.)

(ii) C the error in Q is ·14 % per °C or approximately ·7 % per 1% change in C (1% is, say 15 in 1500 = 5°C rise).

(iii) Cp the error in Q is-·09% per °C or ·3 % per 1% change in Cp (1% is, say 27/2700)

(iv) α the error in Q is-1.2%/per angular degree,

or instead of (ii) and (iii)

(v) C & Cp the error in Q is .044%/°C

There are problems in measuring D-2d, C and Cp accurately in the first place.

Cp should not present a severe problem since the material and its characteristics would be well known and understood.

The problem of measuring D-2d accurately is particularly difficult. Pipe manufacturers tolerances would appear to range up to 3% for the pipe wall thickness and clearly this presents a more severe problem in small bore pipes.

The measurement of C is left until section 2.5 where a method will be proposed to overcome this difficulty.

2.4.2 Other errors in the clamp-on system.

2.4.2.1 Reynolds number effects.

It was mentioned in section 2.2 that for convenience the velocity would be considered uniform throughout the pipe. In reality this is not the case and account must be taken of the velocity profile.

The equation,

$$\Delta t = \frac{2v(D-2d)\cot\theta}{c^2} \qquad 2.36a$$

can be generalised as an integral

$$\Delta t = \frac{4\cot\theta}{c^2}\int_0^{\frac{D-2d}{2}} v(r)\,dr \qquad 2.36b$$

where (D-2d)/2 is the radius of the pipe and dr is an infinitesimal section. Clearly when $v(r) = V$, the integral reduces to 2.36a.

The velocity distribution in the pipe $v(r)$ is dependent upon the Reynolds number Re. The Reynolds number is given by

$$Re = \frac{\rho v d}{\eta} \qquad 2.37$$

where ρ = density
v = mean velocity
d = diameter
η = kinematic viscosity

As an example of Reynold's number, consider the case of interest - water in a 100mm pipe. Then it can be shown that $Re = 10^5 \times v$ and for a range of .5m/s to 10m/s Re varies between $.5\times10^5 - 10^6$.

The equation for $v(r)$ to be inserted into 2.36b varies with the flow region, ie: laminar, transitional or turbulent.

For laminar flow, where the profile is parabolic

$$v = 2\bar{v}(1-r^2) \qquad 2.38$$

where $\bar{v}$ is the true mean velocity

For fully developed turbulent flow (Re > 4000) an approximate equation is

$$v = \frac{(1+2n)(1+n)\left(1-\frac{r}{a}\right)^{1/n}}{2n^2}\,\bar{v}^2 \qquad 2.39$$

and at very high flowrates

$$v = \bar{v} \qquad 2.40$$

Inserting any of the $v(r)$ in the integral 2.36b and performing the integration would result in values for the ratio of $\frac{v_M}{\bar{v}}$, where v_m is the mean velocity.

In the laminar region $\frac{v_M}{\bar{v}}$ is found to be 1.33 and in the turbulent region (Re = 5×10^4 - 3×10^6), empirical measurements yield (134)

$$\frac{v_M}{\bar{v}} = 1.12 - 0.011 \log_{10} Re \qquad 2.41$$

It can be seen therefore that the velocity calculated (through Δt) is 33% over estimated by an ultrasonic flowmeter operating in the laminar region and by approximately 5-7% in the turbulent region (using previously given values for ν).

Inspection of 2.41 shows a decade change of Re to result in a change of $\frac{V_m}{\bar{V}}$ of approximately 1%. Compensation for Re is thus required and this is discussed in section 2.52.

2.4.2.2 Beam shift effects.

A factor of importance in ultrasonic flowmeters is the beam shift due to a change in C, since it may be important to know exactly where to place the transducers. Consider figure 2.2.

The distance of interest is x and its change with C. Solving for x one finds

$$X = \frac{\frac{C}{C_p} \sin\alpha \, (D-2d)}{\sqrt{1-\left(\frac{C}{C_p}\sin\alpha\right)^2}} \qquad 2.42$$

and differentiating wrt C, one obtains

$$\frac{dx}{dC} = \left[\sin^3\alpha \frac{C^2}{C_p^3} \frac{1}{\sqrt{\left(1-\left(\frac{C}{C_p}\sin\alpha\right)^2\right)^3}} + \frac{1}{\sqrt{1-\left(\frac{C}{C_p}\sin\alpha\right)^2}} \frac{\sin\alpha}{C_p}\right](D-2d) \qquad 2.43$$

Using previously given values, calculation for dx yields

$$dx = 4.97 \times 10^{-4} \quad (D-2d) \quad \text{per 1m/s change in C}$$

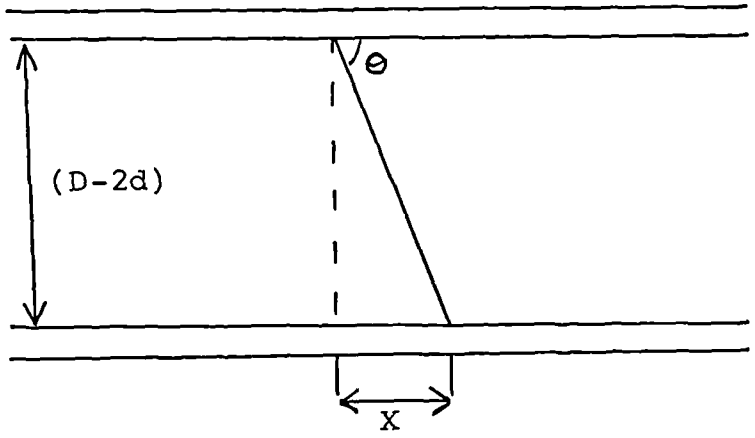

FIG 2.2
Relating to beam shift effects

For a .1m pipe

$dx = 50\mu m$ per m/s change in C

Thus in choosing a C to change by 60m/s would give a beam shift of 3mm in .1m pipe. Hence it can be seen that it would be important to know (roughly) C to enable positioning of the transducers. Also needed would be the likely change in C to ensure that the sound beam did not pass over the transducer and (possibly) miss it altogether. In larger bore pipes this particular problem can be severe.

2.4.2.3 Attenuation and beam spreading effects.

A plane attenuated wave is described by the equation:

$$P_x = P_o e^{-\alpha x} e^{i(kx-\omega t)} \qquad 2.44$$

where Po is the maximum pressure amplitude
k is the wavenumber
α is the attenuation coefficient in nepers/unit distance
x is the distance

For the case of interest the attenuation coefficients are those for water, steel and perspex and at 20°c these are, (Kaye and Laby)

	α (nepers/cm)	f
water	3.6×10^{-4}	1 MHz
steel	4.9×10^{-2}	10 MHz
perspex	.57	2.5 MHz

For solids the attenuation is roughly proportional to f, whilst for fluids it is related to f^2, thus the revised values at 1.25 MHz are

	α(nepers/cm)	f
water	5.6×10^{-4}	1.25 MHz
steel	$61{\cdot}25 \times 10^{-4}$	1.25 MHz
perspex	.28	1.25 MHz

It can be seen, therefore, that the wedge material for this case has a very high attenuation coefficient and in a commercial instrument it would be important to consider the choice of material used for the block.

Beam spreading is related to the frequency of operation and in this case energy is lost because the beam spreads out in a conical fashion. The half-angle is approximately given by $\Theta = \frac{\lambda}{D}$ where λ is the wavelength of sound in the medium and D is the diameter of the (piston) ultrasonic generator.

From the two aforementioned energy loss mechanisms it can be seen that the attenuation puts a limit on the higher frequency and the beam spreading puts a limit on the lower frequency.

2.5 Proposed compensation methods.

From the previous discussions it is clear that it is necessary to compensate for changes in C and Cp and Reynolds number (velocity profile) effects.

The difficulty in measuring C in a clamp-on system is brought about by the fact that neither ℓ (path length) nor Θ is known. In the following section a proposed method for measuring C is suggested.

The manufacturer of clamp-on flowmeters has control over the choice of the wedge material and hence over Cp and $dCp/dtemp$
One possible remedy, to eliminate the effects of changing Cp, would be to select a material with zero temperature coefficient. However, this is unlikely and if a material could not be found with a negligible coefficient then it may be of interest to monitor the temperature of the block. One imagines that this could be achieved simply by embedding a temperature sensor.

The majority of flowmeters in industrial use are operating on turbulent systems. This makes the particular job of compensating for velocity profile effects slightly simpler than it would be if covering the entire range of flows. The method of compensating is discussed in section 2.5.2.

2.5.1. Compensation for changes in C.

By compensation for changes in C is meant the ability to measure C and to track it should it change. A proposed method for doing this is discussed below.

Consider figure 2.3.

Consider the transmission of a wavefront (XX) from transducer 1 to transducer 2 (YY). The wavefront (XX) travels a distance in the wedge before encountering the pipe wall, where, for reasons to be established in chapter 4, the front is normal to the pipe wall. The wavefront then travels across the fluid and onto the far wall, where once again it is normal. Finally, the wavefront emerges and travels a distance before impinging upon the receiver transducer. In a similar manner the reverse procedure occurs from transducer 2 to transducer 1.

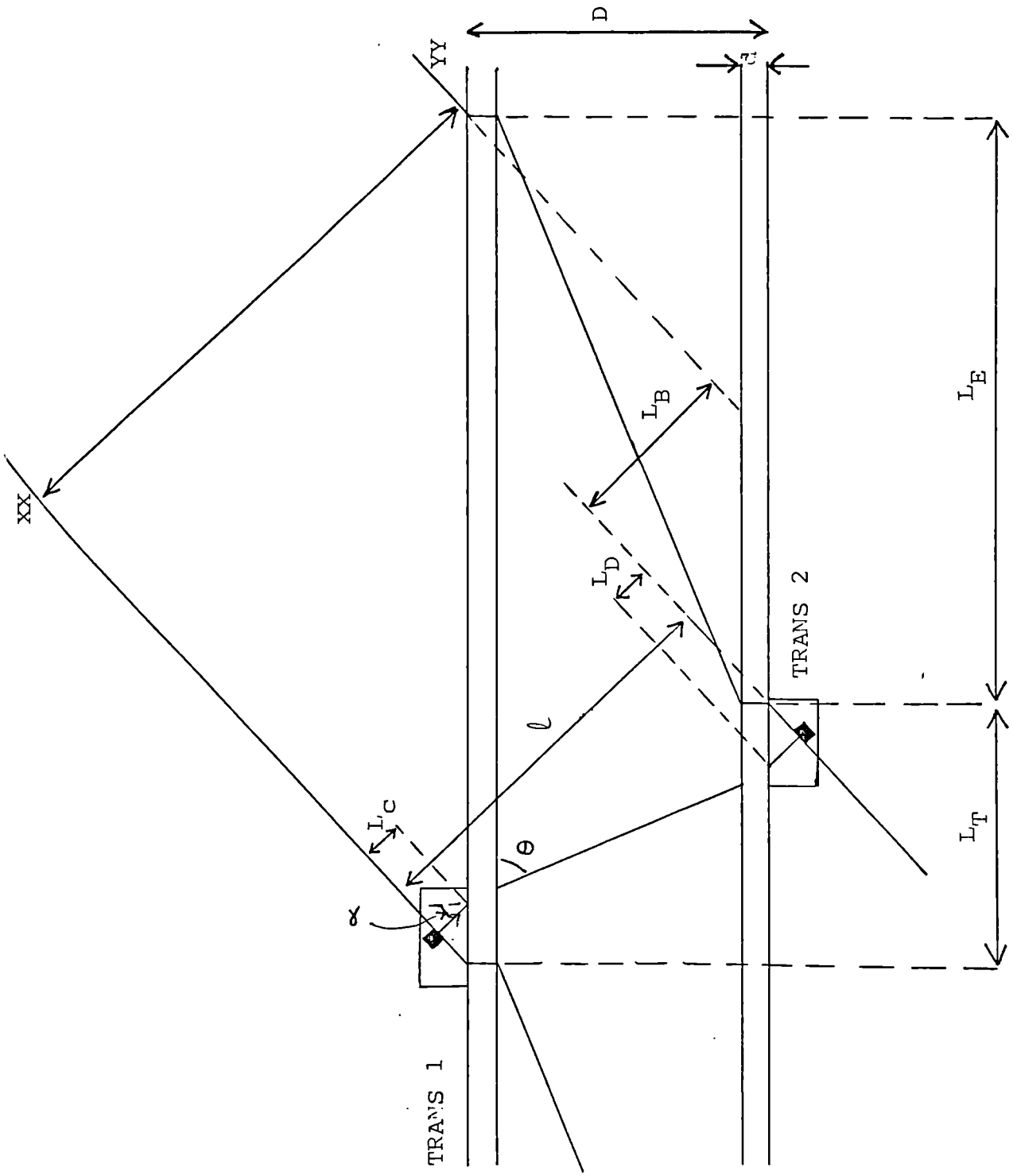

FIG 2.3
Geometry of the Clamp-on system

The overall distance travelled is equivalent to a distance of $L_T + L_E$ in the pipewall or a distance $L + L_B$ in the wedge material. Since the wedge material is under manufacturing control it makes sense to work on this distance.

From geometrical considerations the distance $L + L_B$ is found to be,

$$L+L_B = \left[\frac{(D-2d)\sqrt{1-\left(\frac{C}{C_p}\sin\alpha\right)^2}}{C/C_p} + L_T \sin\alpha\right] \qquad 2.45$$

and dividing $L + L_B$ by C_p yields the time for the wavefront to travel this distance. Hence

$$T_1 = \frac{L+L_B}{C_p} = \left[\frac{(D-2d)\sqrt{1-\left(\frac{C}{C_p}\sin\alpha\right)^2}}{C} + \frac{L_T \sin\alpha}{C_p}\right] \qquad 2.46$$

Now consider figure 2.4a and 2.4b.

In 2.4a it can be seen that the total time T through the electronics, cabling, transducers and pipe section is made up from T_1 + τ
If now the blocks are placed face to face, so that the projection of a centre line from the transducers continues in a straight line, the time T_2 is made up from T_p (the time in the perspex) and τ

$$\text{Since } T_p = \frac{L_C + L_D}{C_p} \qquad 2.47$$

subtracting eliminates the delays and the resulting equation is,

$$(T-T_2) = \left[\frac{(D-2d)\sqrt{1-\left(\frac{C}{C_p}\sin\alpha\right)^2}}{C} + \frac{L_T \sin\alpha}{C_p}\right] - \left[\frac{L_C+L_D}{C_p}\right] \qquad 2.48$$

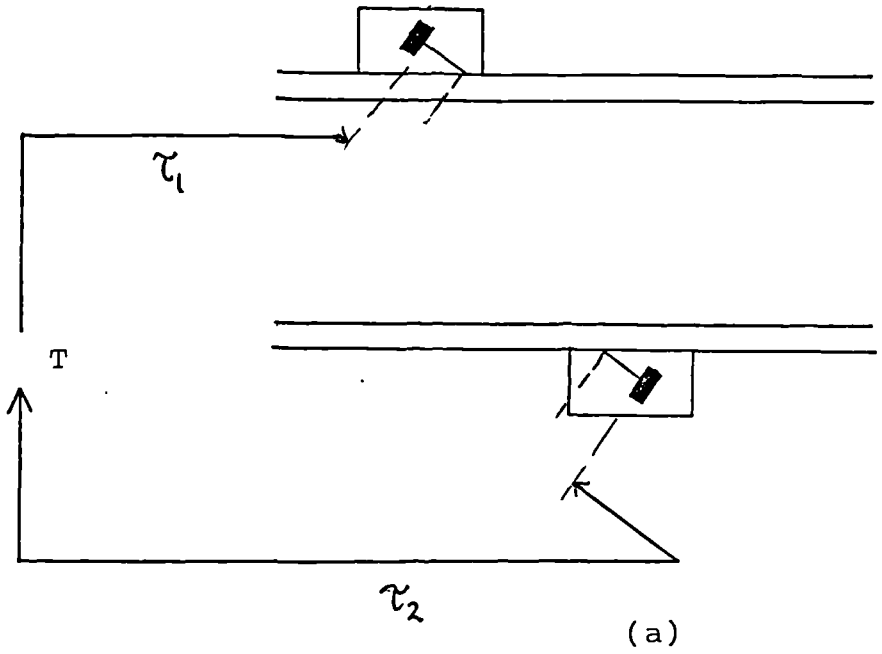

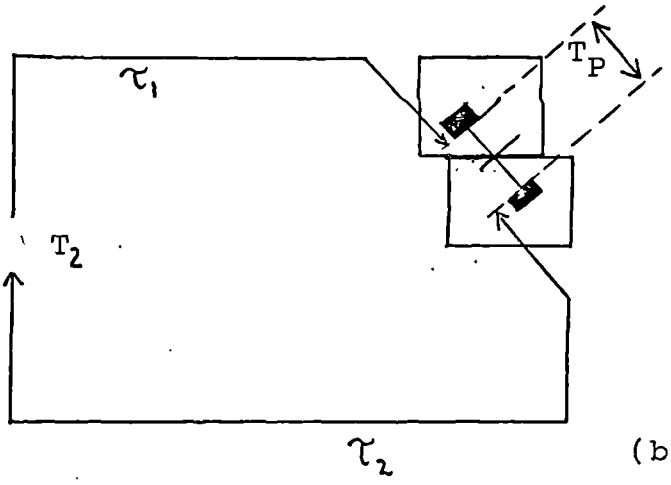

$$\tau = \tau_1 + \tau_2$$

FIG 2.4
Delays in the system

which when rearranged for C becomes

$$C = \frac{1}{\sqrt{\left\{\left[(T-T_2)-\frac{L_T}{C_p}\sin\alpha+(L_C+L_D)\right]\frac{1}{D-2d}\right\}^2+\frac{\sin^2\alpha}{C_p}}} \qquad 2.49$$

Thus C can be obtained from outside of the pipe. Inspection of 2.49 shows that C = f(T, T_2, L_T, C_p, L_C, L_D and D-2d).

Fortunately a lot of the variables are under control and assessing each one in turn one finds

(i) T — T would be of the order of the transit time in one direction, since this value is quite large T can be accurately measured.

(ii) T_2 — T_2 is also of significant size in a clamp-on flowmeter due to the wedge distance) and can be accurately measured, either on site or in a laboratory and the value stored. (Clearly the application and its temperature range needs to be assessed).

(iii) L_T — L_T is a distance and should be accurately measured to within a 1/2 mm.

(iv) Cp — Cp is under strict control and should not present a problem. If temperature monitoring is not engaged then the application and temperature range of the instrument will need further investigation.

(v) L_C,L_D — L_C, L_D are distances in the wedge and should be accurately known.

(vi) (D-2d) — (D-2d) cannot be accurately measured and the error is likely to be of the order of 1% in pipes of nominal bore 100 mm.

For a majority of the variables above it may be possible to calibrate the system and the only problem then would be the correct positioning of the blocks on the pipework. This would require a high quality mechanical jig.

The time T_2 is mainly made up of the time T_p (the time in the wedge), this is because τ will be very small, and as a first approximation to C the terms T_2 and $\frac{L_C + L_D}{C_p}$ could be ignored and removed from 2.49.

Since τ is very small the change in τ will likewise be small.

Now that a method has been proposed for measuring C and a discussion of the variables that are used in its determination has been undertaken, it would be useful to see how the value of C would change for changes in (D-2d) and Cp.

Differentiating 2.49 wrt Cp one finds

$$\frac{dC}{dC_p} = \frac{(D-2d)^2 \sin^2\alpha - \left[(T-T_2)C_p - L_T \sin\alpha + (L_C+L_D)\right]\left[L_T \sin\alpha - (L_C+L_D)\right]}{\sqrt{\left\{\left[(T-T_2) - \frac{L_T \sin\alpha}{C_p} + \left(\frac{L_C+L_D}{C_p}\right)\right]\frac{1}{D-2d}\right\}^2 + \frac{\sin^2\alpha}{C_p^2}\Bigg\}^3}\; C_p^3 (D-2d)^2} \qquad 2.50$$

similarly, differentiation of 2.49 wrt to (D-2d) yields

$$\frac{dC}{d(D-2d)} = \frac{\left[(T-T_2) - \left(\frac{L_T}{C_p}\sin\alpha\right) - \left(\frac{L_C+L_D}{C_p}\right)\right]^2}{\sqrt{\left\{\left[\left[(T-T_2) - \frac{L_T \sin\alpha}{C_p} + \left(\frac{L_C+L_D}{C_p}\right)\right]\frac{1}{D-2d}\right\}^2 + \frac{\sin^2\alpha}{C_p^2}\Bigg\}^3}\; (D-2d)^3} \qquad 2.51$$

solving for $\frac{dC}{C}$ one finds

$$\frac{dC}{C} = \frac{(D-2d)^2 \sin^2\alpha - \left[(T-T_2)C_p - L_T \sin\alpha + (L_C+L_D)\right]\left[L_T \sin\alpha - (L_C+L_D)\right]}{\left\{\left[(T-T_2) - \frac{L_T}{C_p}\sin\alpha + \frac{L_C+L_D}{C_p}\right]\frac{1}{D-2d}\right\}^2 C_p^2 (D-2d)^2} \cdot \frac{dC_p}{C_p}$$

$$+ \frac{\left[(T-T_2) - \frac{L_T}{C_p}\sin\alpha + \left(\frac{L_C+L_D}{C_p}\right)\right]^2}{(D-2d)^2\left\{\left\{\left[(T-T_2) - \frac{L_T \sin\alpha}{C_p} + \frac{L_C+L_D}{C_p}\right]\frac{1}{D-2d}\right\}^2 + \frac{\sin^2\alpha}{C_p^2}\right\}} \cdot \frac{d(D-2d)}{(D-2d)} \qquad 2.52$$

Using approximate values for the variables, as follows

$T-T_2$ = 86 x 10^{-6} seconds
D-2d = .1 m
L_T = .15 m
α = 62.5°
L_C+L_D = .07 m
C_p = 2700m/s

It can be shown that for a 1% error in (D-2d) and a 1% error in Cp (this corresponds to a temperature change of 13.5°C)

$$\frac{dC}{C} = .79\% \text{ (from a 1\% increase in (D-2d) - .077\% (from a 1\% increase in Cp)} \qquad 2.53$$

ie: a .71% error in C

Thus the biggest factor in our ability to measure C correctly is the inaccuracy in determining (D-2d),

If now we return to the prediction of flowrate Q and ask the question what is the effect on Q of an error in D-2d, taking into account that an error in D-2d causes an error in C, the expression that needs to be evaluated is,

$$d\varphi = \frac{\partial \varphi}{\partial (D-2d)} d(D-2d) + \frac{\partial \varphi}{\partial C} \cdot \frac{\partial C}{\partial (D-2d)} d(D-2d) \qquad 2.54$$

The first term of 2.54 causes a 1% error in Q and so we only require to review the second term. $\frac{\partial \varphi}{\partial C}$ and $\frac{\partial C}{\partial (D-2d)}$ are given by equations 2.27 and 2.51

and combining these and dividing by Q results in

$$\frac{d\varphi}{\varphi} = \frac{1}{c}\left[\frac{-\sin^2\alpha}{1-\left(\frac{c}{c_p}\sin\alpha\right)^2}\left(\frac{c}{c_p}\right)^2+1\right]\frac{\left[(T-T_2)-L_T\sin\alpha+\frac{L_c+L_D}{c_p}\right]^2}{\sqrt{\left\{\left[(T-T_2)-L_T\sin\alpha+\frac{L_c+L_D}{c_p}\right]\frac{1}{D-2d}\right\}^2+\frac{\sin^2\alpha}{c_p^2}\}^3}\,(D-2d)^2} \qquad 2.55$$

substituting previously given values results in a value

$$\frac{d\varphi}{\varphi} = 1\%$$

Therefore combining the errors it can be said that if (D–2d) is incorrectly measured then a double error occurs in the estimation of Q.

2.5.2 Compensation for velocity profile effects.

It was shown in section 2.4.2.1 that velocity profile effects cause the ultrasonic flowmeter to over estimate the flow. This effect can be compensated for iteratively by multiplying the estimated (uncorrected) velocity by K_{Re} where

$$V_m = K_{Re}\cdot\bar{V}$$

$$K_{Re} = \frac{1}{1{\cdot}12 - {\cdot}011\log_{10}Re} \quad (3\times10^4<Re<10^6) \qquad 2.56$$

and Re is as previously given.

The calculation of Re does require a knowledge of the constants C and η_0 but since $\frac{V_m}{\bar{V}}$ is a slowly varying function of Re it is not too important to obtain these values with any great accuracy. In fact it is reasonable to stop correction after the first iteration.

CHAPTER 3 ELECTRONIC CIRCUIT DESIGN AND TRANSDUCER SELECTION

3.1 Introduction

The prototype instrument was built along the guideline that the primary objective was to develop expertise from building a complete instrument. The initial design of the instrument stemmed from previous considerations that had laid the foundation such as significant digital content and a leading edge instrument with the capability of being microprocessor controlled. The starting block diagram was, therefore, as depicted in figure 3.1 where the instrument is sub-dividided into a control and firing module, a switch (to direct the firing and received pulses) a pair of receiving/processing modules and a timing system.

The timing system was felt to be the heart of the instrument and, as mentioned in Chapter 1, the timing system chosen was based on the vernier principle and was felt to fulfil the main requirements, which are very stringent (possible accuracy to within $.5 \times 10^{-9}$ seconds on a single shot basis and a fast response time).

Significant effort was put into the timing system and particularly, the detector part of the circuit, which had many guises before reducing to an almost trivial, but novel, circuit. The overall accuracy of the vernier system is in doubt since late into the experimental work it was discovered that the equipment used for testing had questionable accuracy.

However, an overall bound of around $\pm 2 \times 10^{-9}$ seconds was placed on the system but a more significant feature was its excellent repeatability. It was felt that the final answer, to the prediction of flowrate, would lie in the instruments ability to predict a true flowrate and the testing of the timing circuit was, therefore, to ensure correct operation and reasonable accuracy. This approach was adopted for all circuits.

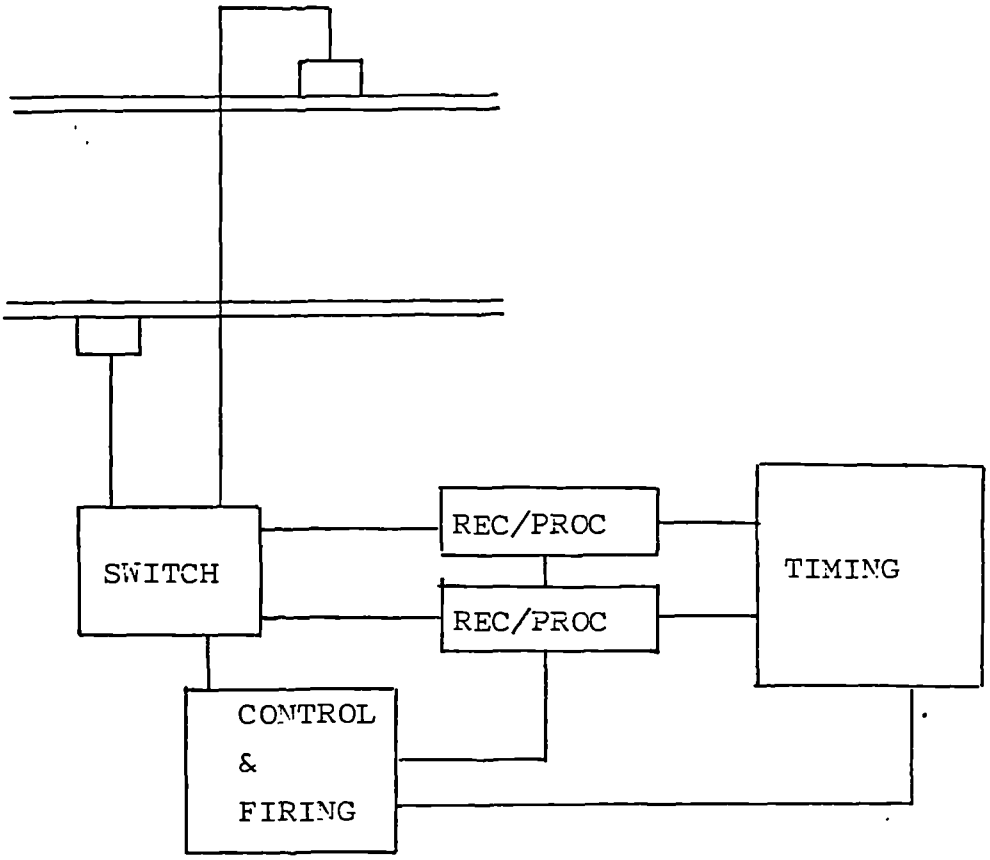

FIG 3.1
Outline of the proposed flowmeter

In the following section, section 3.5, the requirements for the receiving and processing of signals is discussed. Previous work had employed a wide bandwidth video amplifier (SN733) and this had led to noise problems. Although the noise was in part due to poor quality transducers, it was felt wise to exchange the wide bandwidth amplifier for a low bandwidth, low noise amplifier and a suitable device was found in the ZN459 low noise preamplifier.

Following the amplification of the signal there is a requirement to develop a time marker from the leading edge. This is often achieved by monitoring when the signal crosses a threshold and then using the following zero crossing, where the signal has maximum slope, to provide a time marker. A correction is employed to account for the difference in time between the leading edge and the actual point taken. In the case where two similar pulses are received there is no degradation in the signal timing if the two times measured are subtracted. However, under different conditions the signal changes form and it is prudent to ensure that the time marker obtained has its correct time relationship. Clearly necessary for this circuit is the requirement for good quality, fast comparators.

Associated with fast circuits is the possibility of feedback and oscillation because of the high gain employed ($>10^7$). To reduce this possibility it is necessary to take reasonable precautions and these are discussed along with other encountered problems, in section 3.2.
The entire circuitry has been designed to be microprocessor compatible whilst in its present form being hardwired. The reason for this approach was explained earlier. Because of the hardwired approach a control circuit was necessary but in a commercial model its functions would be carried out by the microprocessor. The control and firing circuitry delivers all the necessary synchronisation for the rest of the circuit and produces a firing pulse for the transducers. The circuit uses standard components to derive the synchronisation and a novel single chip device for the firing circuit. This part of the instrument is discussed in section 3.6.

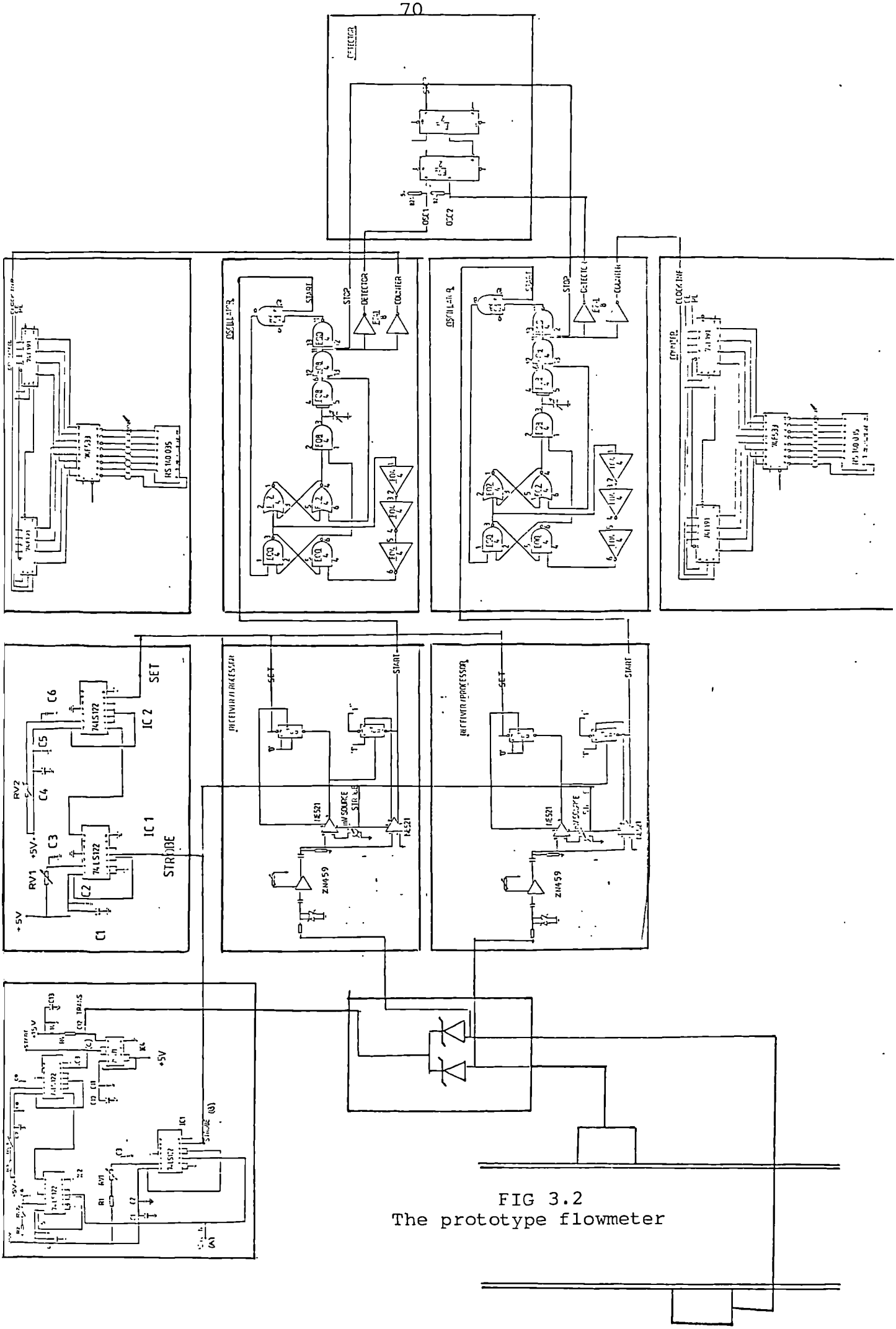

FIG 3.2
The prototype flowmeter

Also discussed in section 3.6 is the auxilliary circuits required for testing the overall instrument and those circuits are a time delay unit and a selector (which allows single or multiple samples through to the timing).

The instrument uses the principle of firing both transducers at once and waiting for the received signals. There is the need, therefore, for a switch mechanism to allow through the firing pulse to the transducers and to allow the received pulses through to the receiver/processors. Initially a multiplexer unit was designed using MOSPOWER FET's configured as switches with small on resistances (rds = .55 and configured as a "T" to reduce feed through). However, although successful, when a component count was taken and the commercial aspects considered the multiplexer was removed and an alternative solution sought. The simplest answer is a pair of high speed isolating diodes with exceptionally fast switching characteristics (of the order of picoseconds).

Because the first transducers used were of a poor quality and appeared very noisy (although this was later contributed to the excitation of unharmonic modes) it was necessary to purchase new transducers. After preliminary investigations it was decided to select a pair of lead Metaniobate transducers. The selection of the transducers is discussed in section 3.3.

When all the circuits are combined an overall instrument is produced and this is shown in figure 3.2.

3.2 Problems encountered in the design of the electronic circuits

During the construction of the flowmeter several noise problems arose and it was decided at an early stage to separate most of the circuits so that the problem of interaction between circuits was reduced.

However, there was a conflicting interest in that one of the prime objectives was to develop a commercially viable instrument. It was decided, therefore, to separate the circuits but not to take extra precautions such as separate supplies for analogue and digital circuitry etc.

External noise is noise radiated from other circuits and introduced by (i) capacitive coupling (electrostatic noise), (screening of circuits eliminates this effect) or (ii) induced by magnetic coupling, in which case screening with ferrous materials is required. Screening with a good ferrous conducting material (such as mu-metal) provides protection from both coupling mechanisms. For the instrument under construction good quality screening boxes were purchased; however, severe noise problems did not exist even with several screening panels removed.

Noise can be transported readily from one part of the circuit to another by the power lines and it was found necessary in the prototype instrument to decouple all power lines at regular intervals. This was achieved using a high quality RF disc capacitor and a tantalum capacitor in parallel.

All circuits were designed on a dense ground plane and all signal interconnections between units was through 50Ω coaxial cable. Although not necessary for short lines (say 200mm) the printed circuit boards were designed as microstrip transmission lines.

The characteristic impedance of the line is given by (ECL data book)

$$Z_o = \frac{87}{\sqrt{\epsilon_r + 1.41}} \ln\left(\frac{5.98h}{0.8w + t}\right)$$

where

h = thickness of board
t = foil thickness
w = track width

For the circuit boards constructed a choice of PCB was made with t = 35 micron, h = 1.6mm and ϵr = 4.9, then for w = 1.5 the value of Zo is 68Ω and for w = 2.5 the value of Zo = 51Ω.

The tracks were designed to be within this range. The importance of this value of impedance increases when transporting a signal from board to board where no discontinuity in the line is wanted.

It was found important to ensure good grounding of IC's since the sudden draw of current, in high speed devices, can cause noise spikes (135). It was also found important to separate tracks to reduce crosstalk and where it was important it was found useful to insert an earth track between signal lines.

The phenomenon of reflections from mismatched terminations must be considered when the rise time is less than the time delay of the line, ie: the time required for the signal to travel twice the line length. It can be seen that if the source has finished rising (or falling) to its new level then when a reflection is returned it will adjust the level accordingly. If on the other hand the line is small wrt rise time the reflection modifies the source voltage during transition and no sharp abruptions are encountered.

There are two common techniques employed for analysing the reflections from mismatched source and terminations and these are both graphical since the input and output characteristics are highly non-linear. These techniques are known as the Bergeron diagram and the lattice diagram.

Within individual modules the lines are short enough so that reflection problems are not encountered. Where the line lengths are long, the techniques above were used to ensure that the signal did not pose a problem.

The most critical signal was felt to be the signal from the oscillator to the detector and to ease this, a buffer was used to drive a line. The buffer has high sink capability and this meant that a pull up resistor could be used at the far end of the line to make (almost) a matched system. The use of a pull up resistor enables more rapid rise times and a higher noise margin.

Other general rules for PCB layout were followed such as separating the analogue and digital circuitry and running the signal lines well away from the power lines.

3.3 Selection of transducers

The transducers used in the early development stages were 1.25 MHz Lead Zirconate Titanate (PZT) transducers. They were eventually rejected for Lead Metaniobate transducers (to be discussed shortly) because of the strong coupling observed between modes.

A piezoelectric disc has two modes of vibration, a thickness mode and a radial mode. The resonant frequency for a thickness mode is given by:

$$f_t = \frac{N_{3t}}{th} \qquad 3.1$$

where N_{3t} is the frequency constant along the axis and th is the thickness. For PZT the value of N_{3t} is of the order of 2000KHz mm
For the radial mode of operation the equation becomes

$$f_r = \frac{N_p}{D} \qquad 3.2$$

where N_p is the frequency constant in the radial direction and D is the diameter of the disc. A value for N_p is about 2000-2900 KHz mm.

Therefore the ratio of $\frac{f_t}{f_r}$ is,

$$\frac{f_t}{f_r} = \frac{N_{3t}}{th} \cdot \frac{D}{N_p} = \frac{N_{3t}}{N_p} \cdot \frac{D}{t} \qquad 3.3$$

and for $\frac{N_{3t}}{N_p} = .9$ and $\frac{D}{t} = 10$ (for a 20mm dia 2mm thick disc)

the radial mode frequency is seen to be at 110KHz, whilst the thickness mode frequency is at 1MHz.

The radial mode frequency was observed at around 110KHz and proved very troublesome. This mode is seen very clearly on a plot of the modulus of impedance versus frequency in figures 3.3, 3.4. This plot shows that more resonances are likely but that the radial mode at 110KHz would appear to be significant. The plots show resonances at 110KHz, 260KHz, 900KHz and 8.2MHz for probe 3 and similar resonances for probe 2, but with an added resonance at 750KHz.

Because the excitation is a pulse the various resonances will all be excited to some extent and the resulting motion of the ceramic face will be a complicated affair. More discussion on these anharmonic resonances can be found in texts (104).

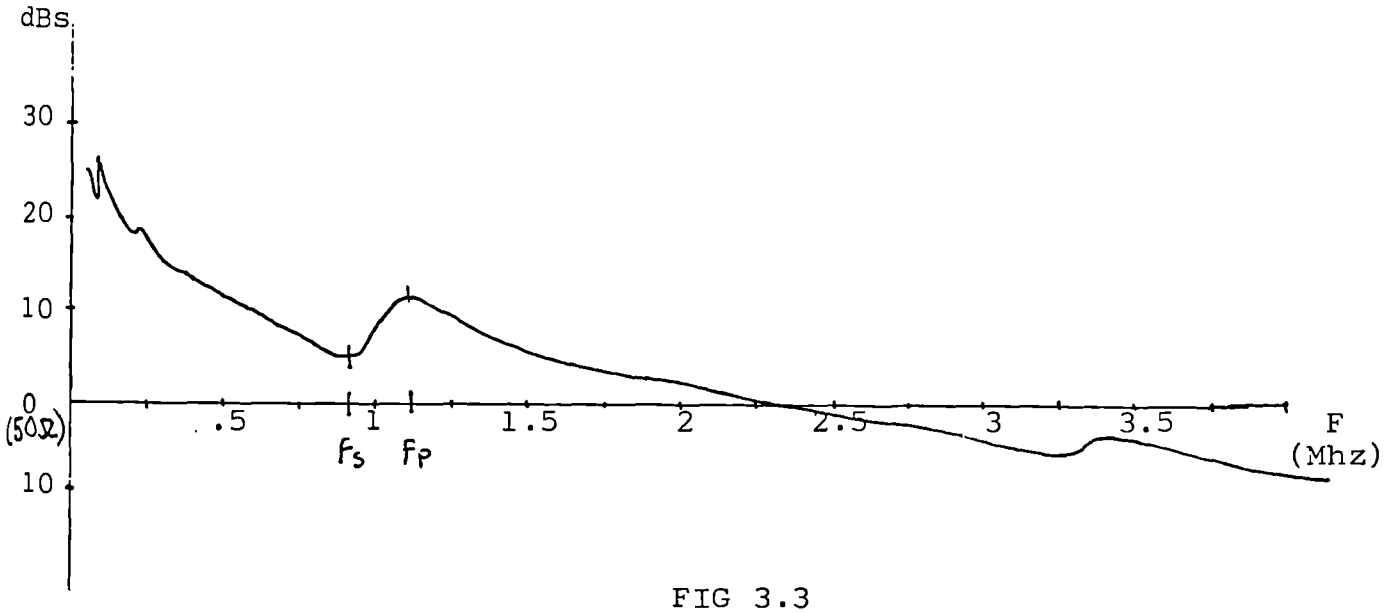

FIG 3.3
|Z| v. frequency (probe 2)

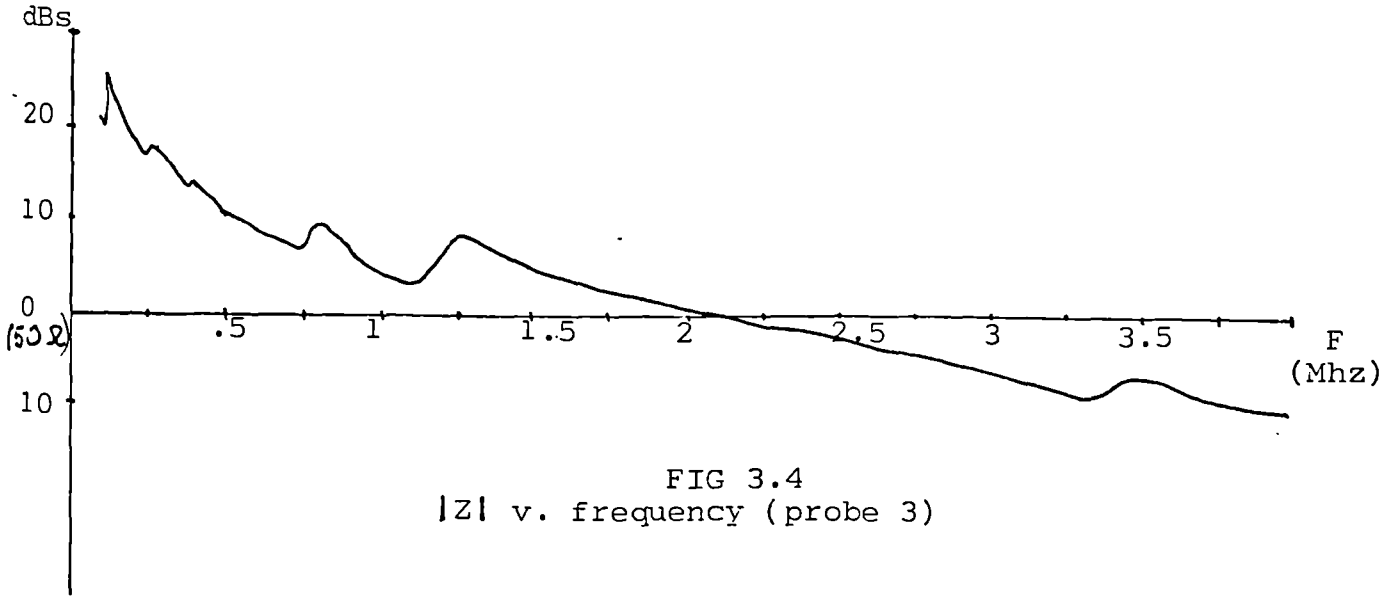

FIG 3.4
|Z| v. frequency (probe 3)

The impedance elements of a transducer around resonance can be approximated by the equivalent circuit of figure 3.5. In this circuit there is a static capacitance C_o, which is the normal capacitance of a pair of plates separated by a dielectric medium ($C = \frac{\epsilon_o \epsilon_R a}{\ell}$).

In parallel with this capacitance is a series arm with elements L_1, C_1 amd R. This arm is known as the motional arm and the elements are equivalent components for the mass (L_1), spring (C_1) and damper (R) of the transducer.

The resonance marked as f_s on probe 3 is known as the series resonance frequency and is the frequency at which L_1 and C_1 cancel and leave R as the impedance (which is real). R is the sum of the mechanical losses in the ceramic plus the acoustic load.

Between f_s and f_p the motional arm becomes inductive until at f_p it tunes with C_o to form another resonant circuit (this time a parallel resonant circuit). The impedance looking into the parallel circuit is very high. After f_p the circuit looks like a capacitor again.

The capacitor C_o partially shorts the input current and the output (acoustic signal) is reduced. An improvement in output can be obtained by tuning out C_o with an inductor (in series or parallel) so that at series resonance the motional arm is resonant and the parallel arm, C_o and tuning inductor, is also resonant but presenting high impedance to the source. For a parallel inductor the value of L is given by:

$$L = \frac{1}{2\pi f_s C_o} \qquad 3.4$$

and for the case of probes 2 and 3 a 22μH inductor was found experimentally to increase the received signal. Even with this improvement the noise was still a significant problem and coupled with the radial mode vibration it was decided to obtain new transducers.

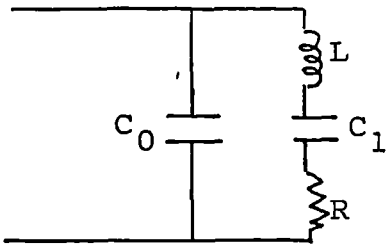

FIG 3.5
Equivalent circuit around resonance

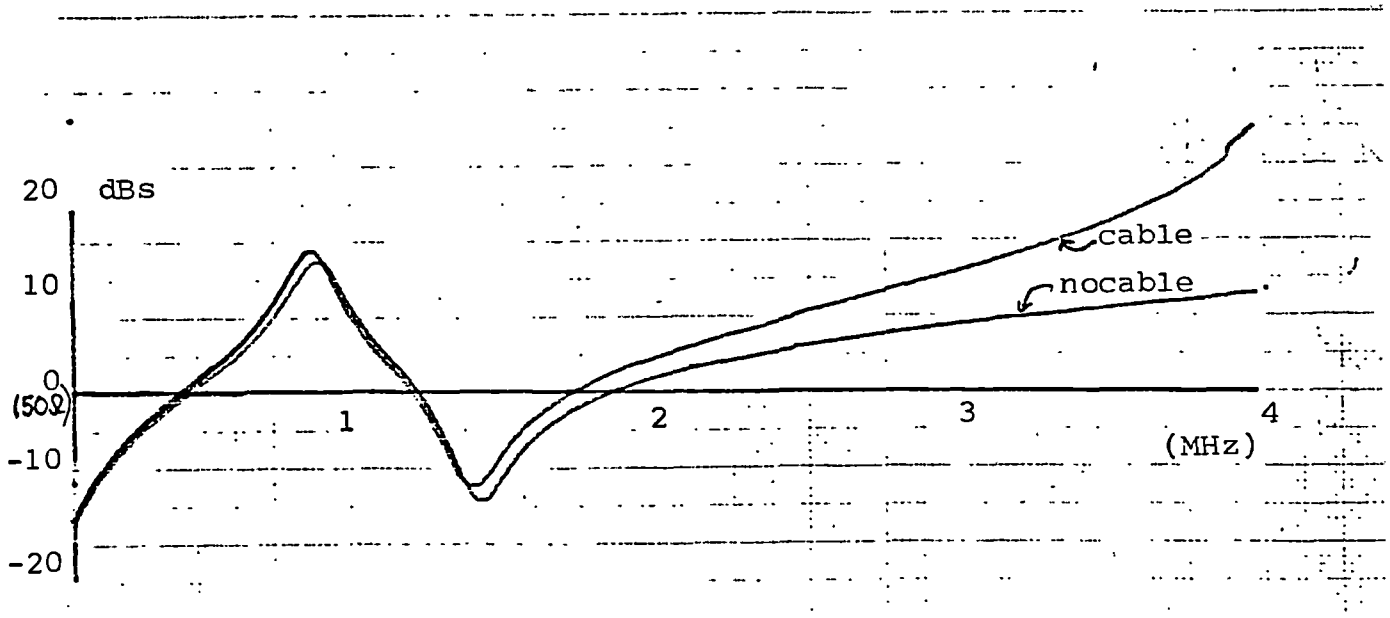

FIG 3.7
Cable capacitance effects (probe 1,unloaded,2 Mtr cable)

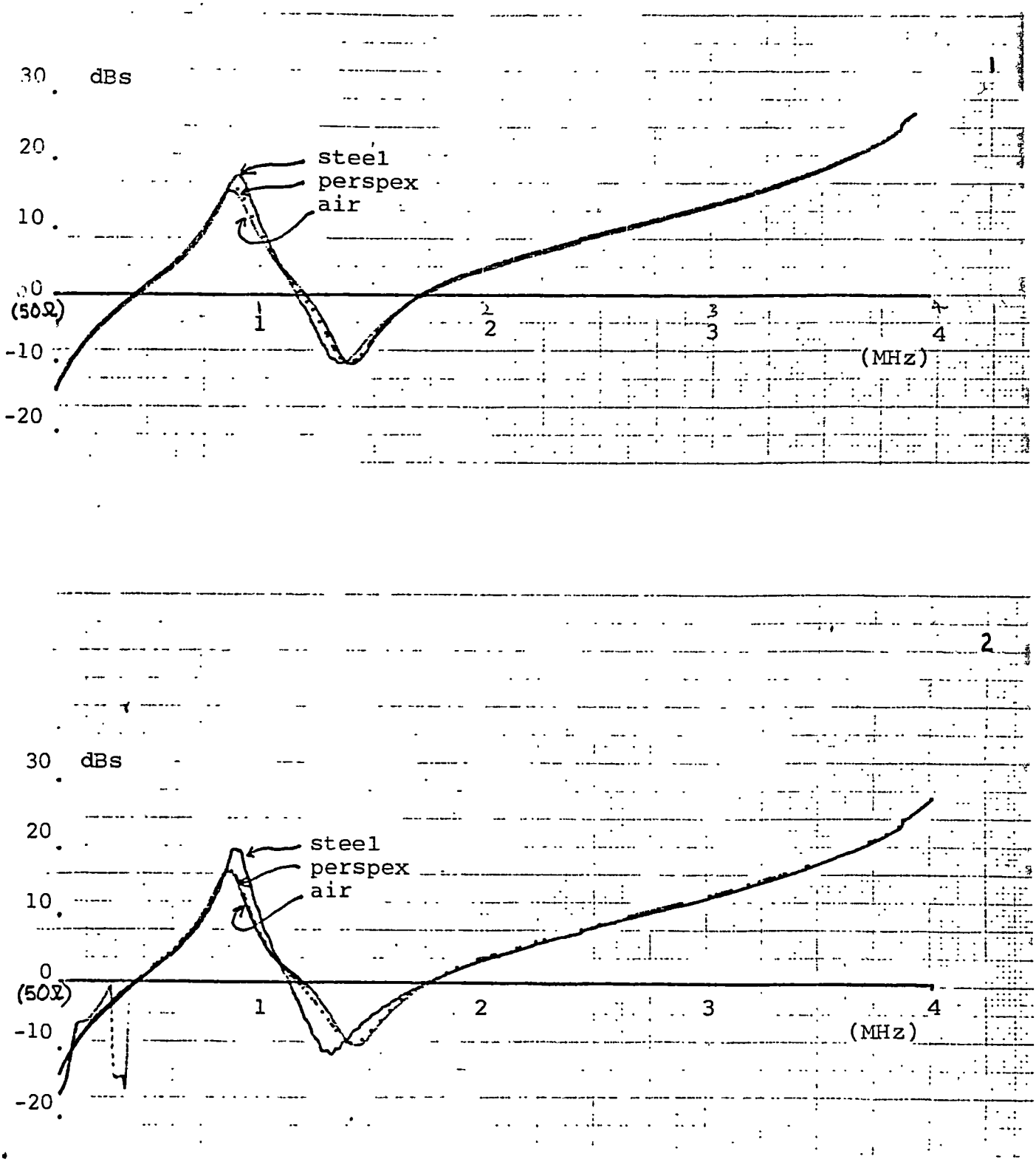

FIG 3.6
|Z| v. frequency (Lead Metaniobate transducers)

The main specification for the new transducers was that the interference between modes should be well separated.

Krautkramer (125) analyses the most common materials for use in transducers for NDT work.

In his analysis, Krautkramer concludes by suggesting Lead Metaniobate as the best material for pulse echo work.

This analysis coincides with almost identical requirements for flowmeter work. The main requirements being:

(i) lower level of resonance from the radial mode
(ii) good piezoelectric coefficients as receiver/transmitter
(iii) separated (in frequency) radial and thickness modes
(iv) low acoustic impedance, to match fluids (Z= 1.5 Pa s/m)

For requirement (i) the coefficient of coupling Kp for the radial mode is low in Lead Metaniobate at .07 and the piezoelectric constants (ii) are as a transmitter d = 85×10^{-12} m/v whilst as a receiver g = 32×10^{-3} V m/N.

To fulfil the requirement of (iii) means that the ratio of must be larger than for PZT. This can be seen to be so by the series resonant frequencies of the plates at 1mm, which for Lead Metaniobate is 1.65MHz and for PZT is 2MHz. This also is a disadvantage in that the (thinner) plates are now more fragile and for higher frequencies exceptional care in construction must be undertaken.

The acoustic impedance of Lead Metaniobate is Z = 20 Pa s/m x 10^6.

A further advantage of Lead Metaniobate is its Curie temperature which is 400°C and its internal damping coefficient which is 1.3. This high damping coefficient means that physically smaller transducers can be made (ie: less backing is required).

It was decided to purchase a pair of commercially available Lead Metaniobate transducers. The transducers are already tuned by a series and parallel inductor of value approximately 15μH.

The transducers were tested and found to work extremely well compared to the previous transducers. A vector impedance plot is shown in figure 3.6 where the characteristics are shown under different loading conditions.

Both transducers are seen to match to each other and at the system frequency observed (1MHz) the impedance is seen to be 10 d B's up on 50 Ω. This means that Z = 158Ω. It was decided not to attempt to match the source to the transducer at this stage.

A particular problem with piezoelectric devices is the cable capacitance C_c between the transducer and receiver. The effect of the cable capacitance can also be seen on a vector impedance plot and is shown in figure 3.7, where it can be seen to 'pull' the curve. Consider the circuit of figure 3.8, where the transducer is effectively a current source (related to the pressure on the face) parallel with the static capacitance (it is assumed that the static capacitance does not change with deformation).
Then

$$\frac{V_L}{V_S} = \frac{C_S}{C_C+C_S} \qquad 3.5$$

As C_c gets larger then the output voltage decreases. A solution, in general, is to use a charge amplifier and a simple circuit is shown in figure 3.9. It can be seen that the C_c of the cable is effectively short circuited by the virtual earth of the amplifier and thus

$$\frac{V_L}{V_S} = -\frac{C_S}{C_f} \qquad 3.6$$

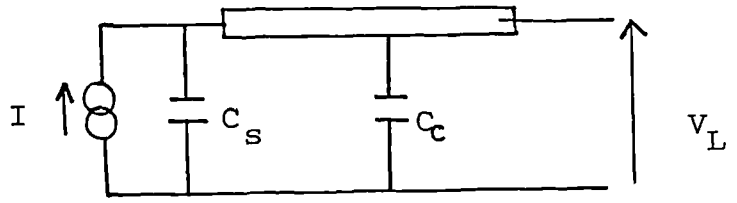

FIG 3.8
Equivalent circuit of a transducer and cable

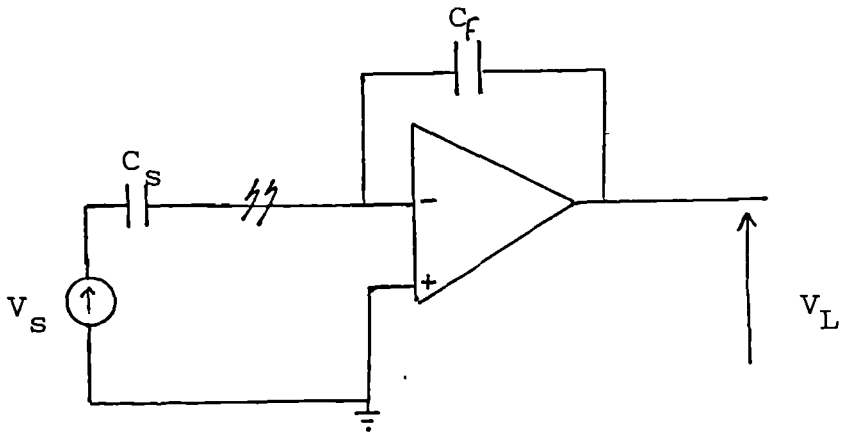

FIG 3.9
The use of a charge amplifier

and is independent of C_c and hence the length of cable. In the case of lead Metaniobate ceramics, the frequency constant has been given as 1.65MHz and thus a frequency of 1.25MHz would require a thickness of .76mm. From $C = \frac{\epsilon_o \epsilon_r a}{e}$ the capacitance is calculated to be $\approx$1740pf. The cable used in the experiments is 2 metres long and its capacitance is 100pf/metre thus 200pf in total.

From 3.5 above the reduced voltage is seen to be $\frac{1740}{1940} \approx .9$ and this figure is considered to be acceptable. It was decided therefore, to develop the flowmeter with a normal voltage amplifier and not, in this instance, to use a charge amplifier. This argument can easily be extended to the case where the charges are varying and a current to voltage convertor is required. In this case the feedback element is a resistor.

3.4 The vernier timing system

It will be recalled that the leading edge system was chosen as part of the specification for the prototype flowmeter. It was also decided to produce a system in as much digital form as possible. A review, therefore, of timing systems was undertaken, and since leading edge implies high speed logic a suitable system that appeared to be fast and digital was that of a vernier timing system.

The vernier timing system, which is at the heart of the electronics is described by reference to figure 3.10. The system consists of two high frequency oscillators two high frequency counters and a detector. The oscillator periods are separated by a small time difference δt. Thus the frequencies of the oscillators will be different and for convenience will be classed as one fast oscillator and one slow oscillator.

The input to the oscillators will be processed logic pulses and will be separated in time, by Δt the time interval that is required to be measured.

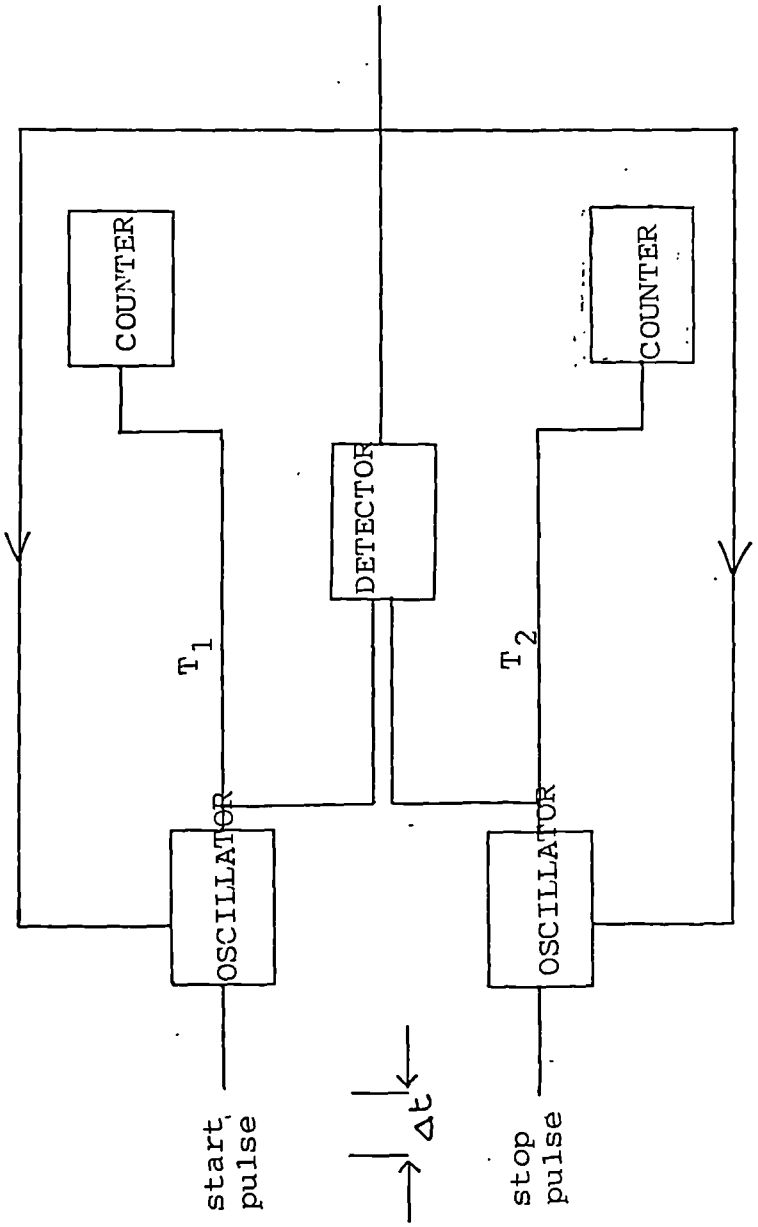

FIG 3.10
The Vernier Timing system

The start pulse is applied to one oscillator which starts oscillating immediately. The stop pulse is applied to the other oscillator, which also starts oscillating immediately. A counter on each oscillator counts the pulses until there is coincidence between the two output pulse trains, and this is detected by the detector. The detector signals the oscillators to stop. The count in the counters is then related to the interval Δt and for this equation there are two possibilities. First, that the slow oscillator starts first and the fast oscillator second, or, secondly the opposite sequence of starting.

Then for the first case (see figure 3.11)

$$N_1 T_1 = N_2 T_2 + \Delta t \qquad 3.7$$

and thus

$$\Delta t = N_1 T_1 - N_2 T_2 \qquad 3.8a$$

or

$$\Delta t = (N_1 - N_2) T_2 + N_1 \delta t \qquad 3.8b$$

where $T_1 = T_2 + \delta t$ 3.9

If the time interval, Δt, is less than one period then $N_1 = N_2$ (since the fast oscillator has caught up on the slow oscillator) see figure 3.12, and,

$$\Delta t = N_1 \delta t \qquad 3.10$$

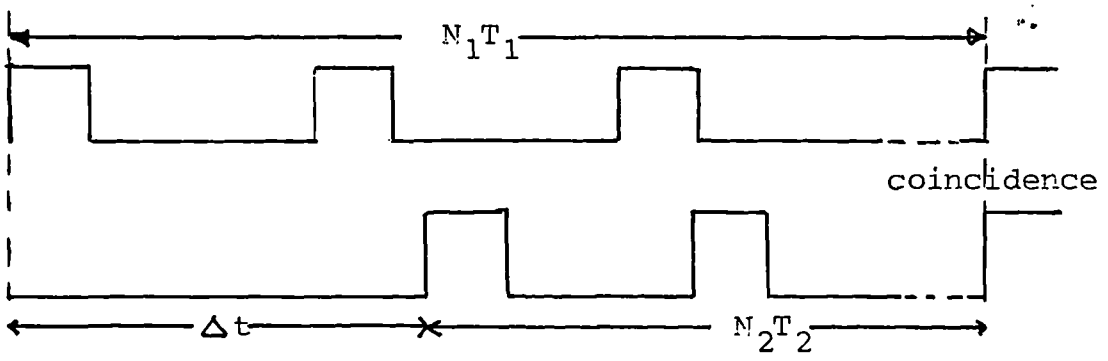

FIG 3.11
Timing diagram of oscillator circuit (slow oscillator starts first)

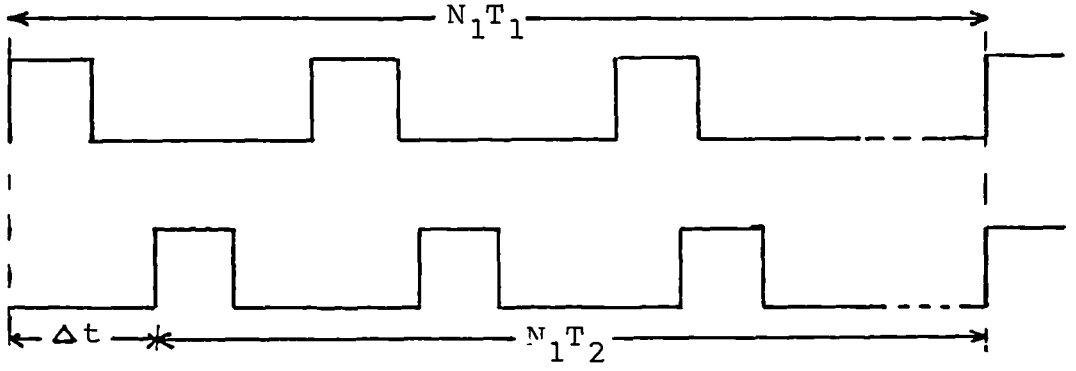

FIG 3.12
Timing diagram of oscillator circuit within one cycle

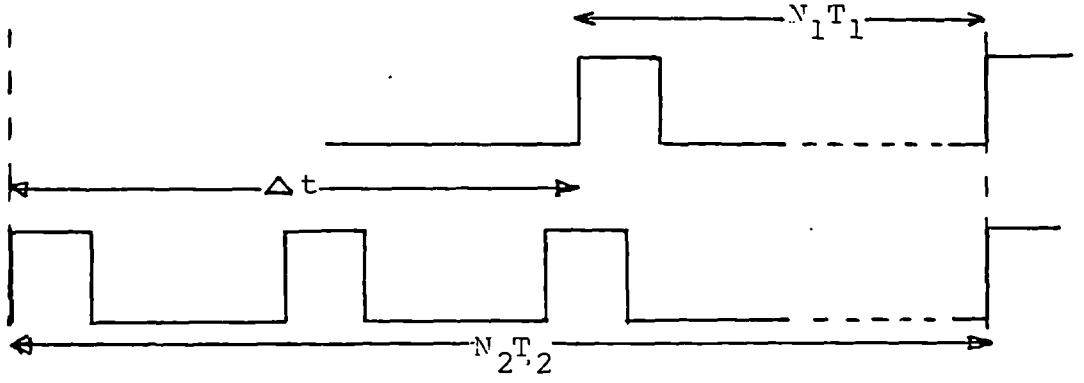

FIG 3.13
Timing diagram of oscillator circuit (fast oscillator starts first)

For the opposite case where the fast oscillator starts first, (see figure 3.13),

$$N_2 T_2 = N_1 T_1 + \Delta t \qquad 3.11$$

$$\therefore \quad \Delta t = N_2 T_2 - N_1 T_1 \qquad 3.12$$

and since $T_1 = T_2 + \delta t$

$$\Delta t = (N_2 - N_1) T_2 - N_1 \delta t \qquad 3.13$$

Combining equations 3.8b and 3.13 results in a single equation

$$\Delta t = |N_2 - N_1| T_2 \pm N_1 \delta t \qquad 3.14$$

where

+ is for oscillator 1 starting first ($N_1 \geq N_2$)

and

- is for oscillator 2 starting first ($N_2 > N_1$)

A significant advantage of the vernier system is that only full developed pulses are counted so that there is no $\pm$ 1 count error as in other counting systems.

3.4.1 Errors in the vernier timing system

3.4.1.1 Errors in the oscillator circuits

Consider equation 3.14,

$$\Delta t = |N_2 - N_1| T_2 \pm N_1 \delta t \qquad 3.14$$

or

$$\Delta t = |N_2 - N_1| T_2 \pm N_1 (T_1 - T_2) \qquad 3.14a$$

and hence

$$\Delta t = f(T_1, T_2)$$

Now

$$d\Delta t = \frac{\partial f(T_1, T_2)}{\partial T_1} dT_1 + \frac{\partial f(T_1, T_2)}{\partial T_2} dT_2 \qquad 3.15$$

and thus

$$d\Delta t = |N_2 - N_1| dT_2 \pm N_1 (dT_1 - dT_2) \qquad 3.16$$

and

$$\frac{d\Delta t}{\Delta t} = \frac{|N_2-N_1|\,dT_2 \pm N_1(dT_1-dT_2)}{|N_2-N_1|\,T_2 \pm N_1(T_1-T_2)} \qquad 3.17$$

$$= \frac{|N_2-N_1|}{|N_2-N_1| \pm \frac{N_1(T_1-T_2)}{T_2}} \cdot \frac{dT_2}{T_2} \pm \frac{N_1}{|N_2-N_1|\frac{T_2}{T_1-T_2} \pm N_1} \cdot \frac{(dT_1-dT_2)}{(T_1-T_2)} \qquad 3.18$$

This equation can be reduced by setting

$$\frac{T_2}{T_1-T_2} = N \qquad 3.19$$

and

$$\frac{T_1-T_2}{T_2} = \frac{1}{N} \qquad 3.20$$

substituting 3.19 and 3.20 into 3.18, results in

$$\frac{d\Delta t}{\Delta t} = \frac{|N_2-N_1|}{|N_2-N_1| \pm \frac{N_1}{N}} \cdot \frac{dT_2}{T_2} \pm \frac{N_1/N}{|N_2-N_1| \pm \frac{N_1}{N}} \cdot \frac{(dT_1-dT_2)}{T_1-T_2} \qquad 3.21$$

Thus the fractional error in Δt is made up of two parts, and these parts are due to the drift in T_2 and the drift in $(T_1 - T_2)$.

For $|N_2 - N_1| = 0$ the error is simply made up of the fractional error in δt, ie $\frac{dT_1 - dT_2}{T_1-T_2}$. As $|N_2-N_1|$ increases the error in (T_1-T_2)

becomes less important since it is reduced by the factor $\frac{N_1/N}{|N_2-N_1| \pm N_1/N}$ the error then in Δt is made up (at large (N_2-N_1) of the drift in T_2, ie $\frac{dT_2}{T_2}$ and the absolute error is given by $d\Delta t = \Delta t \frac{dT_2}{T_2}$, and is thus proportional to the time interval being measured and is a standard error associated with time interval measurement.

Clearly, the importance of highly stable oscillators becomes significant.

It is felt that the differential term $\frac{dT_1-dT_2}{T_1-T_2}$ can be made relatively small by building as nearly identically as possible the oscillators and subjecting them to the same environment. Ideally this would be on a single chip, and thus any drift is likely to affect both oscillators similarly.

3.4.1.2 Errors in the detector

Consider now the detector part of the circuit. If the detector were ideal and had infinite resolution, detection would occur only when the two pulses overlapped. Thus if the system happened to fall into a cyclical pattern, detection would never occur, (this would be if dt was irrational - not possible in a practical system due to jitter). However, it is possible for the system to run for some time before the pulses are close enough to be considered coincident. For repetitive signals, where it is hoped to average, this may not be convenient and therefore it may be better to design for a first pass system such that the detector gives a signal the first time the pulses pass over each other.

In the first pass case consider the detector resolution to be d_R, ie: the detector can only detect when the pulses are d_R apart, then if the difference in period is dt the total system resolution will be R, where

$$R = \delta t + d_R \qquad 3.22$$

It can be seen therefore that the limit to the system resolution is the detector resolution and there is little point in making $\delta t < d_R$.

3.4.2 Design of the oscillator circuits

The design of the oscillator circuits require that they have,

(i) instant start with constant phase and amplitude,
(ii) negligible frequency drift with respect to time or temperature.

The first condition means that high Q tuned circuits or crystal controlled circuits cannot be used since the signal requires time to build up.

A relatively simple circuit that proved successful had been built by Barton and King (83), but this used what is now obsolete logic, MECL II.

It was still possible, however, to obtain data on MECL II from the master references kept by the manufacturer and a similar speed (propagation and transition times) logic was found in the FAST TTL family. FAST is an acronym for Fairchild Advanced Schottky logic.

The range of time intervals that are of interest in flow metering are from approximately 25×10^{-9} seconds (1/2m/s @ 30° in a 100mm pipe) to about 500×10^{-9} seconds (10m/s @ 30° in 100mm pipe). The resolution of a single shot measurement is hoped to be, ultimately, $.25 \times 10^{-9}$ seconds and this would give approximately .5% accuracy at 1m/s for the above conditions. With averaging this bound should be improved considerably.

The difference in frequency of the oscillators is usually set to be of the order of .5%-2%. If a lower value is attempted screening and guarding must be employed to save the oscillators from frequency locking. A figure of 1% was thus chosen, then, since

$$\delta t = .25 \times 10^{-9} \text{ seconds} \qquad 3.23$$

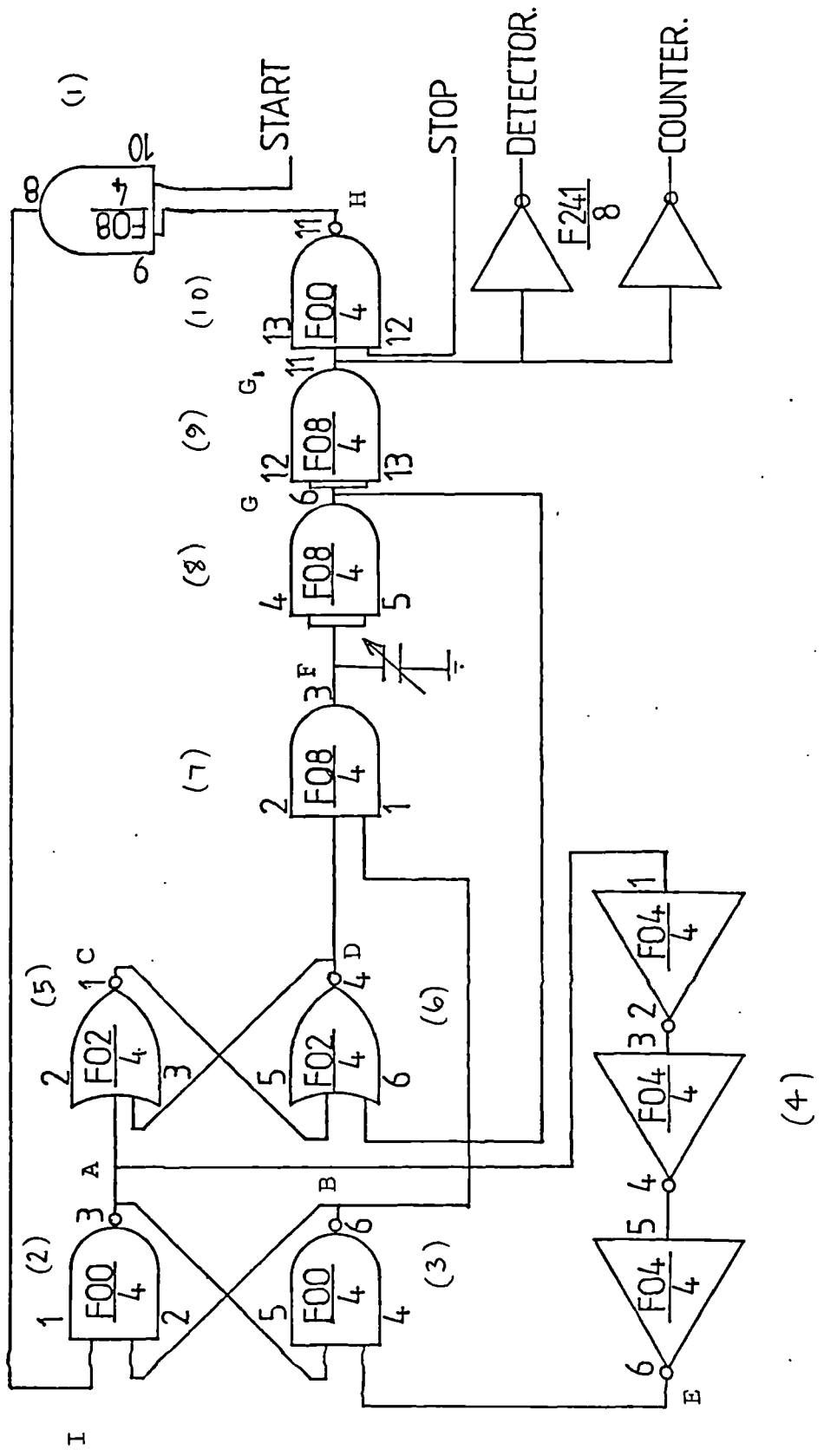

FIG 3.14
The oscillator circuit design

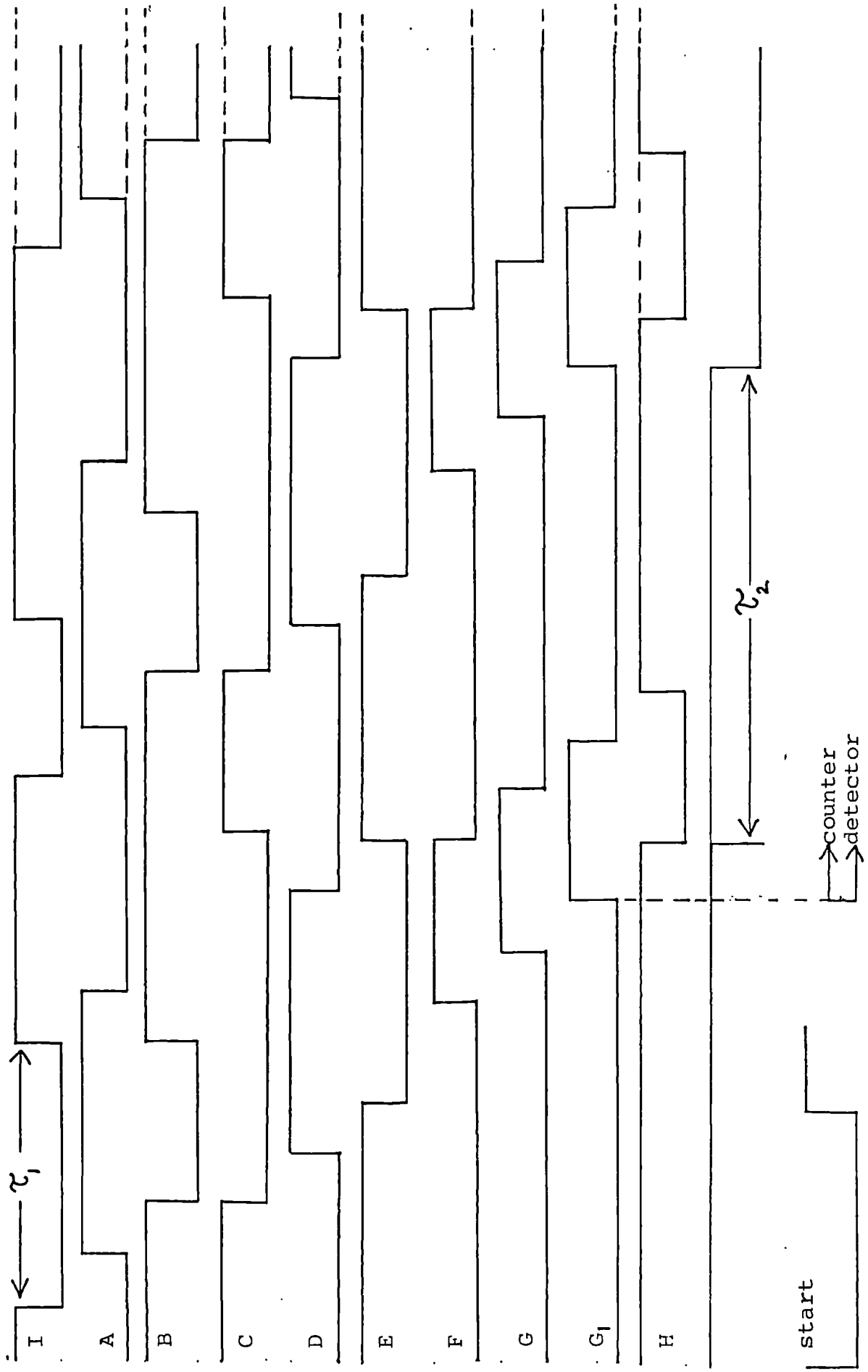

FIG 3.15
Timing diagram of the oscillator circuits

means

$$\frac{f_1 - f_2}{f_1 f_2} = .25 \times 10^{-9} \qquad 3.24$$

and because $f_2 = .99 f_1$ (1%)

then

$$f_1 = 40.4 \text{ MHz}$$

and

$$f_2 = 39.99 \text{ MHz}$$

It was decided to construct an oscillator circuit using FAST elements.

The oscillator would be designed to have a period of approximately 25×10^{-9} seconds and have controllable mark:space ratio and frequency. The circuit that is presently used in the flowmeter is shown in figure 3.14 and the timing diagram based upon typical propagation delays is given in figure 3.15.

A prototype circuit was built which consisted of both oscillators on the same p.c.b. This circuit was found to frequency lock (at about $f_1 = .99 f_2$). It was decided therefore to build both oscillators in separate screened boxes. This was the only precaution taken and both oscillators are powered from the same supply unit. This was felt to be more in line with the project definition, ie: that of constructing a prototype unit with commercial prospects, since it was decided that separate power supplies would not be cost effective.

The circuit consists of a NAND latch, a NOR LATCH and AND,NAND and Invertor gates. The circuit operation is best described by reference to figure 3.14.

The off state of the oscillator is shown on figure 3.14 and 3.15. In the off state a stop signal (at level 0) is present on NAND 10 and to enable the oscillator to function is required to go high. The oscillator now requires a negative going pulse on the start AND (1). The start pulse passes through the AND gate and sets the NAND latch (signal I). The NAND latch going high causes three actions to start simultaneously. Firstly, NAND 3 resets (B goes low). Secondly the signal (A) causes the NOR latch (gates 5 and 6) to reset (ie: C goes to a low level, D goes to a high level). Thirdly the signal (A) is inverted by the invertors to a low level signal and this resets the NAND latch (A goes low after B has gone high).

With B and D signals at a high level the AND gate (7) goes high and so similarly does AND gate 8. The result of AND gate 8 going high is that the feedback signal sets the NOR latch (C high, D low) and thus F and G go low. The pulse meanwhile, has propagated through AND 9 and is shared between two buffers (for the counter and the detector) and the NAND (10) provided the stop signal is still high. The operation is now repeated until a stop pulse (stop going low) is sent. The circuit then settles to the off state.

Frequency control of the circuit is made in two ways. Coarsely by the inclusion of another gate and finely by increasing the output capacitance of one gate. The above effects add one propagation delay to the period, for the coarse adjustment, and by experiment 1 nS per 15 pf of capacitance for fine adjustment. It was found that during construction sufficient control of the frequency was gained by adding capacitance on the gate.

The mark space ratio is controlled by moving the feedback link from G to G1 or by controlling the reset time of the NAND latch.

The timing diagram shown in figure 3.15 was based upon a typical propagation delay per gate of 2.9 nanoseconds and provided all gates exhibited a delay close to this value then the timing diagram would be accurate. However, in digital design, it is good practice to design for worst case contingencies and to thus carry out timing verification.

Timing verification essentially means carrying through a signal (reference) and considering the minimum and maximum delays through the system. Thus early and late times of arrival of pulses can be produced. If, then, in the process of timing verification signals do not appear in their correct time frame, race and/or hazard conditions may be specified and these need to be followed through to define the effect.

The oscillator, so designed, under worst case considerations does possess possible race situations, but the conditions necessary to produce a race situation, were felt to be unlikely for the prototype instrument. It was decided, therefore, to build six oscillators and check the frequency and mark/space ratio. All six oscillators produced a frequency and mark:space ratio within ±5% of the mean value (all components were randomly selected). Thus the typical values would appear to be typical and it was decided to note this point and pursue the main objective, that of a prototype instrument.

The oscillator requires a negative going step pulse which for nominally equal period spacing should be less than τ_1, in width. If the pulse is longer than τ_1, in width the output pulses are delayed and since this delay is propagated through the system a timing offset can occur. It will be shown later that the start pulse meets the criterion required for clean starting.

The stop pulse can be switched on at anytime to enable the oscillators, but a difficulty can exist in the stopping phase.

Consider the output pulse G1 which is used for detection purposes and to restart (via the NAND gate) another complete cycle of the oscillator. This pulse (G1) is NANDED with the stop signal to produce signal H. Therefore, provided the stop signal arrives after one propagation delay and before the return of G1 (this interval is marked as τ_2 on the timing diagram) then one extra pulse only will be counted and the oscillator will settle to the off condition. It will be necessary to subtract one count from the counters, therefore, before converting the count to a time interval.

3.4.3 Design of the counters

The mark:space ratio of the counter pulse (see figure 3.15 the timing diagram) is approximately equal to 3:7 and if the oscillator period is made approximately 25 nanoseconds this means a pulse width of about 7.5 nS. The counter must therefore be able to accept narrow pulse widths of this order. A suitable chip to use is a 74F191 synchronous 4 bit up/down binary counter chip. This chip requires a minimum clock pulse width of 5.5 nanoseconds.

The design of the counter is shown in figure 3.16. The parallel load line ($\overline{PL}$) which overides all other lines is used to load zero into the counters and thus to effectively reset the counters.

The counter has been designed to be bus orientated and the two 4 bit counters are connected via the ripple count ($\overline{RC}$) and clock pulse (CP) to form an 8 bit counter which is then connected to the bus tri-state octal latch 74F533. The output of this chip would then feed the data bus of a microprocessor system.

However, in the present mode of operation the system is hard wired controlled and this feature of microprocessor control is not used. Instead the system output is displayed on a series of LED's. Because of this mode of operation the timing requirements do not present a problem. However, the timing has been verified to ensure correct operation.

The principle of operation is thus as follows:- a low signal is sent to the chip enable $\overline{CE}$ that meets the normal requirements for set up and hold conditions. A low signal is also sent to the latch enable ($\overline{LE}$) of the tri-state buffer. This signal ($\overline{LE}$) means that the latch becomes transparent and when the $\overline{LE}$ goes high, data meeting the timing requirements is latched into the buffer.

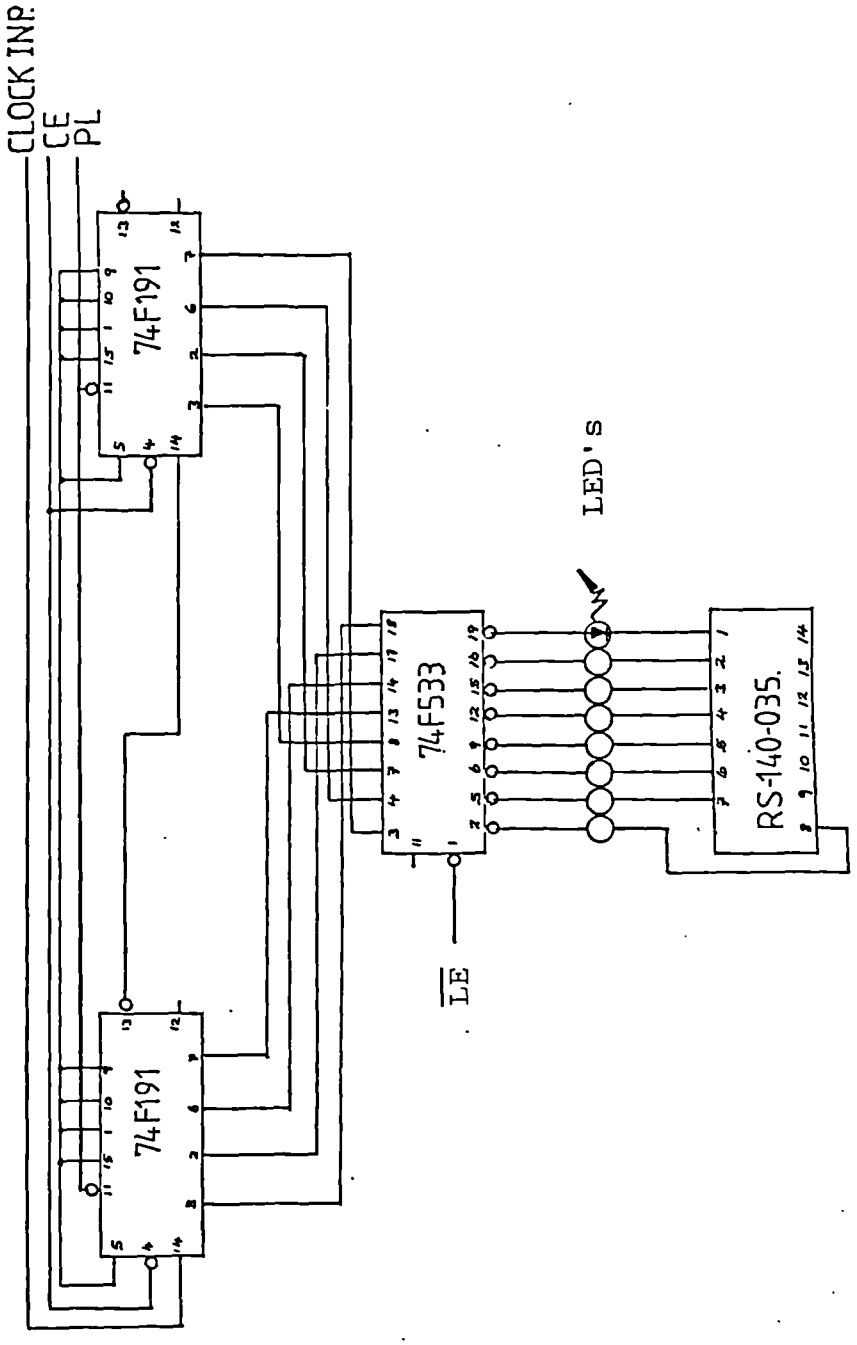

FIG 3.16
The counter circuit design

Thus pulses counted in the counter appear also at the output of the latch. When $\overline{OE}$ (output enable) is set low the output of the latches would be presented to the bus, but in this case because $\overline{OE}$ is held permanently low, appear directly on the LED's. Under bus operation $\overline{OE}$ high would mean that the output was in its high Z state.

The octal latch is an inverting type and it was necessary to design the circuit so that the LED's only lit up when the output was low. This is accomplished by using the pull up resistors to 5V and the latch, thus, sinking current.

The counter's range can be extended by using the ripple count of the second chip as the clock to the other 8 bit counter. This increases the range from 2^8 counts (256) to 2^{16} (65K) and this was found to be necessary when flow testing (see chapter 6).

The counters were built in accordance with the precautions outlined in section 3.2. The counters were built in screened boxes and inputs and outputs were via coaxial cable.

3.4.4 Design of the detector circuit

The detector in a vernier system is a very crucial element and the normal way of detecting coincidence is usually by some comparator circuitry or by an AND gate arrangement.

Although considerable effort was expended in searching for a solution the final choice of circuit would appear trivial, since it is a dual D type flip flop 74F74. Figure 3.17 shows how the flip-flop is configured and a timing diagram is given in figure 3.18.

To consider the operation of this circuit, assume initially that the circuit is reset and Q is a 1. Also assume that the D.type is perfect and no set up or hold times are required. Let $f_2 > f_1$, then, as depicted in figure 3.18, the clock input samples the D input and Q remains at 0 for position T_1. Q will also remain at 0 for position T_2.

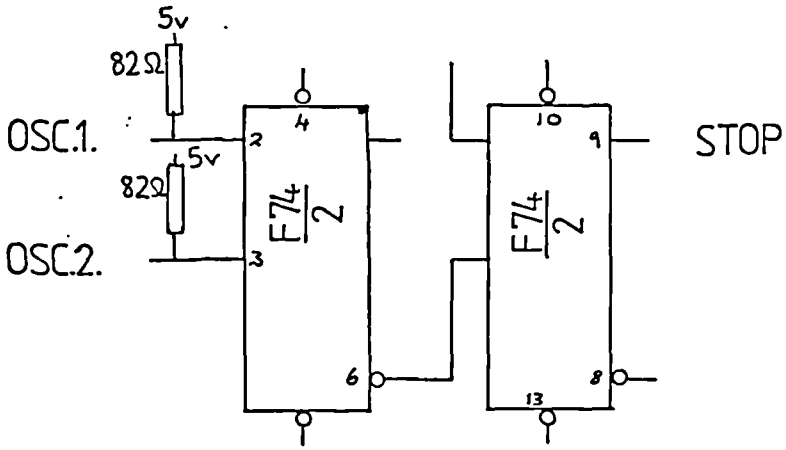

FIG 3.17
The detector circuit design

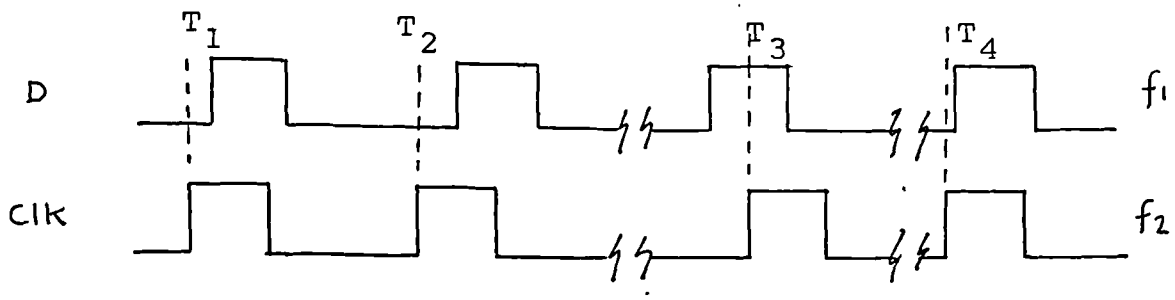

FIG 3.18
Timing diagram of the detector circuit

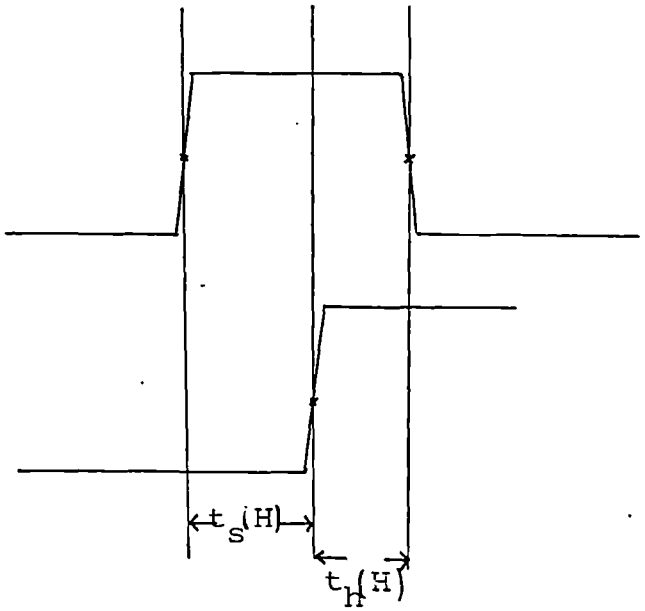

FIG 3.19
The required set-up and hold conditions

Position t_3 will, however, cause a one to be sampled and Φ will go to a one whilst $\overline{\Phi}$ goes to a zero. Because the D-types are positive edge triggered the change of $\overline{\Phi}$ from $1 \rightarrow 0$ does not affect the second D-type.

The clock will now sample a '1' for a further number of cycles (dependent upon the time difference in the oscillators δt) until it reaches position T_4. At position T_4 the clock samples a zero and thus $Q \rightarrow 0$ and $\overline{Q} \rightarrow 1$. With $\overline{Q}$ going to a '1' the second flip flop samples its D input and since this is a zero, it is passed through. This signal stops the oscillators.

The detector therefore searches for a $0 \rightarrow 1 \rightarrow 0$ sequence on its input, or a $1 \rightarrow 0$ sequence. Since these are the only two conditions of interest the detector detects when one pulse passes over the other.

Let us now return to the case of a non perfect D-type flip-flop with set up and hold conditions. For the 74F 74 these are at 25 °c and 5v (FAST data book),

$$\begin{aligned} &\text{Set up} \quad t_s\,(H) = 2nS \\ &\text{hold} \quad\; t_h\,(H) = 1nS \end{aligned}$$

and are explained by reference to figure 3.19. In specifying the times t_s and t_h the manufacturers ensure that they have covered a significant percentage of the population. The figures given are, therefore, likely to be an overestimate.

The particular problem of two signals arriving from different time frames is of great importance in computer construction where it is known as a synchronisation problem.

The output delay of a D-type flip-flop as a function of the set up time has the form shown in figure 3.20. (this figure is taken from Stoll (87)). The figure shows that provided the time of arrival is well before the clock edge then the normal propagation delay tp can be expected for the output to reach its new state. As the edge gets

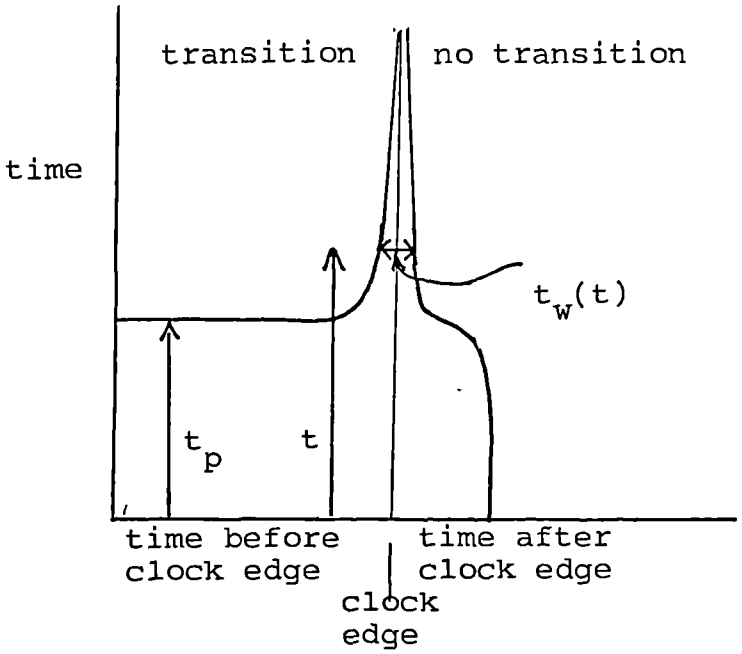

FIG 3.20
Response of a D-type flip-flop

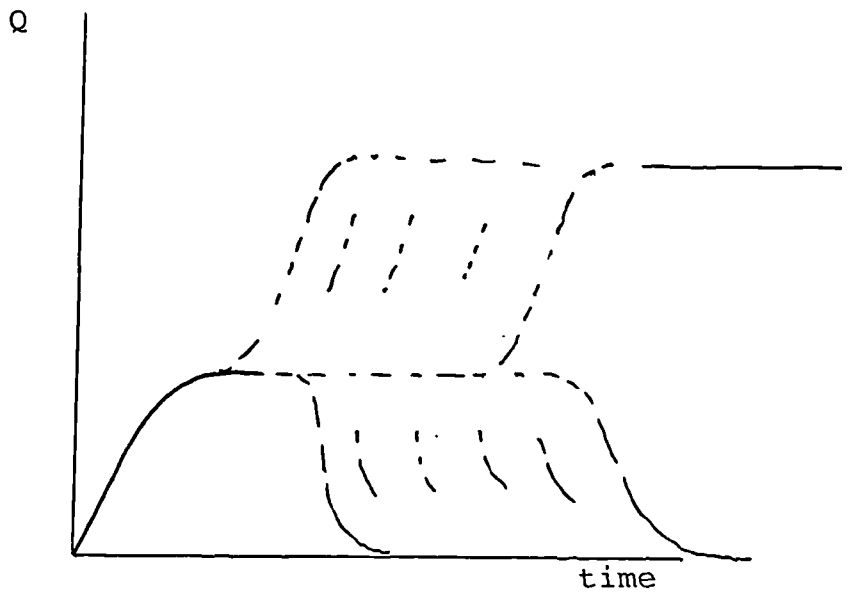

FIG 3.21
The outout trajectories of a D-type flip-flop

nearer to the clock edge, the time for the output response increases (without bound) until after the clock edge no transition occurs. The region of extra delay is known as the meta stable region or that the flip-flop is in a meta stable state. Under this condition of conditional stability the output has trajectories as shown in figure 3.21.

In his paper Stoll uses the concept of a failure window tw, which is the range of input times that will produce output delays greater than t, this is marked on figure 3.20. Stolls equation is:

$$t_w(t) = t_p \, 10^{\frac{-(t-t_p)}{\tau}} \qquad 3.25$$

for regenerative flip-flops
where,

t_p is the normal propagation delay of the flip-flops and τ is the time constant of the resolution of the flip-flop.

The value of τ varies for each logic family and decreases for increasing speed characteristics. A value of given by Stoll for Schottky logic is 2×10^{-9} seconds. (Note that a smaller time would be expected for FAST).

It is of interest, now, to estimate the rate at which the data input will fall into the region t_w. An equation for the MTBF (Mean Time Between Failures) is, from Stoll,

$$MTBF = \frac{1}{2F_c \, F_d \, t_p \, 10^{\frac{-(t_E-t_p)}{\tau}}} \qquad 3.26$$

where

F_c, F_d are the input frequencies

t_p, τ as previously given

t_f = the time of delay that will cause failure.

To estimate the time t_f that will cause failure, it is necessary to review the part of the circuit to which it applies. Consider figure 3.22 which is a figure of the detector elements that make up the path from the oscillator to the detector and back to the oscillator.

The typical delay from the rising edge of G_1 is, given by t_d

$$t_d = t_{p\ (buffer)} + 2xt_{p\ (flip-flop)} \qquad 3.27$$

and

$$t_{p(buffer)} = 6x10^{-9} \text{ seconds typically}$$

and

$$t_{p(flip-flop)} = 5x10^{-9} \text{ seconds typically}$$

thus

$$t_d = 16 \times 10^{-9} \text{ seconds typically}$$

and this time falls within τ_2. Assuming that the period of the oscillators is around 25nS, the value of t_d can be allowed to increase (to 25nS) and thus the time of delay that will cause failure (t_f) is 9nS.

Hence the MTBF is,

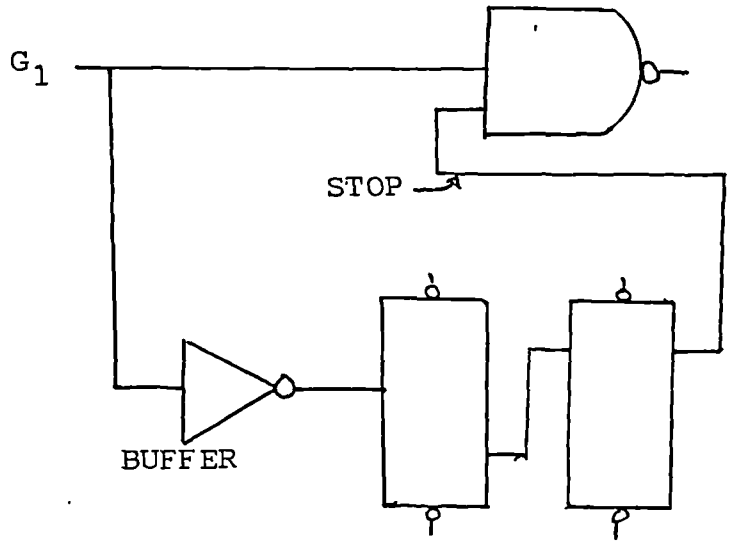

FIG 3.22
The timing path of the detector elements

$$= \frac{1}{2 \times (40 \times 10^6)^2 \times 5 \times 10^{-9} \times 10^{-(9-\frac{5}{2})}}$$

$$\simeq 6{\cdot}25 \times 10^{-6} \text{ secs}$$

where $F_c \approx F_d = 40 \times 10^6$ Hz.

The values of tp and τ have been taken as 5 and 2nS respectively, but it is likely that τ will be smaller for FAST circuits.

Thus for continuous operation of the oscillators one failure could be expected every 250 counts, ie $\frac{6.25 \times 10^{-6}}{25 \times 10^{-9}}$

If the value of t_f (the time to failure allowed) is increased by one period ie: 9nS + 25nS = 34nS, then because of the power relationship in 3.26 the MTBF is increased to 197642 seconds or 7.9×10^{12} counts.

There are thus two problems,

(i) If the stop signal is not returned in time $\tau 2$ (and this occurs on average every 250 counts) then it is likely to occur within the next period since the probability of a failure occuring outside of this total period (ie: first and second periods) is very small, at 1 in 7.9×10^{12}.

The question, therefore is whether to subtract one or two from the final count or indeed 1.004 (1 1/250).

(ii) The output of the first flip-flop, when in the meta stable state, may trigger the second flip-flop because the output may exceed the voltage threshold level of the input of the second flip-flop, and thus the system may be triggered every time the detector enters the meta stable region.

The region around the clock edge that causes problems is very narrow so that when failure is discussed what is really meant is that the detector would not be resolved until the next pulse, which because of δt separation, would not present a problem. Thus this is the resolution of the detector. It is difficult to estimate a figure for the resolution.

The detector was constructed in a screened box following the precautions outlined previously. The inputs and outputs are made via coaxial cable. To ensure fast edges two 82Ω pull- up resistors are used at the input to the detector.

3.4.5 Testing of the timing system

3.4.5.1 Testing the oscillator circuits

The oscillator circuits were tested throughout their construction for correct operation. The periods of the oscillators were found to be approximately $26\text{-}28\times10^{-9}$ seconds and the mark: space ratio was found to be about 3:7 resulting in a pulse width of approximately 8nS (at the 1.5 volt level). A difficulty in measuring the width was encountered, since as discussed previously, the rise and fall times observed were in error because of the systems rise time (ie: the scope).

An experiment was conducted into the associated drift of the oscillators. This consisted of free running the oscillators and measuring the period. A warm up time of approximately half an hour was allowed. The measurements were made using the HP counter/timer (accuracy $\approx 10^{-12}$ seconds).

The result of measuring the medium term drift is displayed in figure 3.23 where the period of both oscillators is displayed against the time after warm up. It can be seen that the periods remain substantially constant.

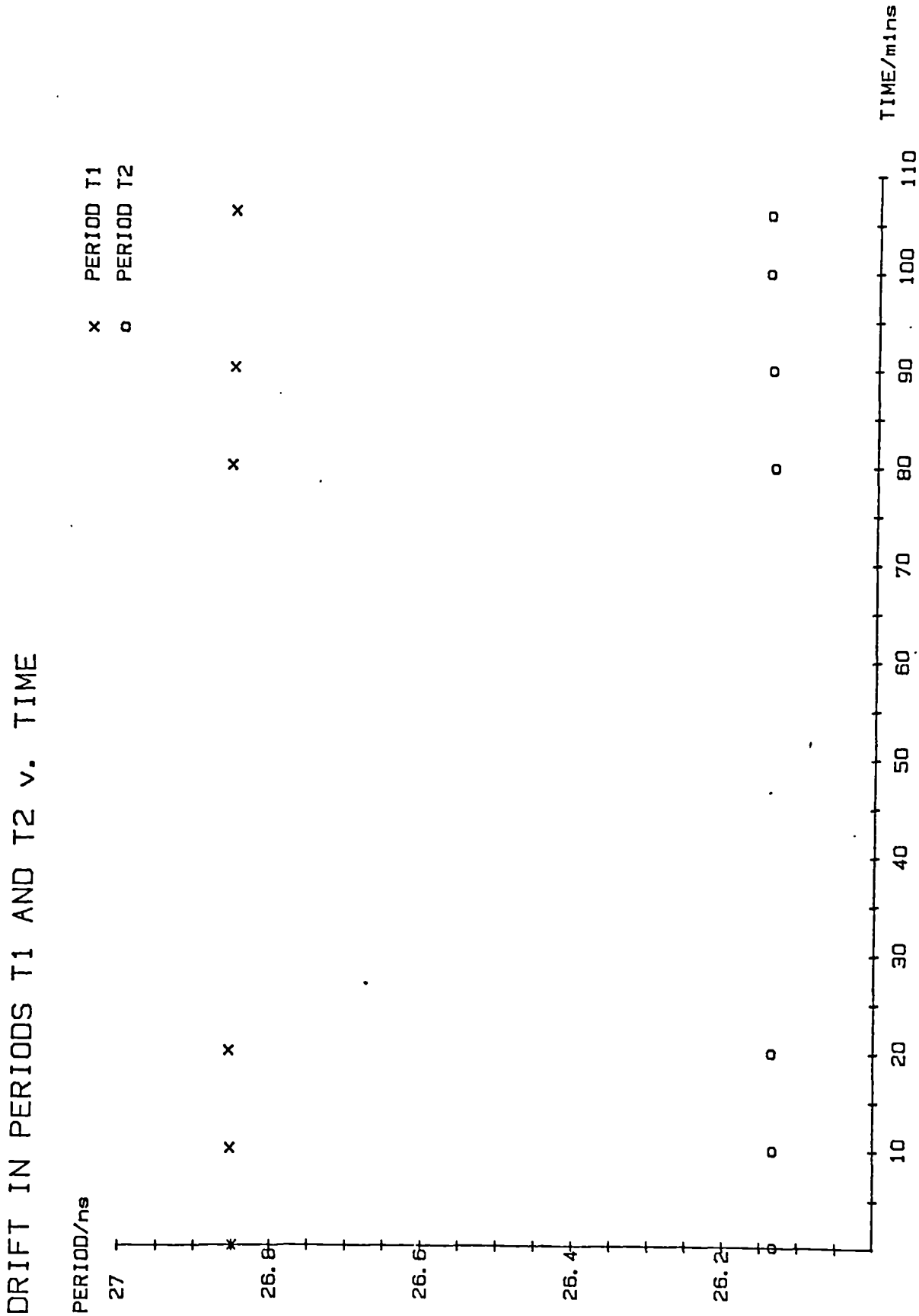

FIG 3.23
Graph of medium term drift in oscillators

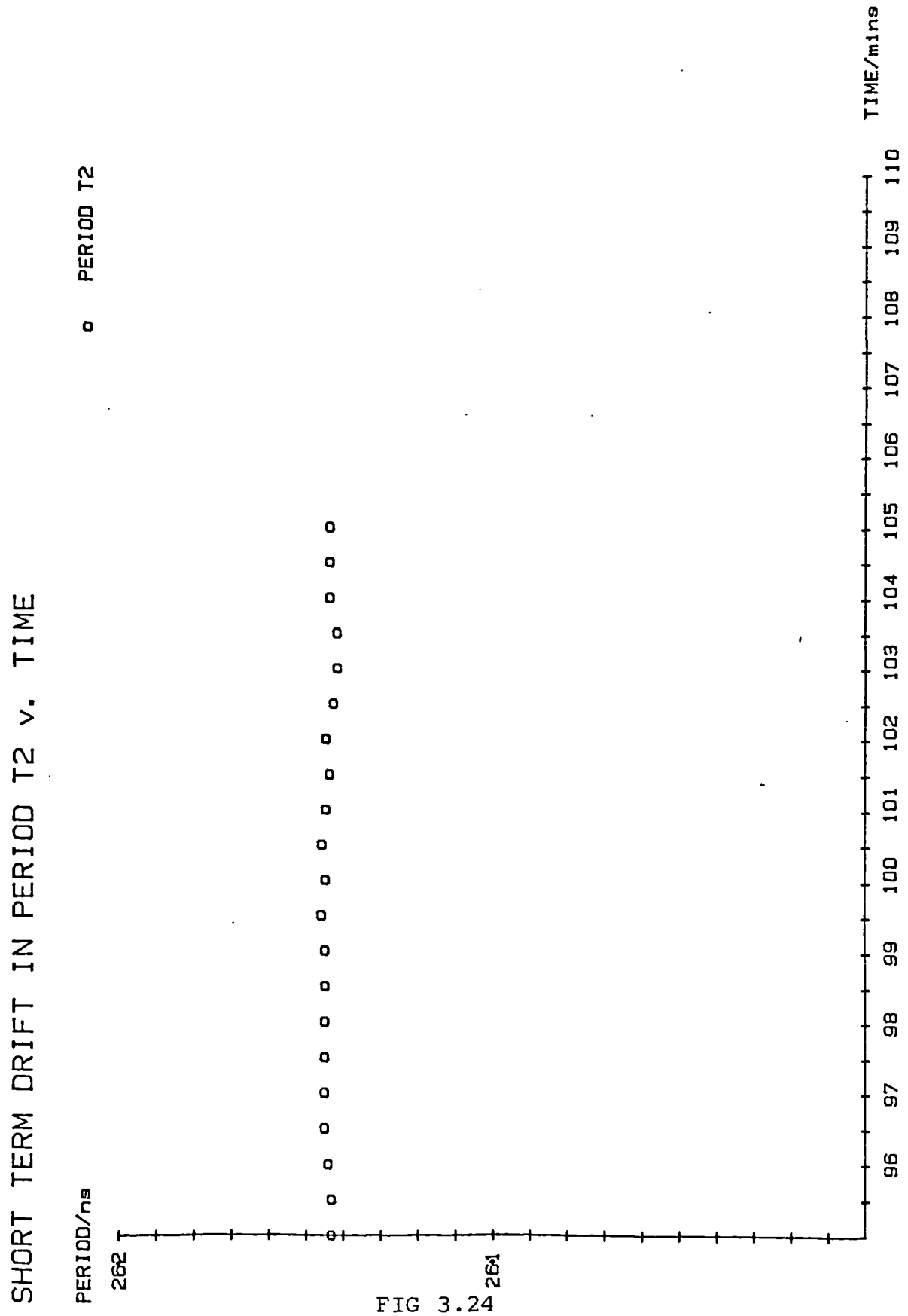

FIG 3.24
Graph of short term drift of oscillators

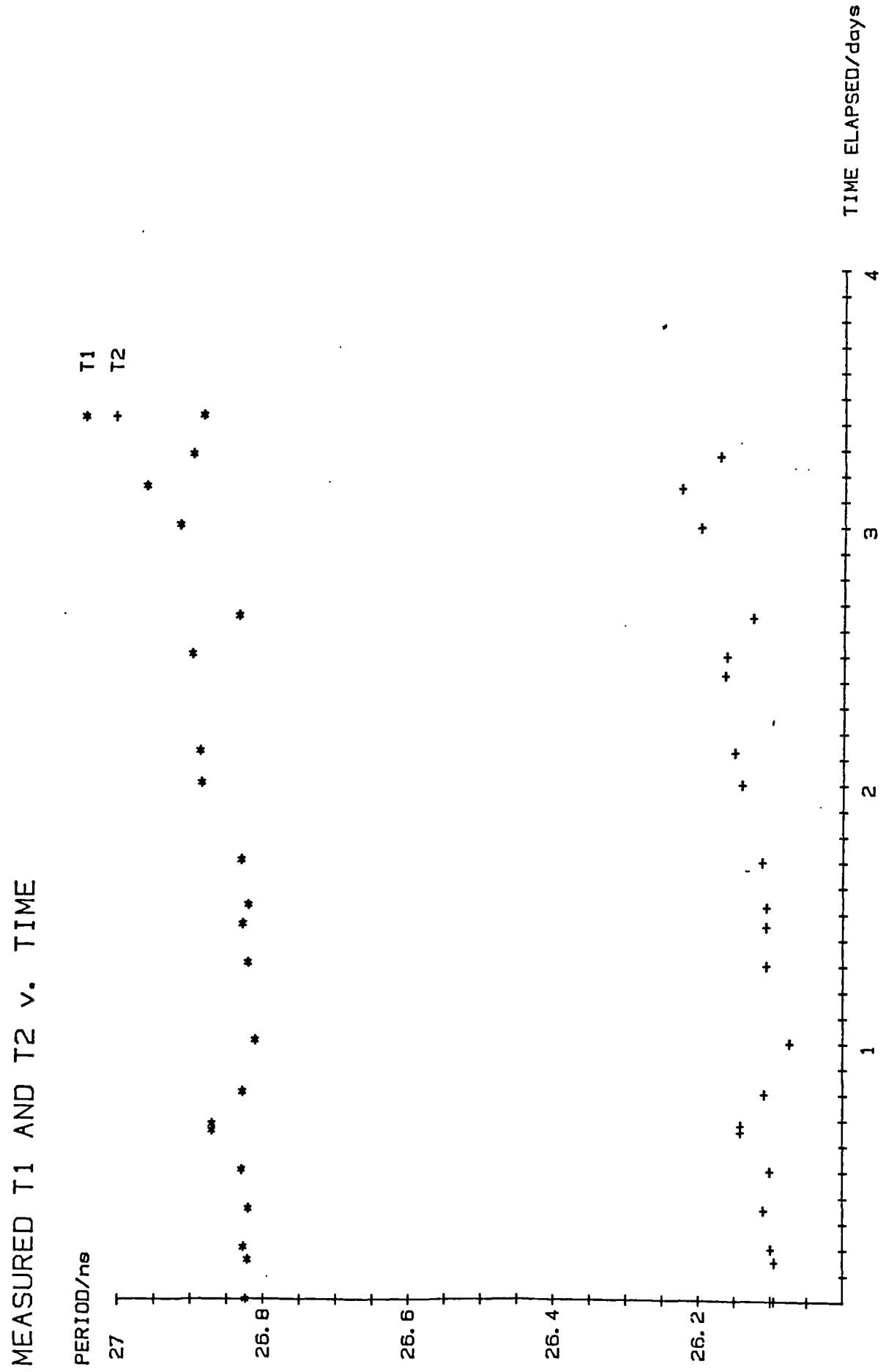

FIG 3.25
Graph of long term drift of oscillators

During the test it was decided to measure the short term drift of one oscillator and the results of this test are displayed in figure 3.24.

The final test, of which the results are displayed in figure 3.25, consists of monitoring the periods over the flow testing of the instrument. In this case flow testing took approximately a month and on four selected days various calibrations were carried out. The graph displays the period of the 2 oscillators against the selected days, which have been marked in hourly intervals.

It can be seen from this test that the oscillators appear to track each other. No special precautions were taken with temperature control but it was noticed that the ambient temperature rose during the month long period. It is felt that this probably accounts for the gradual rise in the periods.

The maximum change in the periods over all tests is tabulated in table 3.1.

Table 3.1

Period of oscillators

Test	Oscillator 2	Oscillator 1	Units	Comments
Short term	26.142		nS	minimum period
test	26.145		nS	maximum period
(10 minutes)	.003		nS	difference
Medium term	26.131	26.848	nS	minimum period
test	26.145	26.857	nS	maximum period
(110 minutes)	.014	.009	nS	difference
Long term test	26.073	26.812	nS	minimum period
(over 1 month)	26.227	26.963	nS	maximum period
	.154	.154	nS	difference
Value of	.71		nS	minimum
δ_t	.739		nS	maximum
(all tests)	.029		nS	difference

Thus over a medium term test the fractional changes are given by:

$$\frac{dT_2}{T_2} = \frac{\cdot 014 \times 10^{-9}}{26\cdot 145 \times 10^{-9}} = \cdot 54 \times 10^{-3}$$

and

$$\frac{dT_1 - dT_2}{T_1 - T_2} = \frac{-\cdot 005 \times 10^{-9}}{\cdot 712 \times 10^{-9}} = -7 \times 10^{-3}$$

Thus to calculate the errors in the timing one uses 3.21,

$$\frac{d\Delta t}{\Delta t} = \frac{|N_2-N_1|}{|N_2-N_1| \pm N_1/N} \cdot \frac{dT_2}{T_2} \pm \frac{N_1/N}{|N_2-N_1| \pm N_1/N} \cdot \frac{dT_1-dT_2}{T_1-T_2}$$

as given previously.

It will be shown that the vernier system is a bidirectional instrument but that for the flow tests it is used in a unidirectional manner which is that the slow oscillator starts first and the fast oscillator second. Then the equation reduces to:

$$\frac{d\Delta t}{\Delta t} \quad \frac{|N_2-N_1|}{|N_2-N_1| + N_1/N} \cdot \frac{dT_2}{T_2} + \frac{N_1/N}{|N_2-N_1| + N_1/N} \cdot \frac{dT_1-dT_2}{T_1-T_2} \qquad 3.28$$

Consider the case where $|N_2-N_1| = 0$, then

$$d\Delta t = \Delta t \, \frac{dT_1-dT_2}{T_1-T_2} \qquad 3.29$$

let $\Delta t = 26\times10^{-9}$ seconds (one period approximately)
and $\dfrac{dT_1 - dT_2}{T_1 - T_2} = -7\times10^{-3}$
then

$$d\Delta t = \cdot182 \times 10^{-9} \text{ secs}$$

As the time to be measured increases (in periods of 26×10^{-9} seconds) the error from $\frac{dT_1-dT_2}{T_1-T_2}$ decreases by the same factor. The net result is that the maximum error from the change in the difference in the periods is constant at .182 nanoseconds and this is expected since the oscillators run through each cycle.

Now the error from $\frac{dT_2}{T_2}$ increases with increasing $|N_2-N_1|$ and for large $|N_2-N_1|$ where N_1/N can be ignored the error is due to the term $\frac{dT_2}{T_2}$, and the absolute error is given by:

$$d\Delta t = \Delta t \, \frac{dT_2}{T_2} \qquad 3.30$$

which for 500×10^{-9} secs is:

$$= \cdot 27 \times 10^{-9} \text{ secs}$$

If the data from the long term tests is used the errors increase by a factor of 5.6 for the differential period change (thus 1.01nS) and a factor of 10.7 for the $\frac{dT_2}{T_2}$ term, (hence 2.9nS).

It can be seen therefore that some form of on board monitoring is required. This can be achieved quite simply by employing a low cost, high quality crystal oscillator and gating the vernier system.

The above errors are considered to be worst case because the oscillators were tested under very loose conditions eg: in opened boxes.

3.4.5.2 Construction of a timedelay unit

The time delay unit (TDU) was required in the testing of the vernier system. Previous work by the author (136) had shown the monotonicity of the vernier system but because the active delays were inconsistent it was difficult to estimate the accuracy.

It was decided to construct a unit with various lengths of time delays provided by pieces of coaxial cable wound upon a plastic former.
The inductance per unit length (L) and the capacitance per unit length (C) of a coaxial cable are functions of the geometry of the cable. An electromagnetic wave progresses with a velocity, in such a cable, of

$$V = \frac{1}{\sqrt{LC}} \qquad 3.40$$

and since the characteristic impedance of a line is given by

$$Z_o = \sqrt{\frac{L}{C}} \qquad 3.41$$

then

$$L = Z_o^2 C \qquad 3.42$$

and

$$V = \frac{1}{Z_o C} \qquad 3.43$$

and thus

$$\text{the delay } td = \frac{\text{dist}}{\text{vel}} = ZoC \text{ per unit distance} \qquad 3.44$$

The cable used was a 50Ω characteristic impedance cable with 100pf/metre capacitance. The time delay was thus approximately 5nS/metre.

It was decided to construct a unit with delays of the order of nanoseconds, 10's of nS and up to 150 nS or so. The values of delays should be selected so that any value in between can be achieved.

To eliminate the possibility of reflections, it was necessary to make each delay individual and to have each end matched with 50Ω connectors. Exact lengths of interconnection cable were then made (with matched BNC's) to form the complete TDU. Thus every delay presents a matched 50Ω system to the driving source.

The length of cable required for a delay of 150 nanoseconds is, therefore, of the order of 30 metres and it was necessary to ensure that a small size was chosen. A suitable cable was found to be a miniature coax type RG174 A/u, with Zo = 50Ω and C = 100pf/m.

The unit was constructed with the BNC cable wound on a round 50 mm former and completely enclosed in a box. The unit was tested functionally and found to work satisfactorily.

3.4.5.3 Tests on the overall system

The counters were tested by allowing through a single pulse and holding the stop control low. In this way a single pulse should register a count of 1. Both counters were tested in this way and performed correctly at all times. The system for testing was set up as shown in figure 3.26. The system consisted of the prototype firing circuit, the selector unit, a BNC connection block and the two timing systems (the HP counter/timer and the vernier system) and the time delay unit.

The selector will be described in section 3.6.4 but for the purpose of this test allowed two pulses through, which were derived from one pulse off a single chip, thus the differential delay between the pulses was negligible.

The connection block was necessary to provide connectors for the vernier system (miniature BNC) and the HP counter timer (standard BNC). a coil was connected in one limb of the connection block to bias the system to some point in the middle of its characteristic. This would then allow the system to be tested over a range through zero, and thus show the bidirectional nature of the vernier timing system.

From the connection block, which has the TDU in one limb and a fixed coil in the other limb, two sets of BNC's were provided in parallel for the vernier system and the HP counter timer. Both cables to the vernier system and to the HP counter were of the same length. The entire system to the HP forms a 50Ω (characteristic) impedance system but for the vernier system the impedance termination is the input impedance of an AND gate.

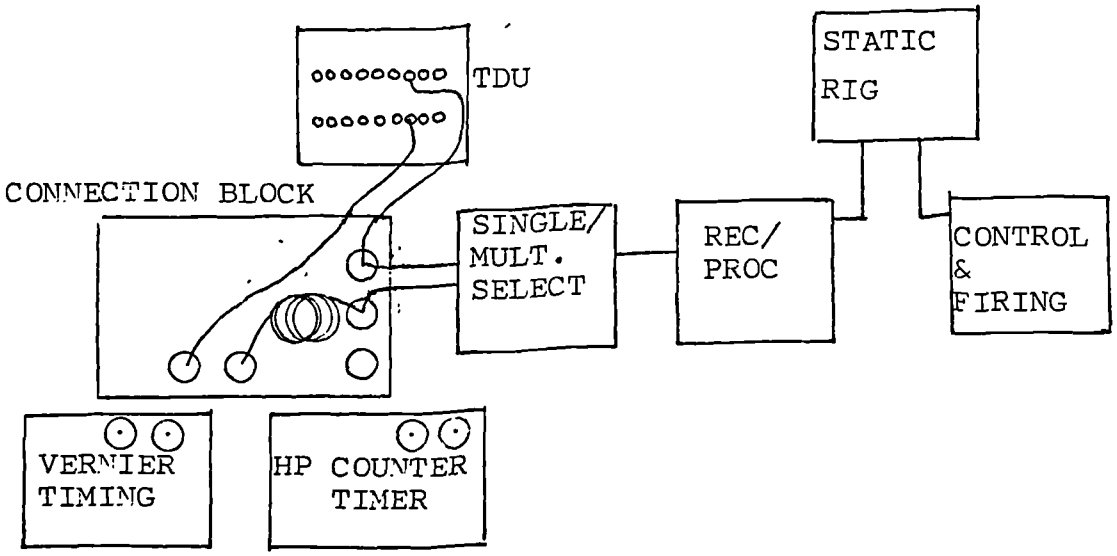

FIG 3.26
Experiment to test the Vernier Timing system

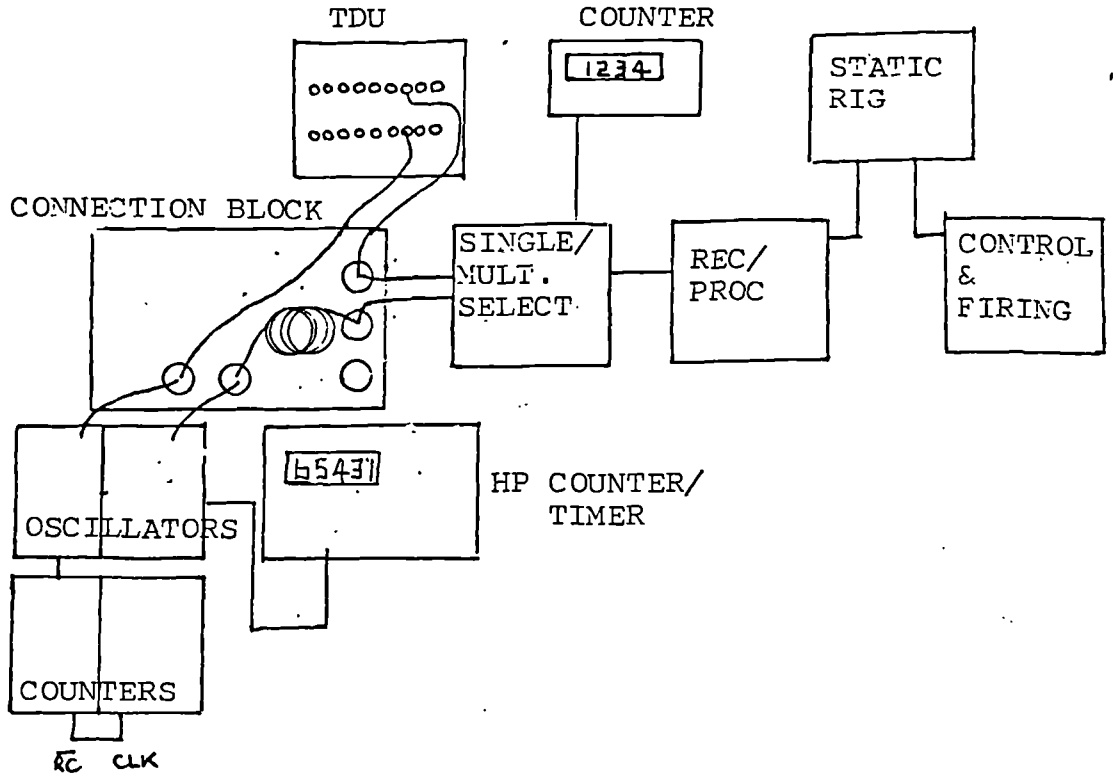

FIG 3.27
Experiment to test the Vernier system in average mode

A difficulty with the HP counter/timer was that to reverse the pulses it was necessary to physically interchange the leads on the inputs, this was felt to introduce a small error since the pulse shapes would not be identical and triggering may not occur on the same point for both pulses. However, it was felt that the important feature of the experiment was to check the bidirectional nature and the stability of the vernier readings.

A further test that was felt important was the limit of operation of the vernier system. In this test it was decided to reduce the difference δt and this was achieved by increasing the gate capacitance and thus decreasing the periods between the oscillators.

The method of testing was that a delay in the TDU was selected and connected to the connection block. The HP counter/timer was connected and the system switched on. A sample of 1000 pulses was allowed through and the mean of the sample and the standard deviation were recorded. This was repeated to obtain a set of 3 results.

The HP counter/timer was removed and the vernier system was connected. The system was connected in single shot mode and ten readings were taken. The vernier system was removed from the connector block and a new value of delay chosen. The tests were repeated as before.

After completing a full set of tests the TDU was tested at selected delays to ensure that no drift had occurred (using precisely the same cables as previously used, all cables were numbered).

The capacitance on the gate of one of the oscillators was adjusted to provide a different δt. The complete tests as given above were repeated. This adjustment was repeated one more time.

The results of testing the system in this way are tabulated in table 3.2. The periods of the oscillators were measured and δt was found to be .774 nS, .396nS and .094nS.

Table 3.2

Results of testing the Vernier system

Test 1 $T1 = 26.697 \times 10^{-9}$ $T2 = 25.923 \times 10^{-9}$ $\delta t = .774 \times 10^{-9}$

N of delay	No of Samples	N_1	N_2	Calculated Δt	Measured Δt (from HP)
2	10	8	3	135.033	137.296 ± .04
3	10	12	10	60.36	62.05 ± .04
4	10	19	19	13.93	16.18 ± .04
5_{71}	10	5	5	3.096	4.5 ± .04
5_{81}	10	4	4	2.32	3.36 ± .04
6	10	22	23	-9.669	-9.14 ± .04
6_{71}	10	28	29	-5.025	-4.9 ± .04
6_{81}	10	27	28	-5.799	-6.0 ± .04
7	10	17	18	-13.54	-14.14 ± .04
7_{81}	10	19	20	-11.99	-11.58 ± .04
8	10	15	16	-15.087	-15.8 ± .04

Test 2 $T_1 = 26.857 \times 10^{-9}$ $T2 = 26.461 \times 10^{-9}$ $\delta t = .396$

N of delay	No of samples	N1	N2	Calculated Δt	Measured Δt (from HP)
2	10	8	3	135.077	137.296 ± .04
3	10	20	18	60.45	62.05 ± .04
4	2	37	37	13.94	16.18 ± .04
	8	36	36		
5_{71}	10	10	10	3.56	4.5 ± .04
5_{81}	10	7	7	2.37	3.36 ± .04
6	10	45	46	-9.037	-9.14 ± .04
6_{71}	10	54	55	-5.473	-4.9 ± .04
6_{81}	10	53	54	-5.869	-6.0 ± .04
7	10	33	34	-13.789	-14.14 ± .04
7_{81}	10	39	40	-11.413	-11.58 ± .04
8	10	32	33	-14.185	-15.8 ± .04

Test 3 $T1 = 26.801 \times 10^{-9}$ $T2 = 26.707 \times 10^{-9}$ $\delta t = .094$

N of delay	No of Samples	N1	N2	Calculated Δt	Measured Δt (from HP)
2	3	14	9	134.69	137.296 ± .04
	7	13	8		
3	1	46	44	57.56	62.05 ± .04
	9	45	43		
4	10	92	92	8.55	16.18 ± .04
5_{71}	10	25	25	2.256	4.5 ± .04
5_{81}	8	13	13	1.11	3.36 ± .04
	2	12	12		
6	4	108	109	-16.59	-9.14 ± .04
	6	109	110		
6_{71}	3	177	178	-10.07	-4.9 ± .04
	5	178	179		
	1	179	180		
	1	180	181		
6_{81}	7	100	101	-17.37	-6.0 ± .04
	3	101	102		
7	1	83	84	-18.89	-14.45 ± .04
	7	84	85		
	2	85	86		
7_{81}	1	97	98	-17.5	-11.58 ± .04
	3	98	99		
	3	99	100		
	2	100	101		
	1	101	102		
8	3	106	107	-16.77	-15.8 ± .04
	7	107	108		

The results of test 3 show that the system becomes highly non linear for small δt and for the discussion that follows these results have been excluded.

There appears to be an offset in the vernier or HP system and it may be more constructive to view the differences in the systems' estimation of delay. If this is done the results are as given in table 3.3.

Table 3.3

Difference in delay values

Delay	HP difference (nS)	Test 1 (.774nS)	Test 2 (.396nS)
2-3	75.246	74.673	74.627
3-4	45.87	46.43	46.51
$4-5_{11}$	11.68	10.834	10.38
$5_{71}-5_{81}$	1.14	0.776	1.19
$5_{81}-6$	12.5	11.989	11.4
$6-6_{71}$	-4.24	-4.644	-3.56
$6_{71}-6_{81}$	0.77	1.1	0.396
$6_{81}-7$	8.45	7.74	7.92
$7-7_{81}$	-2.87	-1.55	-2.38
$7_{81}-8$	4.2	3.1	2.77

For test 1 the difference in the estimated differences arise within .774nS with the exception of delay $7-7_{81}$ (1.32nS) and $7_{81}-8$ (1.1nS). For test 2 the difference in the estimated differences is within a maximum of 1.43nS (for delay $7_{81}-8$).

The results of these tests appear to show that the system (for test 1) is within δt + .55nS and within δt + 1.07nS (for test 2). Because both tests were remarkably repeatable it was concluded that there is probably some non-linearity in the system at start up.

The accuracy of the HP counter/timer is ± 2.2nS where it is assumed that the ± 2nS part is a systematic offset, thus, the difference tables would then be a better guide than the direct results (in table 3.2).

Difficulty was encountered when measuring the low values of delays (with the HP counter/timer). The adjustment of the trigger level by .5 volt caused a difference of .5nS in the reading.

It was decided to test the system under averaging mode and this was carried out by setting up the system as shown in figure 3.27. In this case the two 8 bit counters were connected to form a 16 bit counter and the HP used in totaliser mode to form the other counter. The system in this case was now operated in a unidirectional manner and the only requirement was to exchange the systems (ie: the vernier and HP counter/timer) when testing through the delay.

The results of testing in this manner are given in table 3.5. The system was biased away from the low end (to eliminate problems with the HP counter/timer) and the procedure adopted for testing follows that described in the flow tests, chapter 6. Two readings of the vernier system were taken to ensure that the system was repeatable.

Table 3.5

Results of testing vernier in average mode

Test 4	T1 = 26.832nS		T2 = 26.128nS	δt = .704nS	
Delay value (by HP) nS	Average N_1	Average N_2	Estimated Δt (nS)	Difference between delays HP	Vernier
	36.6584	31.6556			
160.715	36.6646	31.6618	155.82		
	8.0993	5.0989		74.78	72.5
85.935	8.0866	5.0863	83.39		
	16.2929	15.2927		45.8	46.49
40.135	16.2870	15.2868	36.899		
	30.1751	30.1751		15.41	16.36
24.73	30.1593	30.1593	20.5393		
	19.8115	19.8115		7.71	7.29
17.025	19.8154	19.8154	13.25		
	13.3887	13.3887		4.8	4.53
12.185	13.3905	13.3905	8.72		
	12.31	12.31		1.49	.757
10.69	12.3117	12.3117	7.96		
	11.0496	11.0496		.965	.888
9.72	10.9929	10.9929	7.075		

The table shows that the vernier system is very repeatable (worst case is for the last delay and is approximately 5 in 1000). The results also show that measurement within one period always produced the same count in each counter. However, the difference in delays is now equal to 2.28nS for the worst case.

If a straight line is fitted to the data then a relation

$$\Delta t = -3.07 + .9919 \; HP_{time}$$

with a regression coefficient of .99991 is obtained. If now this is used then a set of results estimated from the line is as given in table 3.6.

Table 3.6

Estimate of time from line fit

Predicted Δt from line (nS)	Calculated Δt from vernier (nS)	Difference (nS)
156.35	155,82	.53
82.17	83.39	-1.22
36.74	36.899	-.16
21.46	20.539	.92
13.816	13.25	.56
9.02	8.72	.3
7.53	7.96	-.43
6.57	7.075	-.5

Using the line fit would mean that the system could be contained within +.92 or -1.22 nS.

However, when the values for the delays were compared for the Hp counter/timer, a large discrepancy was observed in the values of the differences. The results of this observation are tabulated in table 3.7.

Table 3.7

Results of delay differences (via HP counter timer)

Delay Difference	Measured value given by HP test 1 & 2 (nS)	Measured value given by HP test 4 (nS)
2-3	75.246	74.78
3-4	45.87	45.8
4-6	25.32	23.09
6-7	5.31	4.84
7-8	1.35	1.495

From these results it was concluded that the Hp counter/timer did not have a systematic offset that was constant but appeared to have a variable offset. The results, therefore, of any time test could not be guaranteed to better than ±2.2nS.

It was decided that further testing of the timing system was futile with the present equipment and that the testing of the overall instrument would be of more use.

However it would seem that the vernier system is very repeatable and (probably) accurate to within ±1.5nS for a δt of approximately .396-.774 ns. The monotonicity of the vernier system has been demonstrated as well as the bidirectional facility.

Before closing this section it is observed that the difference between two nearly identical frequencies is obtainable from the output of a D type flip-flop and that with the present system it may be that the difference frequency (the reciprocal of which is δt) could be used in the calculation of the value Δt.

An experiment was conducted to observe on an oscilloscope the output of the detector flip-flop under free running conditions. The trace was seen to be at the difference frequency, but the period observed was seen to have two values (a value calculated to be δt and a value of δt + (approximately) 26nS, the period of the oscillators). This 'ghosting' observed is probably the result of the failure mode discussed previously.

3.5 The receiving and processing circuit

The purpose of the receiving and processing circuit is to take the signal from the transducer (which is in the form of a damped sinusoid) and to produce a time marker. Because the level of signal is low, it is necessary to include an amplification stage. This is often an automatic gain controlled amplifier (AGC). However, for the present prototype a non AGC amplifier has been used.

The time marker produced must be compatible with the vernier system and must therefore be a negative going pulse of defined duration.

The overall concept of operation of the circuit was that the signal would be amplified, a threshold level on the signal would be chosen and on the following zero crossing a time marker would be produced.

A circuit was built using an amplifier, two comparators and a dual D type flip-flop for gating purposes. The amplifier chosen was a SN 733 video amplifier with large band width (approximately 200 MHz). This circuit appeared to have oscillation and noise problems associated with it and the video amplifier was replaced by a high quality low noise preamplifier the ZN459, which has a lower bandwidth.

A suitable design of circuit was then found to be that of figures 3.28, 3.29. Two circuits were constructed in shielded boxes and because the differential delay between the circuits would be important, it was necessary to design for minimum components in the path from transducer to vernier system. The effective path length is from the transducer through the preamplifier and one comparator to the vernier system.

A suitable comparator with small delays was found to be the NE521. comparator. In fact this is a dual comparator, which is TTL compatible, on one chip. The other comparator was therefore used as the threshold detector. This unit has a guaranteed maximum delay of 12nS for low level signals but this decreases for high level signals. It was noted from the data sheet that the changes in delay time for high level input voltages and for temperature effects was very small (of under 1nS) and thus under given conditions the changes in these should also be small.

However, there is a disadvantage in using the 521 and that is its high offset voltage (resolution between inputs). For the level of signals of interest it was decided that the offset (of approximately 6mV) would not be significant and this was not, at this stage, investigated further. It should be noted, however, that the offset over the

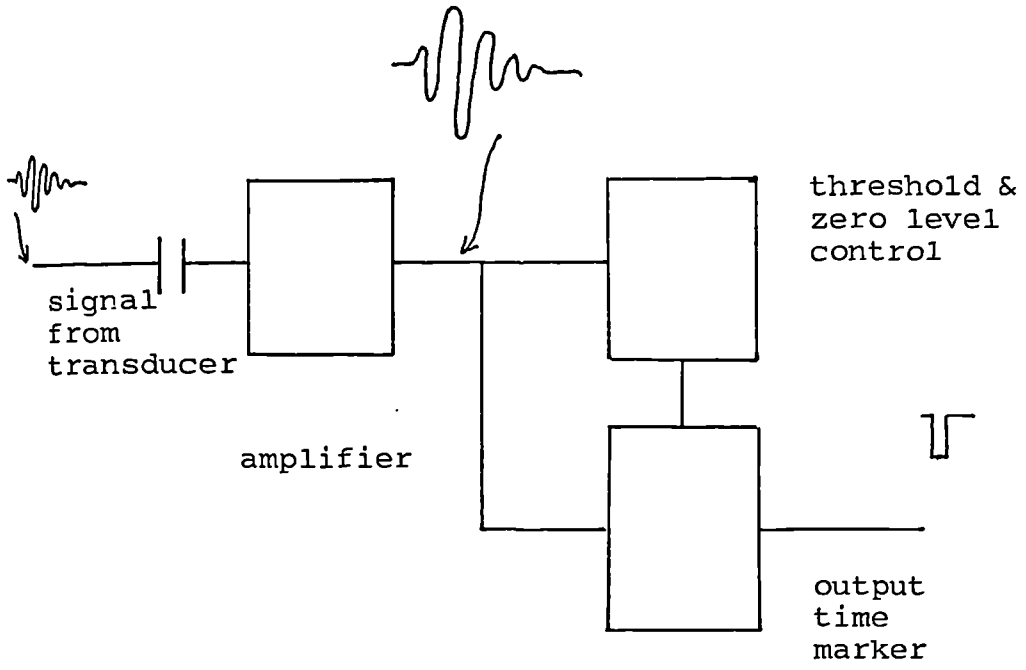

FIG 3.28
Outline circuit of receiver/processor

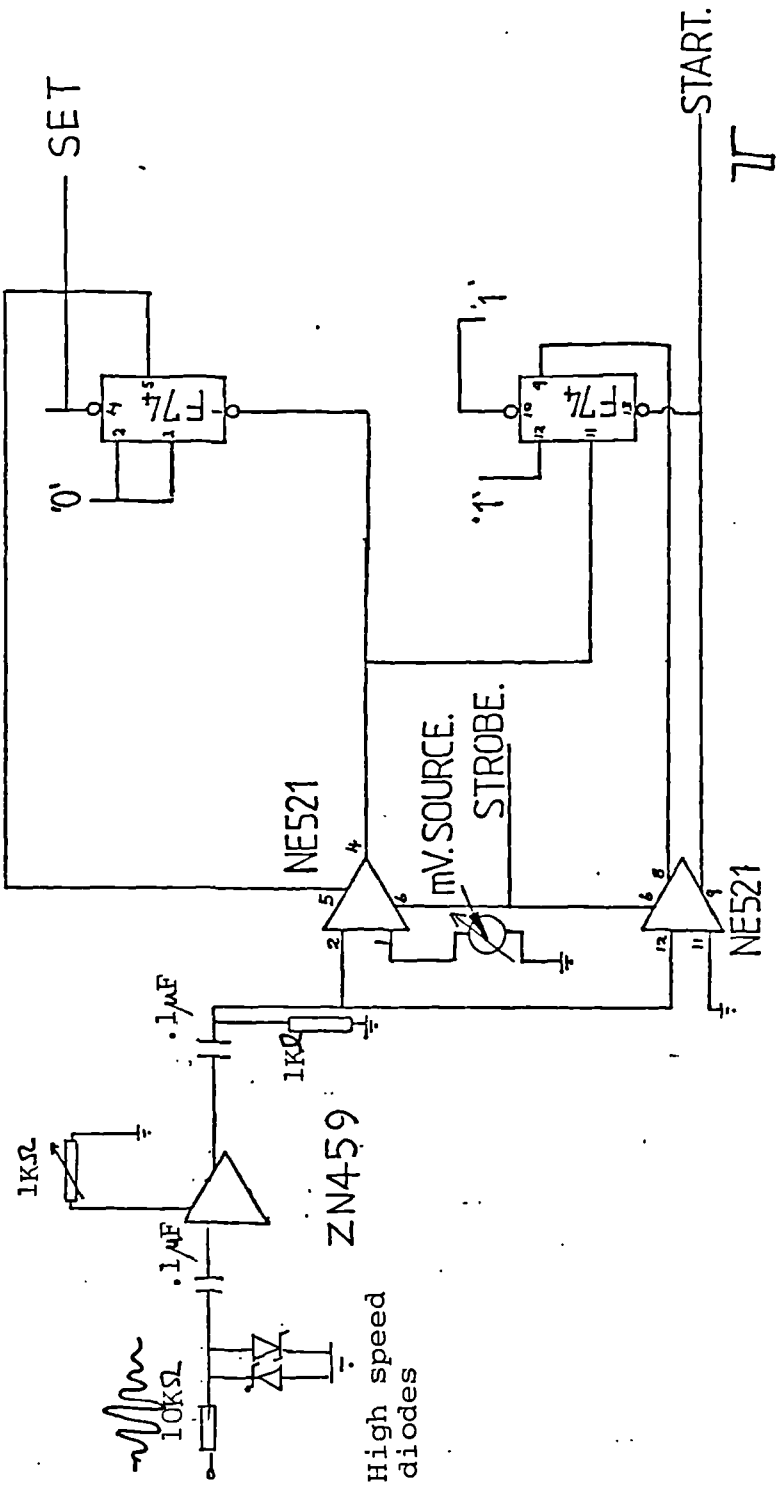

FIG 3.29
Detailed circuit diagram of the Receiver/Processor

temperature range (0-70°c) would be up to 10mV and since this would combine with the bias currents a higher level of overall offset would be encountered. It was considered that the change in the higher level of offset was the important parameter and as this would be small it could be temporarily ignored.

One other design requirement was that the pulse width be of a suitable value to start the oscillators (between approximately 3nS and 15nS). A typical value of delay through the system (producing the start pulse width) is,

from $\overline{C}$ to Q for the flip-flop + strobe to output of comparator.

The listed value of typical delays is $\overline{C}$ to Q = 6.5nS and strobe to output of 3nS. Thus the overall width is approximately 9.5nS and within the desired value.

The threshold detector levels is set by a variable current source and a resistor (which is connected to one leg of the threshold comparator). A range of levels can thus be set.

The design of the circuit has been previously given in figures 3.28 and 3.29. Its principle of operation will now be described by reference to these figures and also to the figure 3.30, the timing diagram.

The transducers are fired by a pulse from the firing circuit, but because there is coupling from the firing circuit to the receiving circuit it is necessary to protect the input of the pre-amplifier. This is achieved by the 10kΩ resistor and the high speed Schottky diodes (V_f=.3 or .4 volts). However some signal is still amplified and it is necessary to strobe off the comparators during this time.

After sufficient time has elapsed for the signal to decay the strobe signal (B) is sent high and thus enables both comparators. (The threshold comparator has a threshold value set on its input). A set signal, derived from the strobe going high, is sent to flip- flop 1

(signal D) and this sets the flip-flop and enables the threshold comparator. The system now waits for a signal above the threshold level set (see the signal in figure 3.31).

When the input signal has been received it is amplified and when it rises above the level (E) set on the comparator, the comparator output falls to zero in approximately 8nS. The output falling to zero, resets the flip-flop, whose Q output now goes low and thus disables the comparator. Disabling the comparator now sends its output high and the entire procedure, from crossing the theshold to the output returning high, has taken approximately 20nS.

The threshold comparator output, in going high has now clocked the second flip-flop and its Q output has enabled the zero crossing comparator. The zero crossing comparator now waits for the signal to go negative and as soon as it does, it sends its output low. The low output resets the second flip-flop which, by disabling the comparator, causes the comparator output to go high, a negative pulse having, thus, been formed. It is this pulse that starts the oscillators.

The circuits were built in accordance with the precautions outlined in section 3.2 and with the manufacturer's suggestion for pre-amplifier layout.

The circuits were tested by applying the same signal to both circuits but delayed by a small piece of coax. The pulses out were found to vary, within $\pm$1nS of each other (at the 3σ level) and this was considered acceptable. It was decided to save further testing until the receiver/processor was incorporated into the overall flowmeter.

The pulse widths were measured and found to be approximately 10nS @ 1.5v level.

The signal to noise ratio of the complete flowmeter circuit under operational conditions was found to be approximately 50 - 52 dB.

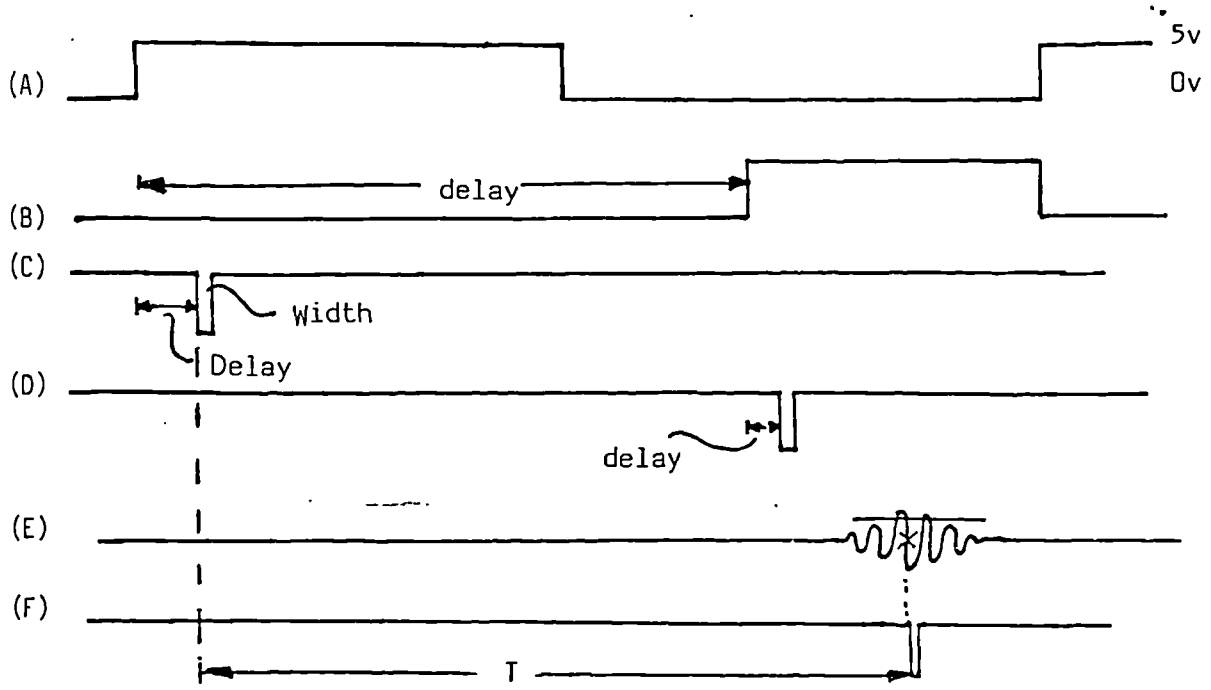

FIG 3.30
Timing diagram of the system's operation

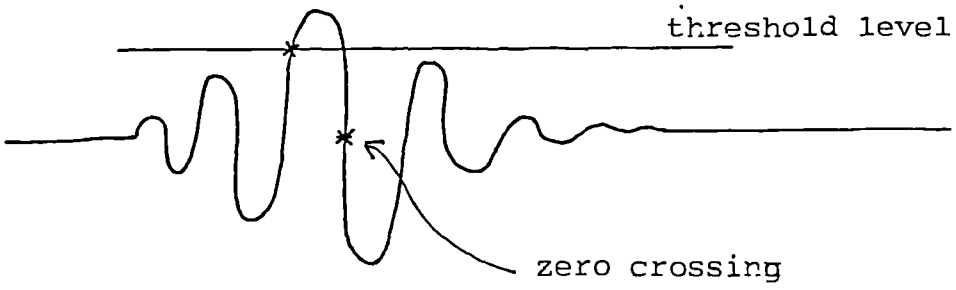

FIG 3.31
Received signal,threshold and zero crossing

3.6 The control and firing circuit

3.6.1 The firing circuit

The impedance of the transducer, seen by the firing circuit varies as a function of frequency, with a real impedance seen at the series resonant frequency of the motional arm.

The standard techniques applicable to exciting the transducer are avalanche transistor techniques, SCR's and charged inductor circuits. All of these methods producing a pulse like waveform (in the time domain) which has a wide frequency band from which the frequencies of interest are selected by the filtering action of the transducer.

Other methods of excitation include gating a sinusoidal waveform at the resonance frequency. This can be of a much lower signal level.

However, for the case of an ultrasonic flowmeter the level of pulse necessary to produce a good signal can be very low (order of volts) and since the signal may be logic generated this clearly is an advantage. It should be noted, though, that a higher firing signal, within the transducers limits, produces a higher received signal and thus requires less amplification. All things being equal the signal to noise ratio is improved over that of a low level firing voltage.

It was decided to produce a variable level signal, of the order of volts, with a high edge speed to produce the higher frequencies.

A suitable chip to meet the requirements is the SN 75471 dual peripheral AND driver. This chip has high current capability (up to 300MA) high voltage output capability (up to 70 volts, latch free) and medium speed switching (typically 10nS fall time).

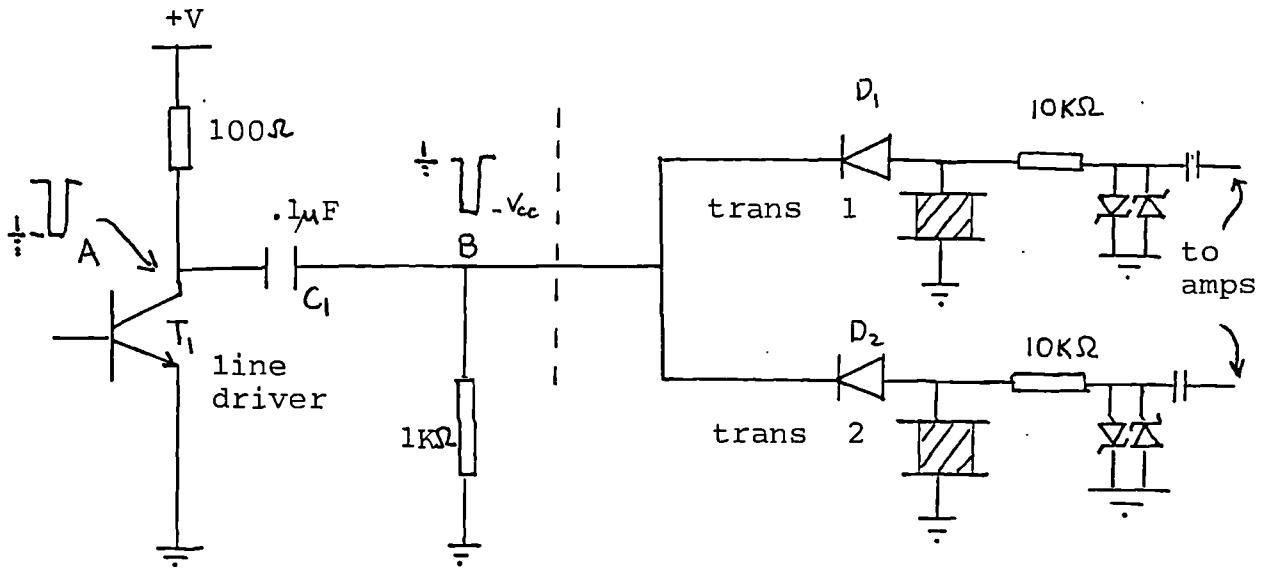

FIG 3.32
The *firing circuit design*

It was observed that by varying the pulse width to match that of the time taken for an accoustic pulse to travel across the crystal, a significant response was obtained. This chip was incorporated into the firing circuit as depicted in figure 3.32.

At switch on the capacitor C1 is charged up to Vcc volts (ie: T_1 is off). The transistor is switched on and point A rapidly falls to ground. Point B follows the rapid fall and falls to - Vcc. The diodes D1 and D2 conduct and current is drawn through the transducers, thus exciting the transducers.

When the transducers are in the receive mode the signal amplitude is insufficient to forward bias the diodes (V_f=.3-.4 volts) and the transducers simply see the 10KΩ and input resistance of the pre-amplifier.

A requirement for the diode isolator circuit is a need for high speed switching diodes and a resistor to allow reverse feed to remove the stored charge otherwise a large reverse diode current flows and the transducer firing signal is degraded. Essentially this means that the anode must follow the signal when switching off. A suitable value of resistance was found to be 1KΩ and the high speed diodes chosen were Schottky barrier diodes type HSCH1001 or 1N6263. These diodes have low turn off voltage and picasecond switching speed. The breakdown voltage of the diodes is rated at 60V.

The firing chip was enclosed with the control circuitry (described next) whilst the diode isolator was constructed in a screened unit with BNC connectors, for input and output.

3.6.2 The control circuit

The control circuit has to perform the timing functions described in the timing diagram. At present the input is derived from a signal source, but in a commercial instrument would be obtained from a microprocessor signal. The present generation of micoprocessors are

also unlikely to be able to perform the width control (directly) of the firing pulse (order of 200-500nS) and so some logic would still be required.

The circuitry chosen, for the timing, is shown in figure 3.33 and consists of three monostable multivibrator circuits (74LS122). These are standard circuits that perform a timing function, which is controlled by an external RC network.

Consider the timing diagram given in figure 3.30 and the circuit diagram given in figure 3.33.

The rising edge of the signal generator is used by two of the monostables to produce delays. Monostable IC1 responds to the signal after a delay, (controlled by RV1, R1 and C3) to produce a strobe signal. The strobe signal is used by the receiving/processing circuits to enable the comparator chip.

Monostable IC2 delays the start of the firing signal and this is controlled by RV2, R2 and C6. The output of this monostable circuit (IC2) feeds the input of IC3, the final monostable circuit. The output of monostable IC3 controls via RV3, R3 and C9 the width of the firing pulse and this is fed to the peripheral driver the SN 75471.

The start signal (used later for test purposes) is derived from the output of monstable IC3. This signal is thus one propagation delay before the firing signal, the propagation delay being approximately 30nS.

This circuit was built and tested and found to perform satisfactorily. It was then committed to PCB form and enclosed in a screened box with input and output via coaxial cabling.

COMPONENT LIST.	
COMP. NO.	DESCRIPTION.
IC1	74LS122
IC2	74LS122
IC3	74LS122
IC4	75471
R1	50kΩ
R2	10kΩ
R3	10kΩ
R4	100 Ω
RV1	50k pot
RV2	20k pot
RV3	20k pot
C1,C4,C7,C10,C13	22 µF Tant bead
C2,C5,C8,C11,C14	22nF Disc
C3	0·0033µF
C6	0·0022µF
C9	33pF
C12	0·1µF Disc

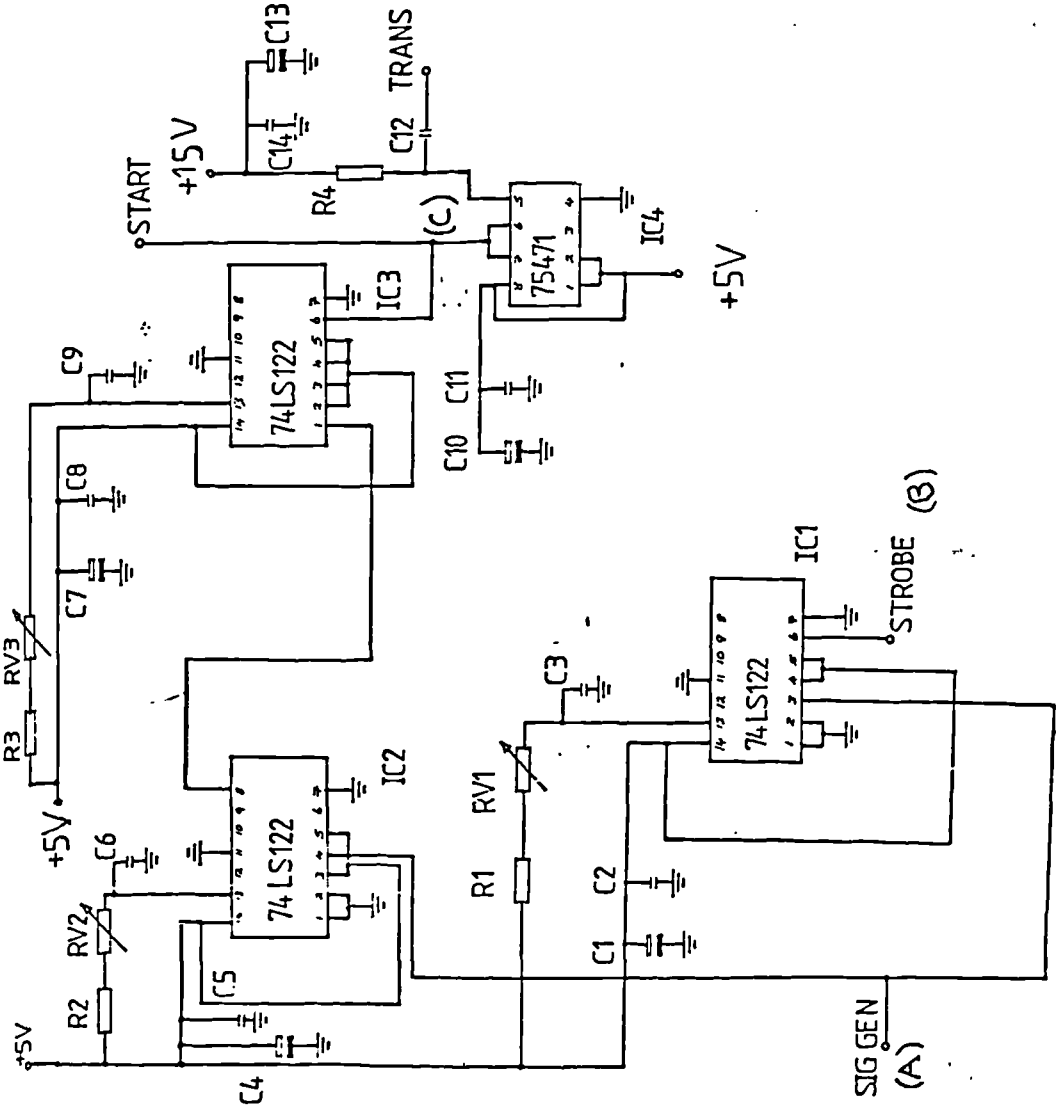

FIG 3.33
The control and firing circuit design

3.6.3 The set circuit

The set circuit is used to enable (or set) the flip-flop for the threshold detector.

The requirements for this circuit are not at all critical and in a commercial instrument this function would be performed by the microprocessor directly.

The requirements for this circuit are for a small width negative pulse for the set input of the flip-flop. Provided the width is greater than the requirements for set up and hold (approximately 6nS) the size is only limited by the reception of the incoming signal.

The set circuit is shown in figure 3.34 and simply consists of two monostable circuits IC1 abd IC2, (these are two of 74LS122). The first IC controls the length of delay from the rising edge of the strobe signal (by the use of RV1 and C3) and the second IC controls the width of the pulse. The width of output pulse is controlled by RV2 and C3.

This circuit was tested and found to work satisfactorily and was constructed in a screened box with input and output BNC connectors.

3.6.4 Auxilliary control circuitry

Because the unit was under manual control it was necessary to check single shot performance as well as averaging or multiple shot performance. It was decided therefore to design a unit that would allow either one pair of pulses through to the timing system or allow multiple pairs of pulses through.

It was decided to insert this circuitry between the reciever/processor units and the connections block to the timers. It was therefore necessary to ensure that any delay affected both lines similarly. This could only be achieved by gating the pulses through the same chip.

COMPONENT LIST.	
COMP.NO.	DESCRIPTION.
IC1	74LS122
IC2	74LS122
RV1	20K pot
RV2	20K pot
C1,C4	22μF Tant bead
C2,C5	22nF Disc
C3	0·0022μF
C6	33pF

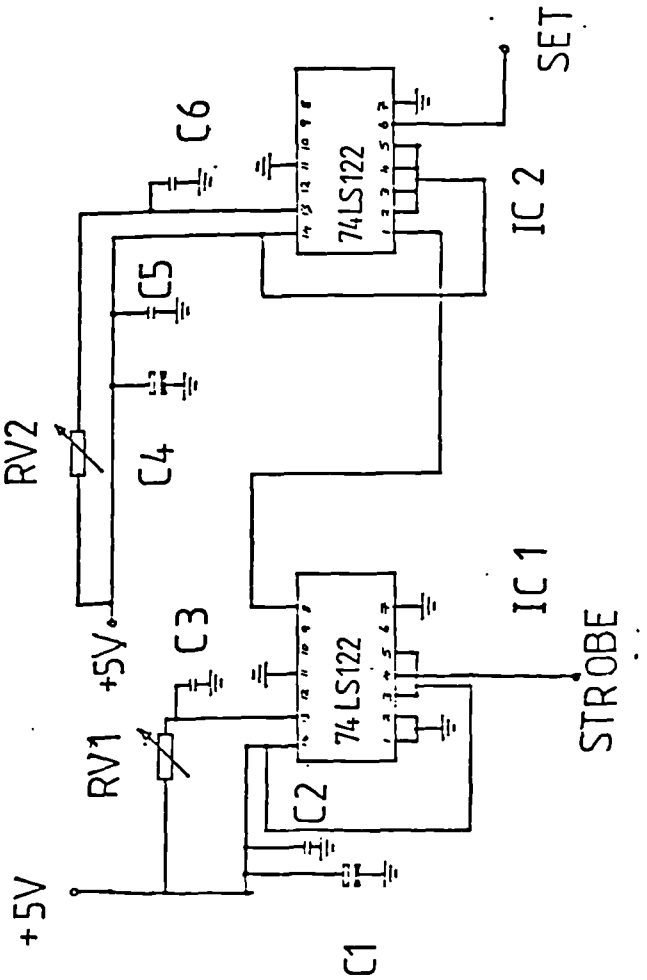

FIG 3.34
The set circuit design

The final circuit designed and used in the flowmeter is shown in figure 3.35 and consists of two NAND latches two NAND delays, a dual D-type flip-flop and a pair of OR gates. The NAND latch on the switch was found necessary after operations using a switch alone produced erroneous results.

Consider firstly the link in position 1 and the latch reset (A1 is high). Under these conditions latch B is permanently set so that B1 is low. When the clock goes high (and this is the L-Z signal derived from the receiver/processor) the low level signal is taken through the D-type and onto the input of both OR gates.

Pulses now arriving on the other leg of the OR gates are passed through (signal normally high but negative pulses). The output signal is fed back and resets the D type flip-flops, which because B1 is low are enabled on the next cycle and the next pair of pulses are allowed through.

In the single mode of operation the link is in position 2 and a change of level on A1 (from 0→1) causes a negative pulse from the NAND gate 2 to set the latch B and thus B1 goes low.

The clock signal (L-Z) now takes the zero through and the process is as described previously. Now however, when the flip-flop goes low to enable the OR gate, the NAND latch is reset (B1-high) and is not enabled further until the switch is used.

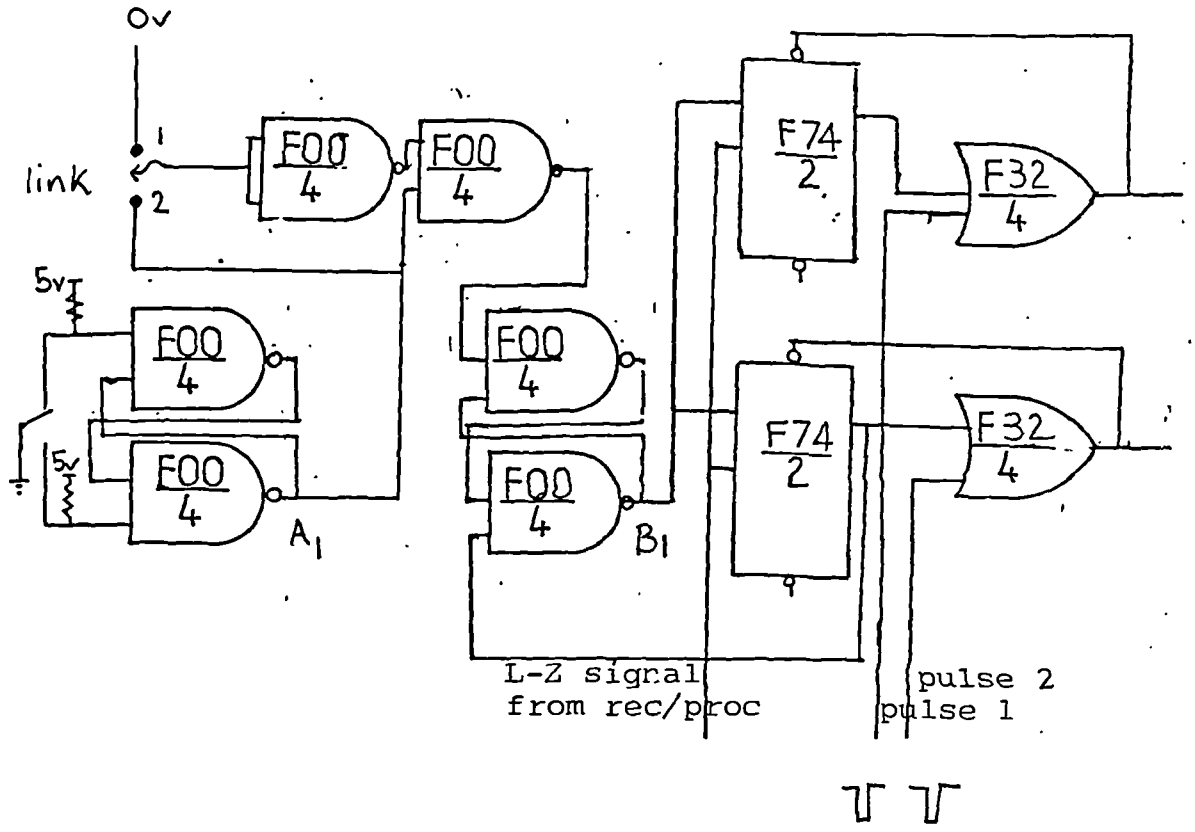

FIG 3.35
The multiple or single pulse selector circuit design

CHAPTER FOUR THE TRANSMISSION OF SOUND THROUGH PLATES

4.1 Introduction

The transmission and reflection of sound through plates is a very complicated subject. Rayleigh and Lamb were the first to investigate the modes of vibration of elastic plates and their models were based on infinite plates of infinite extent. Rayleigh's case was for shear-stress free plates and medium whilst Lamb investigated a plate in a shear-stress free medium.

In many practical situations the dimensions of the system under consideration are sufficiently large to warrant the use of infinite models and the purpose of this chapter is to show the development of an infinite model (in fact two models) which can be applied to the case of clamp on flowmeters.

The first section, section 4.2, reconsiders the case of a free plate and its associated dispersion curves (or modes of vibration). The solution to the transcendental equation relating the free modes to the frequency - thickness is discussed for the case when the modes velocity (C_L) is less than the longitudinal velocity (C_1) and the shear velocity (C_2) in the plate. This is the case of the external angle of incident sound being greater than the second critical angle (i.e. for shear waves). It will be shown that transmission of sound is still possible (for a frequency - thickness product below a certain value) by coincidence with a natural mode of vibration of the plate, either the S_o mode (symmetric) or the A_o (antisymmetric) mode. The relationship between dispersion and transmission curves will be discussed.

For the case of a clamp-on flowmeter the main area of interest is in good transmission with as steep an angle as possible in the fluid. This then relieves the stringent timing requirements and since the relationship between the transducer material and the fluid (in terms of refraction of sound) still obeys Snell's Law, there is clearly an advantage in working at a steep external angle.

Two models are produced for predicting the transmission through plates and these are combined to produce an overall transmission model to yield a total transmission coefficient. The models are checked by applying them to the case of water/plate/water and comparing the results of this model to that of another author, Freedman.

The relationship between dispersion curves and transmision curves is shown clearly.

4.2 Dispersion curves for a free plate

It will be recalled from the introduction that the dispersion equation for free waves in a plate is:

$$\frac{\tan\left(\left(\frac{\omega}{c_1}\right)^2-\xi^2\right)^{1/2}b}{\tan\left(\left(\frac{\omega}{c_1}\right)^2-\xi^2\right)^{1/2}b}+\left\{\frac{4\left(\left(\frac{\omega}{c_1}\right)^2-\xi^2\right)^{1/2}\left(\left(\frac{\omega}{c_2}\right)^2-\xi^2\right)^{1/2}\xi^2}{\left(2\xi^2-\left(\frac{\omega}{c_2}\right)^2\right)^2}\right\}^{\pm 1}=0 \qquad 4.1$$

where the index takes a value of

+1 for symmetric modes
-1 for antisymmetric modes

and

ξ = Wavenumber $\left(\frac{\omega}{c_1}\right)$
ω = Radian frequency
C_1 = Longitudinal wave speed in the plate
C_2 = shear wave speed in the plate
b = thickness of plate

This equation is valid for the region $C_L > C_2, C_1$ i.e. below both critical angles. However, interest is high in the region $C_L < C_2 < C_1$ which is above the critical angles. The reason for this interest stems from the improved distance in the fluid brought about by a steeper transducer angle. The improvement in this distance reduces the stringent requirements needed for the timing system of a clamp-on flowmeter.

It was decided therefore to produce dispersion curves for the region $C_L < C_2 < C_1$ and the equation used was that of 4.1, but now with the trigonometric tangent functions replaced by the hyperbolic tanh since the terms of form $\left(\left(\frac{\omega}{c}\right)^2 - \xi^2\right)^{1/2}$ now become complex.

The equation in real terms is therefore:-

$$\frac{\tanh\left(\xi^2-\left(\frac{\omega}{C_2}\right)^2\right)^{1/2} b}{\tanh\left(\xi^2-\left(\frac{\omega}{C_1}\right)^2\right)^{1/2} b} = \left\{\frac{4\left(\xi-\left(\frac{\omega}{C_1}\right)^2\right)^{1/2}\left(\xi-\left(\frac{\omega}{C_2}\right)^2\right)^{1/2}\xi^2}{\left(2\xi^2-\left(\frac{\omega}{C_2}\right)^2\right)^2}\right\} \quad 4.2$$

where the index and terms carry the same meanings as previously given.

A small interactive, iterative program was written to solve numerically this transcendental equation (program name RAY 2,3). The results of the program were then used to produce a plot on a HP plotter.

It was discussed earlier that the reason for this work was to improve the understanding of the transmission through plates and this impetus came from a commercial flowmeter that appeared to operate under the Lamb mode of operation and which had been used in previous work (137). The transducer arrangement for this commercial instrument was X-rayed and it was this X-ray that showed up the large angle of the transducer position (approximately 58°). This instrument had been obtained for a particular pipe and it was felt therefore, that the same data should be used in the programs RAY 2,3.

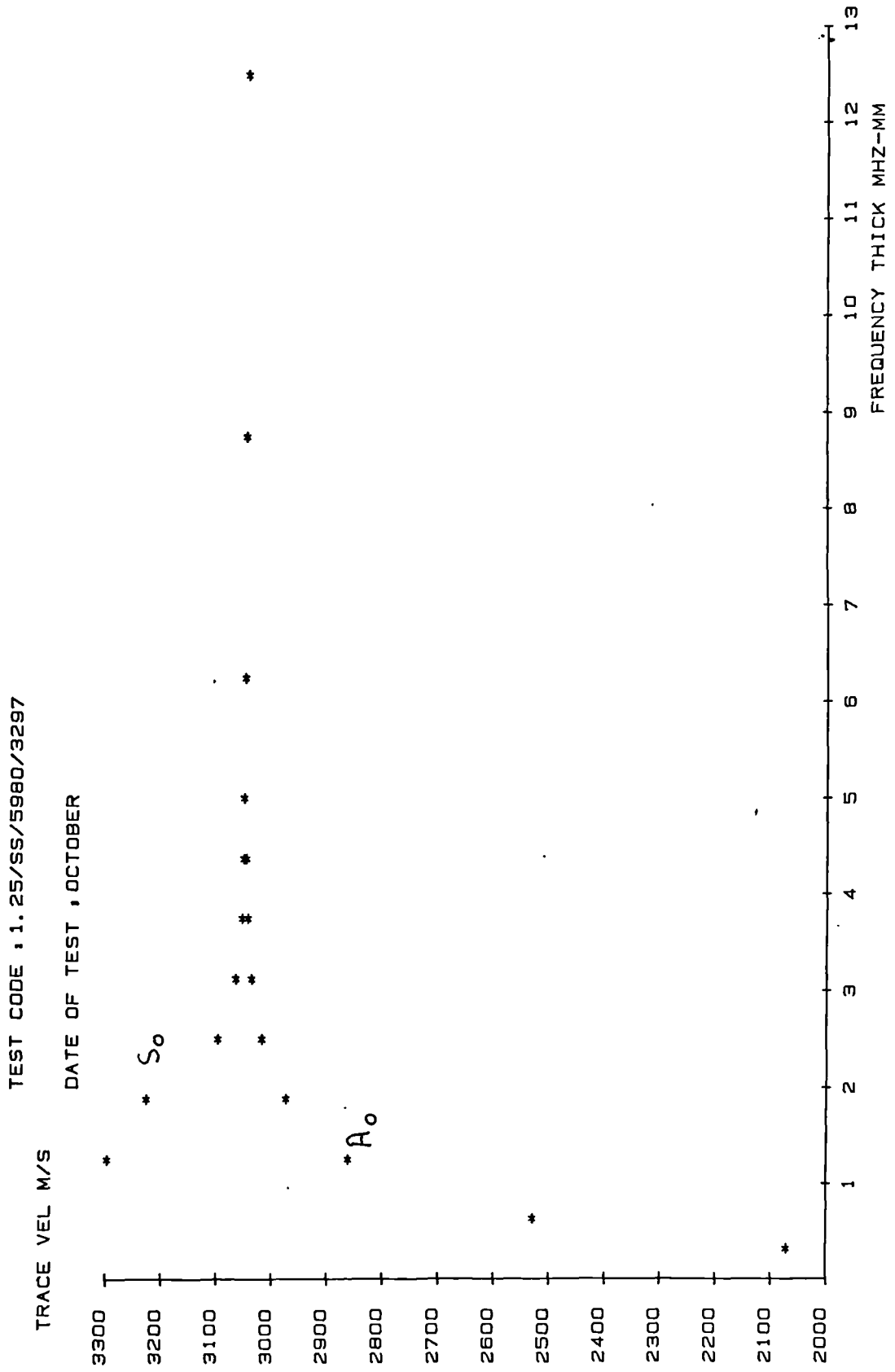

FIG 4.1
Plot of trace velocity v. frequency thickness (s/s plate 3 mm)

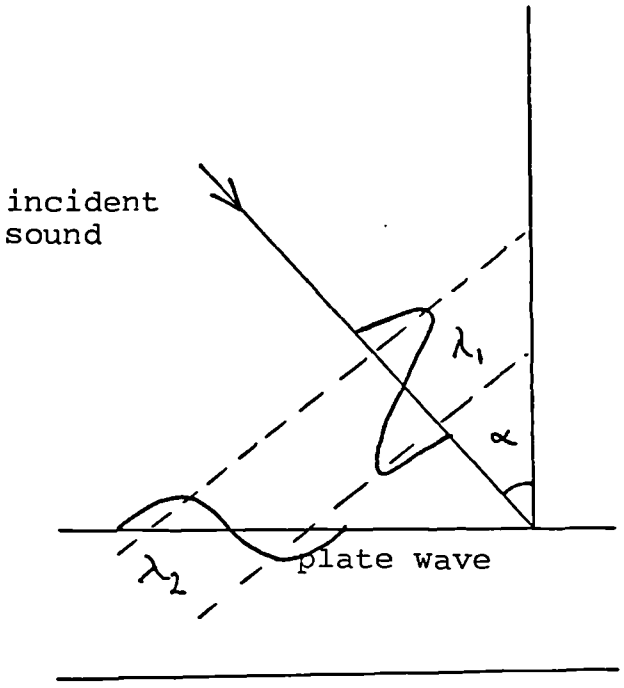

$$\lambda_1 = \frac{C_1}{f} \qquad \lambda_2 = \frac{C_2}{f}$$

$$C_1 = C_2 \sin \alpha$$

FIG 4.2
Phase relationship between incident and plate waves

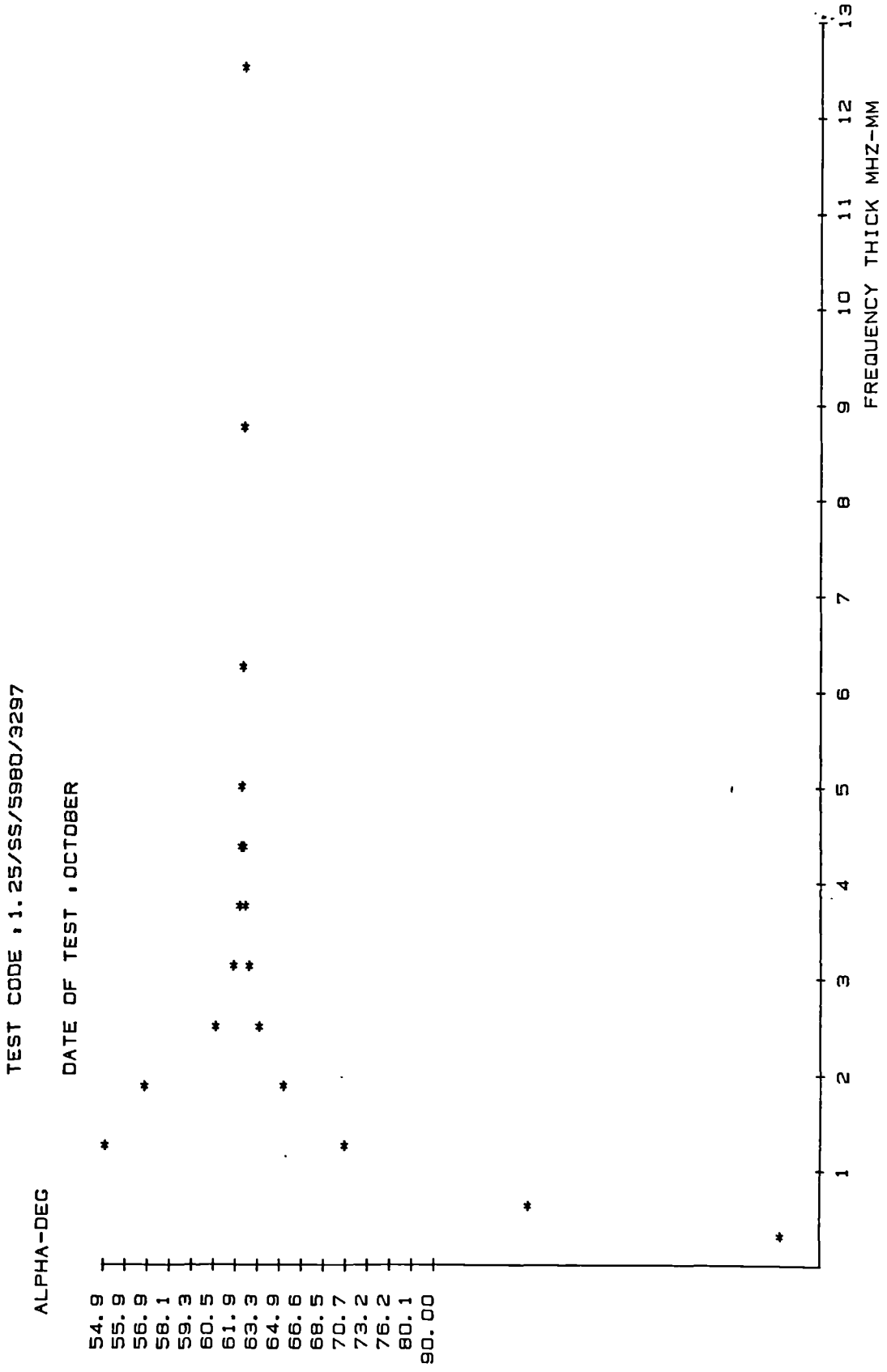

FIG 4.3
Plot of transducer angle v. frequency thickness (s/s plate 3 mm)

This application data supplied was,

thickness of wall = 3mm
material = stainless steel, grade 316S

The additional information required by the program was,

Frequency = 1.25 MHz
Long wave speed = 5980 m/s
Shear wave speed = 3279 m/s

The program was run using the supplied data and when the curves are plotted the result is as shown in figure 4.1.

There are two curves displayed and these are marked as the A_o mode and S_o mode. The curves are seen to combine at approximately 4MHz mm. The A_o mode has a curve that is seen to produce lower trace velocities with smaller F x D products. However, there is a cut-off value of trace velocity at which the angle of the incident sound is at 90° to the plate. This can be seen more easily from figure 4.2. The incident sound wavelength has to match the trace wavelength, to excite the mode, through the angle α. Thus when the incident sound is at 90° the waves are superimposed and the limiting condition is the velocity of waves in the block. For the case of perspex the velocity is 2700m/s and this therefore corresponds to the lowest value of trace velocity.

For the case of a perspex block on a pipe wall the corresponding angle of incidence would be as shown in figure 4.3. This is now a plot of the dispersion curves but with incident angle versus frequency-thickness.

The critical angle for shear waves in this condition is approximately 54.9^{o} which results in a trace velocity of approximately 3297 m/s which is the velocity of shear waves in the plate.

Of more interest to clamp-on flowmeters is the angle that the beam makes within the fluid. This angle can be plotted and is shown in figure 4.4, against frequency thickness. Note that this is the angle with repect to the pipe wall and not to the normal. It can be seen that the internal angle varies slowly with the transducer angle.

In all figures, although the S_o mode appears to stop it does infact continue across the line corresponding to the 2nd critical angle and then levels off and remains at a constant value for reducing F x D, down to zero.

Further inspection of the curves show that the curves settle to a value of trace velocity of 3049 m/s. This corresponds to the Rayleigh velocity (the velocity of surface waves on a half space) which is given as 3048 m/s (Kaye & Laby). Therefore as far as the sound is concerned a plate of frequency-thickness greater than approximately 4MHz mm appears as a half space. Rayleigh waves decay exponentially into the plate.

Throughout the preceeding argument it has been assumed that the free plate modes differ little from the modes of a plate that is ligthtly loaded. This is shown to be the case (see for example Freedman) and is the topic of the next section.

Complete curves are given by various authors, (eg. Freedman or, Fiorito, Madigosky and Uberall) for the case of vacuum/plate/vacuum and for the case of water/plate/water.

4.3. The transmission of sound through plates and its application to clamp on ultrasonic flowmeters

It was decided to investigate the transmission of sound through plates with the object of producing a transmission model for clamp-on flowmeters. This in turn will, it is hoped, produce more accurate flowmetering by positioning the transducers at an optimum angle.

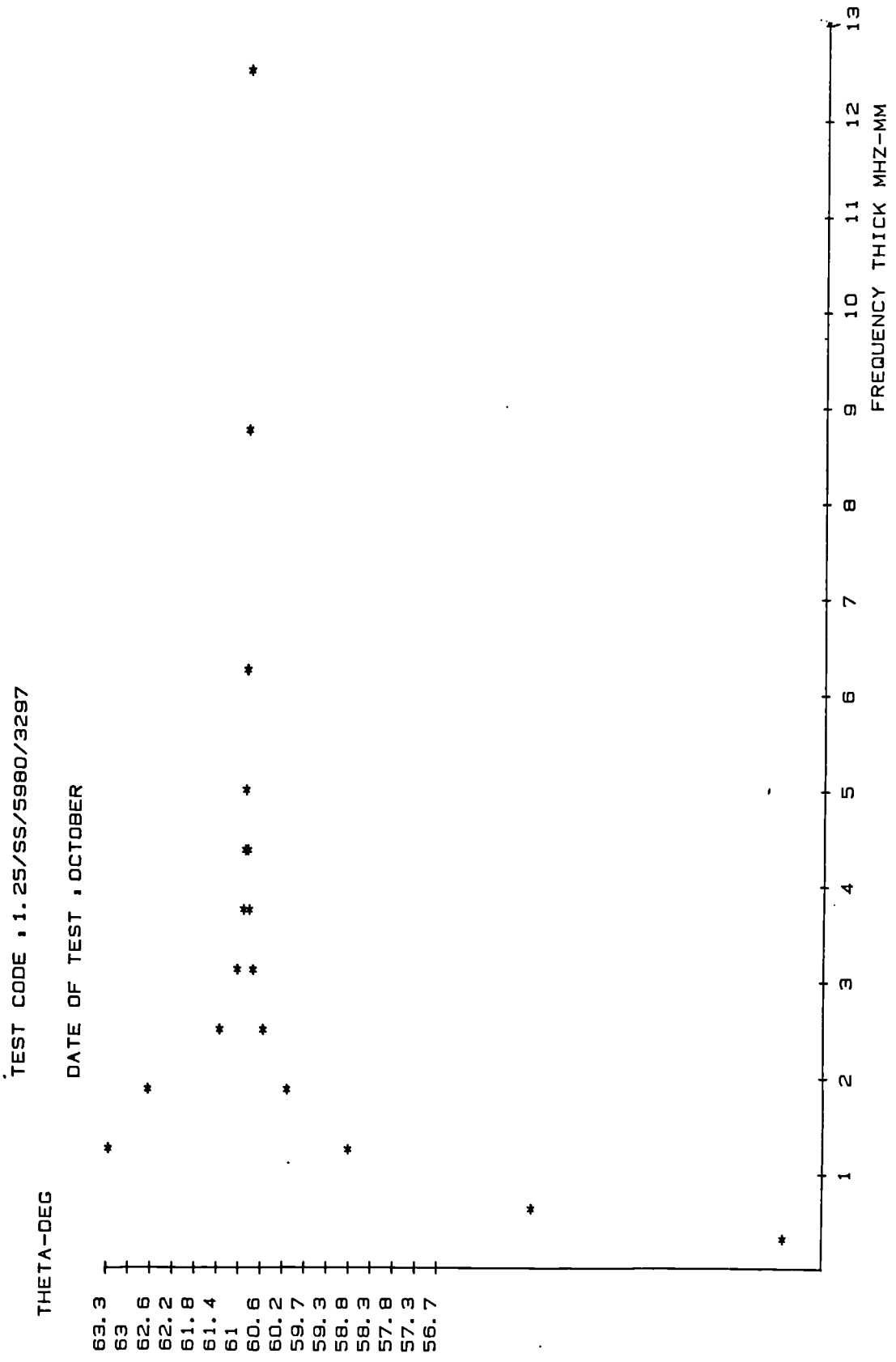

FIG 4.4
Plot of fluid angle v. frequency thickness (s/s plate 3 mm)

If an optimum position can be found then this will have benefits with regard to smaller amplification or firing levels and thus improved signal to noise ratios.

A shematic diagram of a clamp-on ultrasonic flowmeter is depicted in figure 4.5. Of interest is the ratio of received sound to transmitted sound which is an important quantity in the design of the head unit.

If the reflected wave in the fluid can be excluded two simple models can be produced. Provided the internal bore is sufficiently large the returning reflection can be considered negligible and therefore ignored (at least to a first approximation). The practical operation of the flowmeter i.e. with a narrowbeam and under pulse operation also rules out a 'total' model.

Hence suitable models are:-

(i) a solid/plate/fluid model
(ii) a fluid/plate/solid model

Both models are for flat, infinite plates and half spaces. A literature search provided no ready solutions for the above cases.

Before analysing in detail the solutions to the above models, it is worth while considering on a qualitative basis the effect of varying the angle of incidence.

Consider the angle to be at 0° and slowly rotated. As the angle increases a first critical angle is reached at which the plate longitudinal waves become inhomogeneous i.e. travelling on the surface and confined to within approximately one wavelength into the medium (decaying exponentially). When a plate is many wavelengths thick transport of energy across the plate is then principally due to the shear wave.

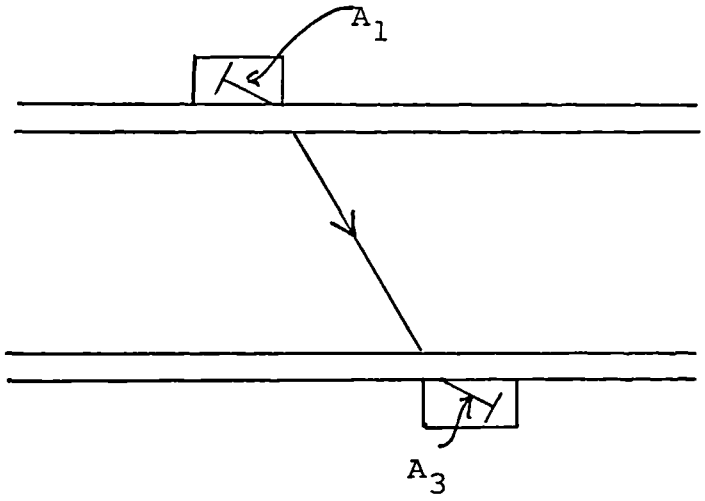

FIG 4.5
Schematic diagram of a clamp-on flowmeter

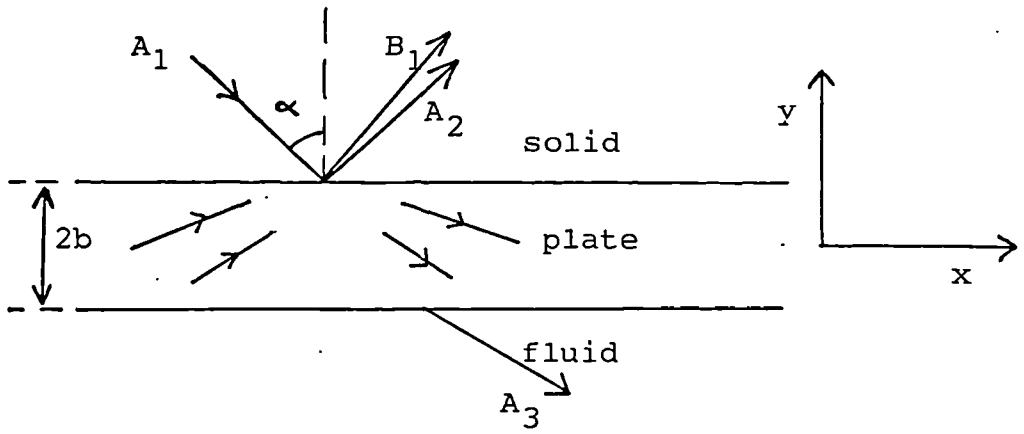

FIG 4.6
Solid/plate/fluid structure with incident wave A_1

Further rotation of the angle results in a second critical angle at which the shear waves now become inhomogeneous. Now if the plate is very thick there is no energy transport mechanism and to all intents and purposes the plate looks like a half space.

Through all angles from normal incidence to beyond the critical angle, plate waves are excited and transmission is high even when working beyond the critical angle for shear waves, provided that the plate is not too thick. If the plate is thick then beyond this critical angle only a Rayleigh wave (a surface wave) and not a Lamb wave (or plate wave) is excited.

4.3.1. The solid/plate/fluid model

The first model chosen for analysis is depicted in figure 4.6. It consists of two half spaces separated by an isotropic, elastic, solid plate of thickness 2b.

An incident, infinite, longitudinal wave of frequency ω impinges upon the plate making an angle α with the normal. This wave gives rise, via mode conversion, to two further waves in the solid, a longitudinal and a shear wave. Four waves are possible in the plate (two longitudinal incident and reflected and two shear waves) and a final wave, longitudinal, is in the fluid.

The model is 2 dimensional and thus allows us to set

$$U_z = \frac{\partial}{\partial z} = 0 \qquad 4.3$$

By Helmholtzs theorem the displacement vector $\underline{U}$ can be written in terms of a scalar potential Φ (longitudinal wave potential) and a vector potential $\underline{H}$ (shear wave potential).

Thus:

$$\underline{u} = \nabla \Phi + \nabla \times \underline{H} \qquad 4.4$$

In terms of x and y components

$$u_x = \frac{\partial \Phi}{\partial x} + \frac{\partial H_3}{\partial y} \qquad 4.5$$

and

$$u_y = \frac{\partial \Phi}{\partial y} - \frac{\partial H_3}{\partial x} \qquad 4.6$$

The wave equations are:

$$\nabla^2 \Phi = \frac{1}{c_1^2} \frac{\partial^2 \Phi}{\partial t^2} \qquad 4.7$$

and

$$\nabla^2 H_3 = \frac{1}{c_1^2} \frac{\partial^2 H_3}{\partial t^2} \qquad 4.8$$

where

c_1 = longitudinal wavespeed = $\sqrt{\frac{\lambda+2\mu}{\rho}}$

and

c_2 = shear wave speed = $\sqrt{\frac{\mu}{\rho}}$

λ and μ are the Lamé constants of the elastic medium and ρ is the density. For a medium supporting longitudinal waves only the constant μ is set equal to zero.

The potential in the solid is assumed to be a wave travelling between the x direction of the form,

$$\Phi = f(y)\, e^{i(\xi x - \omega t)} \qquad 4.9$$

Substitution in the wave equation

$$\frac{\partial^2 \Phi}{\partial x^2} + \frac{\partial^2 \Phi}{\partial y^2} = \frac{1}{c^2} \frac{\partial^2 \Phi}{\partial t^2} \qquad 4.10$$

results in an ordinary 2nd order differential equation

$$\frac{d^2 f(y)}{dy^2} + \alpha^2 f(y) = 0 \qquad 4.11$$

where

$$\alpha^2 = \left(\left(\frac{\omega}{c_1} \right)^2 - \xi^2 \right) \qquad 4.12$$

Solutions of the form $e^{\pm i \alpha y}$ with arbitrary constants satisfy this equation. Thus the solution is given by

$$\Phi = A_1 e^{i(\xi x - \alpha y - \omega t)} + A_2 e^{i(\xi x + \alpha y - \omega t)} \qquad 4.13$$

Which is the longitudinal potential in the solid. A_1 and A_2 are arbitrary constants and correspond to the amplitude of the longitudinal waves. The direction of the waves is given by the spatial component of the exponent, thus $(\xi x - \alpha y)$ corresponds to the wave travelling in the x direction and negative y direction, (ξ and α assumed positive).

In a similar manner the shear potential can be found.

Thus assuming a potential of the form:

$$H_3 = i\,h(y)\,e^{i(\varepsilon x-\omega t)} \qquad 4.14$$

and solving the wave equation results in,

$$H_3 = i\left\{B_1 e^{i(\varepsilon x-\beta y-\omega t)} + B_2 e^{i(\varepsilon x+\beta y-\omega t)}\right\} \qquad 4.15$$

where i has been included for later convenience.

In this equation

$$\beta^2 = \left(\left(\frac{\omega}{c_2}\right)^2 - \varepsilon^2\right) \qquad 4.16$$

The model only contains an incident longitudinal wave thus the coefficient $B_1 = 0$ and the sound fields in the solid become,

for longitudinal waves;

$$\Phi_s = A_1 e^{i(\varepsilon x-\alpha y-\omega t)} + A_2 e^{i(\varepsilon x+\alpha y-\omega t)} \qquad 4.17$$

and

for shear waves

$$H_{3s} = i\left(B_2 e^{i(\varepsilon x+\beta y-\omega t)}\right) \qquad 4.18$$

Similarly the potential in the fluid is found to be

$$\Phi_f = A_3 e^{i(\varepsilon x - \alpha_f y - \omega t)} \qquad 4.19$$

where

$$\alpha_f^2 = \left(\left(\frac{\omega}{c_f}\right)^2 - \varepsilon^2\right) \qquad 4.20$$

The potentials in the plate are given by

$$\Phi_p = G_1 e^{i(\varepsilon x - \gamma y - \omega t)} + G_2 e^{i(\varepsilon x + \gamma y - \omega t)} \qquad 4.21$$

and

$$H_{3p} = i\left\{D_1 e^{i(\varepsilon x - \Omega y - \omega t)} + D_2 e^{i(\varepsilon x + \Omega y - \omega t)}\right\} \qquad 4.22$$

where

$$\gamma^2 = \left(\left(\frac{\omega}{c_{1p}}\right)^2 - \varepsilon^2\right) \quad \text{and} \quad \Omega^2 = \left(\left(\frac{\omega}{c_{4p}}\right)^2 - \varepsilon^2\right) \qquad 4.23$$

Therefore for the three media a set of potentials that describe the sound fields, have been found.

The potentials can now be converted to displacements by using equations 4.5 and 4.6. For brevity the factor $e^{i(\varepsilon x - \omega t)}$ will be omitted.

Hence for the solid

$$u_x = i\xi(A_1 e^{-i\alpha y} + A_2 e^{i\alpha y}) - \beta(B_2 e^{i\beta y}) \qquad 4.24$$

and

$$u_y = i\alpha(-A_1 e^{-i\alpha y} + A_2 e^{i\alpha y}) + \xi(B_2 e^{i\beta y}) \qquad 4.25$$

and for the fluid;

$$u_{x_f} = i\xi A_3 e^{-i\alpha_f y} \qquad 4.26$$

and

$$u_{y_f} = -i\alpha_f A_3 e^{-i\alpha_f y} \qquad 4.27$$

and for the plate;

$$u_{x_p} = i\xi(G_1 e^{-i\gamma y} + G_2 e^{i\gamma y}) + \Omega(D_1 e^{-i\Omega y} - D_2 e^{i\Omega y}) \qquad 4.28$$

and

$$u_{y_p} = i\gamma(-G_1 e^{-i\gamma y} + G_2 e^{i\gamma y}) + \xi(D_1 e^{-i\Omega y} + D_2 e^{i\Omega y}) \qquad 4.29$$

At this stage the boundary conditions need to be specified and it is important to consider the conditions under which a clamp-on flowmeter would operate. Most clamp-on flowmeters are of the portable kind which means that the transducers would be attached to the pipe using a non-setting coupling compound. Under this condition, of transverse slip, the stress τ_{xy} would be zero, i.e. no tangential force would

be communicated across the interface. It is assumed that the couplant forms an infinitely thin strip. The full boundary conditions would be, therefore,

for the top surface,

$$y = b$$

$$U_{y_{solid}} = U_{y_{plate}} \qquad \text{ie: normal displacement is continuous}$$

$$\tau_{yy_{solid}} = \tau_{yy_{plate}} \qquad \text{ie: normal stress is continuous}$$

and

$$\tau_{xy_{solid}} = \tau_{xy_{plate}} = 0 \qquad \text{ie: no tangential stress}$$

At the bottom surface of the plate

$$y = -b$$

$$U_{y_{plate}} = U_{y_{fluid}}$$

$$\tau_{yy_{plate}} = \tau_{yy_{fluid}}$$

and

$$\tau_{xy_{plate}} = 0 \qquad 4.30$$

The stresses τ_{xy} in the plate and solid and τ_{yy} in the plate, solid and fluid need to be calculated. The stress tensor is (from Graff) given by,

$$\tau_{ij} = \lambda \varepsilon_{kk} \delta_{ij} + 2\mu \varepsilon_{ij} \qquad 4.31$$

where

$$\varepsilon_{ij} = \tfrac{1}{2}(u_{i,j} + u_{j,i}) \qquad 4.32$$

and this is used to calculate the stresses in the media, thus:-
in the solid;

$$\tau_{yy} = \rho C_1^2 \left[i\xi u_x - \alpha^2 (A_1 e^{-i\alpha y} + A_2 e^{i\alpha y}) + i\beta\xi (B_2 e^{i\beta y}) \right] - 2C_2^2 \rho i \xi u_x \qquad 4.33$$

and

$$\tau_{xy} = \rho C_2^2 \left[-\xi\alpha (-A_1 e^{-i\alpha y} + A_2 e^{i\alpha y}) - i\beta^2 (B_2 e^{i\beta y}) + i\xi u_y \right] \qquad 4.34$$

in the fluid:-

$$\tau_{yy} = \rho_f C_f^2 \left[-(\xi^2 + \alpha_f^2) A_3 e^{-i\alpha_f y} \right] \qquad 4.35$$

and in the plate

$$\tau_{yy} = \rho_p C_{1p}^2 \left[i\xi u_{xp} - \gamma^2 (G_1 e^{-i\gamma y} + G_2 e^{i\gamma y}) + i\Omega\xi (-D_1 e^{-i\Omega y} + D_2 e^{i\Omega y}) \right] - 2C_{2p}^2 \rho_p i \xi u_{xp} \qquad 4.36$$

and

$$\tau_{xy} = \rho_p C_{2p}^2 \left[-\gamma\xi (G_1 e^{-i\gamma y} + G_2 e^{i\gamma y}) + i\Omega^2 (-D_1 e^{-i\Omega y} - D_2 e^{i\Omega y}) + i\xi u_{yp} \right] \qquad 4.37$$

Fitting the boundary conditions for the displacements and stress results in a set of seven simulataneous equations with 8 unknowns. Therefore the equations can, of course, only be solved in ratiometric terms.

The resulting set of equations is given below in 4.38 in matrix form:-

It was decided to solve the equations numerically using the Institute's VAX 11/780 computer. A fortran program was written which called a suitable library subroutine (NAG LIBRARY ROUTINE F04ADF). This is a routine for solving complex simultaneous linear equations.

The routine solves for x (of Ax=B) using Crouts factorisation with partial pivoting on the elements of A and then back substitution (for a fuller description of this technique see, for example Goult et al (138)).

Initial attempts at trying to solve the matrix failed because the matrix was ill-conditioned (see Goult et al, loc sit), which essentially means that the elements of A were too large. The matrix was conditioned and is given in its new form in 4.39.

After this conditioning the program ran successfully and it was decided to test the results produced.

Two tests were considered, the first test was to establish an energy balance equation. This test would establish that the energy in the reflected beams and transmitted beam matched that of the incident beam. It is assumed that the plate is lossless and that no energy is absorbed or given out.

The second test was to reduce the model to that of a fluid/plate/fluid case and to check the results against documented cases, so forming a comparison. As an intermediate step it was decided to construct a fluid/plate/fluid case exactly which would form a direct comparison and then to check the degenerated solid/plate/fluid case against this.

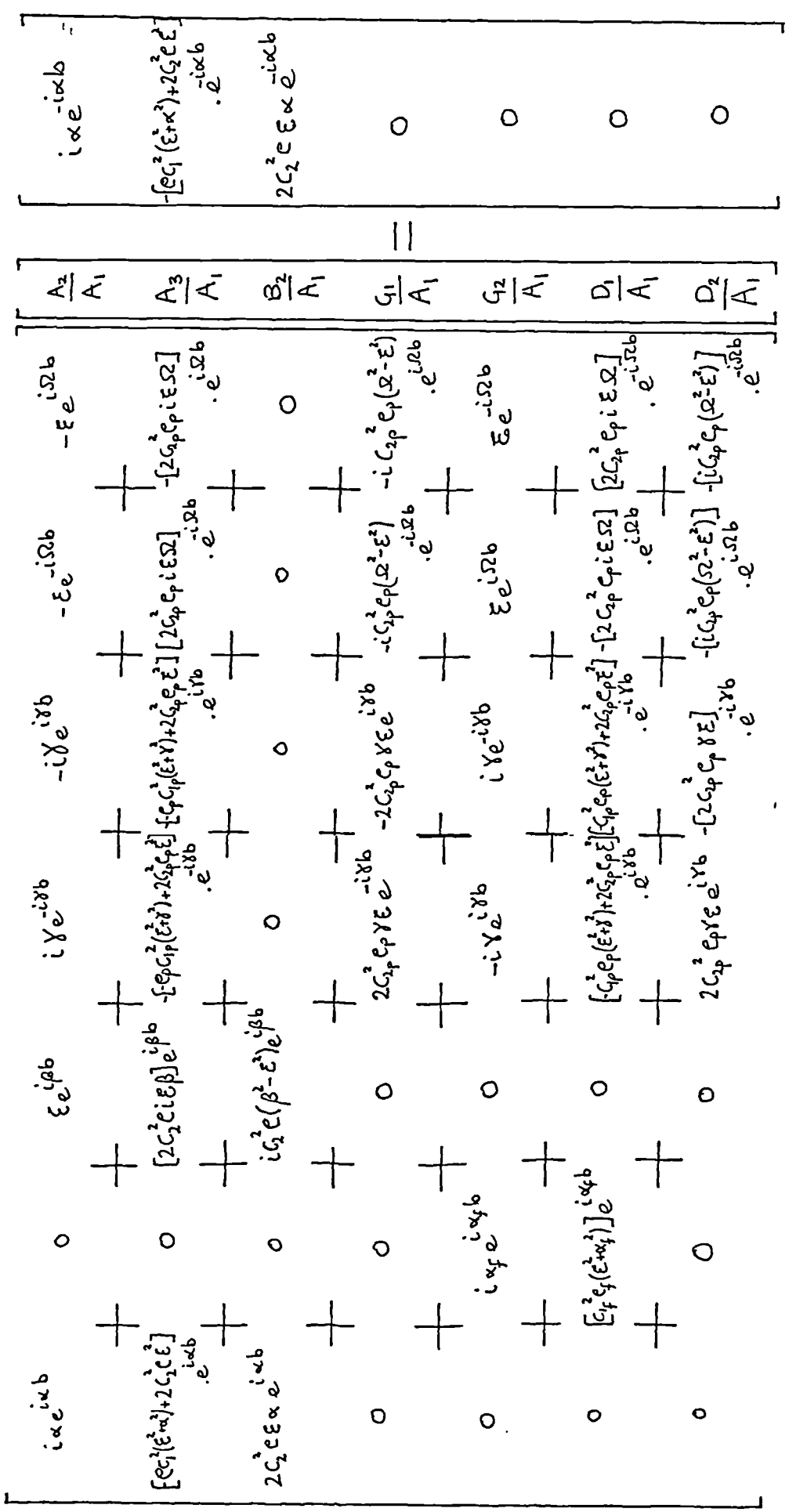

matrix equation 4.38

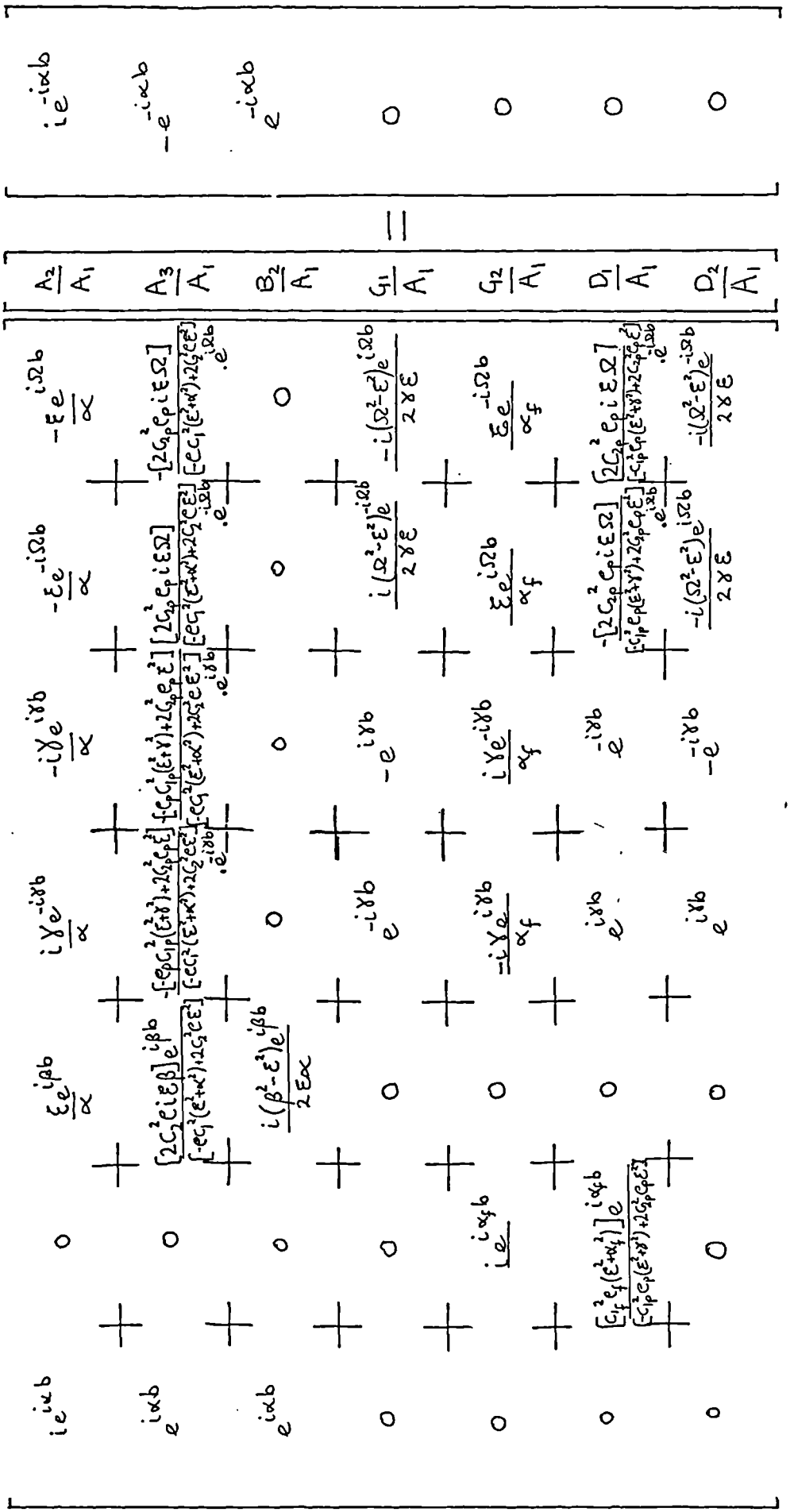

matrix equation 4.39

4.3.1.1 The Energy Balance

The energy in a wave is the sum of its kinetic and its potential energies. The total instantaneous energy E is given in any standard text, as

$$E = \tfrac{1}{2} \rho_0 \left(\dot{u}^2 + \frac{P^2}{\rho_0^2 c^2} \right) V_0 \quad \text{joules} \qquad 4.40$$

where

ρ_0 = density
V_0 = volume, chosen small enough such that u can be considered constant
$\dot{u}$ = particle velocity
p = pressure

The energy density is $\epsilon = \frac{E}{V_0}$ and using $P = \rho_0 c \dot{u}$ where

$\rho_0 c = Z$, the acoustic impedance, the energy density is found to be

$$\epsilon = \rho_0 \dot{u}^2 \qquad \text{joules}/m^3 \qquad 4.41$$

Since $\dot{u}$ is a function of time, a time average must be obtained. Carrying out the required integration the average energy density is found to be, for an incident wave of amplitude A_1 of potential and wave number K,

$$\bar{\epsilon} = \tfrac{1}{2} \rho_0 |A_1|^2 K^2 \omega^2 \qquad 4.42$$

It is more convenient to consider the intensity which is defined as the mean rate of flow of energy through a unit area normal to the direction of propagation, ie: $\frac{dE}{dt}$

If the propagation velocity is C then the flow is

$$I = \bar{\epsilon} C = \tfrac{1}{2} \rho_0 c |A_1|^2 K^2 \omega^2 \quad \text{watts/m}^2 \qquad 4.43$$

for longitudinal waves.

In a similar manner the intensity of shear waves is found to be

$$I = \tfrac{1}{2} \rho_0 C_2 |B|^2 K_2^2 \omega^2 \quad \text{watts/m}^2 \qquad 4.44$$

where the suffix 2 refers to shear waves.

It is now necessary to consider the effective areas of the beams in the energy balance. Consider figure 4.7 and a wave of unit area making an angle Θ with the normal. Consider also a reflected wave.

It can be seen that the ratio of areas, $\frac{A}{1} = \frac{\beta}{K_2} \frac{K_1}{\alpha}$ 4.45

since $\beta = K_2 \cos \Theta_2$

and $\alpha = K_1 \cos \Theta_1$

It can also be shown that the fluid long wave area is given by

$$\frac{\alpha_f}{\alpha} \cdot \frac{K_f}{K} \qquad 4.46$$

Thus a system of waves has an energy balance given by

Energy in	=	Energy in	+	Energy in	+	Energy in
Incident Longwave		Reflected Shear		Reflected long		Transmitted long

$$\tfrac{1}{2} \rho_0 C_L K_L^2 |A_1|^2 = \tfrac{1}{2} \rho_0 C_2 K_2 |B_2|^2 \frac{\beta}{\alpha} \cdot \frac{K_L}{K_2} + \tfrac{1}{2} \rho_0 C_L K_L^2 |A_2|^2 + \tfrac{1}{2} \rho_f C_f K_{fL}^2 |A_3|^2 \cdot \frac{\alpha_f}{\alpha} \frac{K_L}{K_{fL}} \qquad 4.47$$

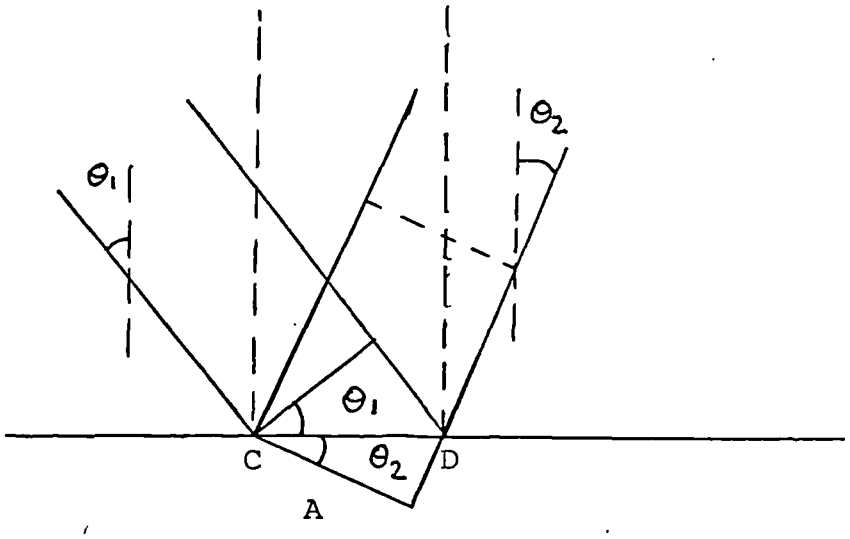

FIG 4.7
Energies in waves

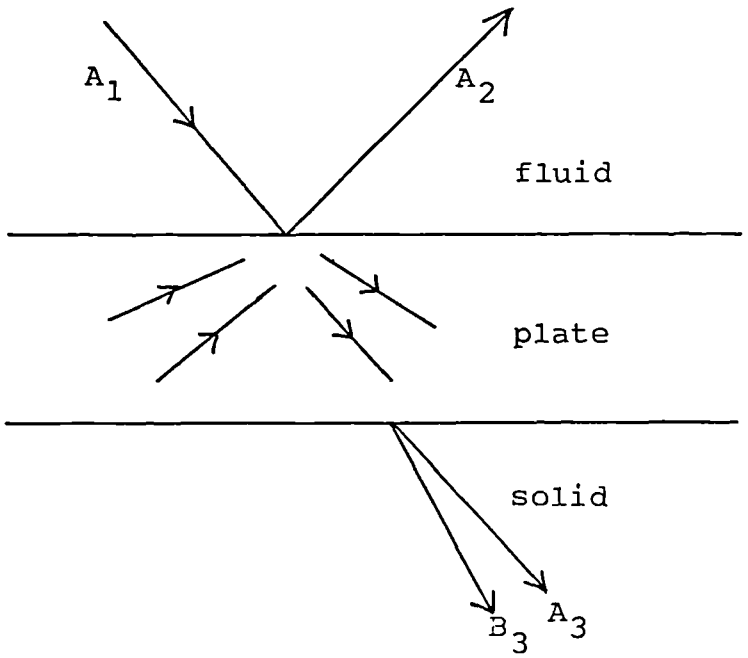

FIG 4.8
Fluid/plate/solid structure with incident wave A_1

and rearranging and reducing the equation, results in,

$$1 = \frac{\beta}{\alpha}\left|\frac{B_2}{A_1}\right|^2 + \left|\frac{A_2}{A_1}\right|^2 + \frac{\rho_f}{\rho_0}\frac{\alpha_f}{\alpha}\left|\frac{A_3}{A_1}\right|^2 \qquad 4.48$$

In the transmission programs the variable assigned to the energy balance is ENBAL (this is the RHS of previous equation) and thus should always read unity.

4.3.2 The fluid/plate/solid model

The model for this case is depicted in figure 4.8.

The incident wave (A_1), in this case, gives rise to a reflected wave in the fluid, four waves in the plate and two waves in the solid, a shear and a longitudinal wave.

In a similar manner to the previous case, assigning potentials and solving the wave equations results in a set of potentials for the three media.

These are:-

in the fluid,

$$\Phi = A_1 e^{i(\xi x - \alpha y - \omega t)} + A_2 e^{i(\xi x + \alpha y - \omega t)} \qquad 4.49$$

where

$$\alpha^2 = \left(\left(\frac{\omega}{c_1}\right)^2 - \xi^2\right) \qquad 4.50$$

in the plate,

$$\Phi_p = G_1 e^{i(\varepsilon x - \gamma y - \omega t)} + G_2 e^{i(\varepsilon x + \gamma y - \omega t)} \qquad 4.51$$

and

$$H_{3p} = i\left\{ D_1 e^{i(\varepsilon x - \Omega y - \omega t)} + D_2 e^{i(\varepsilon x + \Omega y - \omega t)} \right\} \qquad 4.52$$

where

$$\gamma^2 = \left(\left(\frac{\omega}{c_{1p}}\right)^2 - \varepsilon^2\right) \qquad \Omega^2 = \left(\left(\frac{\omega}{c_{2p}}\right)^2 - \varepsilon^2\right) \qquad 4.53$$

and in the solid,

$$\Phi_s = A_2 e^{i(\varepsilon x - \kappa_s y - \omega t)} \qquad 4.54$$

and

$$H_{3s} = i\left\{ B_3 e^{i(\varepsilon x - \xi y - \omega t)} \right\} \qquad 4.55$$

where

$$\kappa_s^2 = \left(\left(\frac{\omega}{c_{1s}}\right)^2 - \varepsilon^2\right) \qquad \Sigma^2 = \left(\left(\frac{\omega}{c_{2s}}\right)^2 - \varepsilon^2\right) \qquad 4.56$$

The boundary conditions are effectively a reverse of the previous conditions,

for the top surface

$$y = b$$

$$Uy_{fluid} = Uy_{plate}$$

$$\tau yy_{fluid} = \tau yy_{plate}$$

and

$$\tau xy_{fluid} = 0$$

and for the bottom surface

$$y = -b$$

$$Uy_{plate} = Uy_{solid}$$

$$\tau yy_{plate} = \tau yy_{solid}$$

and

$$\tau xy_{plate} = \tau xy_{solid} = 0 \qquad 4.57$$

Calculating the diplacements for the three media, the stresses as required and fitting the boundary conditions given above results in a matrix of seven equations in 8 unknowns.

In conditioned form the results are presented in equation 4.58.

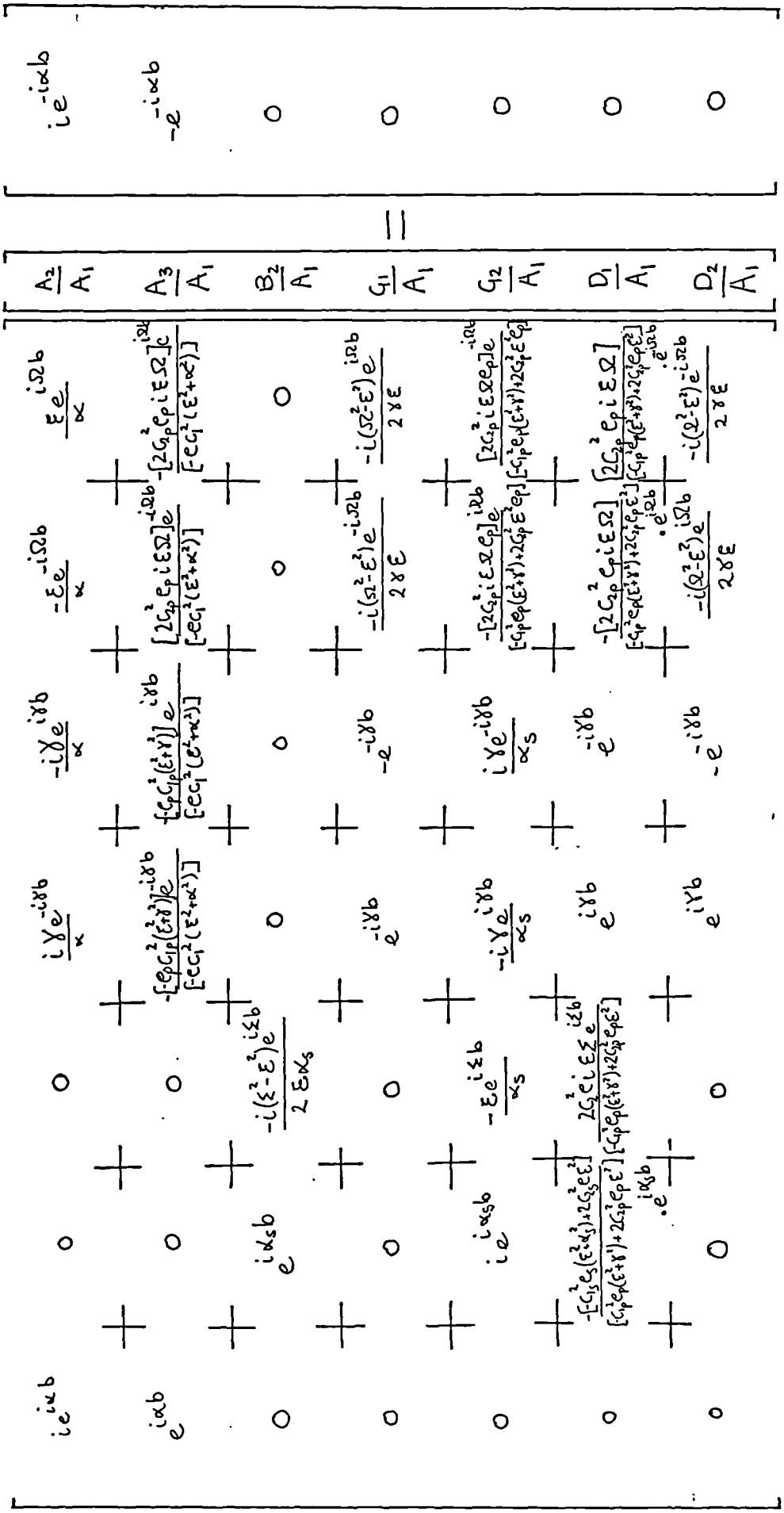

matrix equation 4.58

This matrix was coded into a program in a similar manner to the solid/plate/fluid case. The energy balance equation was included in the model as previously discussed.

4.3.3. The fluid/plate/fluid case

As discussed previously, it was felt that a direct comparison could be made more easily if a new program was written.

It was found that when the main program was run and the value of C_2 (the shear wave speed in the solid) was set to zero a divide-by-zero error occurred. It was necessary therefore to insert a low value of C_2 but is was not known if this would lead to inaccuracies.

The model in this case is shown in figure 4.9. Assigning potentials in the normal manner and performing the requisite computations results in a set of potentials,

in the fluid;

$$\Phi = A_1 e^{i(\varepsilon x - \alpha_f y - \omega t)} + A_2 e^{i(\varepsilon x + \alpha_f y - \omega t)} \qquad 4.59$$

where

$$\alpha_f^2 = \left(\left(\frac{\omega}{c_{1f}}\right)^2 - \varepsilon^2\right) \qquad 4.60$$

in the plate

$$\Phi_p = G_1 e^{i(\varepsilon x - \alpha y - \omega t)} + G_2 e^{i(\varepsilon x + \gamma y - \omega t)} \qquad 4.61$$

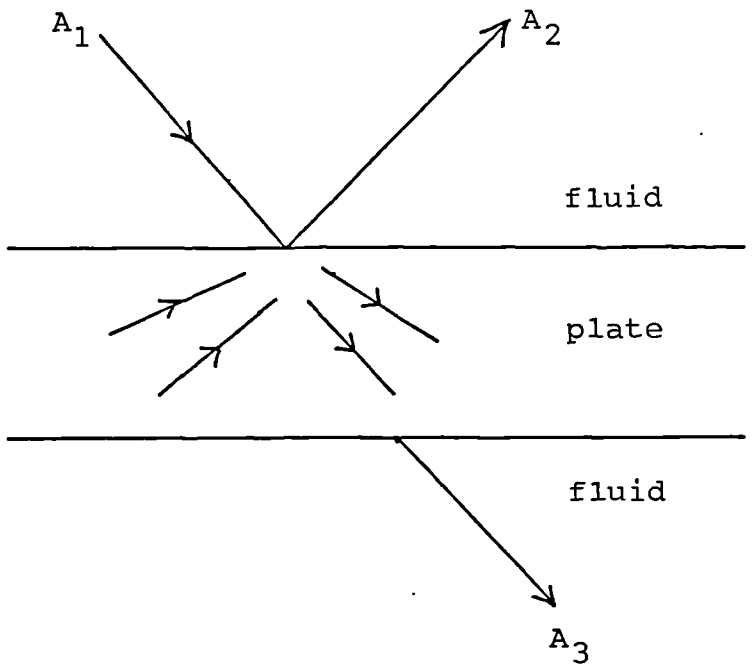

FIG 4.9
Fluid/plate/fluid structure with incident wave A_1

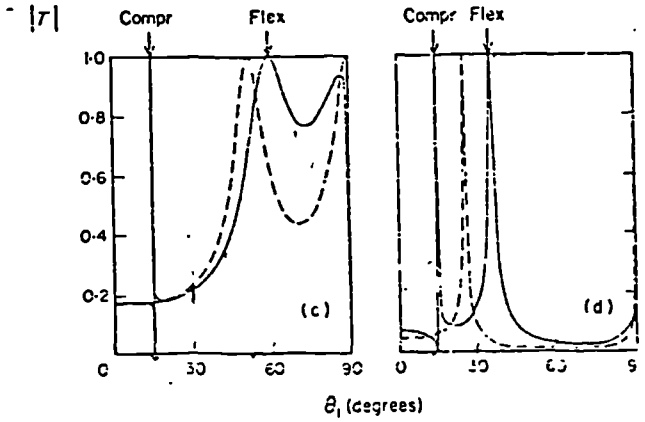

FIG 4.10
Freedman's curves

and

$$H_{3p} = i\left(D_1 e^{i(\varepsilon x - \Omega y - \omega t)} + D_2 e^{i(\varepsilon x + \Omega y - \omega t)}\right) \qquad 4.62$$

where

$$\gamma^2 = \left(\left(\frac{\omega}{c_{1p}}\right)^2 - \varepsilon^2\right) \qquad \Omega^2 = \left(\left(\frac{\omega}{c_{2p}}\right)^2 - \varepsilon^2\right) \qquad 4.63$$

and in the fluid

$$\Phi_f = A_3 e^{i(\varepsilon x - \kappa_f y - \omega t)} \qquad 4.64$$

where κ_f has the same meaning as before.

The displacements and stresses are calculated as before and fitted to the boundary conditions which for this case are,

on the top surface

$$y = b$$

$$Uy_{fluid} = Uy_{plate}$$

$$\tau yy_{fluid} = \tau yy_{plate}$$

$$\tau xy_{plate} = 0 \qquad 4.65$$

and on the bottom surface y = -b the same conditions apply.

Carrying out the requisite manipulations, a 6x6 matrix (in conditioned form) is produced. This is given in equation 4.66.

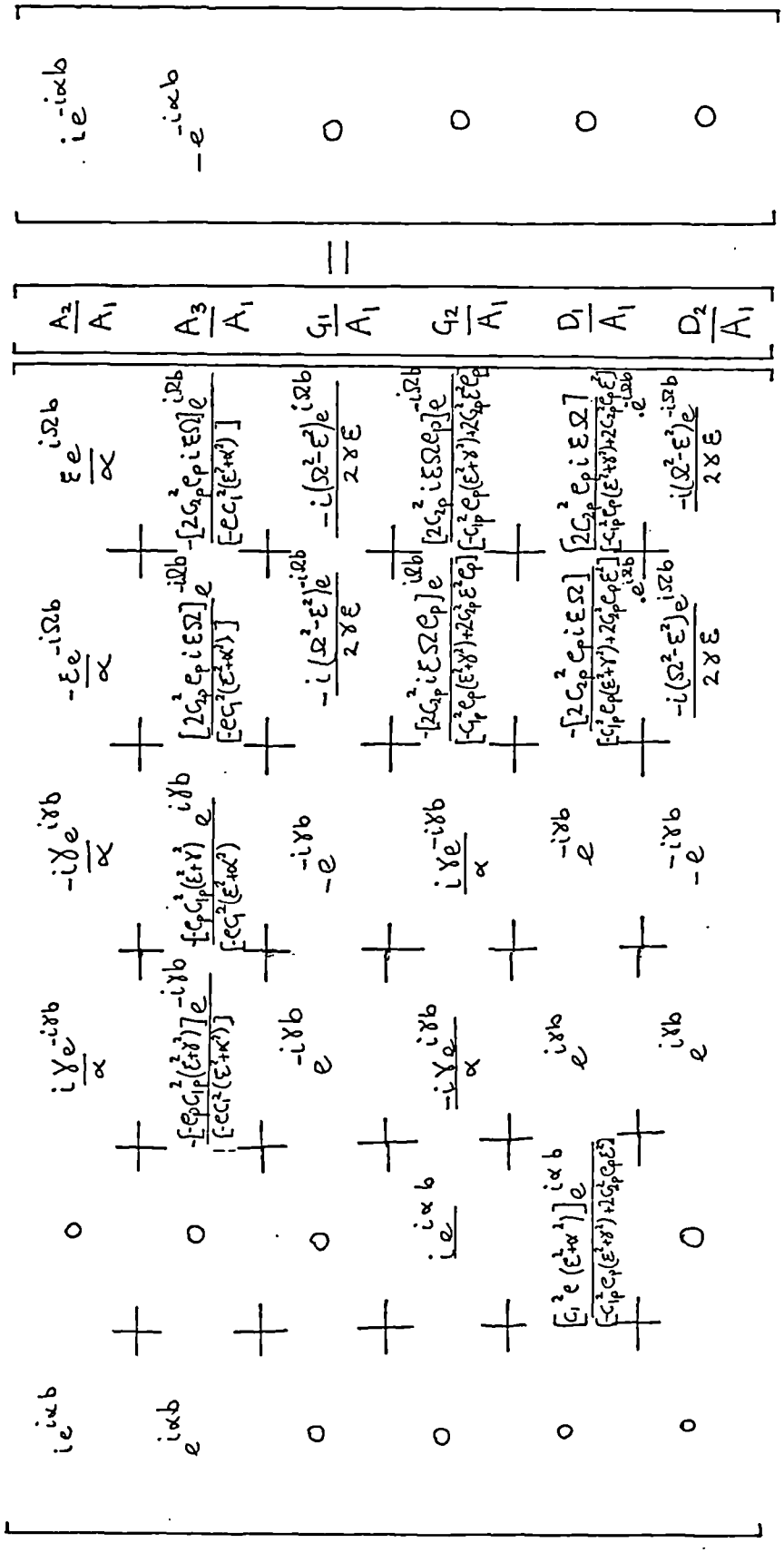

matrix equation 4.66

4.3.4 Program description and testing

4.3.4.1 Program descriptions

There are 3 main programs, they are

(i) TPLATE A for the solid/plate/fluid case
(ii) TPLATE B for the fluid/plate/solid case
(iii) TPLATE LS for the fluid/plate/fluid case

In addition there are two derivatives of TPLATE A and TPLATE B named as:

(iv) TPLATE AA
(v) TPLATE BB

These programs have the added facility of being able to pass data to a file (TPLATEAA) and being able to access the file (TPLATEBB).

The information passed is the ratio of $\frac{A3}{A1}$ and the corresponding

angle and this is used as the incident wave in the second model.

All programs are written in FORTRAN and run on a vax 11/780 under V.M.S. Input data is put on a file and results data is also outputted to a file.

The main program steps are:

(i) Assignment, declarations and input of information.
(ii) Calculation of matrix coefficients.
(iii) Call to NAG subroutine.
(iv) Testing the energy balance.
(v) Writing to results and graphics files.
(vi) Call to graphics routine and saving processed data to a file.

In addition the system needs to be commanded to plot a file.

In all of the programs the choice of step size for the angular variable is set at 1/2°. This is because it was felt that the accuracy of setting up the transducers could not be guaranteed better than 1/2°. To save errors occuring at normal incidence and at 90° these step points were not included in the programs.

4.3.4.2 Program testing

Complete testing of the programs was not possible because other solutions for the models did not exist except for the fluid/plate/fluid case and it was decided therefore to test this first.

Exhaustive testing of other solutions would have entailed point by point calculations and comparisons. It was felt that this approach, whilst rigorous, was too time consuming and it was decided therefore to compare produced curves by eye. It was felt that if the curves were in agreement in this method of testing it would suffice for practical considerations.

For all the cases tested and for all cases discussed in this thesis the energy balance always returned the value of unity.

A published curve for the fluid/plate/fluid case is given in Freedman's paper, for various plate thicknesses normalised to the shear wavelength.

It was decided to check two of Freedman's curves (for d/λ_s = .12 and d/λ_s = .38) against those produced by program TPLATE LS. The parameters for Freedman's curves are given in Table 4.1.

Table 4.1

Freedman's Parameters

	Density kg/m^3	Long Velocity m/s	Shear Velocity m/s
Water	1000	1500	0
Steel	7800	5979.7	3426.3

The curves from Freedman's paper are reprinted for d/λ_s = .12 and d/λ_s = .38 in figure 4.10.

The data used in TPLATE LS was, as given above, but in addition, two other variables were required, ω and b and these were,

ω = 6283100 rad/s
b = .0001947 m

The value for 2b (=d) was calculated from d/λ_s = .12 and $c_s = \lambda_s f$

The result of the plot is shown in figure 4.11 and can be seen to have the same features as Freedman's curve. However, the details of the very sharp peak at approximately 15° are missed as a consequence of the step size chosen (1/2°).

As a check on programs TPLATE A and TPLATE B the same data was used but because C_2 was needed a value of $1x10^{-9}$ m/s was used.

No difference in the curves nor in the results could be detected between the results produced by TPLATE LS and the other two programs. These results were produced (as with all the programs) using double precision and subsequently truncated to 8 decimal figures for printing purposes.

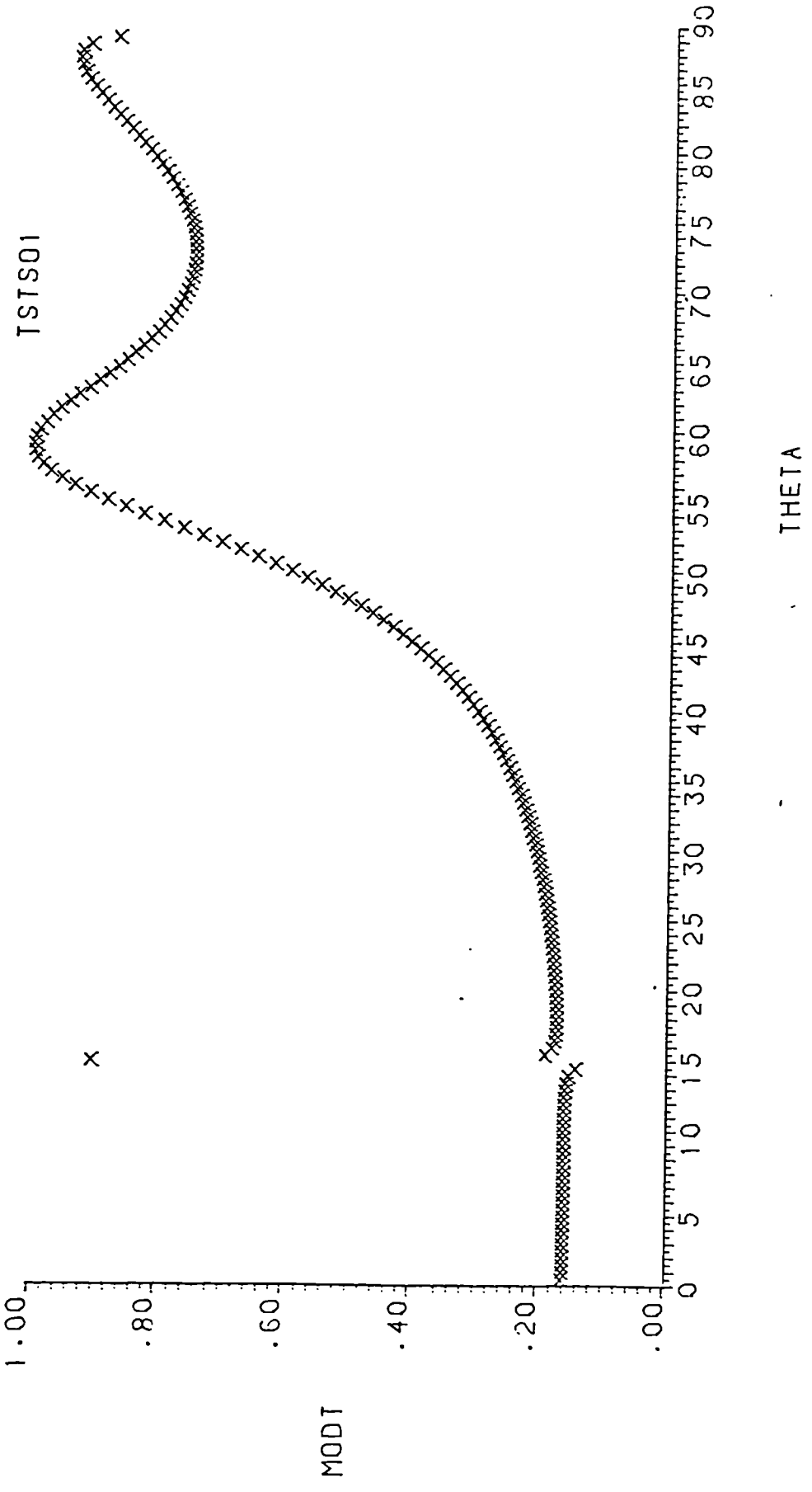

FIG 4.11
Transmission plot (TPLATELS TSTS01)

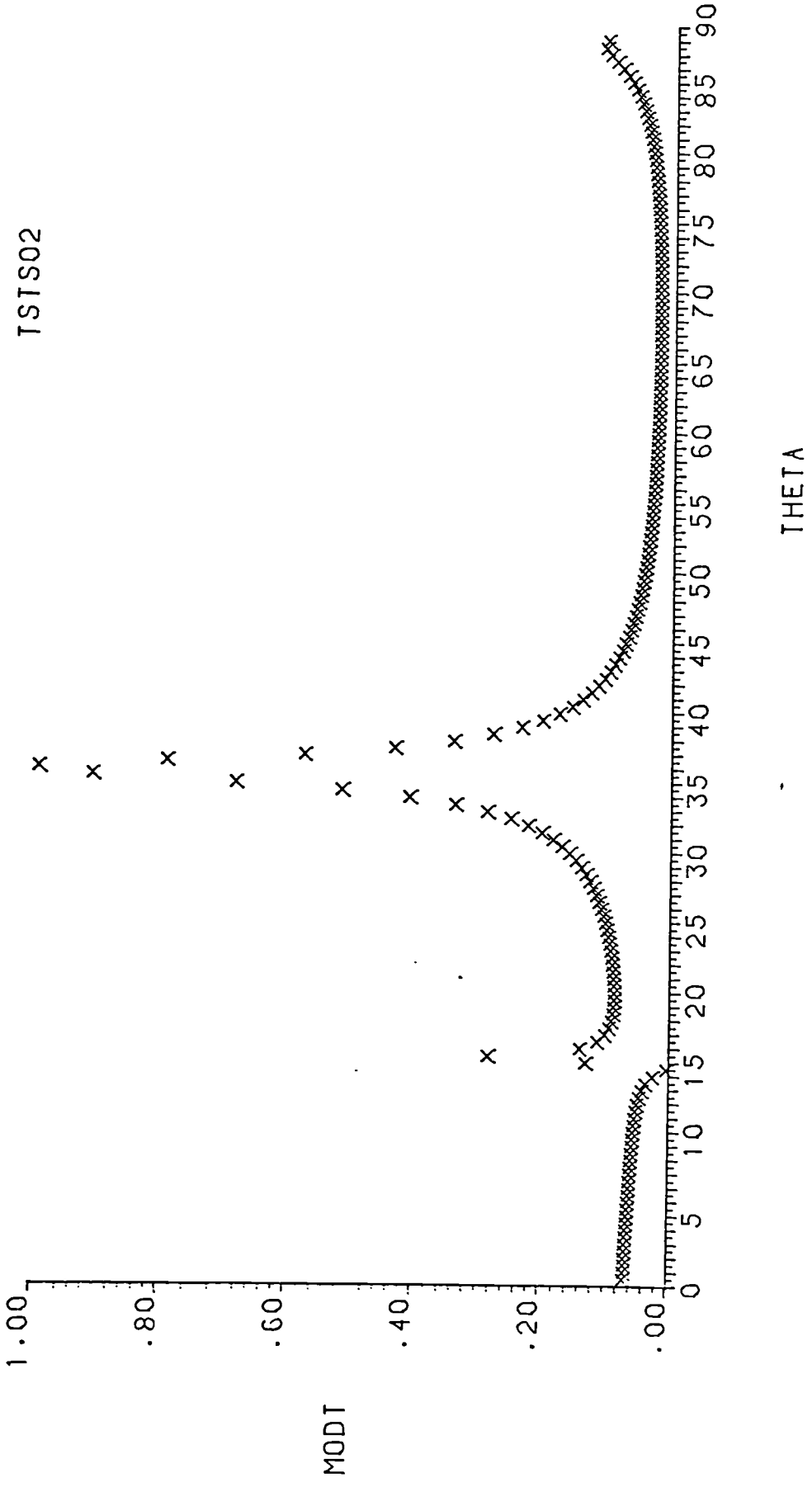

FIG 4.12
Transmission plot (TPLATELS TSTS02)

The programs were then rerun using data for $d/\lambda_s = .38$ (b=.0006168m). Once again all programs produced identical results and the result of TPLATE LS is shown in figure 4.12. It can also be seen to have the general form of Freedman's curve but again the precise details of the peaks has been lost.

It is concluded that the program TPLATE LS is sufficiently accurate for its purpose and that the programs TPLATE A and TPLATE B are acceptable as models for the fluid/plate/fluid case provided the value of C_2 is set small.

4.3.5 The transmission curves for a fluid/plate/fluid in terms of the dispersion curves for a free plate.

The dispersion curves for a steel plate in water are shown below in figure 4.13. The curves are taken from Freeman as calculated from the work of Sides using the values given in table 4.2.

The values of six frequency-thickness variables (or normalised thicknesses) were chosen as being of interest. The six values chosen were,

$$d/\lambda_s = \cdot 12\,,\ \cdot 38\,,\ \cdot 55,\ 1\,,\ 1{\cdot}75\,,\ 2{\cdot}5$$

and cover a range of interesting areas.

The values were converted into acceptable data for the program TPLATE LS (in terms of b) and along with the other data given in table 4.2 was written into the input file. The program was run and the curves produced are coded TSTS01-TSTS06 and are shown in figures 4.14-4.19 respectively.

The peaks of the transmission curves are drawn as small circles on the dispersion curve figure 4.13. The transmission maxima can be seen to lie on the dispersion curves. (For light loading the dispersion curves

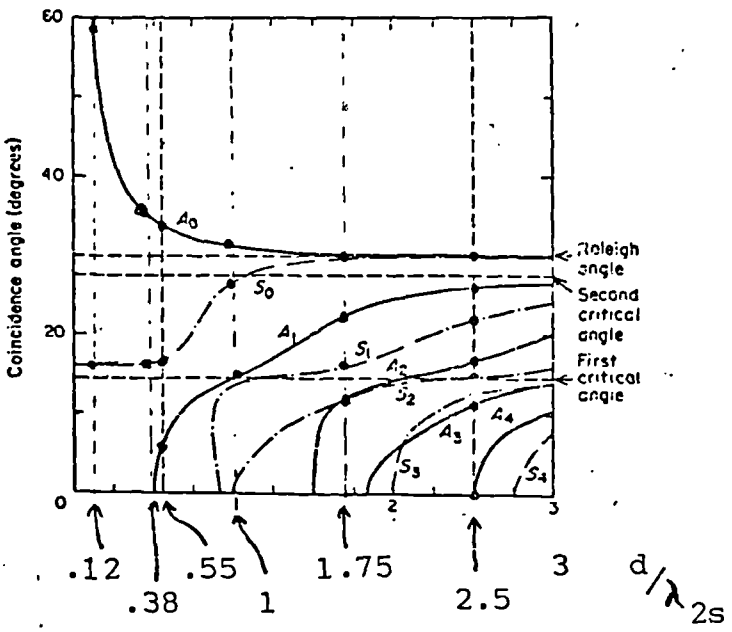

FIG 4.13
Dispersion curves of a steel plate in water (Freedman)

Material	Water	Steel
Density (kg m^{-3})	1000	7800
Dilatational velocity (m s^{-1})	1500	5979·7
Shear velocity (m s^{-1})	0	3246·3
λ (N m^{-2})	$2{\cdot}25\times10^{9}$	$114{\cdot}5\times10^{9}$
μ (N m^{-2})	0	$82{\cdot}2\times10^{9}$

First critical angle (degrees)	14·5278
Second critical angle (degrees)	27·5204
Rayleigh angle (degrees)	29·9163

TABLE 4.2
Parameters for the water-steel model (Freedman)

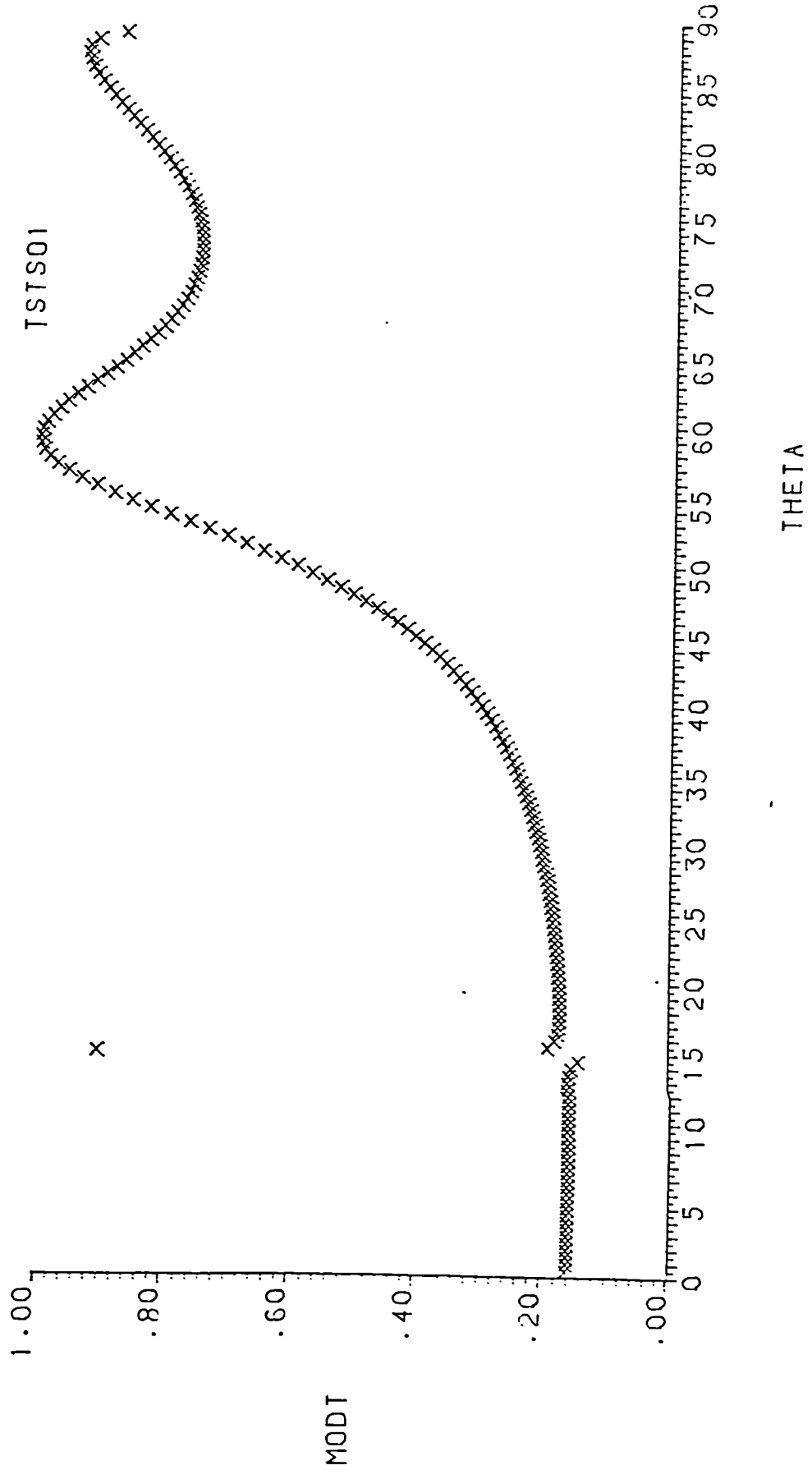

FIG 4.14
Transmission plot (TPLATELS TSTS01)

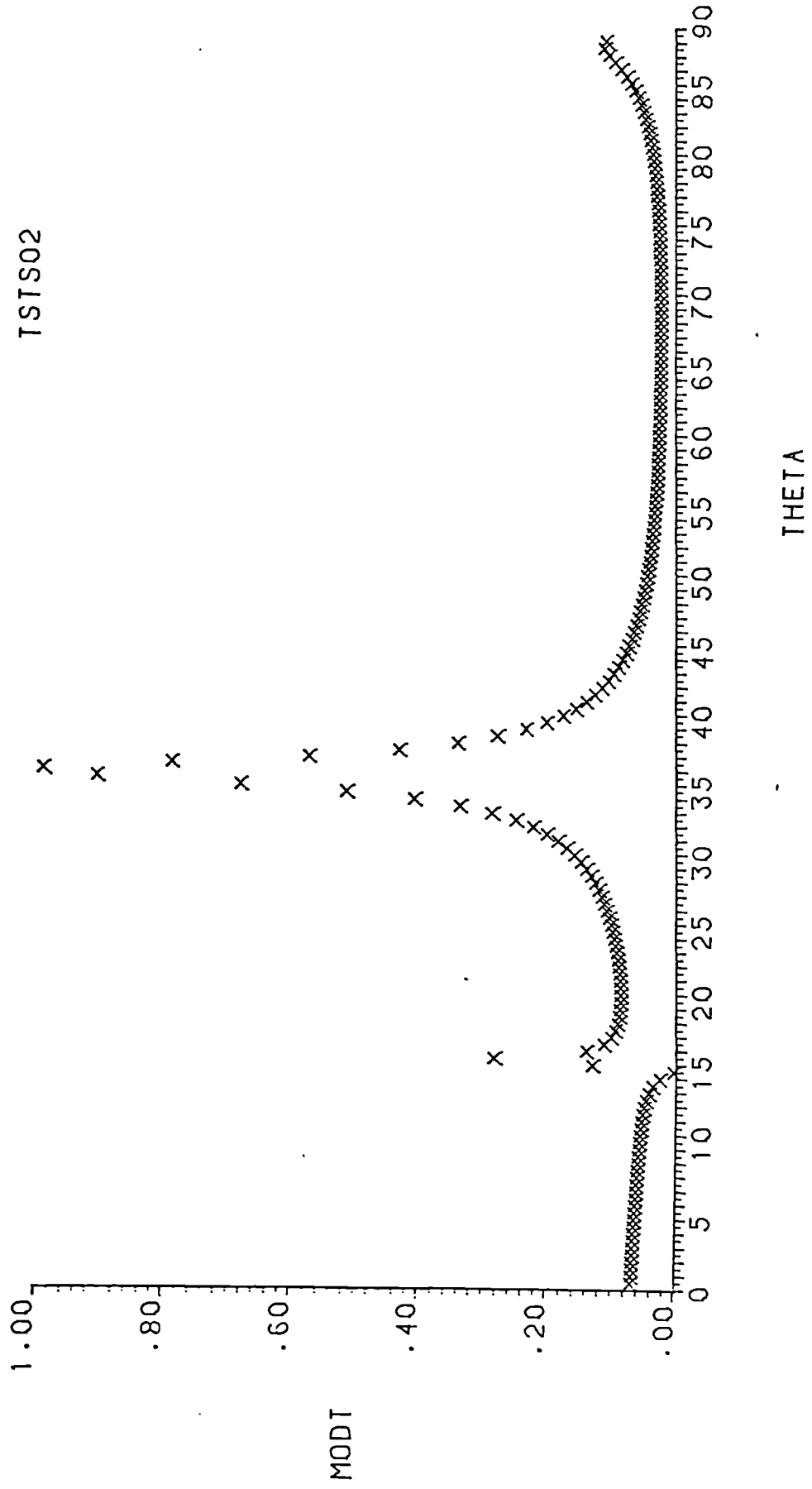

FIG 4.15
Transmission plot (TPLATELS TSTS02)

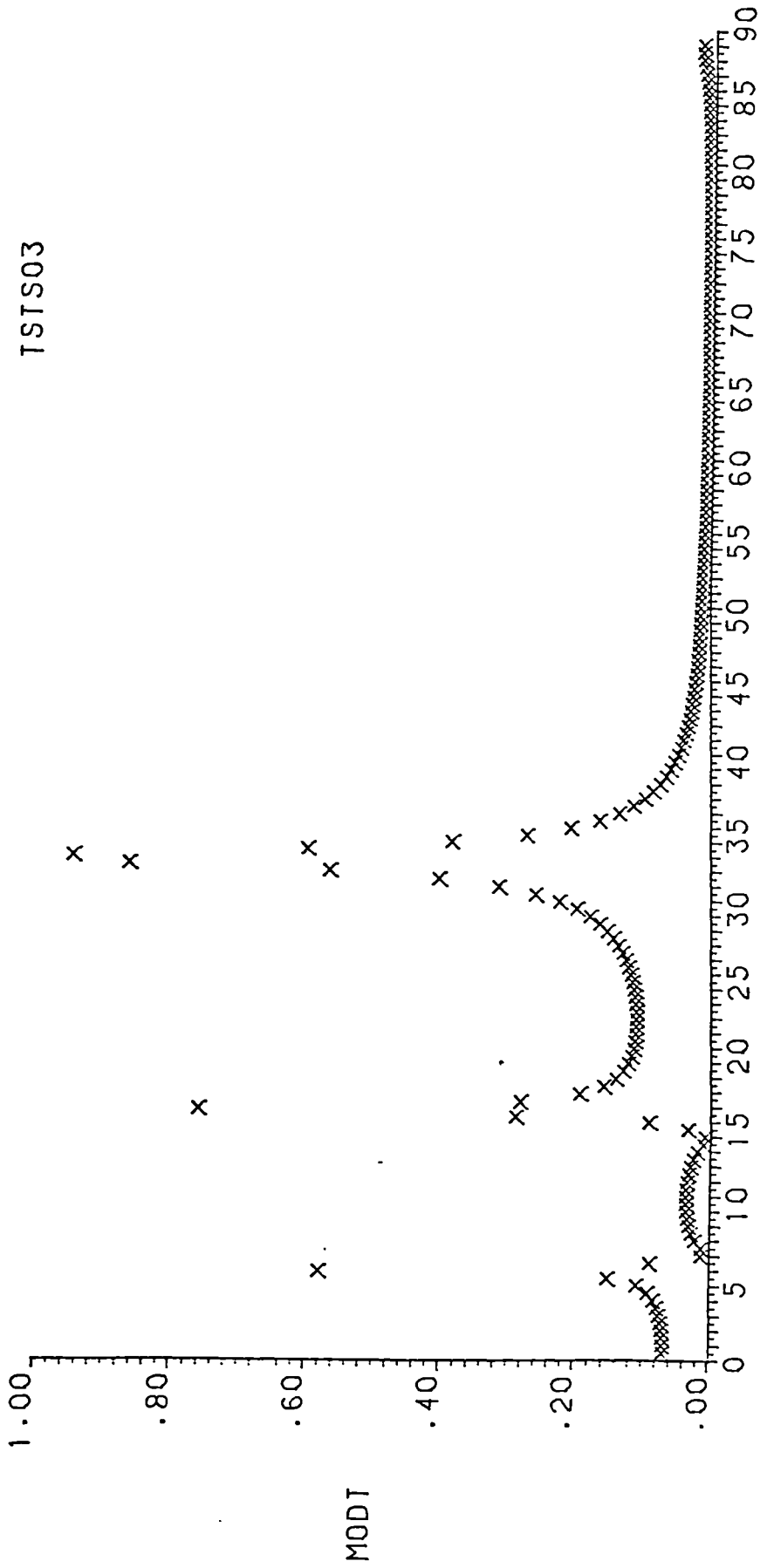

FIG 4.16
Transmission plot (TPLATELS TSTS03)

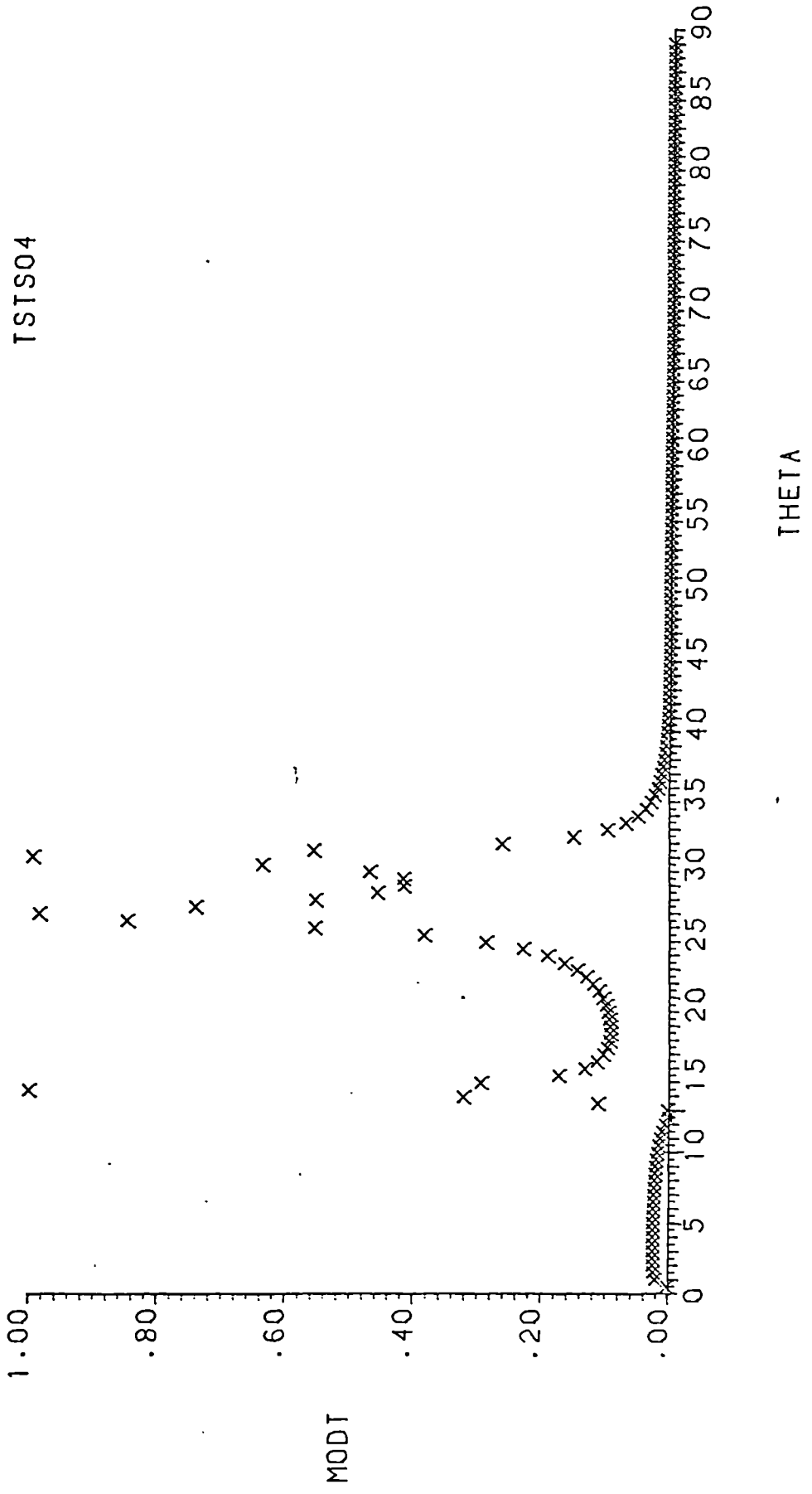

FIG 4.17
Transmission plot (TPLATELS TSTS04)

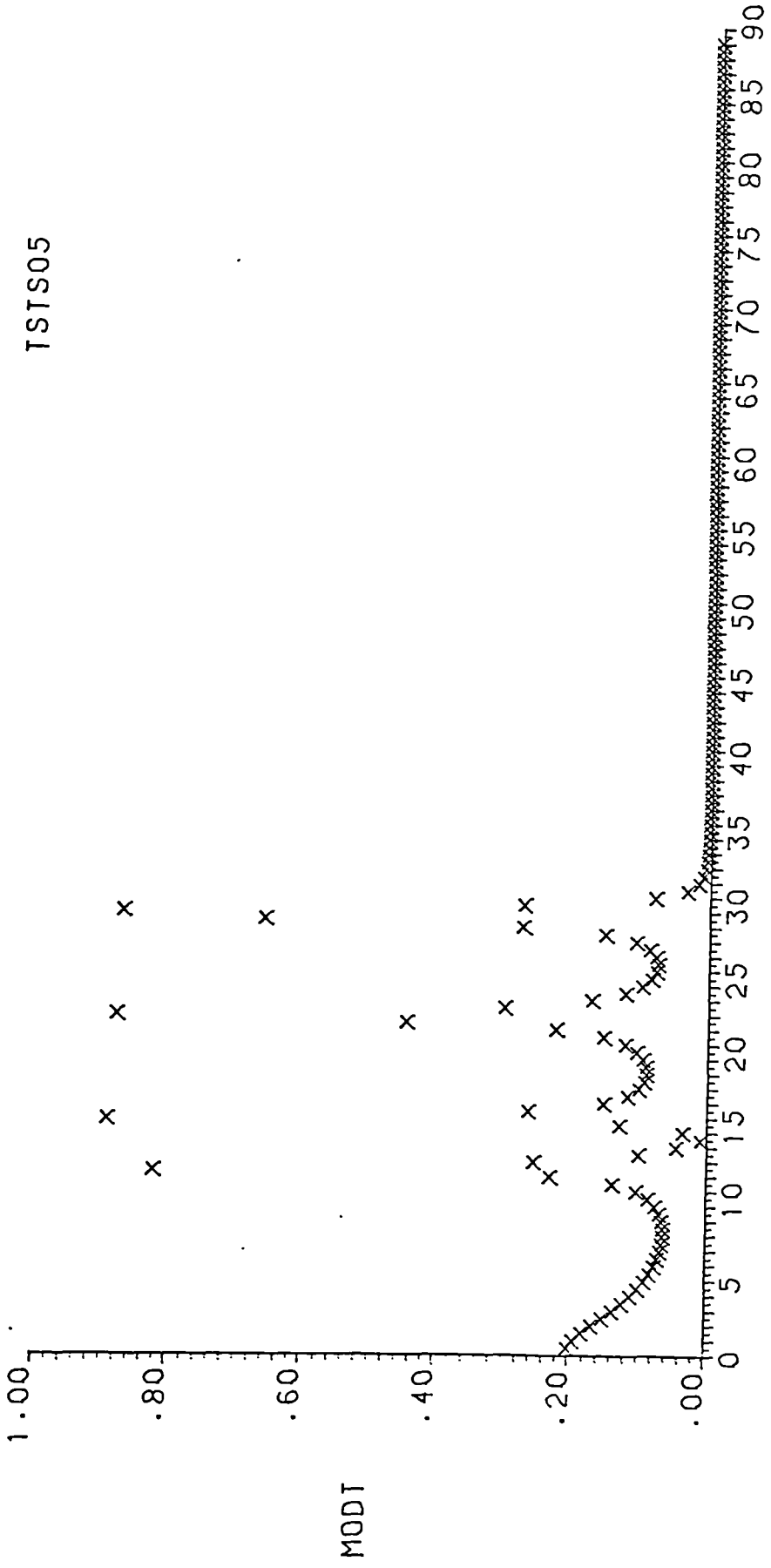

FIG 4.18
Transmission plot (TPLATELS TSTS05)

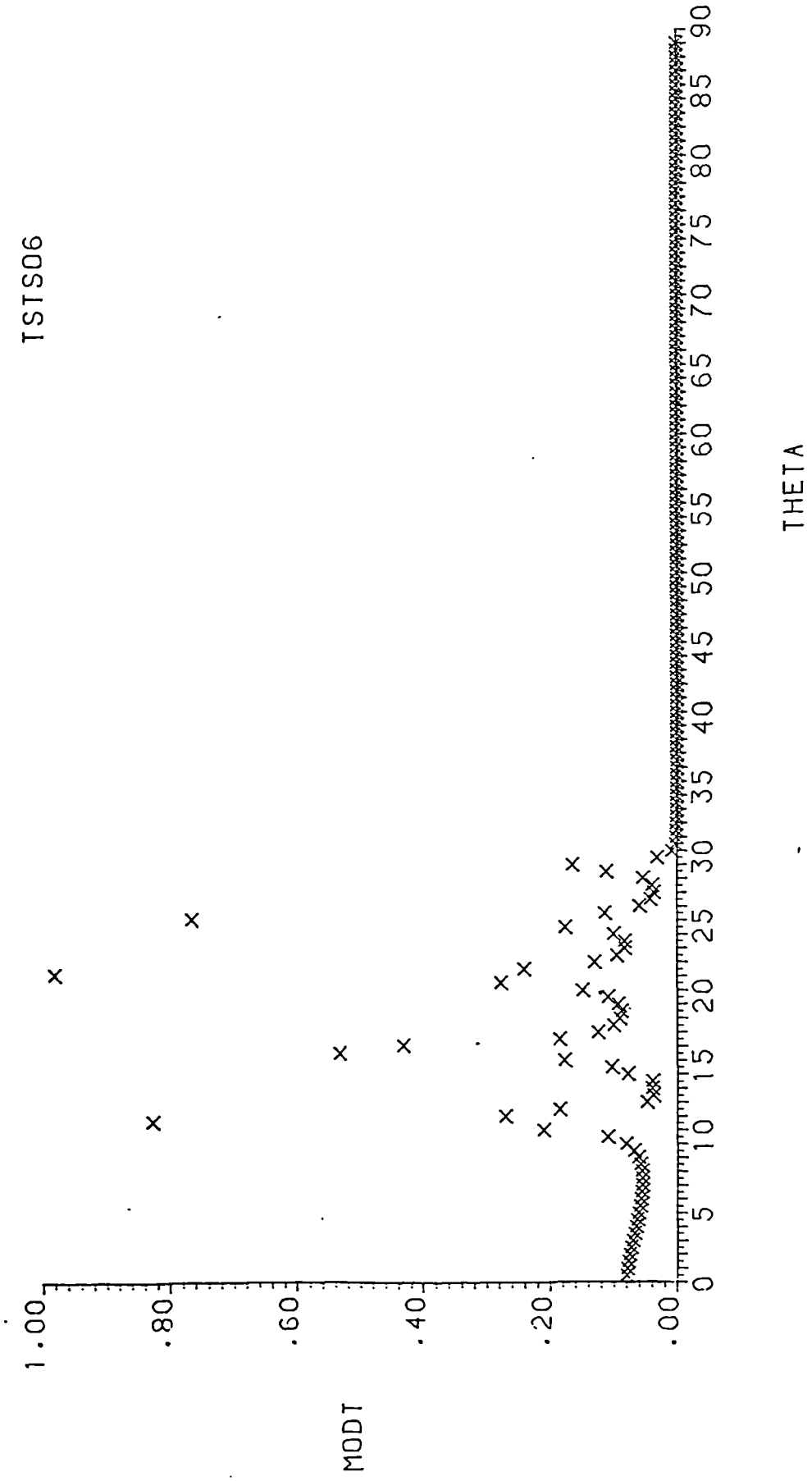

FIG 4.19
Transmission plot (TPLATELS TSTS06)

shown in figure 4.13 are not significantly different from the free plate curves and either set of curves could have been chosen).

Consideration of curve TSTS01 (for which $d/\lambda_s = .12$) shows that peaks of transmission occur at approximately 15°, 60° and 88°. The peak at 15° corresponds to the S_o mode whilst that at 60° corresponds to the A_o mode. Transmission at both of these angles should be high as discussed in previous sections. The peak at 88° is unexpected but has been observed in other work and is considered to be due to Stonely waves. However, these waves are only of interest near grazing incidence.

In the second curve TSTS02 (for which $d/\lambda_s = .38$) it is observed that the A_o mode has now travelled significantly down the curve whilst the S_o mode has more or less stayed at the same position, and is now at the knee of the curve shown in figure 4.13.. The A_o mode is seen to intersect the curve at 36° whilst the S_o mode intersects the curve at 16°.

The third curve TSTS03 (for which $d/\lambda_s = .55$) is seen to intersect three modes, the A_o, S_o and A_1 modes. The A_o mode is now at 34° and is on a slower changing part of the dispersion curve. The S_o mode is seen to be still on the knee of the curve and is at 16.5°. The new mode intersected is A_1 and is at 7°, this mode has a low frequency cut off of $d/\lambda_s = .5$ (in accordance with equation 1.3) and since the curve TSTS03 is for a value of $d/\lambda_s = .55$ it can be seen to be intersected very close to cut off, where the cut off would correspond to the normal thickness-stretch mode at normal incidence.

The following curve TSTS04, (for which $d/\lambda_s = 1$) has several interesting features. From inspection of the dispersion curves one would expect to find five peaks but infact the transmission diagram has only 3 peaks at approximate angles 14°, 26°5 and 30.5.

The first peak, one would expect should occur at normal incidence, for here the curve S_2 has a limiting value (ie: cut off value) of 1 wavelength. However it was shown by Schoch (43) that at this value the plate is exercising tangential displacement only and there is no coupling to the fluid. At this low frequency cut off the value of S_2 corresponds to an integral number of shear half wavelengths. From equation 1.3, $d/\lambda_s = 1$ and at this position $v = \infty$, thus the entire surfaces of the plate are only shearing. In fact, further inspection of TSTS04 does show that at 1/2° there is no transmission.

A zero of transmission (thus total reflection) is seen to occur at approximately 13° and would appear to correspond to the S_1 mode. This angle is very close to the first critical angle for longitudinal waves (ie: $\sin^{-1} \frac{1500}{5979.1} = 14.527°$). Schoch (loc cit) explains in his paper that transmission should be zero at this angle for the S family of curves since they are also undergoing purely tangential displacement. Brekhovskikh (47) shows by a limiting process that total reflection and transmission at this angle is a function of plate thickness (at constant frequency) and that total reflection occurs for integral shear half wavelengths of plate thickness and this corresponds to the intersection of the S family of curves with the first critical angle. The peaks, therefore, on the transmission diagram correspond to the A_1, S_o and A_o modes respectively. The A_1 mode is seen to be very close to the first critical angle and this is the point at which the homogeneous longitudinal wave changes into an inhomogeneous wave on the plate surface. If the results are considered, this wave is seen to produce significant plate waves.

Transmission curve TSTS05 (for which $d/\lambda_s = 1.75$) shows that transmission peaks occur at four angles, approximately 12.5, 16°, 23° and 30°. The mode intersected at 30° is now the amalgamation of the two modes S_o and A_o and this is clearly seen by the curves coming together on the dispersion diagram (figure 4.13) and as previously discussed in section 4.2, where these two curves were dealt with specifically. This mode is now very narrow (consider TSTS04 as a comparison), and is seen to be reducing in accordance with increasing FxD. This effect is well explained in Freedman.

Consideration of curves TSTS01 - TSTS05 show the gradual coalescence of the A_o and S_o modes and as shown in TSTS05 are very close together. The limiting value for this combination is the Rayleigh angle (29.916°) and is approached at approximately $d/\lambda_s = 2$.

The final curve presented (TSTS06) is for $d/\lambda_s = 2.5$ and shows clearly the almost total cancellation of the combined A_o and S_o modes. Transmission now is very low and this cancellation effect is described in more detail by Viktorov (39).

Thus it can be seen that in the case of a thick plate, eg: $2b > 9$ mm at a frequency of 1MHz, transmission by resonance excitation of modes A_o and S_o is not possible. Referring to the case of a clamp-on flowmeter it would mean that for thick walled vessels the angle of the transducers (wrt the normal) must be chosen to be below that of the second critical angle and preferably to excite a higher order mode, (of course there is a trade off with frequency of operation, lower frequency allowing thicker walled vessels). This problem clearly highlights the difficulty in trying to make one flowmeter for all pipe thicknesses.

Further inspection of TSTS06 reveals a difficulty in interpretation (once again due to the 0.5° step size). Inspection of the dispersion diagram would suggest that 8 peaks should be intersected but for previously explained reasons the S_2 mode would not be expected. The number of modes described by TSTS06 would appear to be 5 and occur at angles of 11.5, 17°, 22°, 26.5 and 30°. These would then correspond to dispersion curves A_3 or S_3, A_2, S_1, A_1 and A_o and S_o. It is possible that with finer step sizes the modes A_3 and S_3 could be separated. The A_4 mode has not been intersected but it is probably due to the value of ω used in the program which was 6283100 rad/s and not exactly $2\pi f$ rad/s. This would then make d/λ_s slightly less than 2.5 at 2.4999 and since the cutoff is $\frac{2fd}{C_s} = 1,3,5$ etc, the $d/\lambda_s = 2.5$ value would not be intersected.

As a further case of interest it was decided to investigate on a cursory basis, the case of water/brass/water as was done by Plona (41).

The dispersion curves reprinted in figure 4.20 are taken from Plona (loc cit). In this case the axis is marked in terms of FxD (MHz mm) instead of a thickness/shear wavelength ratio d/λ_s.

It was decided to choose two values of FxD and those were FxD=1 MHz mm and FxD = 2 MHz mm. The data of table 4.3 was used as the input information and

Table 4.3
Data for brass tests

ω	=	6283100	rad/s
C_{1f}	=	1500	m/s
C_{1B}	=	4700	m/s
C_{2B}	=	2110	m/s
b (FxD=1)	=	.0005	m
b (FxD=2)	=	.001	m
ρ_B	=	8500	kg/m^3
ρ_f	=	1000	kg/m^3

the corresponding curves are reproduced in figure 4.21 and 4.22. TSTB01 shows transmission peaks at approximately 25°, 59° and 86°. The peak at 86° is probably due to Stonely waves.

The peaks at 25° and 59° correspond to curves S_o and A_o respectively. Although the peaks do not exactly coincide with the dispersion curves this is probably due to the curves being those for vacuum/brass/vacuum and not for water/brass/water. Plona suggests a difference in the curves of the order of 1%, and this probably accounts for the discrepancy. The same reasoning should be extended to the second test TSTB02.

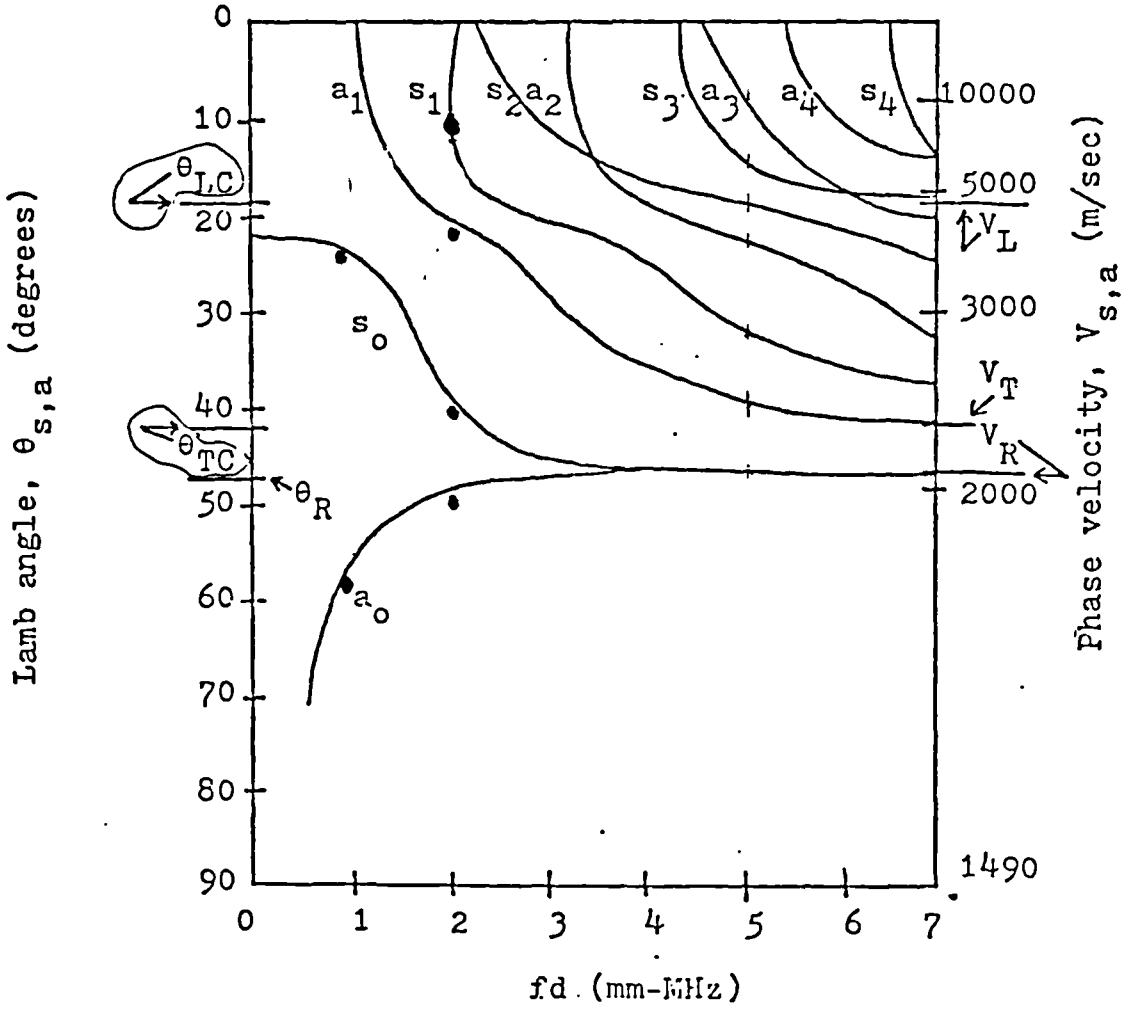

FIG 4.20
Dispersion curves for a brass plate in water (Plona)

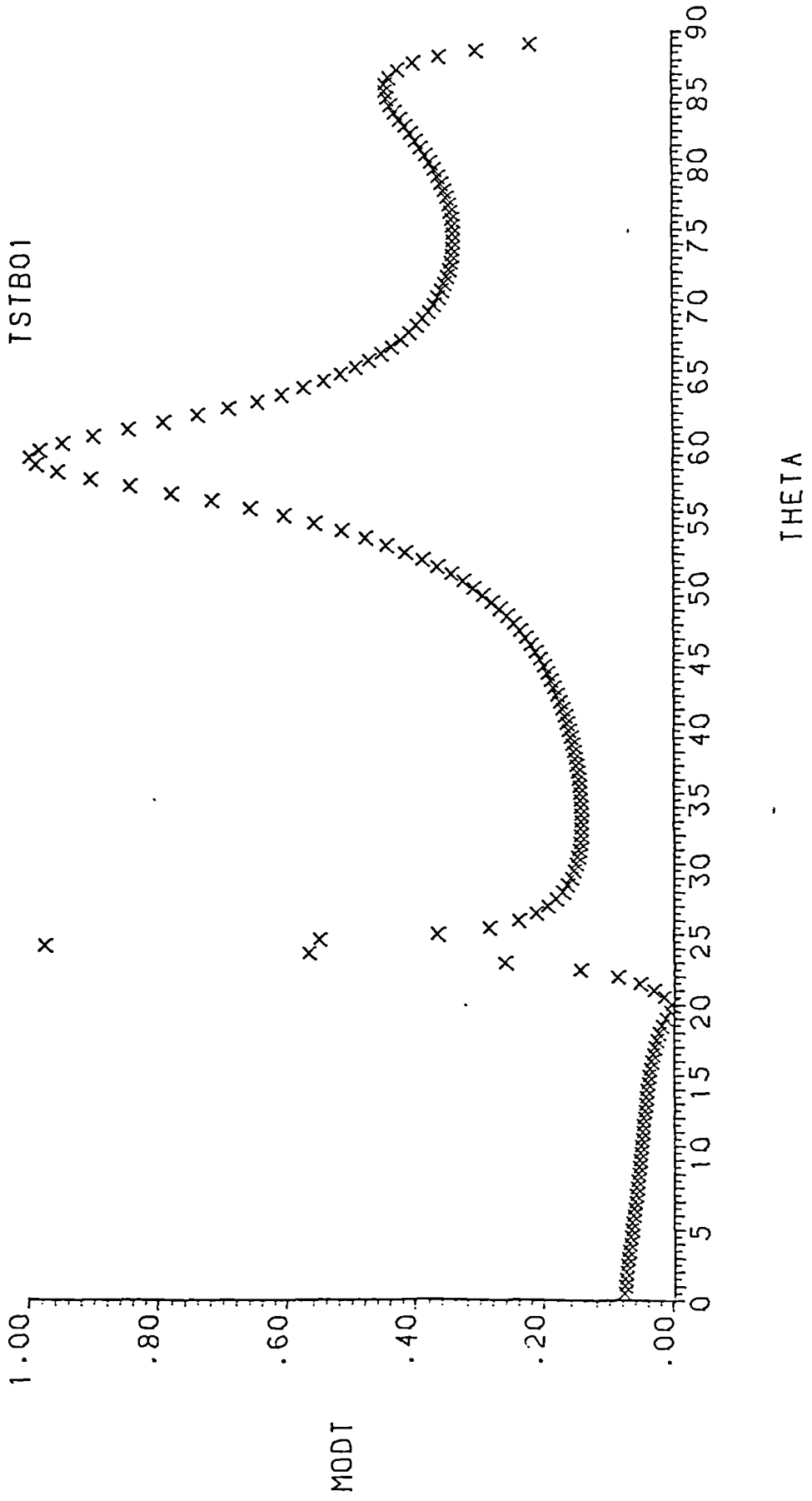

FIG 4.21
Transmission plot (TPLATELS TSTB01)

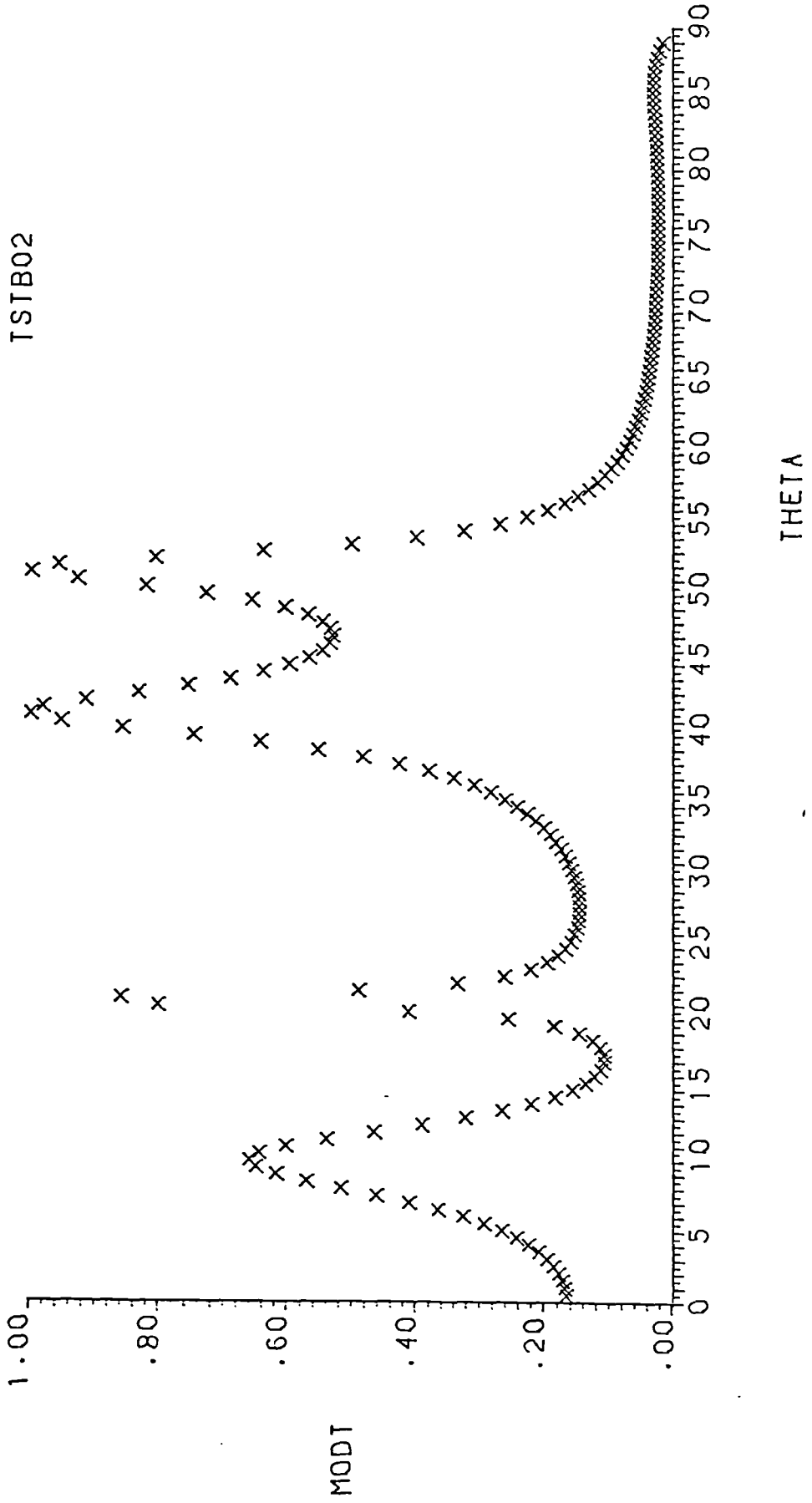

FIG 4.22
Transmission plot (TPLATELS TSTB01)

The second curve (TSTB02) shows peaks of transmission occurring at approximately 10°, 21°, 42° and 53° which corresponds to modes S_1, A_1 and S_o and A_o. The S_o and A_o modes are seen to be combining.

The transmission curves for the brass case are generally seen to be broader than those for the steel case. This is due to the higher acoustic impedance of steel 46 644 Pas/m being less loaded by the fluid than in the case of brass where the acoustic impedance is approximately 39950 Pas/m.

CHAPTER 5 EXPERIMENTAL WORK ON THE STATIC (ZERO) TEST RIG.

5.1 Introduction

The work of the previous chapter led to a model for the prediction of the transmission coefficient through a pair of plates. The purpose of this chapter is to experimentally check the theory and to form a comparison.

It was necessary to build a static (zero) test rig and since an earlier model had shown promise but had lacked refinements it was chosen as the basis for the new model. The design of the model will be described in section 5.2 and its features and disadvantages will be discussed.

The rig was used with typical pipe sections to produce experimental transmission curves with and without correction for attenuation in the blocks (the transducer blocks were found to have high attenuation). The two cases corresponding to the two real cases of blocks with high and low attenuation. It is shown that transmission is possible for the case of large angles (ie: greater than the 2nd critical angle).

The data of the pipe sections tested was used to produce theoretical curves and these are compared with the experimental curves. It will be shown that there is rough agreement between the curves.

It was shown in chapter two that a difficulty exists in the measurement of C from outside of the pipe wall and a proposed solution was put forward. This solution was tested on the static rig and found to be a valid method. The presentation of the results will be given in section 5.4 which will also include the necessary measurements to show that the speed of sound can be measured without recourse to removing the transducer blocks.

Finally tests will be presented for the effects on the zero of clamping/reclamping and temperature.

5.2 Design of zero test rig.

A first prototype static (zero) test rig was built, but was found to have many drawbacks. The chief drawbacks, after preliminary testing were found to be,

(i) That the small physical size of the rig did not allow sufficient axial movement of the transducers to cover the range required.

(ii) That it was difficult to previously position (in either the axial or angular position) the transducers.

(iii) That initial setting of the blocks diametrically opposite was difficult.

(iv) That constant pressure on the blocks could not be maintained.

For the first test rig, several sets of transducer blocks were designed. However, these too had several faults and the main ones were:-

(i) That the transducers were not held in a well defined position.

(ii) That the transducers were not held against the block with a constant pressure.

(iii) That the blocks were not long enough ensure that the sound beam did not return to the transducers.

(iv) That the rotating mechanism of the blocks did not produce pure block material in front of the transducer for every position (in fact a variety of air, interfaces were encountered in traversing the angular region.)

However, even with the above faults, the first static rig produced encouraging results for transmission plots but the confidence in the rig was low.

It was decided to build a second model to overcome the above difficulties. This model is shown in figure 5.1, along with a typical selection of pipework. The main features of the rig are its mechanical sturdiness and its high repeatability with respect to positioning in the axial and angular position.

The position of the transducer platform (marked 1 on the picture) is controlled from the gearing (2) on top of the rig, through four identical screw threads (3). A pointer (4) indicates the position of the platforms against a high quality graduated scale (5) marked in 1mm divisions.

The entire gearing and platform mechanism (6) can be wound in or out to accommodate between 75mm and 150mm pipes. This is accomplished via the belt driven gears (7) on the side. This mechanism provides parallel movement in or out. Although not used in the experiments for this thesis the gearing and platform mechanism can be rotated.

All the pipe sections are sealed across their bottoms with a plate that fits flush into the pipe holder (8). To ensure no movement during the experiments there are four clamps (9) to hold, rigidly, the plate.

A picture of the transducer mechanism is shown in figure 5.2 and an exploded picture of the transducer and cylinder arrangement is shown in figure 5.3.

The transducer body is held on the transducer platform by two Allen screws (10) which allow easy, accurate positioning of the transducer blocks across a diametrical chord. The transducer blocks are secured to the sprung body (11).

The springs (12) and roller (13) arrangement allow the transducer face to take up a natural position against the pipe wall under constant pressure. Guides at the top and bottom (14) prevent the block from moving sideways. The scale (15) is graduated in 1/2° steps and the pointers (16) are displaced by 45° so as to allow the use of a

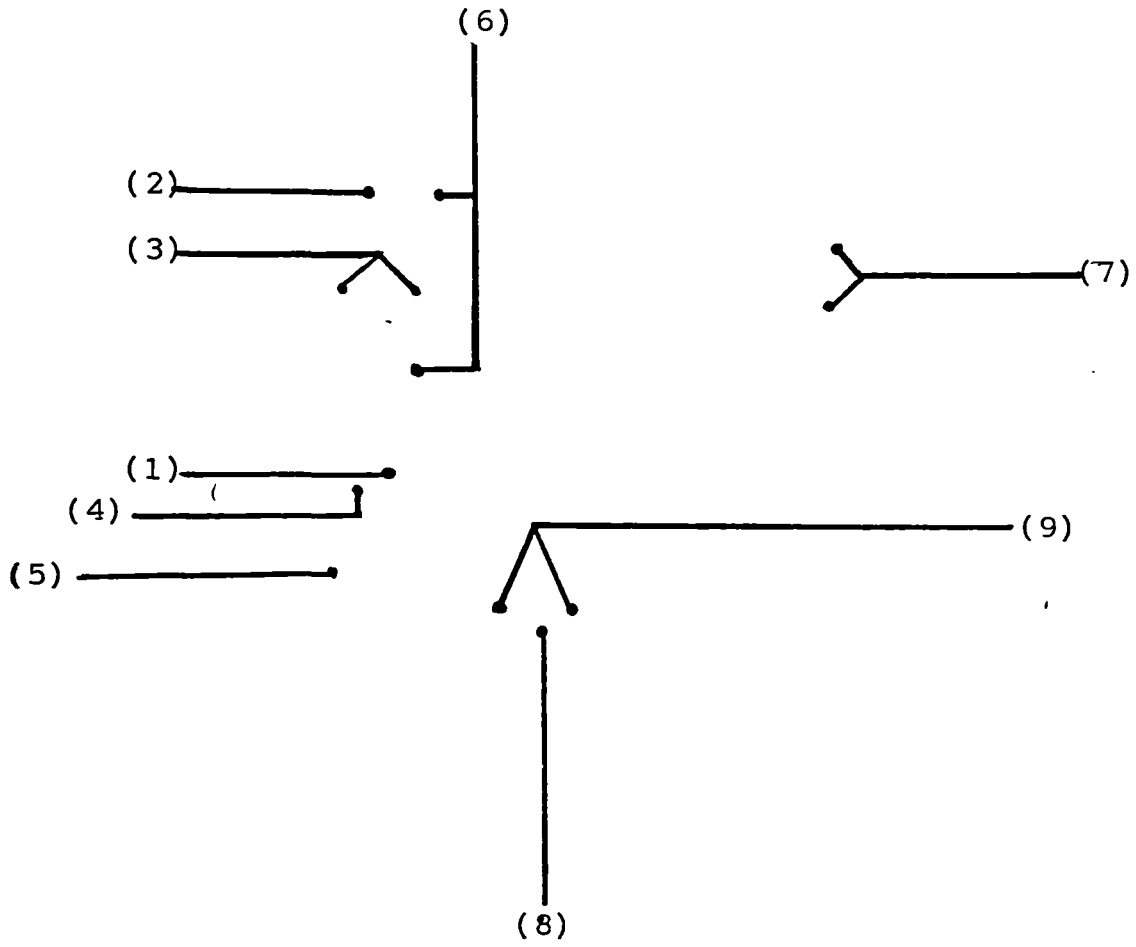
(6)
(2)
(3)
(7)
(1)
(4)
(5)
(9)
(8)

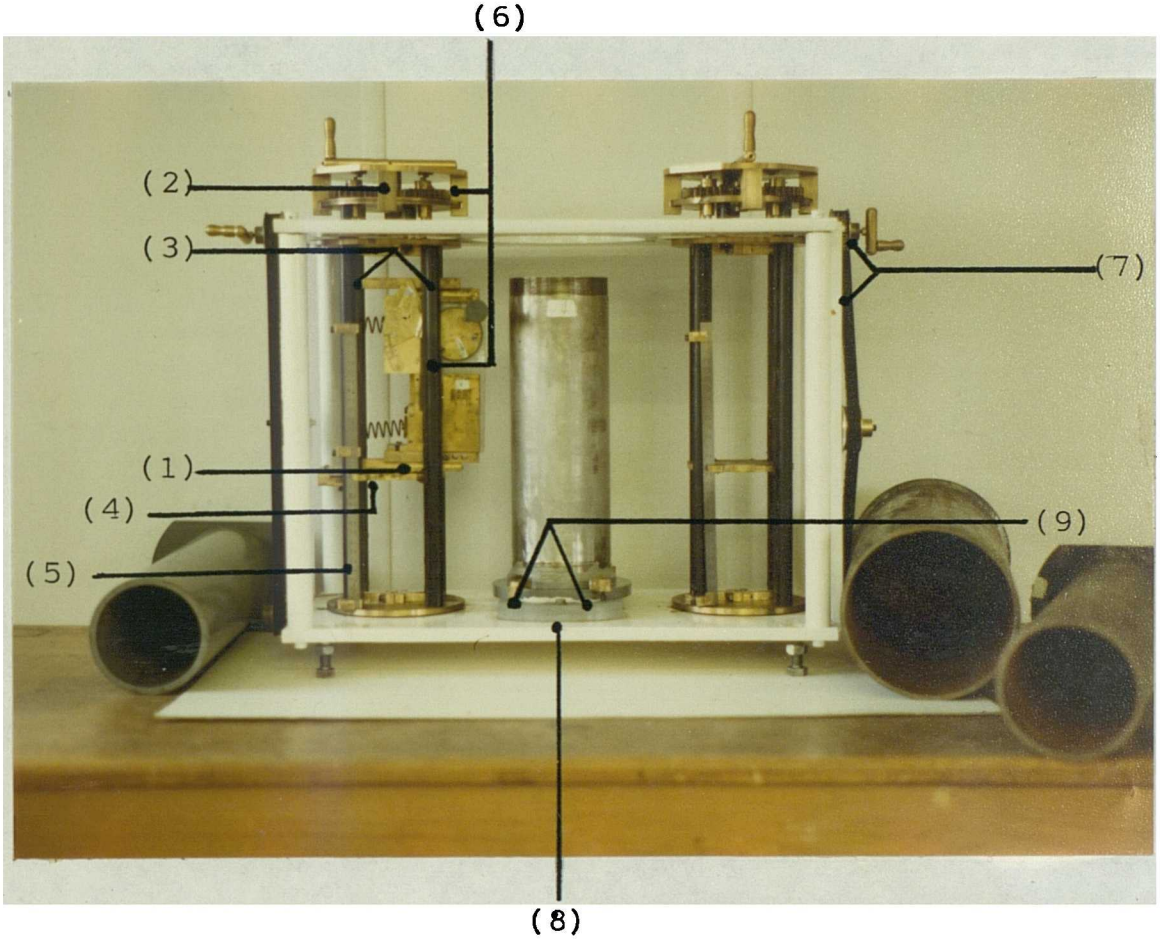

FIG 5.1
The static (zero) test rig

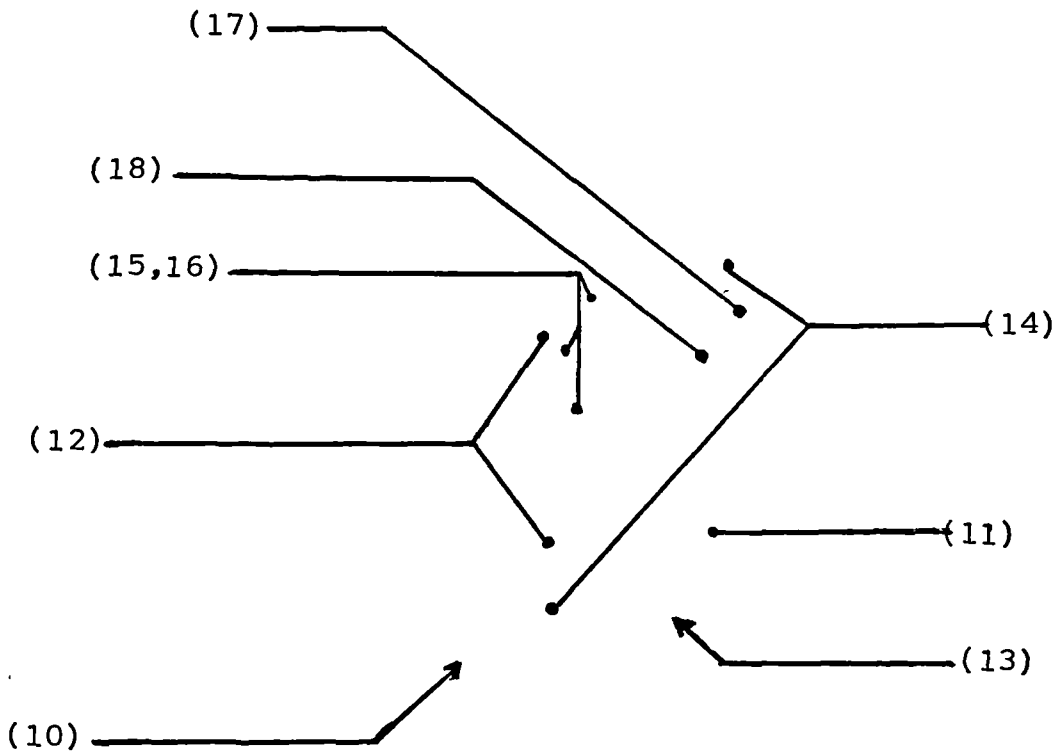
(17)
(18)
(15,16)
(14)
(12)
(11)
(13)
(10)

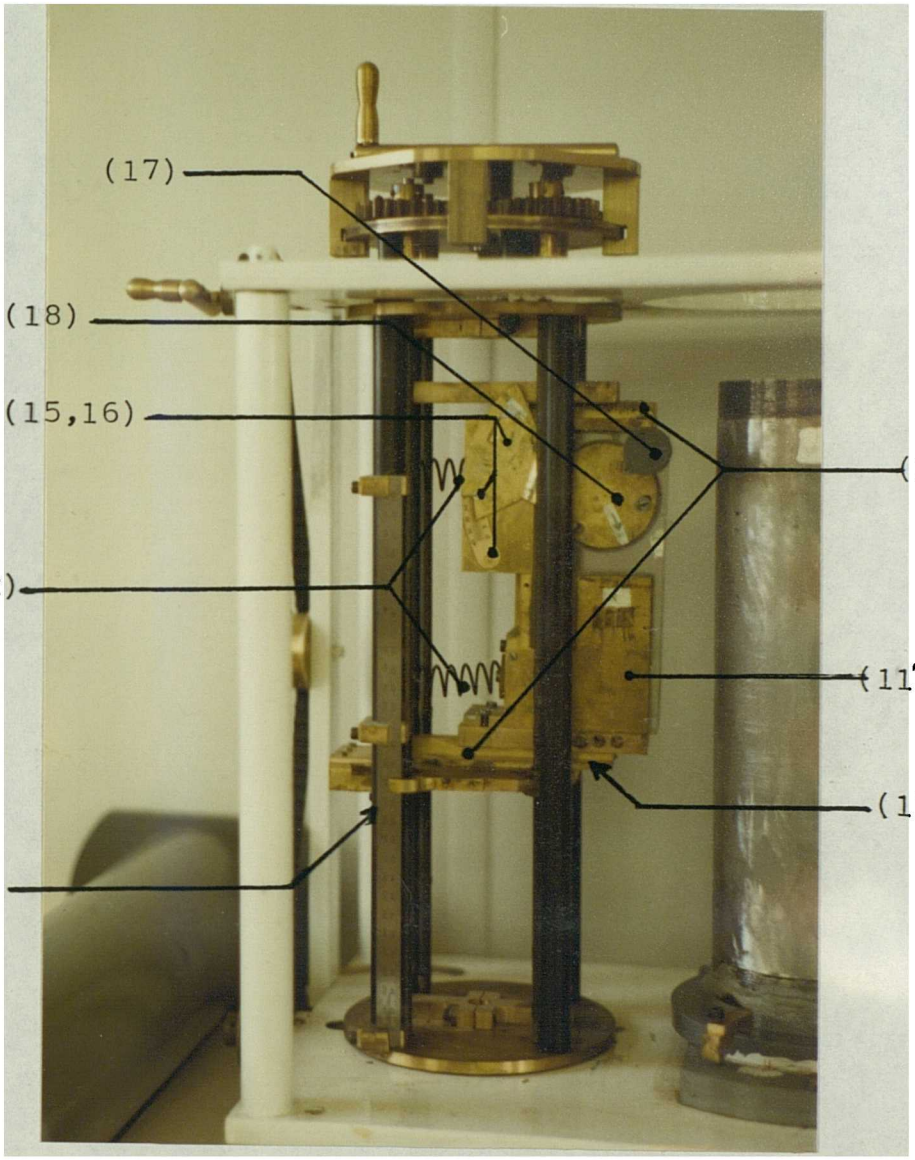

FIG 5.2.
The transducer mechanism

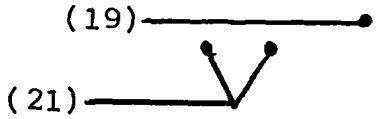
(19)
(21)

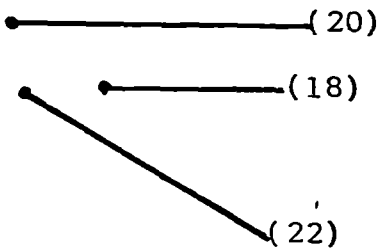
(20)
(18)
(22)

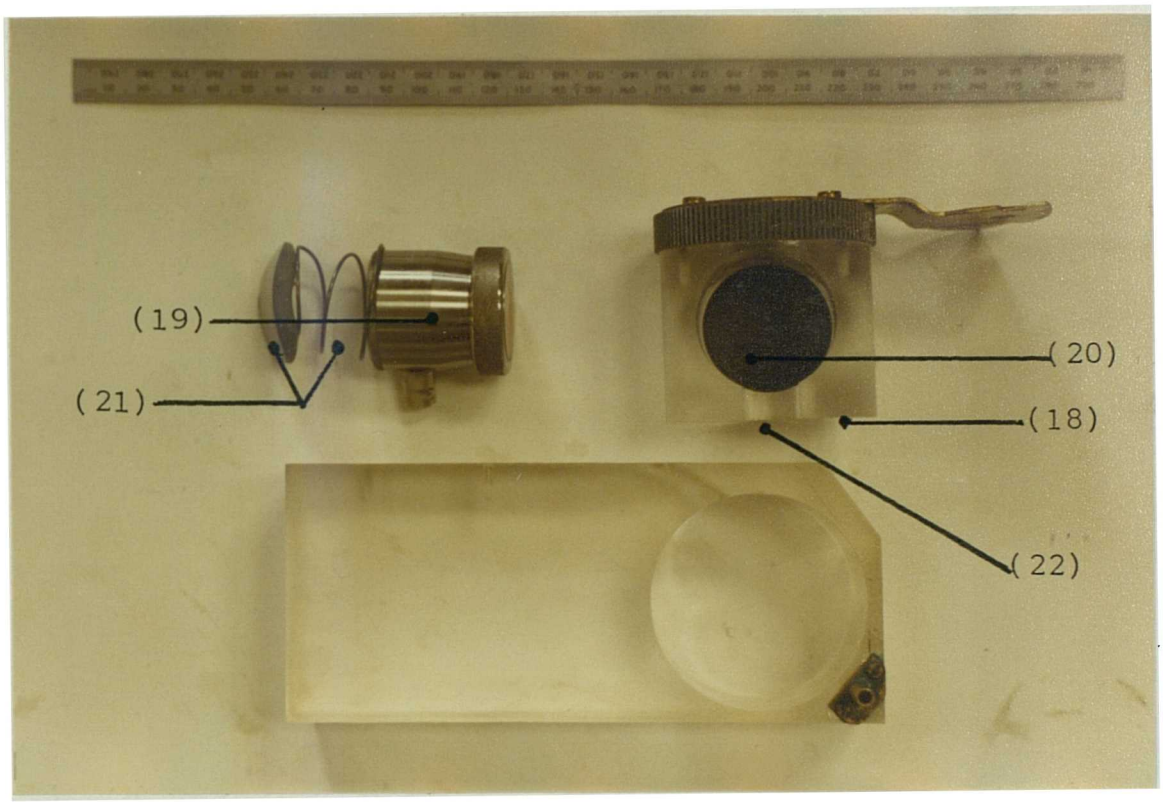

FIG 5.3
Exploded view of transducer and cylinder arrangement

compressed scale (the scale is marked 0-45° and 45°-90° and the pointers arranged so that only one scale can be read). A small knob (17) controls the rotation of the transducer cylinder (18) in the block. The blocks are made out of perspex and are designed so that large angles (wrt the normal) can be used without the beam first hitting the side wall.

The transducer (19) fits snugly into a cylindrical slot (20) cut into the cylinder and is held against a polished face by a cap and spring (21). A further cap ensures that the tension is evenly spread over the transducer. The transducers were chosen to have right angle BNC connector and a small slot is cut sideways (22) into the cylinder to accept this conection.

Most of the drawbacks, discussed previously, had now been overcome but after preliminary testing it was found that the level of received signal varied and it was observed that the only factor, to which this could be attributed, was the interfaces between the transducer and pipe.

It was decided to investigate the interfaces between the transducer and cylinder, the cylinder and block and between the block and the pipe.

An experiment was conducted on the interface between the transducer block and pipe wall whereby varying amounts of coupling compound was used and the received signal observed as a trace on an oscilloscope. The signal observed, under identical conditions apart from the amount of coupling compound, varied from no signal (dry-face) through to maximum signal (well lubricated face) and then stayed at maximum signal for increasing amounts of couplant.

Clearly when the blocks are moved up and down the pipework the amount of couplant is reduced. However, even under the worst conditions a reasonable signal was observed and although it was extremely difficult to put a value on the loss it was found that provided a little time was allowed for the couplant to 'relax' a figure of approximately 5% loss could be used.

A study of the second interface, the one between the block and cylinder revealed that higher signal loss was likely. In this case the rotation of the cylinder caused previously trapped air bubbles to break and form streaks in front of the beam. These bubbles and streaks could be easily viewed by backlighting the perspex. The amount of bubbles and streaks, in the sound path, varied with position and with the rotation of the cylinder. The amount of air initially trapped was also a factor.

By exercising extreme care, it was possible to insert the cylinder with new couplant and reduce considerably the amount of trapped air. Within a certain time and dependent upon the amount of use the problem of streaks and bubbles reappeared. The signal was never entirely lost since there was always some couplant in the interface. A figure of loss between the two angular movements was found to be approximately 8%.

The third interface between the transducer and cylinder prove to be consistently well lubricated mainly because there was no relative movement between the transducer and cylinder.

Attempts were made to try and reduce the amount of trapped air by using more and less viscous coupling materials (eg: grease, oil and detergent) but they did not improve the situation.

However, for slow movement about a point the volume of trapped air did not change significantly and peaks of transmission were observed. These tests will be presented in section 5.3.3.

A further serious problem encountered was the attenuation of the sound beam in the perspex. The attenuation of sound in perspex is very much higher than it is in steel and water and this was previously discussed in Chapter 2.

The dimensional diagram of the transducer block is shown in figure 5.4 and it can be seen that when the transducer is normal to the pipe the distance the sound beam travels (in the perspex) is considerably

shorter than that when the transducer is at its limit (approximately 70°). (Clearly the distance travelled in the perspex is a function of angle). The effect of this will be discussed in section 5.2.1.2.2.

The overall mechanical repeatability of the rig is within +1/2mm (axially) and with regard to the angular positioning is set by eye approximately ±1/4° but also offset by 1/2°.

5.2.1 Temperature and attenuation effects in the rig.

5.2.1.1 Temperature coefficient of gain.

The curves of transmission against angle, to be presented later, were produced by observing the received signal on the output of the amplifier. Because the gain of the amplifier is temperature dependent it was decided to try to measure this effect.

The static rig was set up with the electronics operating in the normal manner. The electronic units were enclosed in screened modules and the system allowed five minutes to warm up (this value would be allowed in any experiment). A digital temperature probe was inserted into the screened box in the vicinity of the amplifier, and a trace of the received signal was observed on the oscilloscope. The system was left running and readings of amplitude and temperature were noted. The water temperature was kept constant to within ±1/2°c. It was found impossible to calculate a temperature coefficient for the following reasons,

(i) the system came upto temperature and then changed very slowly with time

(ii) if the coefficient was the typical value quoted in the data sheet (.2%/°c) then it would have meant observing 4mV in 2000 mV per 1°c change, (ie: the received signal level).

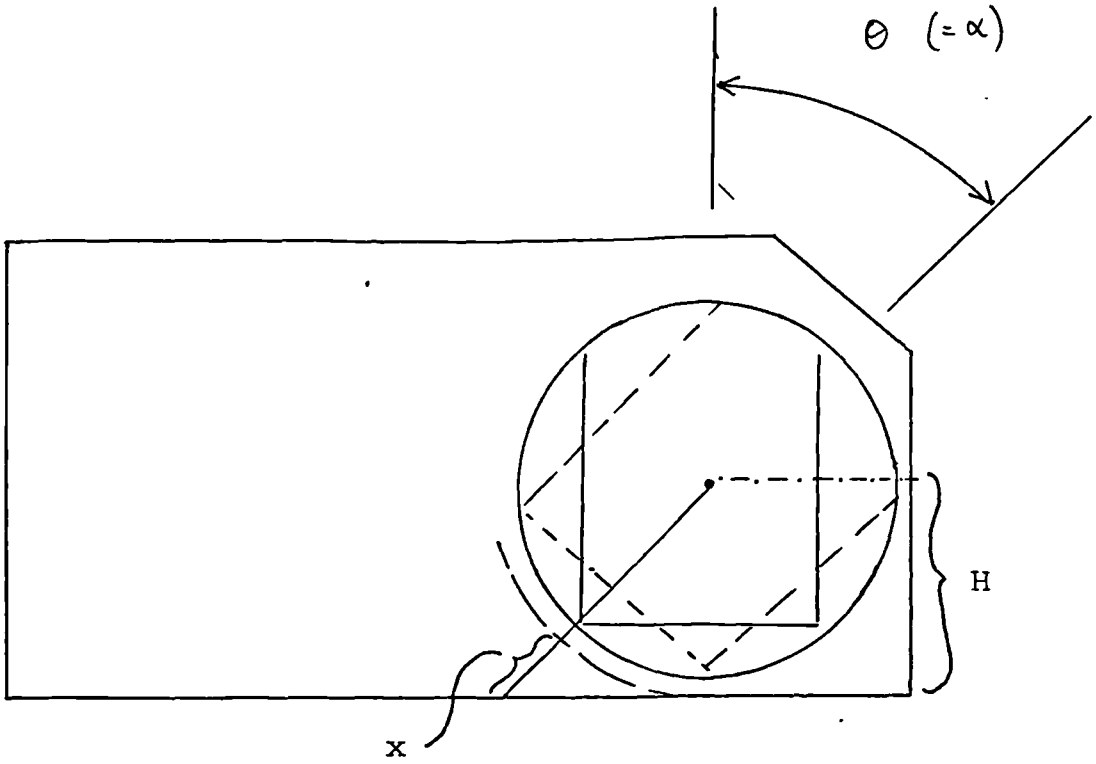

FIG 5.4
Dimensions of the transducer block

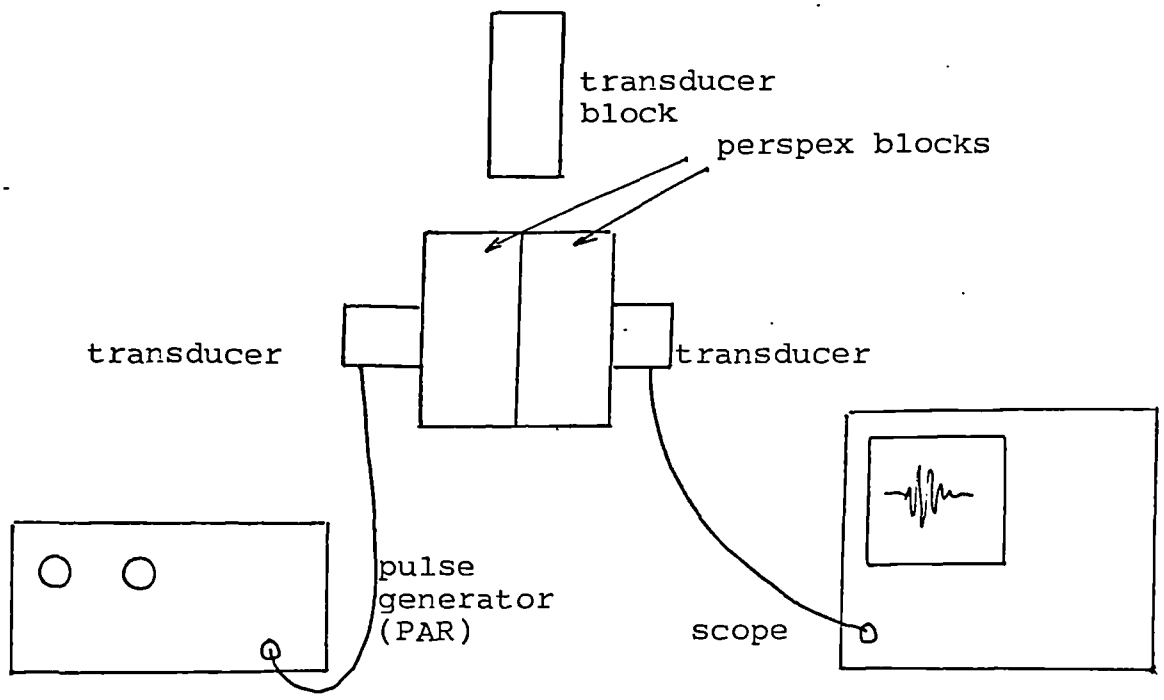

FIG 5.5
Experiment to measure the attenuation coefficient

(iii) artificially increasing the temperature would have produced a value but this was felt to be of little use, because it was not the normal mode of operation of the instrument and the temperature distribution would not be known.

Because a value could not be calculated it was decided to use the typical value as an estimate of the coefficient. Thus over a temperature range of 6° the change in amplitude would be about 1.2%. The figure of 6° is the likely control of temperature on the flow tests to be discussed later.

5.2.1.2 Attenuation in the rig.

The attenuation of sound is a function of temperature and for (distilled) water the values at three temperatures are given below (Kaye & Laby), in Table 5.1.

Table 5.1

Attenuation coefficients

$\frac{\alpha}{f^2} \times 10^{17}$	36	25	19	nepers s^2/cm
Temp	10	20	30	^{o}C
@f=10^6				
α=	$.36\times10^{-3}$	$.25\times10^{-3}$	$.19\times10^{-3}$	nepers/cm
n=	3.127×10^{-3}	2.17×10^{-3}	1.65×10^{-3}	dB/cm

It can be seen, therefore, that over the range 10°c - 20°c the attenuation changes by $.095 \times 10^{-3}$ dB/cm per °c. Therefore over a working range of approximately 10°c the change would be approximately $.095 \times 10^{-2}$ dB down (about .01%). This effect can therefore be ignored.

The values for the attenuation in water steel and perspex were given in Chapter 2. However, it was stressed that the composition used in the manufacture of plastics greatly affects its properties. It was decided therefore, to measure experimentally the value of α, the attenuation coefficient.

5.2.1.2.1 Measurement of the attenuation coefficient in perspex.

The experiment to measure the attenuation coefficient was set up as shown in figure 5.5.

The pulse generator repetition rate was set low enough so that all reflections had died before a new pulse was launched.

A measurement of the maximum amplitude of the pulse envelope was noted under conditions,

(i) block 1 and block 2 together
(ii) block 1 and block 2 with the transducer block between

Care was exercised to ensure that sufficient couplant was applied and that air was excluded. The results of the experiment are given in Table 5.2 for two values of frequency. The attenuation in solids is roughly proportional to f.

Table 5.2

Measurement of attenuation coefficient

Signal frequency	1	MHz
Max amplitude case (i)	.7	Volts
Max amplitude case (ii)	.36	Volts
Block dimension	4.15	cms.
α @ 1MHz	.16	nepers/cm
n @ 1MHz	1.39	dB/cm
α @ 1.25MHz	.2	nepers/cm
n @ 1.25MHz	1.73	dB/cm

The figure for 1.25MHz compares favourably with the figure given by Kaye and Laby (evaluated at 1.25MHz) viz:-

.2 nepers (EXP) versus .28 nepers/cm (K+L)
or
1.7 dB/cm (EXP) versus 2.5 dB/cm (K+L)

Note that the value of α found experimentally also takes into account the beam spreading effects.

5.2.1.2.2 Correction factor for transducer blocks.

Figure 5.4 shows the transducer block used on the static (zero) rig. It can be seen that the excess distance the sound beam has to travel in the perspex (ie: the distance over that travelled when the transducer is at normal incidence), is given by

$$X = H\left(\frac{1}{\cos\theta} - 1\right)$$

where θ is the angle turned and H is the distance at normal incidence (H = 3.175cm) and since the same distance is travelled on the other side of the pipe the total distance is,

$$= 2H\left(\frac{1}{\cos\theta} - 1\right)$$

The signal loss is therefore

$$= n\,2H\left(\frac{1}{\cos\theta} - 1\right) \qquad \text{dB}$$

and since signal loss n = 20 log $\frac{V2}{V1}$, the ratio $\frac{V2}{V1}$ can be found from

$$\frac{V_2}{V_1} = \text{Antilog}\left(\frac{n\,2H}{20}\left(\frac{1}{\cos\theta} - 1\right)\right),$$

where V_2 and V_1 are the voltages received on the transducers.
Thus the ratio $\frac{V_2}{V_1}$ is the ratio that the signal is down on the value at normal incidence. Hence to correct for attenuation losses the received signal must be adjusted by the above factor.

5.3 Comparison of theoretical and experimental transmission curve.

5.3.1 Pipe sections and materials.

It was decided to produce theoretical transmission curves for a number of typical pipe sizes and materials. Four pipe sections were chosen and the dimensions, material and sound speeds for these sections are given in table 5.3. Also given in table 5.3 are the material constants for perspex.

Table 5.3

Pipe section parameters

	bore size (mm)	material (mm)	wall thickness (mm)	density (kg/m^3)	longit. speed (m/s)	shear speed (m/s)
Pipe 1	100	stainless steel	3.1	7800	5979.7	3246.3
Pipe 2	100	mild steel	6.3	7900	5940	3100
Pipe 3	150	mild steel	5.3	7900	5940	3100
Pipe 4	100	ABS	7.12	1080	2160	884
Perspex			1190	2700-	1330 2760	

There are two cases of interest in the production of experimental curves. Firstly, the actual signal received through the transducer blocks, (ie: with attenuation) is important in relation to the actual construction of transducers. Secondly, the corrected signal response to show the comparison with the theoretical curves. It was decided, therefore, to consider both options and these will be presented in section 5.3.3. on experimental results.

5.3.2 Theoretical curves.

It was decided to run TPLATE AA and TPLATE BB using the data given in the previous section. The main resonant frequency of the system was around 950KHz-1MHz and it was decided to run the programs at frequencies above and below this value so as to cover a range. The frequencies chosen were 850KHz and 1.25 MHz.

The results of running the programs are shown in figures 5.6-5.13, where each plot has a code in the top left hand corner corresponding to the conditions of test. The code is made up as follows:

SS 4 L BB

- BB — Transmission through both walls
- L — L = lower frequency 850KHz; Blank = high frequency 1.25MHz
- 4 — Pipe size 4 = 100mm; 6 = 150mm
- SS — Material SS = Stainless steel; MS = Mild steel; ABS = ABS plastic

Figures 5.6 and 5.7 show the results of running the program for the stainless steel case. In figure 5.6 the frequency is 850KHz and it can be seen that the two modes coresponding to A_o and S_o are well separated. It can also be seen that transmission through the plates should be possible right up to 89^o.

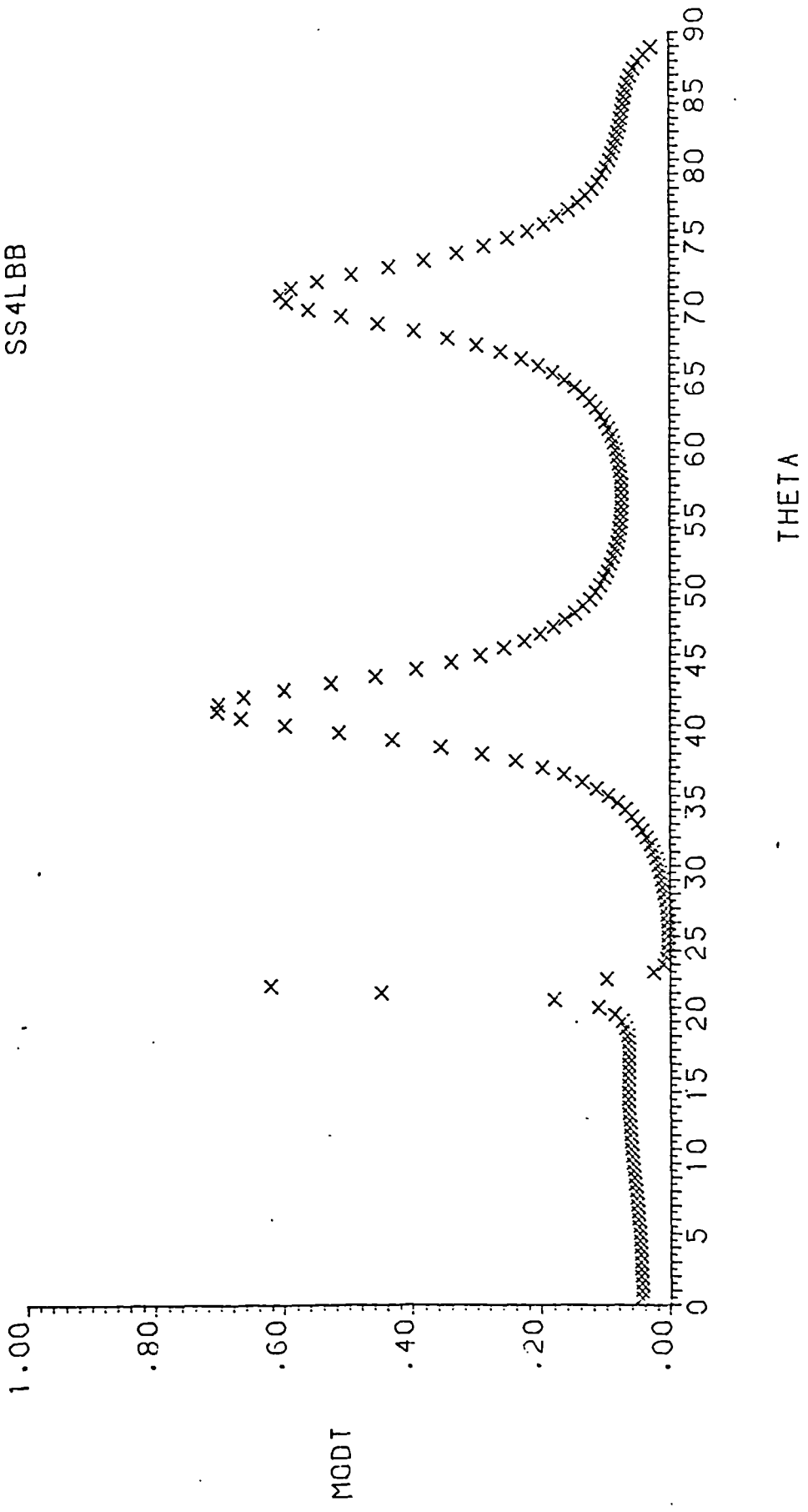

FIG 5.6
Transmission plot of S/S section at .85MHz

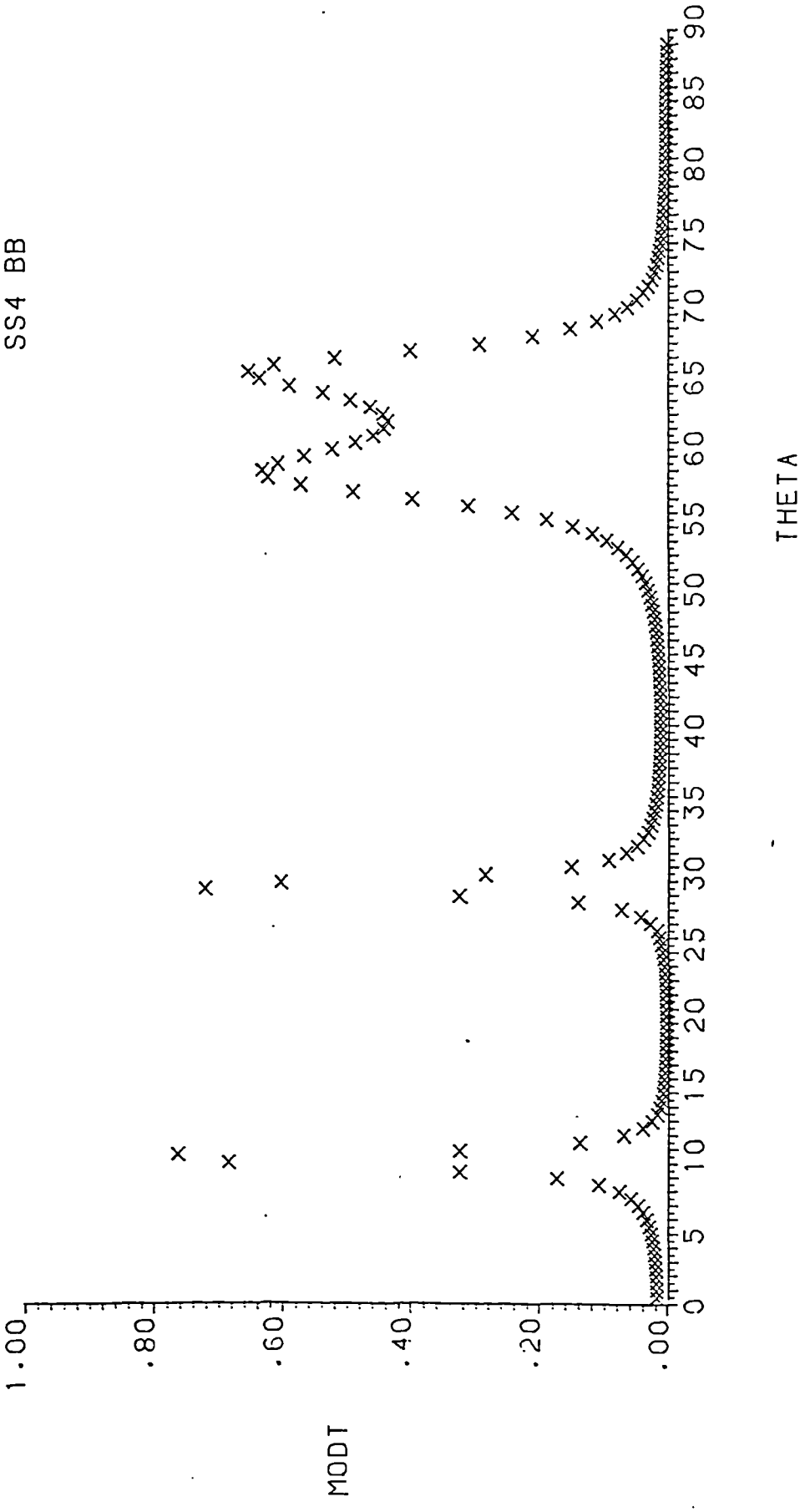

FIG 5.7
Transmission plot of S/S section at 1.25 MHz

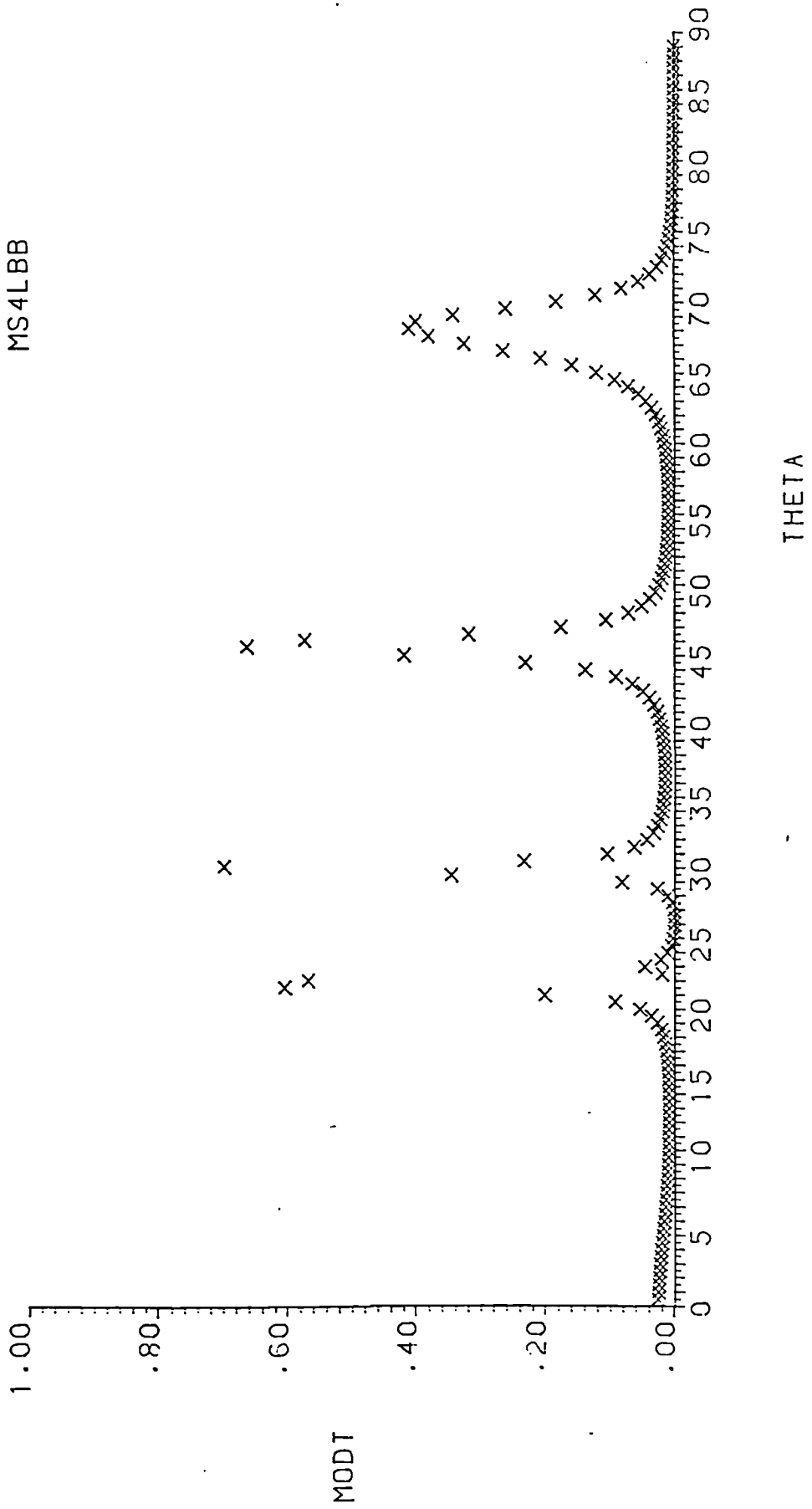

FIG 5.8
Transmission plot of M/S section at .85 MHz (thick wall)

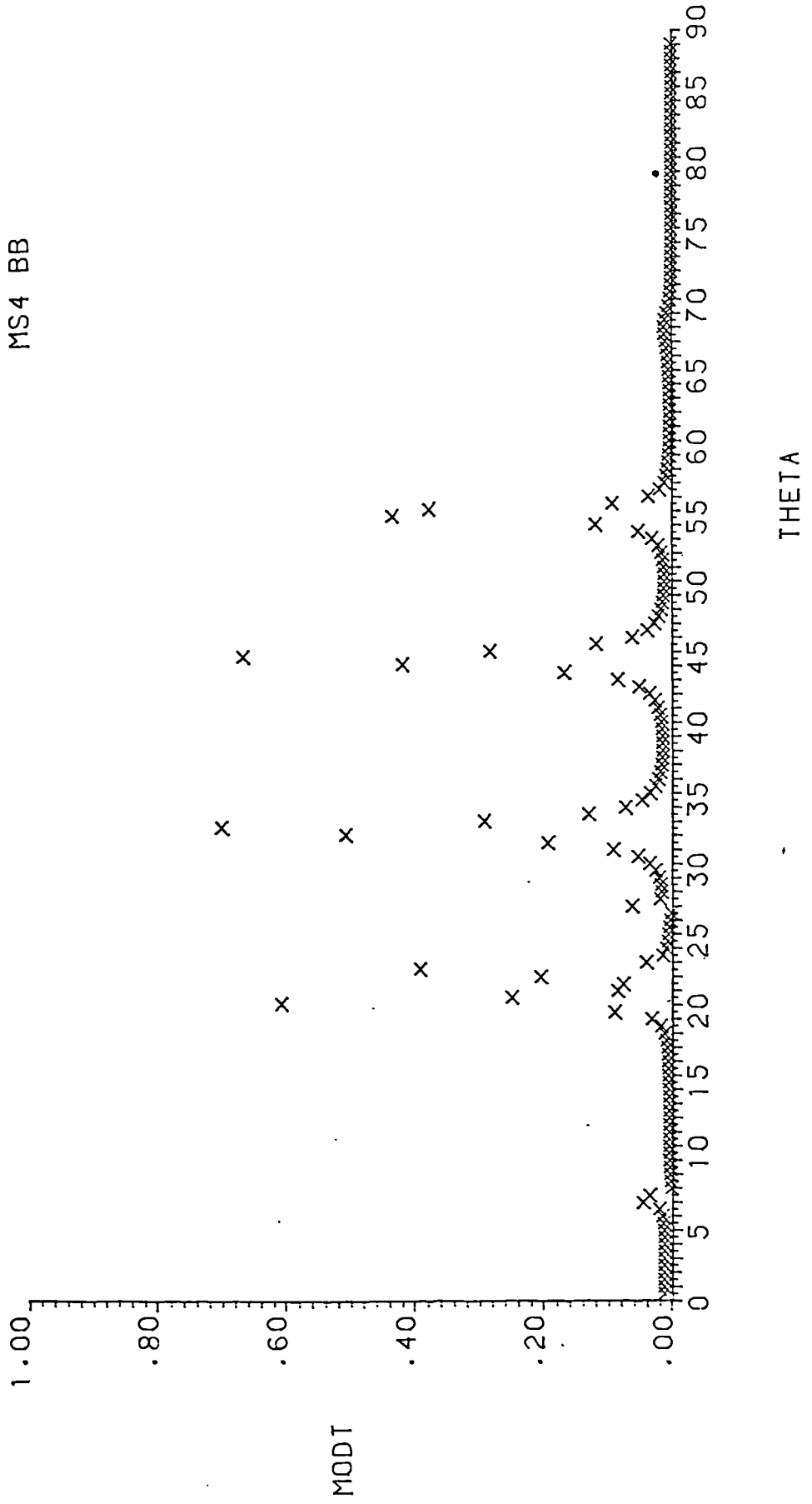

FIG 5.9
Transmission plot of M/S section at 1.25 MHz (thick wall)

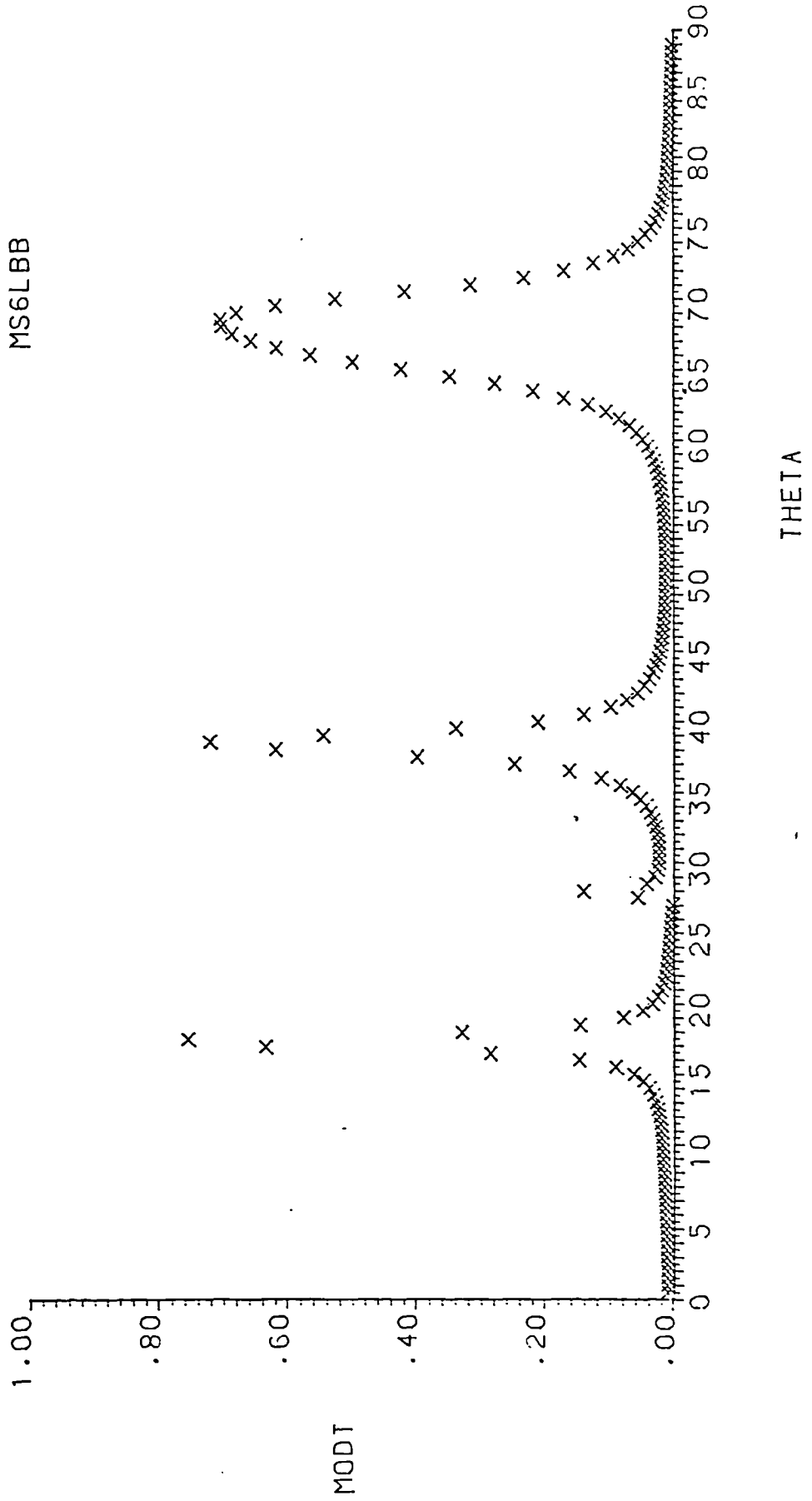

FIG 5.10
Transmission plot M/S section at .85 MHz (thin wall)

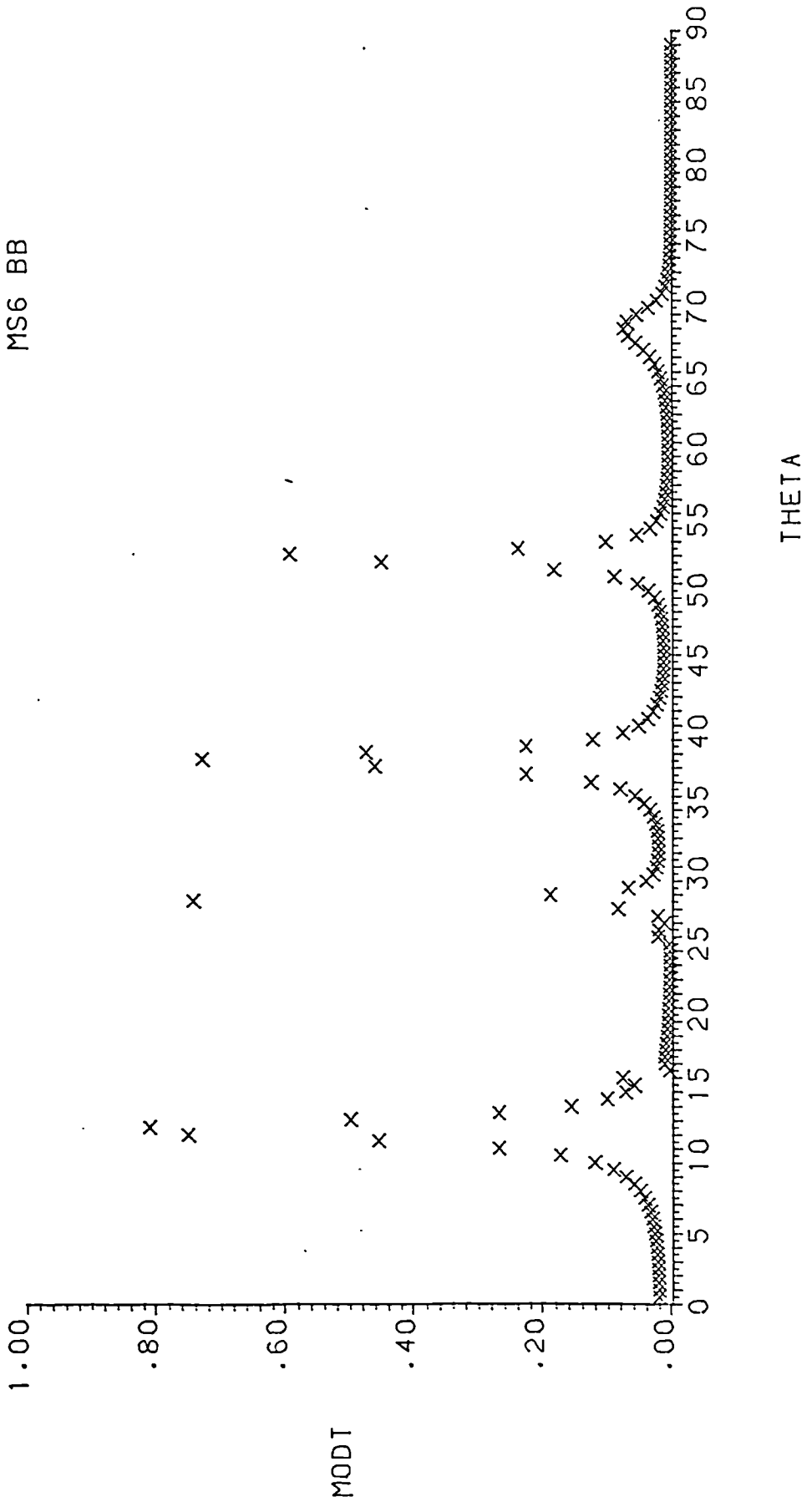

FIG 5.11
Transmission plot of M/S section at 1.25 MHz (thin wall)

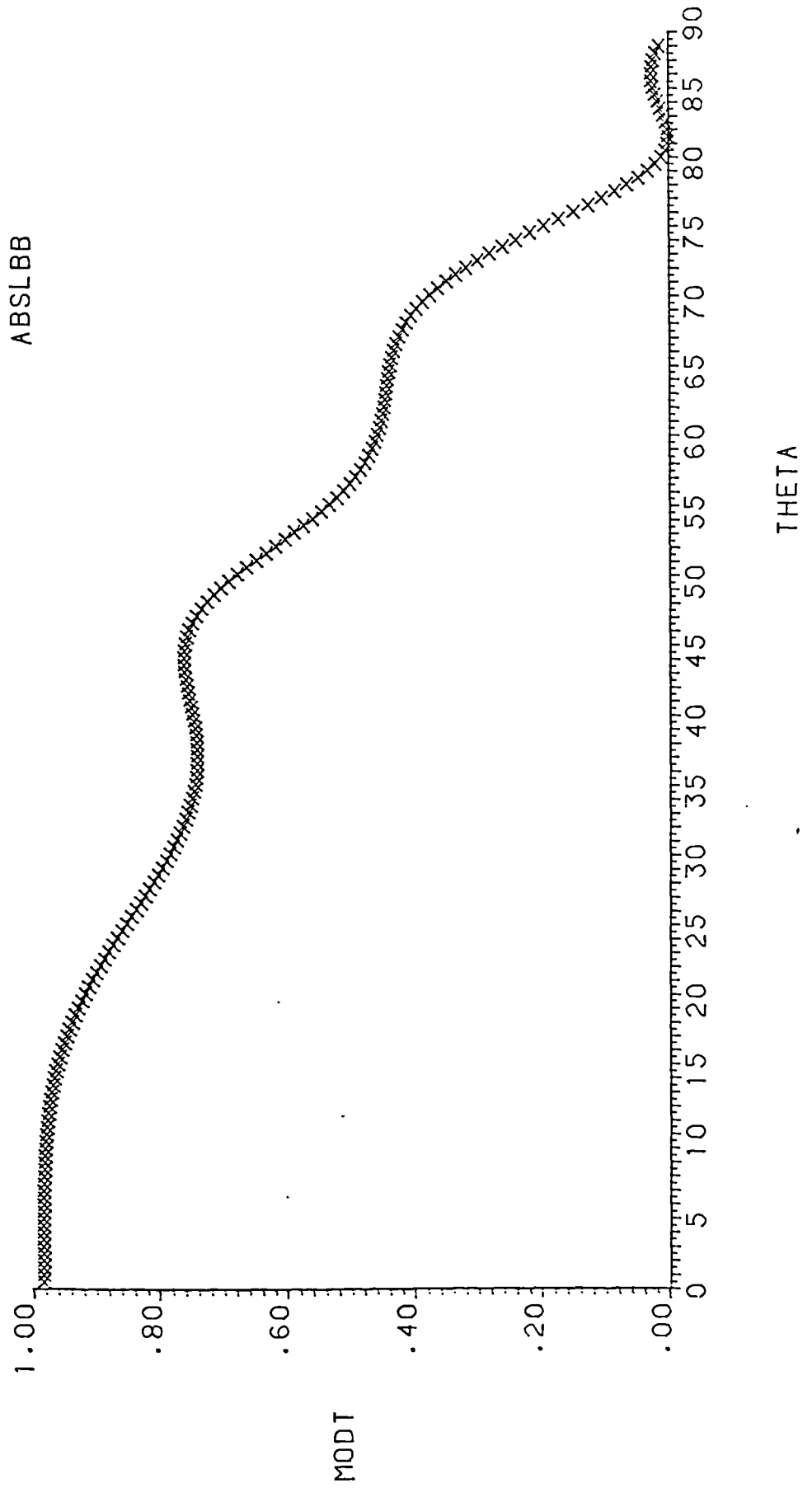

FIG 5.12
Transmission plot of ABS section at .85 MHz

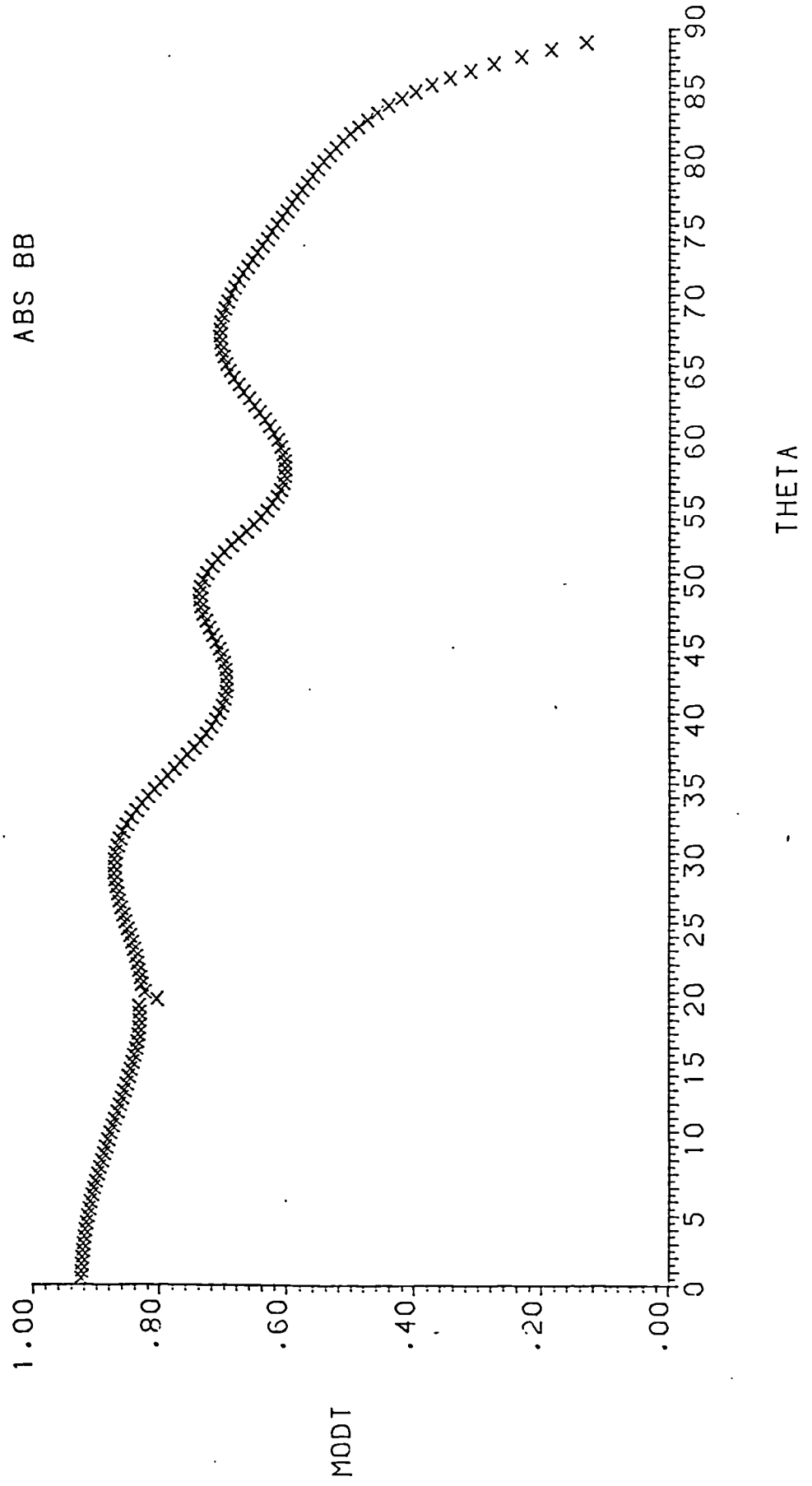

FIG 5.13
Transmission plot of ABS section at 1.25 MHz

In the higher frequency case (figure 5.7) the modes have now joined and transmission could be expected, at a significant level over approximately 15° (56°-69°). A further mode has now been excited but this mode and the other mode are both very narrow and may require precise positioning.

Figures 5.8 and 5.9 are the results of running the program for pipe 2 (the mild steel 100mm pipe). In figure 5.8 the results (at the low frequency) show that transmission would be possible at an angle of 67°-71° plus four other modal points (although one of these, at 24° is very small). However, in figure 5.9, at the higher frequency, the mode at 67°-70° has now almost totally disappeared, and as far as the sound is concerned at this angle, the pipe wall begins to look like a half space. Other modes are now intersected but all modes are now very narrow.

The results of testing the same material but with a slightly smaller wall thickness are shown in figures 5.10 and 5.11, which are figures for pipe section 3, the 150mm section. It should be noted that the model used in the TPLATE programs does not take into account the nominal bore thus the only variable is the wall thickness.

It can be seen that there are similarities between figures 5.8 and 5.11 (the 100mm low frequency cases) but now because the wall is thinner the mode is more pronounced in the 150mm pipe case. A similar observation can be made about figures 5.11 and 5.9 but now the mode (A_o, S_o) is still existent in the thinner walled vessel and the other modes are slightly wider than in the 100mm pipe case.

The final figures presented are for the ABS case (figures 5.12 and 5.13). In this case the acoustic impedance mismatch between perspex and ABS is very small and one would expect very good transmission (3213×10^3 Pas/m (perspex) against 2333×10^3 Pas/m (ABS)). This expectation is borne out by the results shown in the figures. In terms of dispersion curves it would appear that the condition for light loading is not fulfilled, hence the modes are considerably broader and in fact overlap to such an extent that transmission nulls are not produced.

5.3.3 Experimental curves

Preliminary experience with the static (zero) test rig showed that the error possible in a reading was of the order of 5% for the pipe transducer interface and 8% for the cylinder interface, and approximately 1% for the gain variation due to temperature effects. Because only one transducer block was moved at a time the overall error from the above sources would be approximately 14%. During the test program it was observed that another error was possible and that this was due to the sound beam reflecting inside the pipe, striking the top and/or bottom surfaces and reinforcing the signal either destructively or constructively.

A test was conducted whereby small amounts of water were added to the section and a note made of the change in amplitude of the signal. The error was found to be of the order of 12% for the worst case. Combining all errors would therefore result in a worst case error possibility of 26%. In practice the errors in repeatability were found to be, in general, less than 12% and particular attention was paid around transmission peaks to ensure signal repeatability.

The experimental procedure for the production of transmission curves used the test setup as shown in figure 5.14. This consisted of a HP function generator driving a transducer and the transmitted, received and amplified signals displayed as traces on the oscilloscope.

The function generator was switched into sine wave operation and initially set at the resonant frequency of the system .950-1MHz. However, the stability of the function generator was questionable and it was observed that the amplitude of the received signal drifted in agreement with the frequency drift of the generator. Since a drift about the resonance frequency meant a considerable loss in level, it was decided to operate well away from resonance at 1.25MHz. Drift in the frequency was still observed but with very little change in the amplitude. This frequency was also chosen to form a direct comparison with the theory.

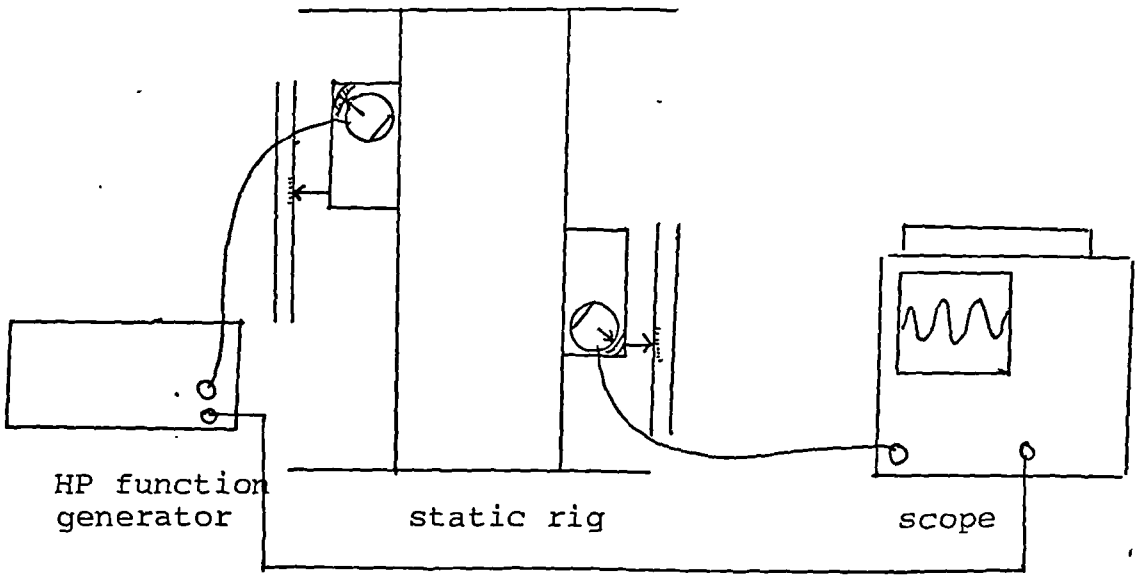

FIG 5.14
Experiment to measure actual transmission curves

The input signal amplitude was monitored and kept constant throughout the experiment.

The transducers were mounted on the platforms and the 100mm Stainless steel pipe section was inserted into the rig. The transducers were lubricated and mounted against the pipework at set positions. Care was taken to ensure that the cylinder blocks were well lubricated and had very little trapped air.

Expected angles of transmission were set on the cylinders and the platforms were adjusted until a peak transmission was observed. The angles of both transducers and the axial positioning was then adjusted and at every adjustment a recording of the amplitude level, position and angle was made.

A program was written to process the data and produce a plot similar to the theoretical plots produced by the TPLATE programs. This simply meant normalising the data and using the same axis as the theoretical plots. The data was fed into a file and read by the programs (READ. PLOT).

The resulting plot for the stainless steel case is shown in figure 5.15. This figure shows where the maximum transmission can be observed for a practical situation. The peaks on this curve are seen to be at angles 8°, 33° and 66° and should be compared with the theoretical curve produced and shown in figure 5.7. The peaks, according to the theory occur at 10°, 30°, 59° and 66°.

If the dual peaks of the theoretical curve are considered as one then a form of rough agreement can be observed. However, the width of the peaks for the experimental case are wider and this will be discussed later.

When the data is corrected for attenuation effects, as described earlier, the resulting plot is as shown in figure 5.16 and shows a slight shift in angular position and a marked difference in amplitude.

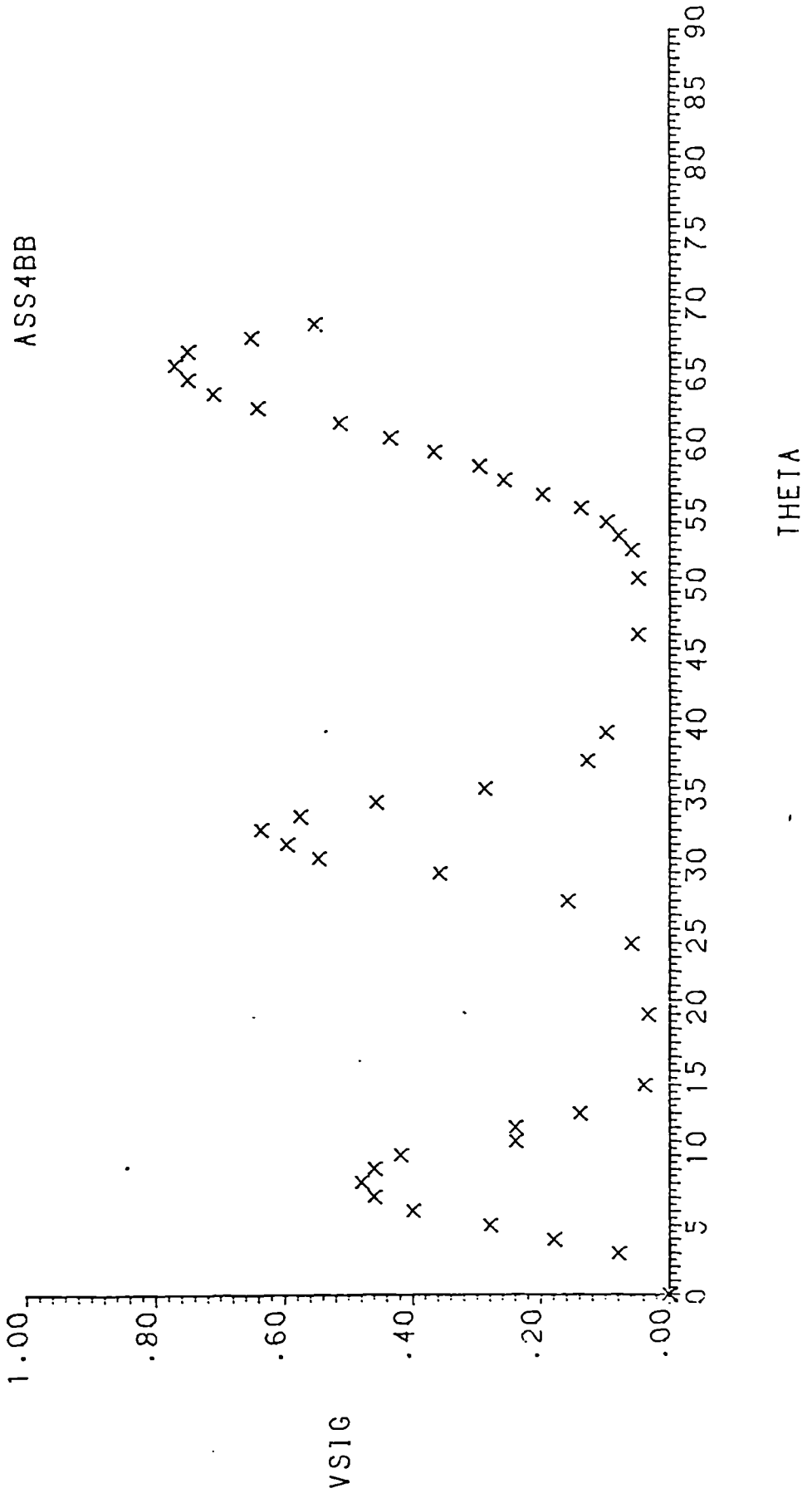

FIG 5.15
Transmission plot (actual) of S/S section at 1.25 MHz (uncorrected)

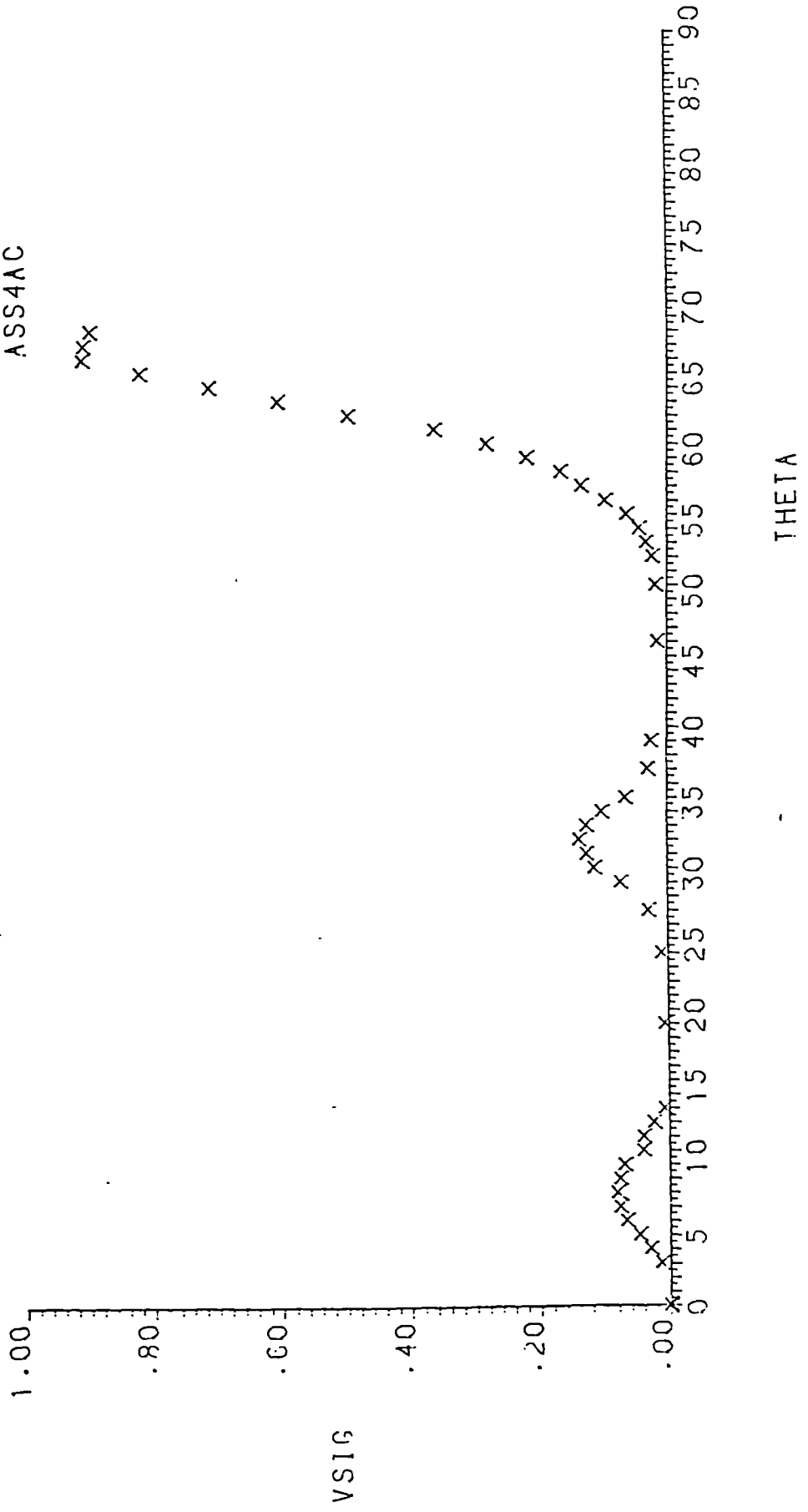

FIG 5.16
Transmission plot (actual) of S/S section at 1.25 MHz (corrected)

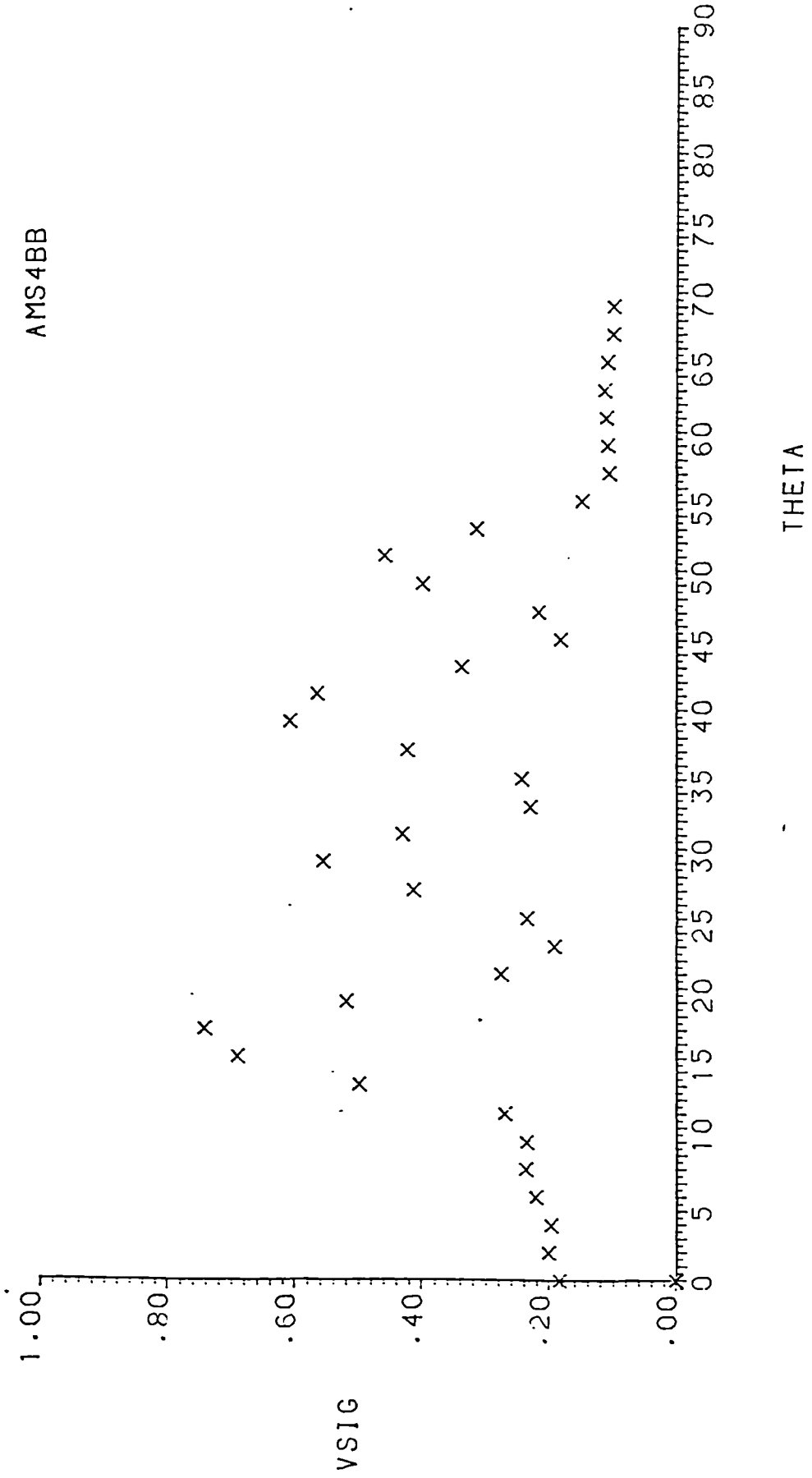

FIG 5.17
Transmission plot (actual) of M/S section at 1.25 MHz (uncorrected)

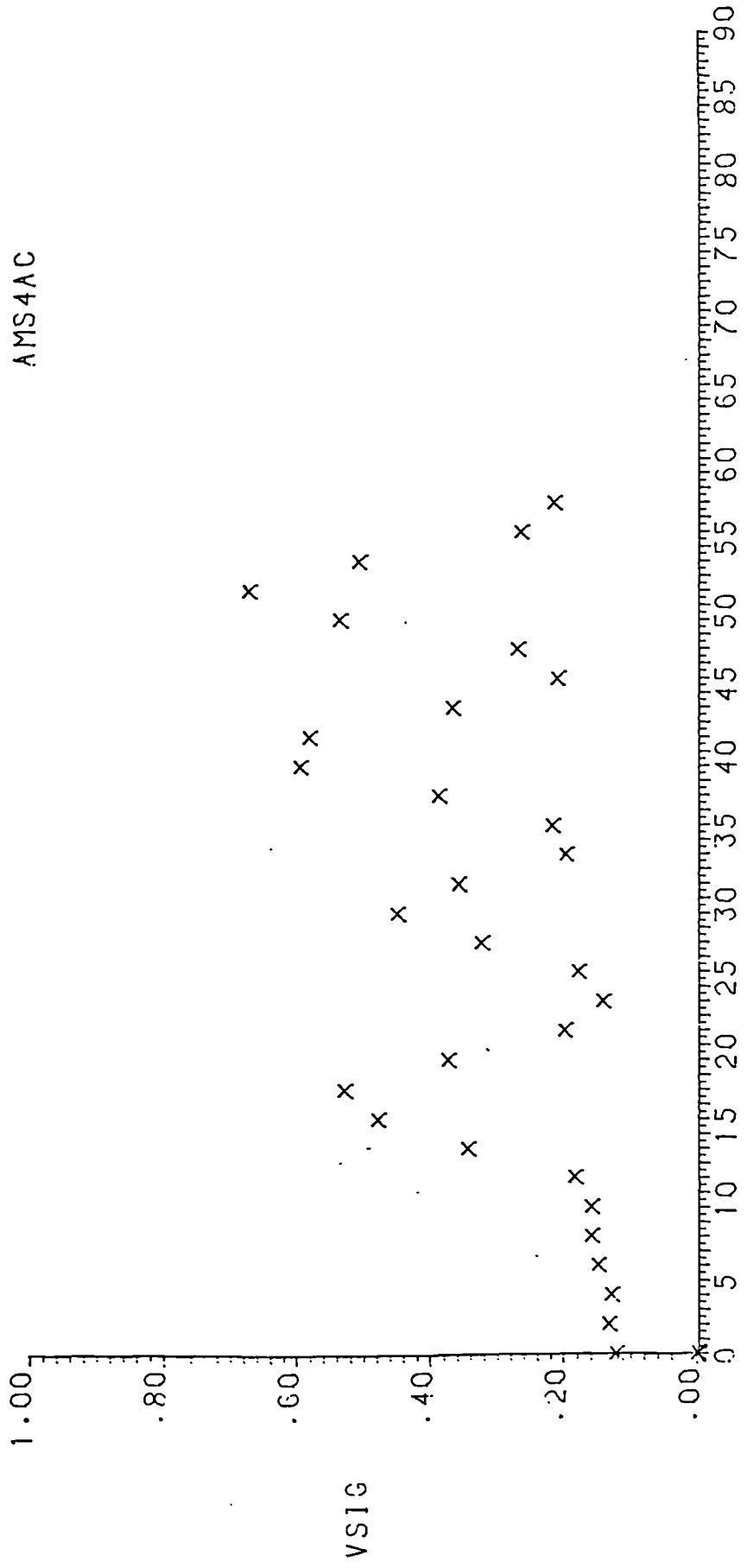

FIG 5.18
Transmission plot (actual) of M/S section at 1.25 MHz (corrected)

It was felt that a better approach to the procedure would be to integrate along the entire path for each particular angle. This would then ensure that all the transmitted sound would be collected and this may account for the change in the signal levels encountered in the stainless steel case. It was also felt, that, from the repeatability point of view, the signal loss would be lower.

The system was set up as previously described but now with the 100mm mild steel pipe section. The amplitude of the input signal was monitored and kept constant throughout the experiment. The platforms were set at a particular position and all interfaces were well lubricated. The angle was set in 2° steps and the platforms were separated in 10mm steps. Readings of angle, position and signal level were recorded. In all over 900 positions were recorded.

At several positions a repeat measurement was taken after some time. This entailed returning to the angles and axial position previously used. The signal amplitude was then measured and compared with the previous reading. In general the result was a reading within 12%, although in one case a high error was observed (aproximately 20%).

For each particular angle the resulting amplitude was averaged and fed into a data file. The resulting plot (normalised) is shown in figure 5.17 and the attenuation corrected plot is shown in figure 5.18. It can be seen that there is little difference in the plots and it would suggest that the method of integrating the sound is more accurate for comparison purposes with the theory, since the theory assumes total collection of sound.

Comparison of figure 5.18 with the theoretical curve of figure 5.9 shows a form of rough agreement. The angles of peak transmission, found experimentally are at 18, 30.5°, 41.5 and 52.5 whereas, those produced by the theory are at 21°, 23.5, 33.5, 45.5 and 56. If one assumes that the two peaks at 21 and 23.5 are observed as one experimentally then there would appear to be an offset of approximately 3°-4°. Allowing for the fact that the system has a small offset (order 1/2°) the error cannot be totally eliminated and as yet no reason can be found for this systematic type error.

However, it is of interest to consider the differences between the model chosen and the experimental results.

In the theoretical model, infinite plane waves impinge upon an infinite plate (flat plate). In the experimental model the transducer produces a sound field that is finite and this impinges upon a cylindrical, finite, plate. Furthermore the beam has a near field of length n= in which the pressure field changes rapidly with position, n=57.8mm for the present case under consideration. In this region the radiated wave is not plane. Thus the final result is that the transducer produces a beam that insonifies mainly alone a line on the pipe and then with varying pressure.

A further difference between the model and static rig is the transducer block. This has finite dimensions but in the model has infinite dimension. The block is also assumed to have no tangential stress coupling with the pipe. In reality there is probably a small amount of coupling.

When a Lamb mode is generated in the pipe wall it travels in both directions. At the end of the pipe the wave is reflected and thus interferes with the incident wave. However, the time taken to travel to the end wall varies with position, but is usually of sufficiently long time not to interfere with the transmitted wave but possibly with the received wave. This will clearly be different from the theoretical case in which a wave is assumed in one direction only. Also, important to this argument is the fact that modes decay at different rates (see eg: Viktorov) and thus the reflection will be of different amplitudes.

The widths of the modes observed in the experimental case are considerably larger than those in the theoretical case. A possible reason for this is the absorption in the plate, which is not included in the theoretical model. The effects of absorption are shown in the work of Madigosky and Fiorito.

5.4 The measurement of C from outside of the pipe.

The equation proposed for obtaining C from outside of the pipe is (2.49)

$$C = \frac{1}{\sqrt{\left\{\left[(T-T_2) - \frac{L_T}{C_p}\sin\alpha + (L_C+L_D)\right]\frac{1}{D-2d}\right\}^2 + \frac{\sin^2\alpha}{C_p^2}}}$$

where the variables have the following meanings:

T = time measured through pipe section
T_2 = time measured with the blocks face-to-face
L_C, L_D = the length of the centre line of the beam in the perspex
$D-2d$ = internal diameter
α = the angle the transducer makes with the normal
C_p = speed of sound in perspex
L_T = distance between the intersections of transducer planes with the pipe.

The measurement of D-2d and is straight forward. The measurement of L_C, L_D and L_T is dependent upon the block being used and this is discussed in the following section. The measurement of Cp is relatively straightforward and this is discussed in section 5.4.2.
As a check on the value of C it was decided to measure C independently and this was carried out by using the test box and is discussed in section 5.4.3.

5.4.1 Measurement of L_C, L_D and L_T

Consider the block and pipe dimensions as shown in figures 5.19 and 5.20.

The distance L_T is,

$$= C\text{- to -}C \text{ distance} - 2M + 2[(M-y)+Q]$$

and L_C, $L_D = \frac{r}{\cos\alpha}$ (assuming blocks are identical).

5.4.2 Measurement of the speed of sound in perspex.

A necessary requirement for the calculation of C from outside of the pipe is, amongst other things, a knowledge of Cp, the sound speed in the perspex.

Two blocks of perspex were cut from the same piece of material as that used in the construction of the transducer blocks. The blocks were cut so as to fit the test box. They were then left along with the rest of the apparatus to attain room temperature.

The water and brass plates were removed from the test box and one piece of perspex was lubricated and inserted into the box. A firing pulse (of a low repetition frequency) was launched and a simultaneously derived start pulse was sent to the HP counter/timer, set in time interval mode. The pulse received from the back face of the block was processed and a stop signal sent to the HP counter/timer. A precise timing measurement was made (for n=1000) and recorded.

The second perspex block was lubricated and inserted firmly against the first block so as to ensure good contact and the exclusion of air bubbles. A second precise timing measurement was made.

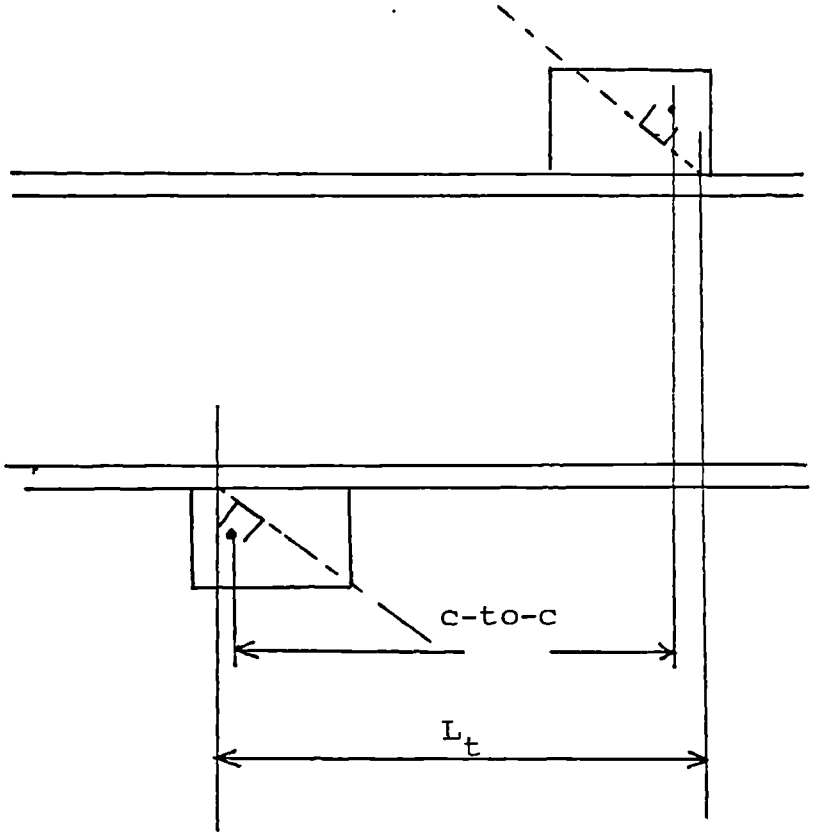

FIG 5.19
Static rig transducer dimensions

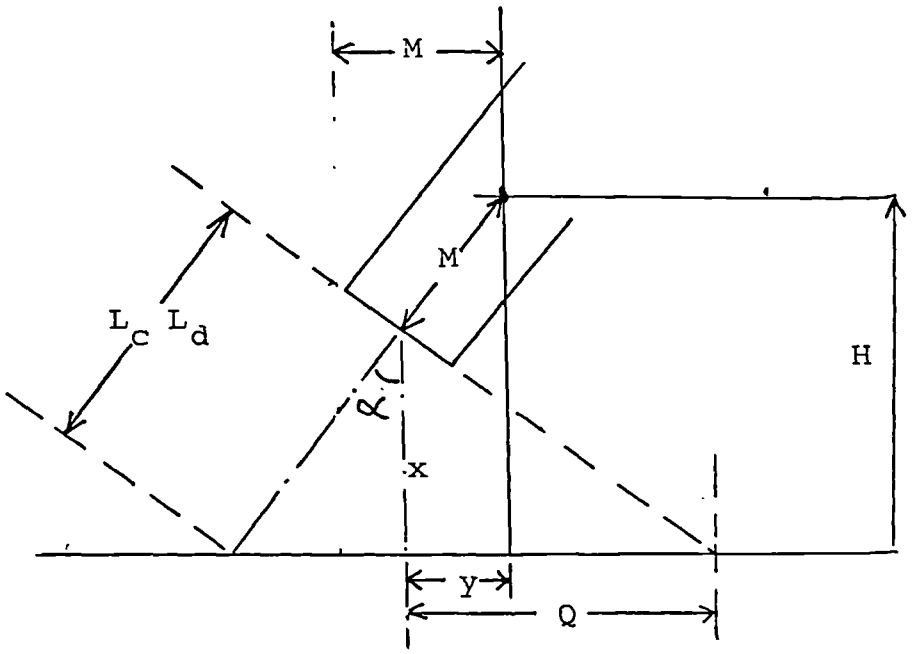

FIG 5.20
Exploded transducer dimensions

The second block was accurately measured using vernier calipers.

The temperature was recorded at 20.3°C and the value of Cp was calculated to be 2707 m/s. This compares favourably with Cp=2700 @ 20°C given by Kaye and Laby.

5.4.3 Measurement of the speed of sound in water.

An amount of water was drawn off from the rig and poured into the test box. The two brass plates were inserted and the system was set up as shown in figure 5.21. All apparatus was left to attain room temperature.

The repetition rate of the firing circuit was made low enough so that the effect of reflections could be ignored. The firing pulse was launched and received off the first brass plate where it was processed by the receiver/processor circuit. A start pulse was derived from the firing pulse and a stop pulse was obtained from the receiver/processor. Both pulses were delivered to the HP counter/timer set in time interval mode.

The strobe gating was adjusted and the experiment was repeated with the second brass plate acting as a reflector.

The times for both experiments were accurately measured on the HP counter/timer. The distance between the brass plates was also accurately measured using a pair of vernier calipers. The temperature of the fluid was measured at 21°C. The value of C was calculated to be 1485.88 m/s. This compares favourably with that given by Kaye and Laby at 20°C (1482.9 m/s) if the coefficient (temperature) is taken into account (3 m/s/°C).

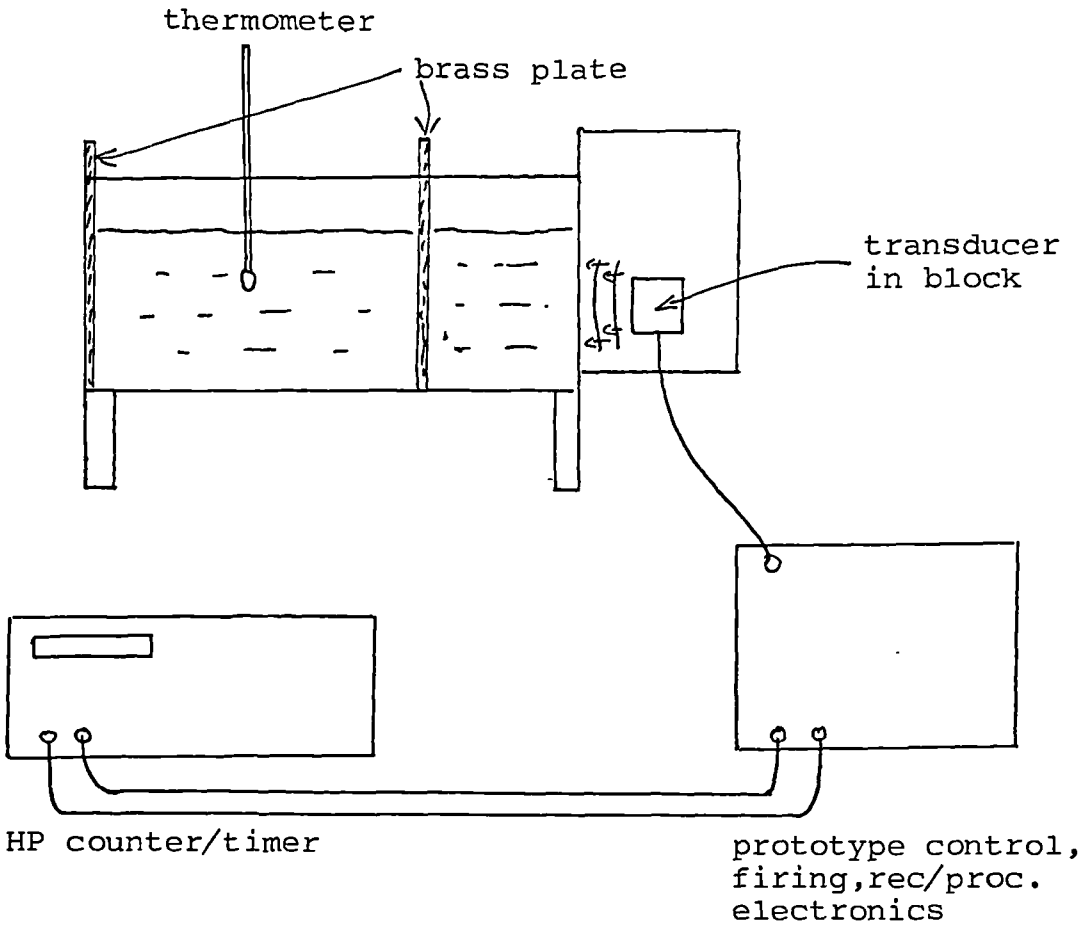

FIG 5.21
Experiment to measure the speed of sound in water

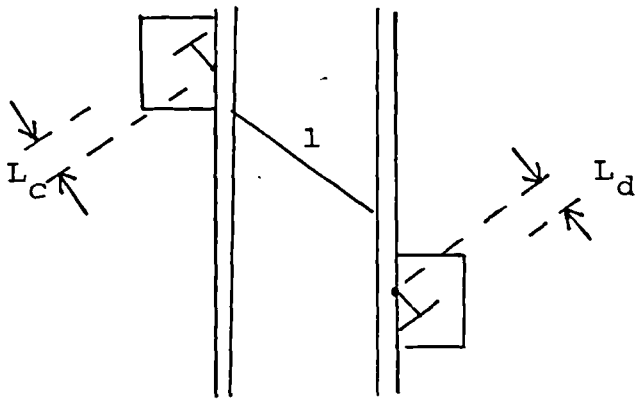

FIG 5.22
Model used in measurement of $\frac{dT}{T}$

5.4.4 Measurement of times T and T_2

An experiment was set up to measure the times T and T_2. The blocks were carefully placed on the pipe and all distances were recorded. The transducer was excited by the firing pulse (which also produced the start pulse for the HP counter/timer). The received pulse was processed by the receiver/processor and produced a stop pulse for the HP timer/counter. A precise timing measurement was made over 1000 samples.

The blocks were removed from the pipe and placed face to face so that a beam was continuous from the centre of one transducer to the centre of the other. Another timing measurement was made (for T_2).

The results of the measurements and the calculation for C is shown in table 5.4. The experiment was repeated at a new position and the results of this test are also shown in table 5.4.

The correction factor for the times T and T_2 will be discussed further in Chapter six, the flowtests, but is essentially due to the fact that the pulse forms are different for the plastic (perspex) and for the pipe configurations. When the time is considered from the leading edge the correction factors are as given in table 5.4.

Table 5.4

Relating to the calculation of C

	Test 1	Test 2	
C-to-C	.185	.195	m
M	.02025	.02025	m
H	.03175	.03175	m
α	62.5°	62.5°	
L_C'L_D	.0485	.0485	m
L_T	.1724	.1824	m
C_p	2707	2707	m/s
Temp	21°	21°	celcus
T	118×10^{-6}	121.25×10^{-6}	seconds
T_2	37.914×10^{-6}	37.914×10^{-6}	seconds
D-2d	.1027	.1027	m
Correction T	3.5×10^{-6}	3.5×10^{-6}	seconds
Correction T_2	2.8×10^{-6}	2.8×10^{-6}	seconds
Calculated Value of C	1517	1517.8	m/s
Measured Value of C	1486	1486	m/s
% error	2.09	2.1	%

Although the error in measuring C would appear high (2%) it was felt that this was probably caused by errors in alignment and measurement of distances. It was felt that the same value of C at another position (test 2) confirmed the consistency of the theory. It was decided to leave further testing of C until the flow tests.

5.4.5 Measurement of dT/T

It was decided that in a practical model it would be unrealistic to expect T_2 to be measured every time. It would probably be given a value at a particular temperature and a temperature coefficient and would be stored in memory. It would then be important to know how T varied with temperature and it was decided to calculate $\frac{dT}{T}$ both experimentally and theoretically for a simplified model.
This model is shown in figure 5.22.

The time T across the model is given by

$$T = \frac{L_C + L_D}{Cp} + \frac{L}{C}$$

and

$$dT = \frac{\partial T}{\partial Cp} \cdot \frac{\partial Cp}{\partial temp} \cdot dtemp + \frac{\partial T}{\partial C} \cdot \frac{\partial C}{\partial temp} \cdot dtemp$$

using previously given values $\frac{dT}{T}$ can be calculated to be

$$\frac{dT}{T} = -.116\%/^{\circ}C$$

The apparatus was set up as shown and the system was allowed to come up to temperature and was monitored over a five hour period. The results of this test are given in Table 5.5.

A similar experiment was conducted over a second day and these results are also shown in table 5.5.

Table 5.5

On the measurement of dT/T

	Test 1	Test 2	
Time	118.278	118.234	μS
Temp	19.0	19.1	°c
Time	117.984×10^{-6}	118.070	μS
Temp	21.2	20.1	°c
dT	-133nS/°c	-164nS/°c	
$\frac{dT}{T}$	-.113%/°c	-.138%/°c	

The temperature probe used had an error of +.2°c and this is thought to account for the slight change in the absolute value.

Thus the values -.113% and -.138% /°C appear close to the predicted value.

5.4.6 Repeat Measurement of C without T_2.

A repeat experiment of the measurement of C was conducted without measuring T_2 and the results of this are given in Table 5.6. This experiment entailed reassembling the rig as previously set up for test 1 and repeating the procedure. A correction for temperature difference (17.2° in this experiment as opposed to 21°C in the other experiments) has been included, in the correction of T. No correction factor has been allowed for T_2. This is because T_2 varies much slower with temperature than T, ie: $\frac{dT_2}{T_2} = \frac{2}{2700}$ as opposed to $\frac{dT}{T} = \frac{3}{1480}$ per °C

Table 5.6
Repeat measurement of C

C-to-C	.185	m
M	.02025	m
H	.03175	m
α	62.5	
L_C, L_D	.0485	m
L_T	.1724	m
Cp	2707	m/s
Temp	17.2°	celsus
T	118.530×10^{-6}	seconds
T_2	37.914×10^{-6}	seconds
D-2d	.1027	m
correction T	3.5×10^{-6}	seconds
correction T_2	2.8×10^{-6}	seconds
correction for temp range	3.8x (-133) 3.8x (-164)	seconds x 10^{-9}
corrected T	114.525×10^{-6}	seconds
range	114.407×10^{-6}	
calculated	1516.8	m/s
C range	1519.1	m/s
uncorrected value of C calculated	1507.04	m/s
previous values of C corrected by $\frac{\partial C}{\partial \text{temp}}$	1505.6 1506.4	m/s

This experiment shows that the model used for the calculation $\frac{dT}{T}$ is valid and can be used to predict the change in C.

If the value of time measured (T) is corrected to that at 21° (as previously tested) by using the factor $\frac{dT}{T}$ produced by experiment, the values of C found are 1516.8 and 1519.1 and encompass the previous values of 1517 and 1517.8.

If, on the other hand, the uncorrected value is used then calculation yields that C = 1507m/s and this compares with a probable value of C of 1505.6-1506.4 m/s and it can be seen therefore that this proposed method of the measurement of C tracks the change in C without recourse to the measurement of T_2. Clearly a significant change in temperature would require an adjustment to T_2.

5.5 Clamp/reclamp tests and differential tests.

It was decided to test the effect of clamping and reclamping the transducers upon the differential time. For this test the experiment was set up as shown in figure 5.23. The transducers and pipe wall were cleaned and relubricated. The received signals were adjusted to be equal at the 2v peak envelope and the processed signals were delivered to the HP counter/timer (set in time interval mode). The temperature of the water was recorded.

The test was initiated by recording the readings produced over 1000 samples for no movement of the transducers. The transducer on one side was wound in and out a total of 4 times and a reading was taken (test 2-5). This was repeated on the second transducer (test 6-10). No further couplant was added.

[Throughout the following tests small modifications were made to the instrument, which essentially consisted of extending the time difference. The results are therefore reproduced in terms of the difference observed in the mean, over 1000 samples.]

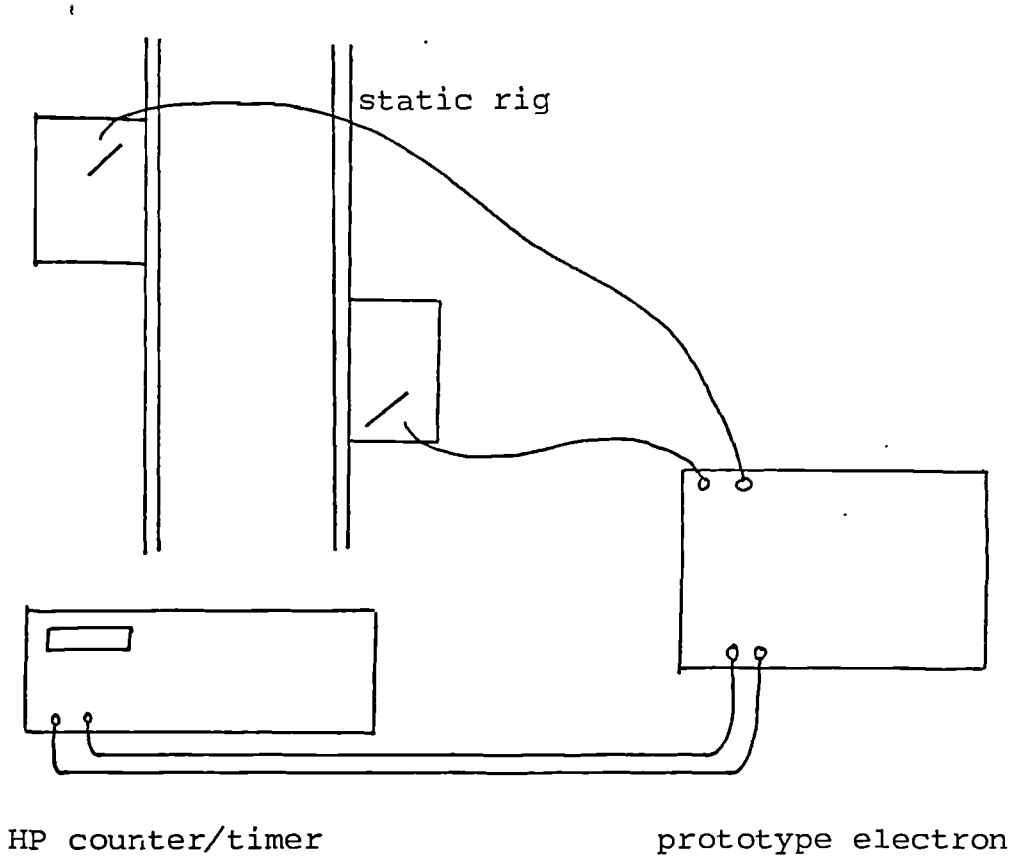

FIG 5.23
Experiment to test clamping/unclamping and other effects

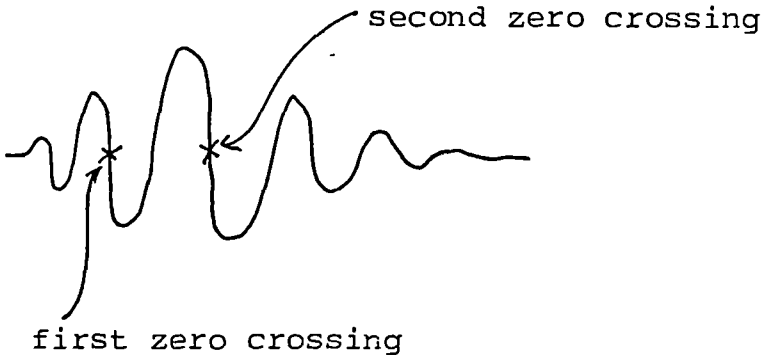

FIG 5.24
The selected zero crossings

The results of this test are given in Table 5.7.

Table 5.7
Clamp/reclamp test

Test 1		Test 2		Test 3		Test 4		Test 5	
Change in (Mean) (nS)	σ (nS)	Change (Mean) (nS)	σ (nS)	Change (Mean) (nS)	σ (nS)	Change (Mean) (nS)	σ (nS)	Change (Mean) (nS)	σ (nS)
0	1.12	.1	1.13	.1	1.12	.1	1.13	0	1.15
.1	1.13								
.2	1.14								
.1	1.12								

note all changes taken from starting value
Temperature 19.1°c

Test 6		Test 7		Test 8		Test 9	
Change (Mean) (nS)	σ (nS)	Change (Mean) (nS)	σ (nS)	Change (Mean) (nS)	σ (nS)	Change (Mean) (nS)	σ (nS)
-.1	1.09	.2	1.13	.1	1.11	.2	1.17
0	1.11	.1	1.14	.1	1.11	.2	1.17
.1	1.08	.2	1.15	.2	1.17	.2	1.17

Temperature 19.2°c

it was concluded that clamping/reclamping had no significant effect on the differential time.

5.6 Effects of zero crossing and temperature on the differential delay.

It was decided to monitor the effect of temperature on the differential delays at two values of zero crossing. Figure 5.24 shows the first zero crossing selected for test 1 and also the second zero crossing selected for test 2. The results are given in table 5.8 and are for the two tests which were carried out on separate days.

Table 5.8
Effect of zero crossing on differential time

Time into Expt	Test 1 Mean (ns)	(1st crossing) σ	Temp 1 (^{o}C)	Test 2 mean (ns)	(2nd crossing) σ	Temp 2 (^{o}C)
0	8	1.2	18.6	11.05	.74	17.6
30	7.72	1.19	18.8			
41	8.1	1.19	19.0	11.01	.76	17.8
57	8.1	1.2	19.3			
69	8.33	1.2	19.5			
73				11.11	.73	18.25
112	8.13	1.18	20.0			
168				10.76	.72	19.55
189				11.04	.74	19.85
214				10.90	.75	20.25
294				11.06	.75	21.3
Max Change	.61		1.4	.35		3.7

It was concluded that the second zero crossing produced less scatter. The +30^{o} reading was + 2.4ns.

A second experiment was conducted on the second zero crossing in which a quantity of hot water was mixed into the pipe and a period of 12 minutes was allowed to let the system settle. The times, temperature and mean value were taken. The results are given in table 5.9.

Table 5.9
Temperature effect on the zero crossing

Time into expt	Mean (ns)	n=1000	(ns)	Temp °C
12	10.94		.87	41.4
21	10.8		.91	41
33	10.81		.81	39.2
47	10.9		.83	37.7
62	11.02		.86	36.1

It can be seen that there is no significant difference, when working at different temperatures, in the differential value measured, although there would appear to be some more scatter at the higher temperature. This scatter may possibly be due to circulating thermal currents. Since the pipe is standing upright the component of velocity of the currents would add to the delay.

A difference in the differential delay is to be expected, since the cycle to cycle variation of the transducer is not constant. However, the value of around 3nS (taken from Table 5.3) is significant and highlights the importance of selecting the correct zero crossing.

CHAPTER 6 TESTING THE PROTOTYPE INSTRUMENT.

6.1 Introduction

It was decided to test two commercial instruments, a spool piece instrument and a clamp-on instrument to provide, firstly, accuracy and repeatability information and secondly, 'hands on' experience.

The DFEI has at its disposal a test rig with traceable calibration standards of .29% uncertainty overall. The flow meters were tested in this rig under straight pipe configurations and, for the clamp-on instrument, under disturbance conditions, and the results of these tests are reported in section 6.2.

The prototype instrument, which has been described in detail in chapter 4, was tested on the rig in a functional manner, to show that it performed correctly. A procedure was then developed for the testing of the instrument. It was necessary to carry out preliminary tests to evaluate the constants relating the measured time Δt to the velocity. This part of the work is described and presented in section 6.3 and a procedure is described for the analysis of the results.

The detailed testing of the instrument is covered in section 6.4 and analysis of the instruments performance is made for zero tests and flowtests. The performance of the instrument is shown to be repeatable and reasonably accurate.

The measurement of C external to the pipe has been discussed in chapter 2 and a proposed method has been put forward. This method has been tested in full and the limitations found. The measurement of C is found to be acceptable, using the method outlined, provided certain precautions are taken. This section of the work is presented in section 6.5.

Finally, the results of all testing are discussed in section 6.6 and a comparison made between the commercial clamp-on flowmeter and the prototype instrument. A specification for the prototype instrument is drawn up and presented. Possible remedies that could be used in a commercial instrument, to improve the performance, are discussed.

6.2 Flowtesting of commercial ultrasonic flowmeters

It was decided to test two commercial ultrasonic flowmeters, one a clamp-on flowmeter and the other a spool piece instrument. The objective of the testing was not to compare instruments but to obtain an indication of accuracy levels and gain experience as a user.

The clamp-on flowmeter manufacturer required the user to furnish some application information before supplying the flowmeter. The information requested (and that given is indicated in brackets) is given below:

(i) pipe size, wall thickness, pipe material and grade pipe lined or not. (100mm, 3mm, stainless steel 316S, not lined).

(ii) fluid, temperature range, flow range, maximum Reynolds number. (Water, 15°-25°c, 240-4870LPM,10^6).

(iii) horizontal or vertical installation, indoors or outdoors, full or partially full pipes. (Horizontal and vertical possible, indoors, full pipes).

Other secondary information was required and this was also given.

The spool piece version was designed to operate on any fluid but the manufacturers were asked to supply the instrument for water and with a range up to 10m/s (100mm pipe).

The claims of the instruments accuracy are given in table 6.1

Table 6.1
Manufacturers Specifications

Clamp-on Flowmeter

Accuracy	± 1-3%	actual flow	(internal calibration)
	± .25-1%	actual flow	(external calibration)
Repeatability	.003m/s		

Figures given for a 5 minute integration period.

Spool piece Instrument

Accuracy	± 1% of rate	(0.3m/s - 12m/s)
Repeatability	±.3% of rate	(for 0.3m/s)

No integration time specified.

The two instruments were code named S for the spool piece version and C for the clamp-on version.

It was decided to test the instruments for straight pipe configurations and for disturbance effects (ie: a valve upstream). Additional tests for the clamp-on flowmeter were that of clamping/reclamping. Because it was felt that both meters would respond similarly for the disturbance tests, it was decided to test only the clamp-on meter in the disturbance configuration.

6.2.1. The flow test rig

A diagram of the flow test rig is given in figure 6.1.

The flow rig consists of a reservoir, four long sections of pipe, 2 pumps and a variety of valves to control the flow and two reference turbines. A data acquisition system collects the data.

The reservoir has a steel baffle which breaks up the flow and allows entrained air to escape more easily.

The four limbs of the pipework are approximately 75 diameters long and are constructed from 100mm nominal bore mild steel and plastic pipework. A flow straightener is included in the inlet section to ensure swirl free profiles.

The two pumps can be switched into operation and the flow controlled to cover two ranges of 0-4m/s and 4m/s - 10m/s (approximately).

In the bottom two limbs of the rig a pair of high quality reference turbines are mounted. The turbines have traceable calibrations to National Standards.

The pressure and temperature can be measured at the points indicated on the diagram.

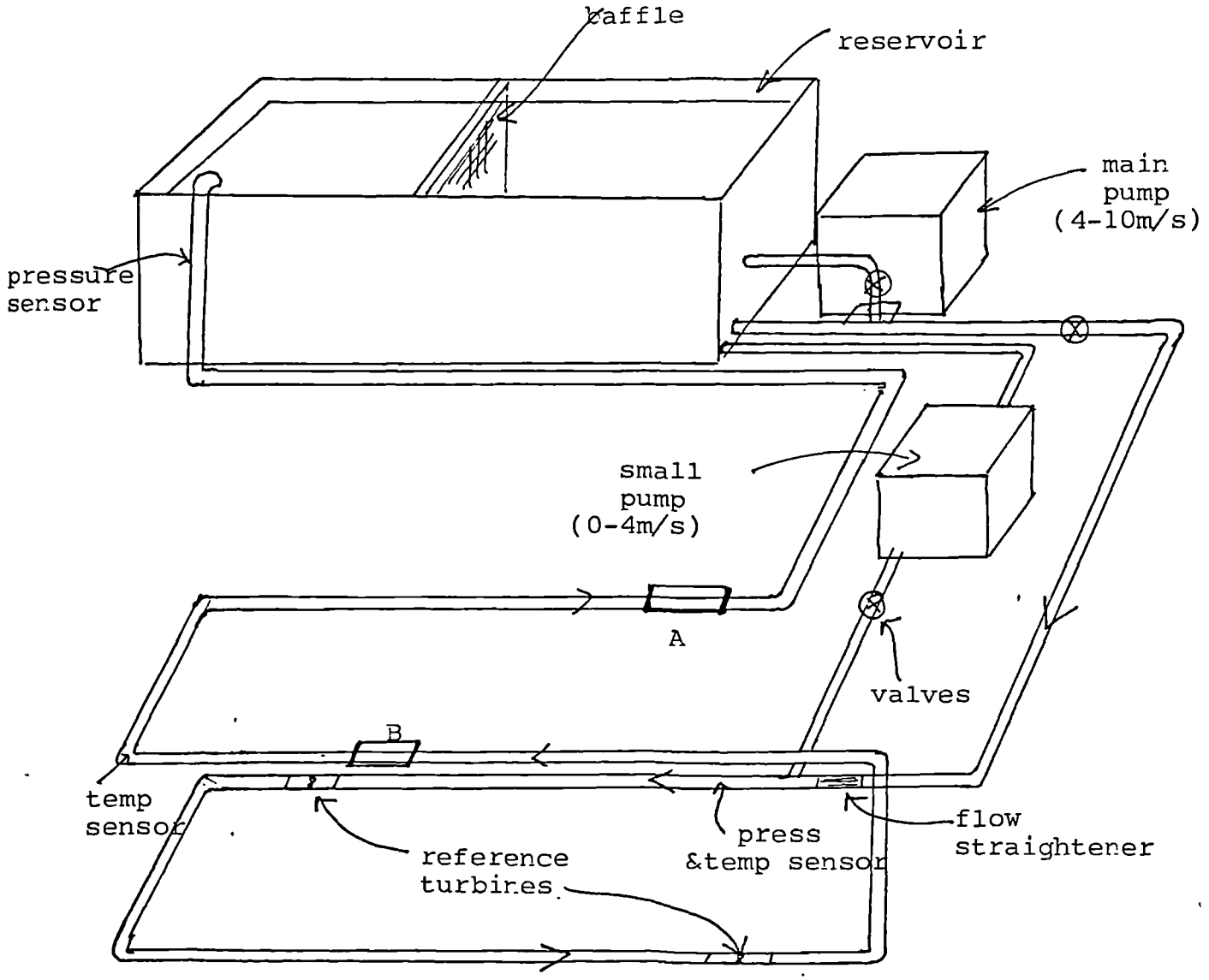

FIG 6.1
The flow test rig

6.2.1.1 The turbine reference meters

The two reference turbines used for calibration are:

(i) A kent PTW (Serial 1002 - wafertype) 100mm

(ii) A Fisher Controls 7104 (Serial 104/0843/81) 100mm

The turbine meters were calibrated at the CEGB calibration centre, Hams Hall, which is a British Calibration Service (BCS) accredited station to $\pm$.2% with a 95% confidence level.

A program was written to fit a straight line to the data and hence produce a meter factor. For both turbines it was decided to fit two straight lines. The meter factors were found to be, for the Kent

$$y = 4591.68 + .00058x \quad (P/m^3) \quad x > 92.95$$

$$y = 4612.6174 - .2246x \quad (P/m^3) \quad x < 92.95$$

and for the Fisher

$$y = 7995.1572 + .0056x \quad (P/m^3) \quad x > 154.37$$

$$y = 8016.5884 - .133x \quad (P/m^3) \quad x < 154.37$$

using the data the random uncertainty associated with the lines plus the systematic uncertainty of the measuring facility produces an overall uncertainty of, for the

Kent: $\pm$ .21%

and Fisher: $\pm$ .21%

The turbines were recalibrated after the tests (at the National Engineering Laboratories, East Kilbride) and the line fits were found to be:

Kent: $y = 4601.4$

and Fisher: $y = 8032.1 - 0.035\,X$

with uncertainty of line fits of,

Kent: $\pm$ .23%

Fisher: $\pm$ .2%

It was thus taken that the calibration had not shifted significantly during the tests (of the order of .2% for both turbines).

6.2.1.2 The data acquisition system

The data acquisition system consists of a S100 computer with facilities for the measurement of pulses, temperature and pressure. Incorporated into the computer is a real time clock (counting 10ms pulses).

In the system it is important to ensure that sufficient pulses are counted to reduce the error from the ± 1 count. Similarly it is important to ensure that the time is counted over a long enough period to reduce the error (as a percentage) of the $\pm$10ms pulse.

If more than 1000 pulses are counted then the error is less than 1/1000 = .1% If, for the timing, a period of more than 20 secs is timed the error will be $10 \times 10^{-3}/20$ = .05% If these figures are added and then summed in quadrature with those of the turbine then the overall uncertainty of a flowrate measurement is

$$F_u = \sqrt{E_{turb}^2 + E_{sys}^2} = \sqrt{.21^2 + .15^2}$$

$$\therefore \quad F_u = .26\ \%$$

For all of the tests carried out for this thesis the previous count and timing were used as the minimum requirements.

6.2.2 The flowtesting of the commercial flowmeters

The instruments were physically checked and inserted into the flowrig at positions marked A and B. (The clamp-on meter at A and the spool piece meter at B).

Both instruments were carefully set up in accordance with the manufacturers instruction booklets.

In the case of the spool piece instrument this meant calculating a calibration factor from the pulse rate, full scale flowrate , and a calibration constant specific to the instrument. This calibration factor was then set on a series of switches in the flowmeter electronics.

It was also necessary to zero the instrument at no flow condition. Essentially this means checking that there was no fault indication and balancing the light output of two LED's.

For the clamp-on instrument the set up procedure consisted of checking that there was no fault condition, checking the signal strength and zeroing the instrument.

An additional feature of the clamp-on flowmeter is a switch that sets the instrument into either an external mode or internal mode. In the internal mode case, the constants for the application (as effectively given in the information requested) are programmed into the device. In the external mode the user sets the zero and full scale value.

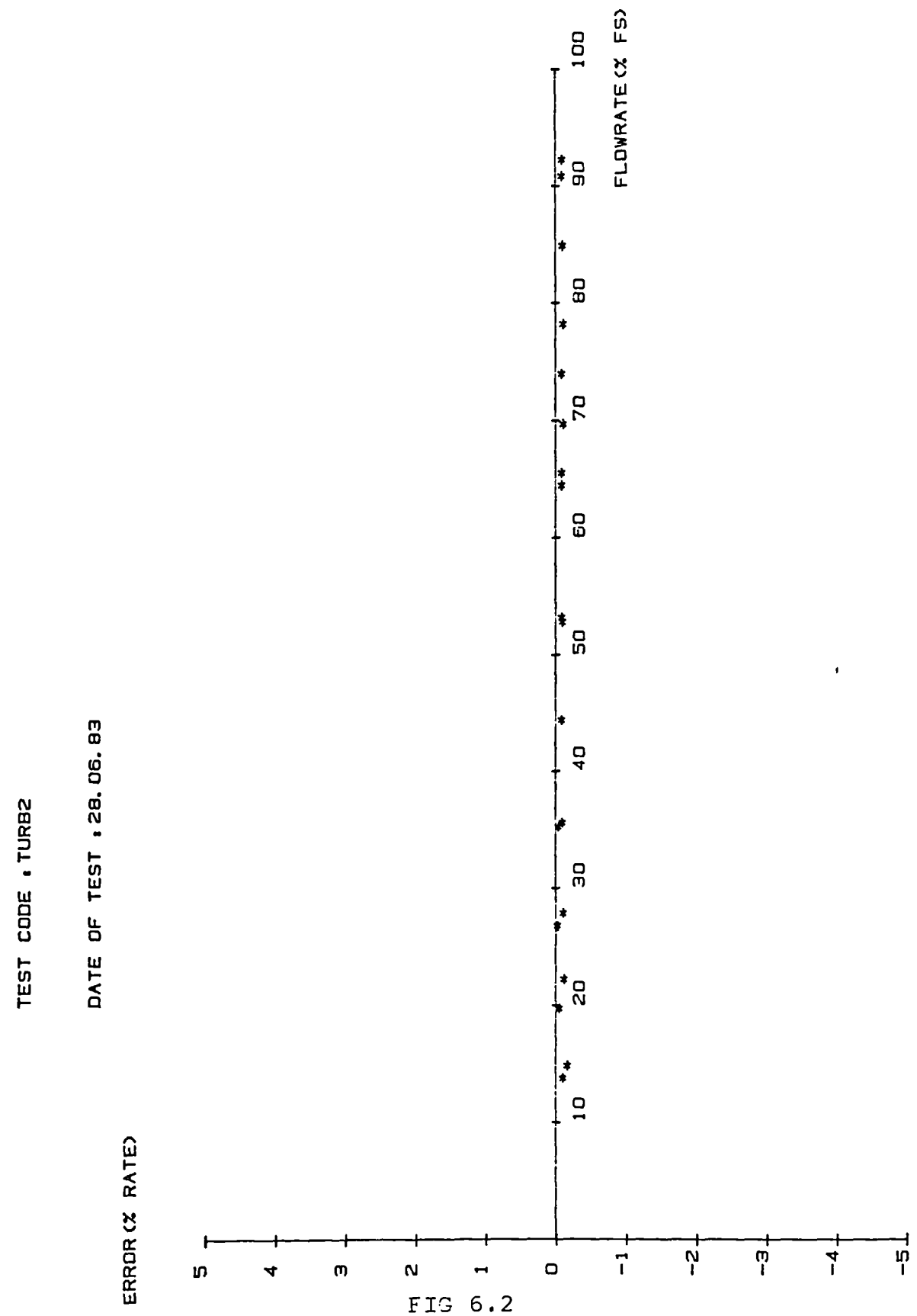

FIG 6.2
The turbine error curves (TURB2)

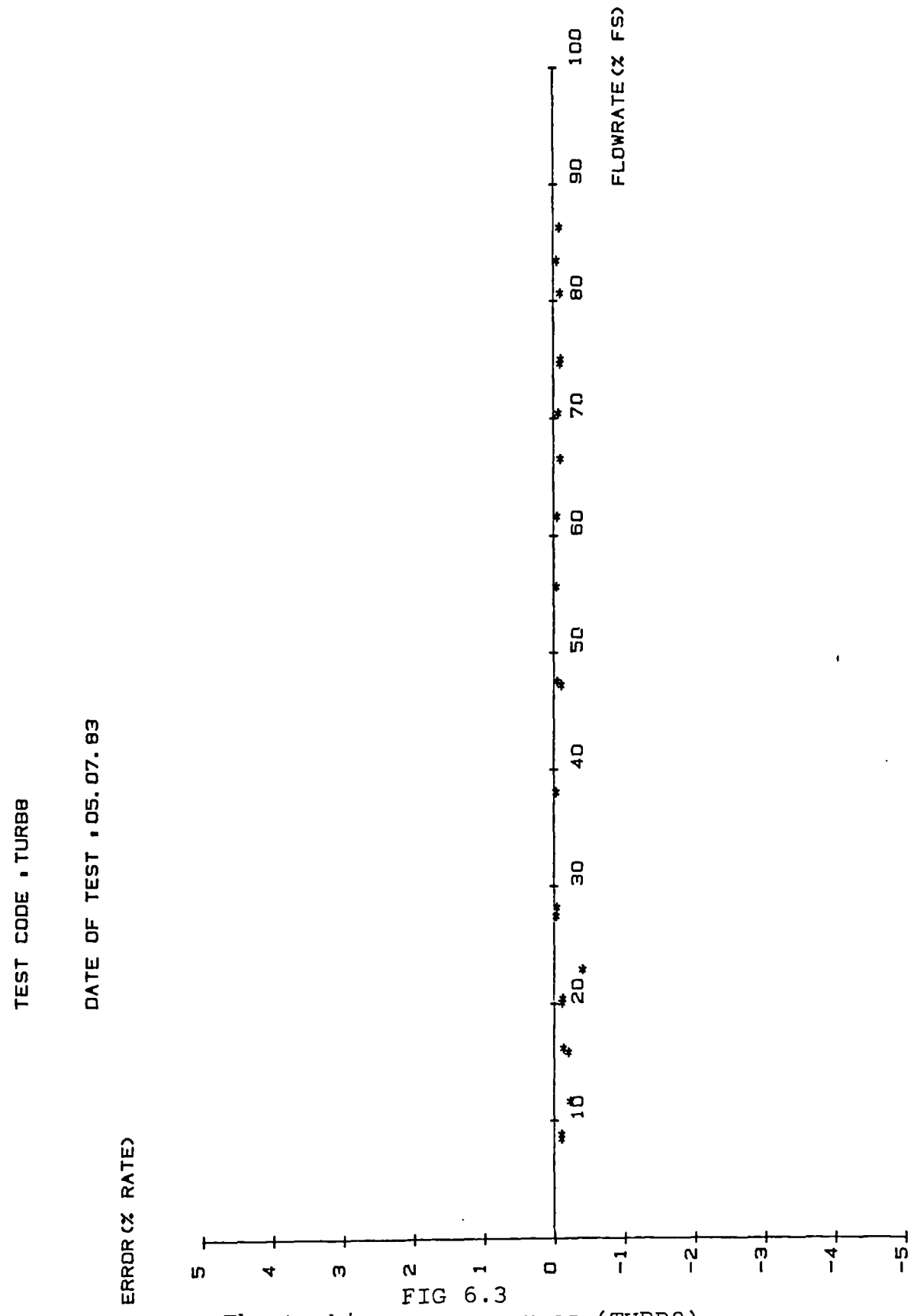

FIG 6.3
The turbine error curves (TURB8)

Preliminary checks were carried out to ensure that the systems were working correctly. The typical error between the turbines is shown in figures 6.2 and 6.3 for two cases, one under flowtest 2 conditions and one under flowtest 8 conditions. It can be seen that agreement is very good.

A warm up period of at least 15 minutes before each test was allowed for both instruments and all data was collected using a program called USTEST 2. As discussed in the data acquisition section it was necessary to collect sufficient pulses and measure sufficient time to reduce errors from these sources. In the tests at least 2000 pulses and 20 secs were used.

The maximum flowrate range of the instruments was:

Kent	260	m^3/hr	$\approx$	9.2	m/s	in a 100mm pipe
Fisher	260	m^3/hr	$\approx$	9.2	m/s	in a 100mm pipe
Spool piece Instrument	144	m^3/hr	$\approx$	5.1	m/s	in a 100mm pipe
Clamp-on Instrument	344	m^3/hr	$\approx$	12.2	m/s	in a 100mm pipe

Note that the clamp-on instrument's range exceeds that of the (calibrated) turbines. It was decided to establish 10m/s as 100% full scale flowrate ($\approx 283 m^3$ /hr).

Preliminary tests on both instruments indicated that the instruments were out of specification. The manufacturer of the spool piece instrument and the agent for the clamp-on instrument were contacted. They both agreed that correct procedures were being followed with their respective instruments.

The spool piece instrument was only tested in straight pipe configuration over the same number of tests as the clamp-on meter. It was observed that when the meter went over range (approximately over 6.5m/s (184 m^3/hr)) the instruments accuracy changed dramatically from

±2% to approximately - 100% at change over and then reduced with increasing flow to about - 70% at full flow (260m^3/hr).

The tests were conducted in blocks of 3 after sufficient time had been allowed for the new flowrate to establish itself. Provided the turbine readings were in close agreement the sets of 3 readings for all instruments were averaged and the result of each instrument calculated as a percentage of flowrate of the Fisher turbine, ie:

$$\% \text{ error} = \frac{\text{Instrument reading - Fisher reading}}{\text{Fisher reading}} \times 100$$

6.2.2.1 The spool piece flowmeter test results.

Figures 6.4 and 6.5 show typical results obtained for the spool piece instrument. The temperature of the fluid in the rig was within ± 3° of 17°c.

All tests show a decreasing error (turning negative) for increasing flowrate. The range of errors are within +2% and - 1.5% The repeatability appears to cover approximately a 1% band.

The low end of the range of this flowmeter was not tested below approximately 0.6m/s (17 m^3/hr) where the turbine accuracy is questionable. As stated previously the upper limit was found to be 6.5m/s (184 m^3/hr).

This instrument has been removed from the market by the manufacturers and has been superceded.

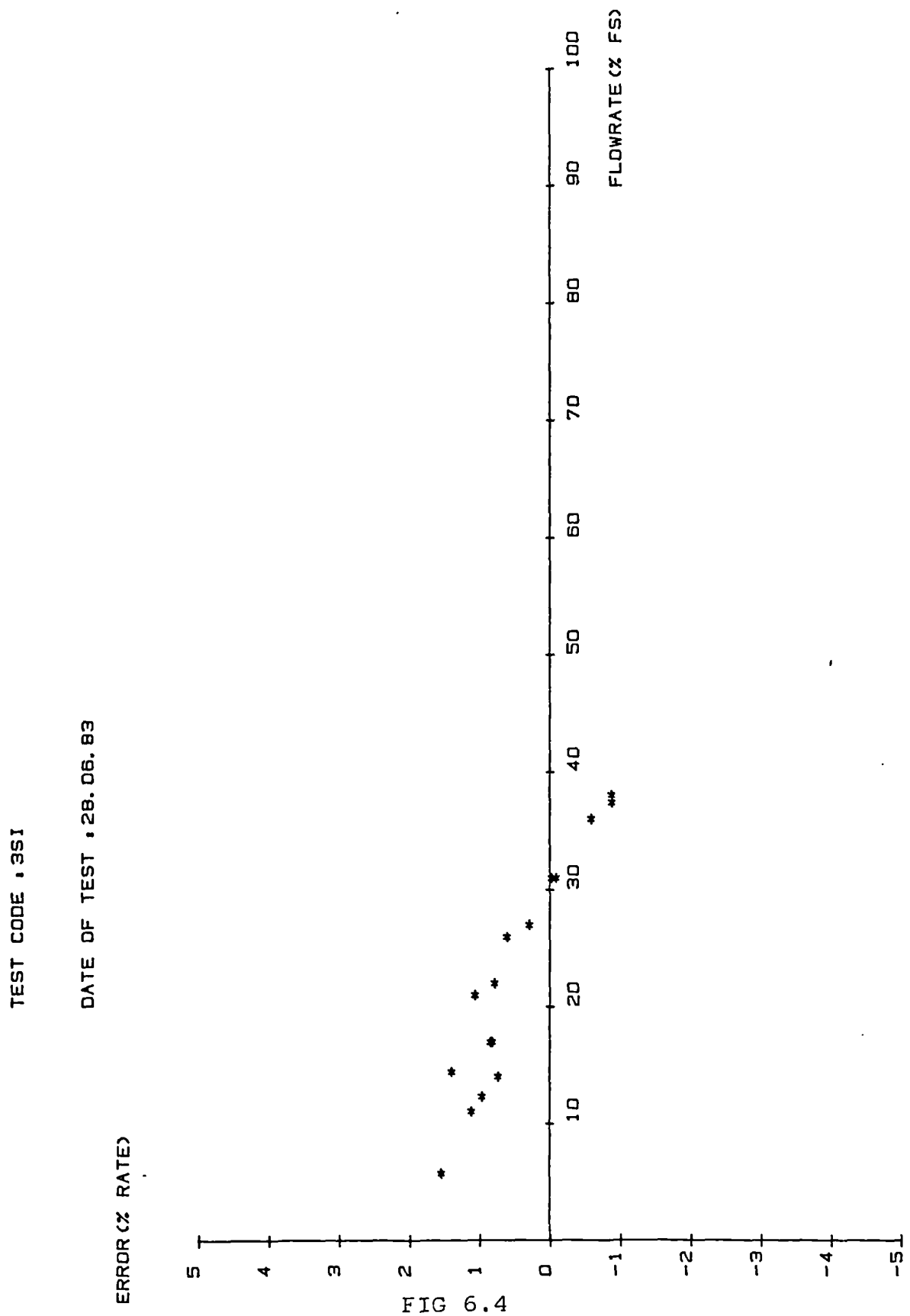

FIG 6.4
Flow test result 3SI

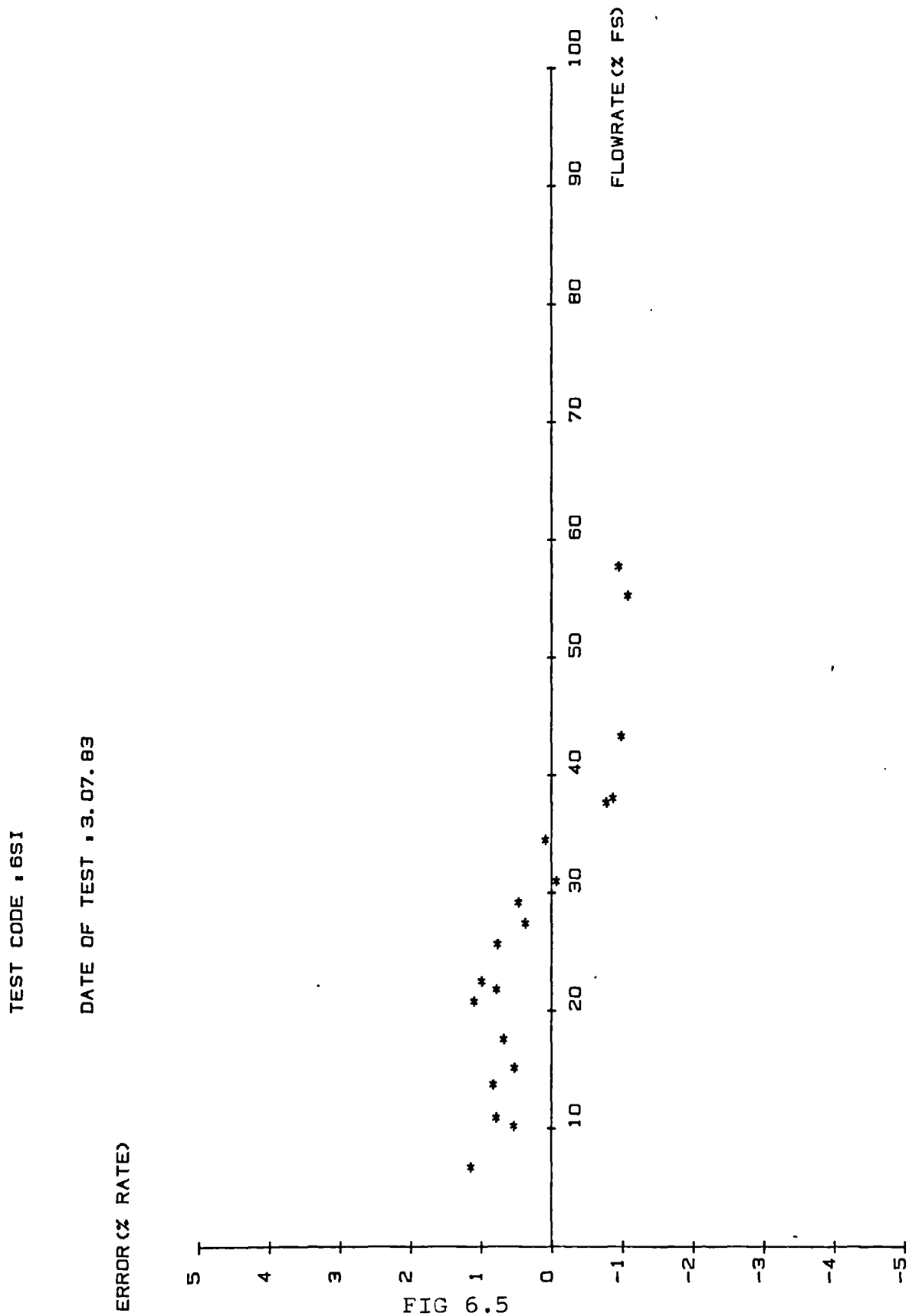

FIG 6.5
Flow test result 6SI

6.2.2.2 The clamp-on flowmeter test results

The clamp-on version was tested under internal and external calibration and with disturbances (a valve) upstream of the instrument. The results, to be presented, have a testcode in the top left hand corner and this is constructed as follows:

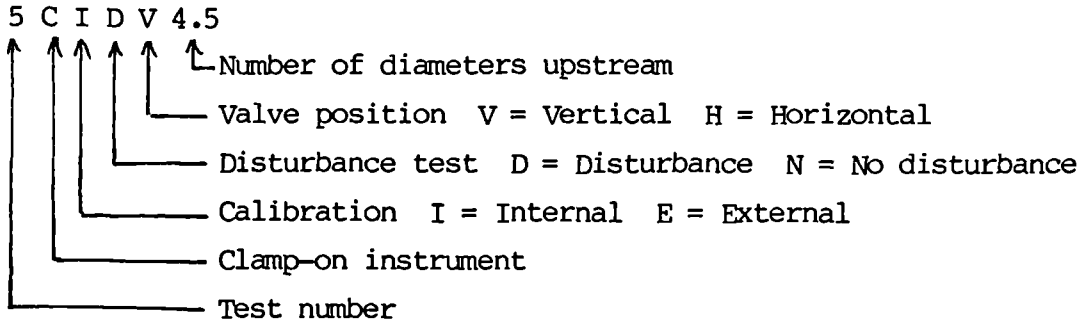

The procedure used for calibrating the clamp-on meter was as follows:

(i) Clean the pipe and transducers, mount the track and correctly position the lubricated transducers.

(ii) Set calibration switch to internal or external position.

(iii) Place the unit into fault position (ie: no signal mode).

(iv) Place the unit into memory mode.

(v) Adjust the analogue calibration potentiometer until the display reads the value for maximum flow at 10v D.C. measured on the output connector of the meter.

(vi) Return all switches to the operating position, set the value of maximum flow displayed and output voltage into the program USTEST 2 and set the calibration switch to internal or external position.

(vii) If calibration switch set to external position, adjust span to read maximum value under flow conditions (via calibrated turbine reading).

(viii) Check instrument zero.

The above procedure was carried out before every test. The zero observed for all tests appeared to be very stable and slightly scattered about zero (±1,0 reading LPM).

A difficulty was encountered when setting the analogue calibration potentiometer. This was found to drift about and although, at the beginning of a test, a corrected value was used in the program, it was possible to find a drift of approximately 1% of rate at the end of the test. This difficulty was expressed to the agents who were aware of this problem.

It was decided to test the clamp-on flowmeter for repeatability with respect to clamping/unclamping. The instrument was set upon the pipe and adjusted in accordance with the manufacturers instructions for external calibration.

A value of flow at approximately 90% of FS was set into the flowmeter and the zero was checked. A test was conducted and the results of this test are shown in figure 6.6, IACEN.

The transducers were removed, cleaned, and recoupled to the pipe and a further test carried out. The result of this test is shown in figure 6.7, IBCEN and shows an offset of approximately 1% with respect to the previous test.

A repeat reclamping was carried out and the results of this test are shown in figure 6.8, ICCEN. For this test the transducers were removed, cleaned and replaced. The instrument was not adjusted in any way and the zero was checked.

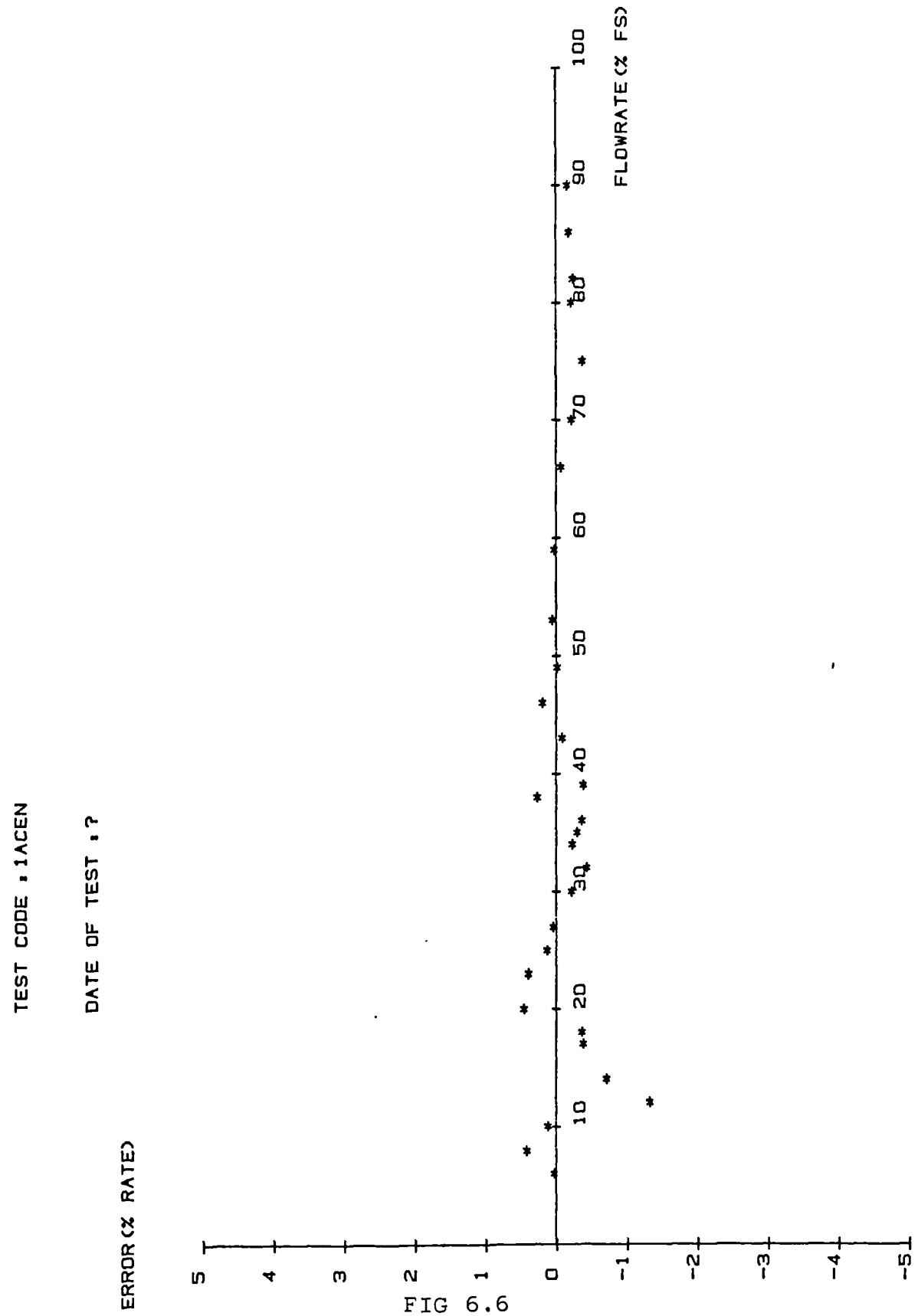

FIG 6.6
Flow test result 1ACEN

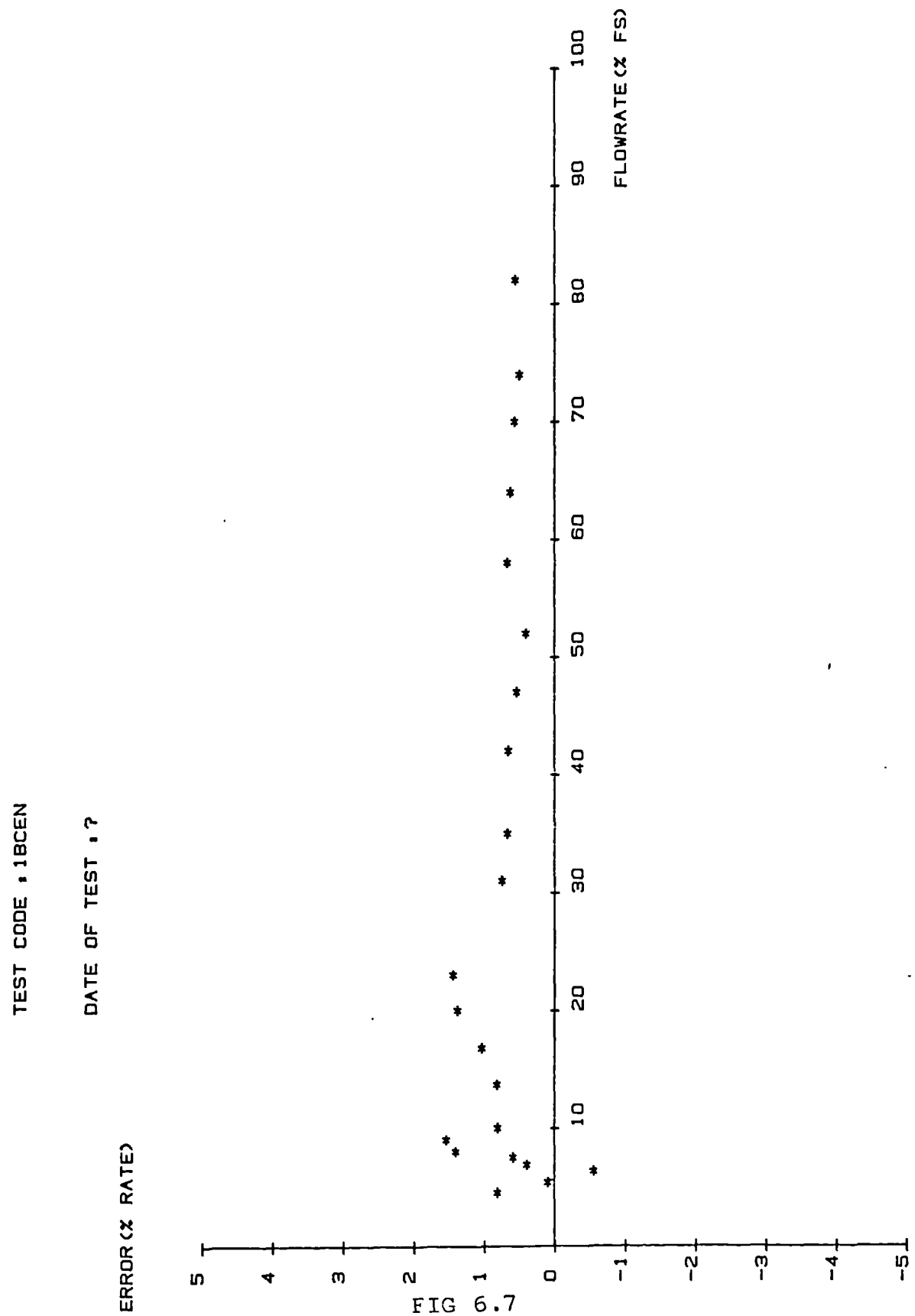

FIG 6.7
Flow test result 1BCEN

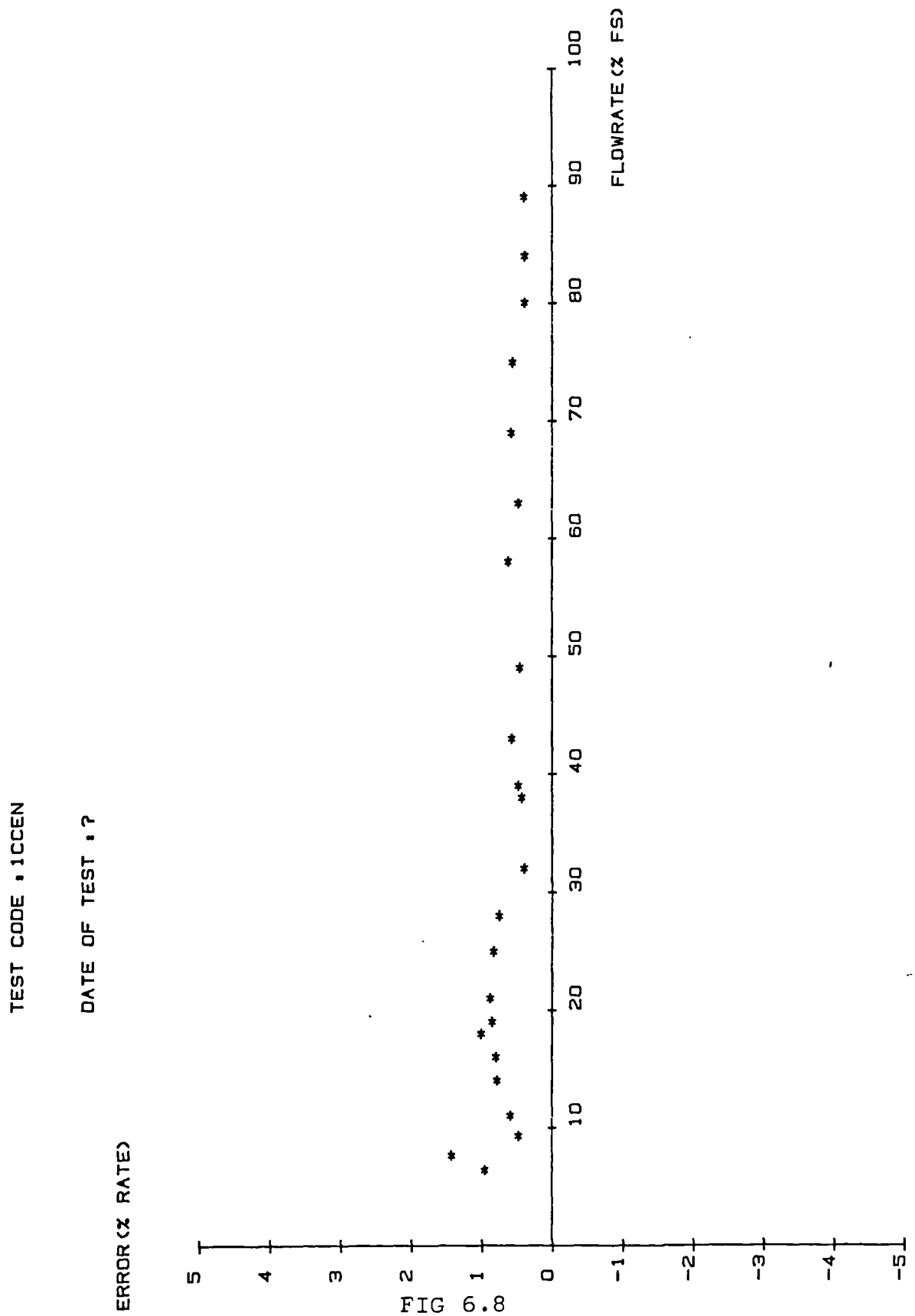

FIG 6.8
Flow test result 1CCEN

It was concluded that, apart from the drift in the calibration offset, the instrument would appear to be repeatable to within about 1%.

It should be noted that the instrument has a mounting track with detachable transducers. For the above tests clamping/reclamping meant that the transducers were removed but the track was left in place. Because the repeatability was of the order of only 1% it was decided against complete clamping/reclamping of the flowmeter for the remaining tests since this would consume a significant amount of time.

For the first test (figure 6.9, 2 CEN) which is a simple calibration under external calibration the results effectively show the linearity of the instrument and the repeatability with time (3 months) from the previous tests. It can be seen that between 20% FS and 92% FS the instruments performance is exceptional and infact compares with the errors produced between the two turbines. Below 20% FS the error starts to rise sharply. The time associated with 1m/s for this instrument is of the order of 50ns and the increase in error around this region suggests either/or both a zero offset introducing a larger percentage error with decreasing flow or a resolution error in measuring the small time.

It was decided to retest the instrument under low flow conditions and figure 6.10, 3CEN shows the result of this test. The results of this test agreeing reasonably well with the previous test.

Figure 6.11 (4CIN) is a straight-line test on internal calibration. It can be seen that errors here are of the order of 9% - 10%. Before and after this test the zero was checked to ensure that there wasn't an offset in the system. Several points were rechecked to ensure that they fell close to the original points.

(These results have subsequently been confirmed by later tests (1 1/2 - 2 years) (139). These results are surprising when one considers the application information supplied and that the system was operated under ideal conditions. The Reynolds number selector was set for a Re number

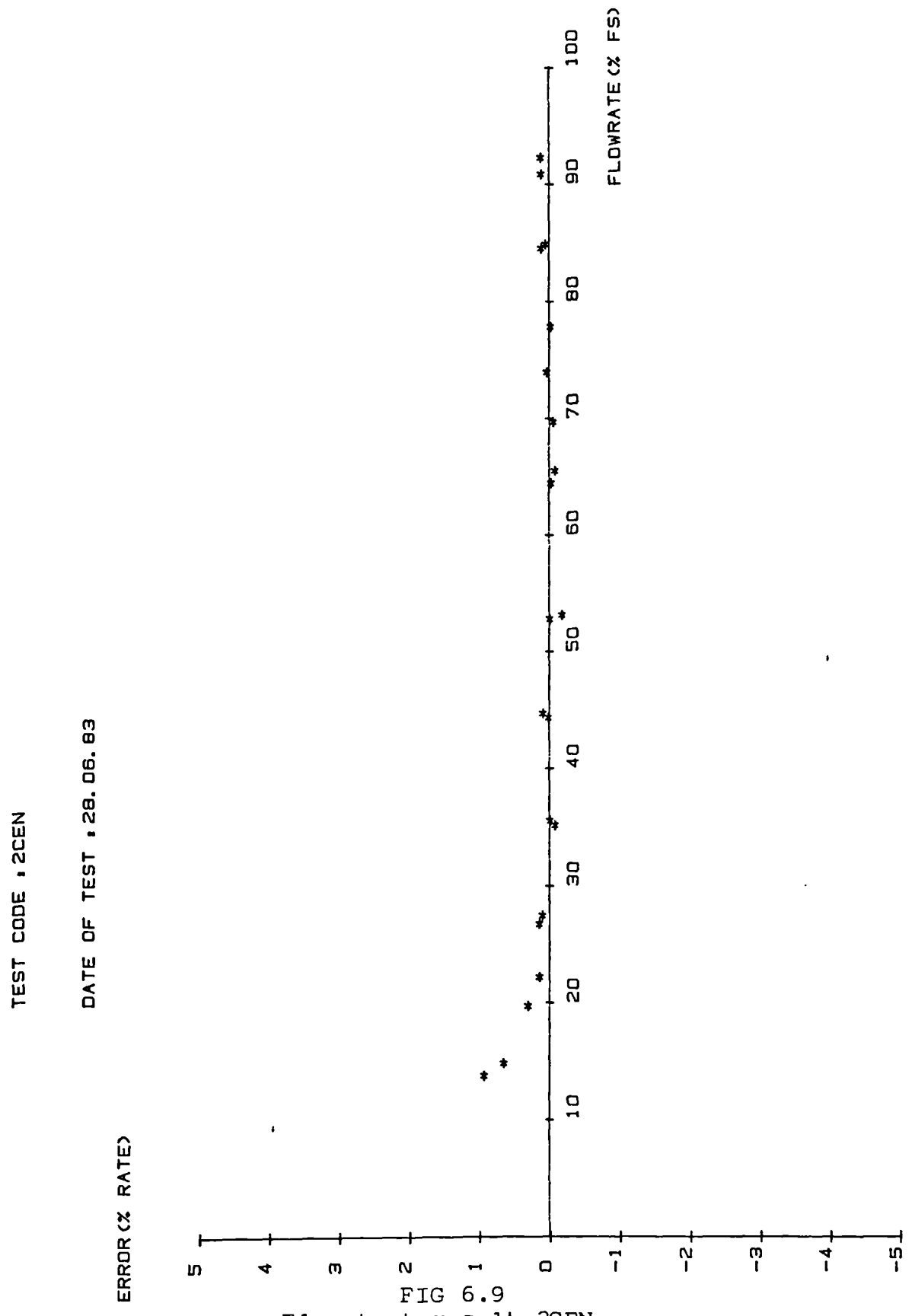

FIG 6.9
Flow test result 2CEN

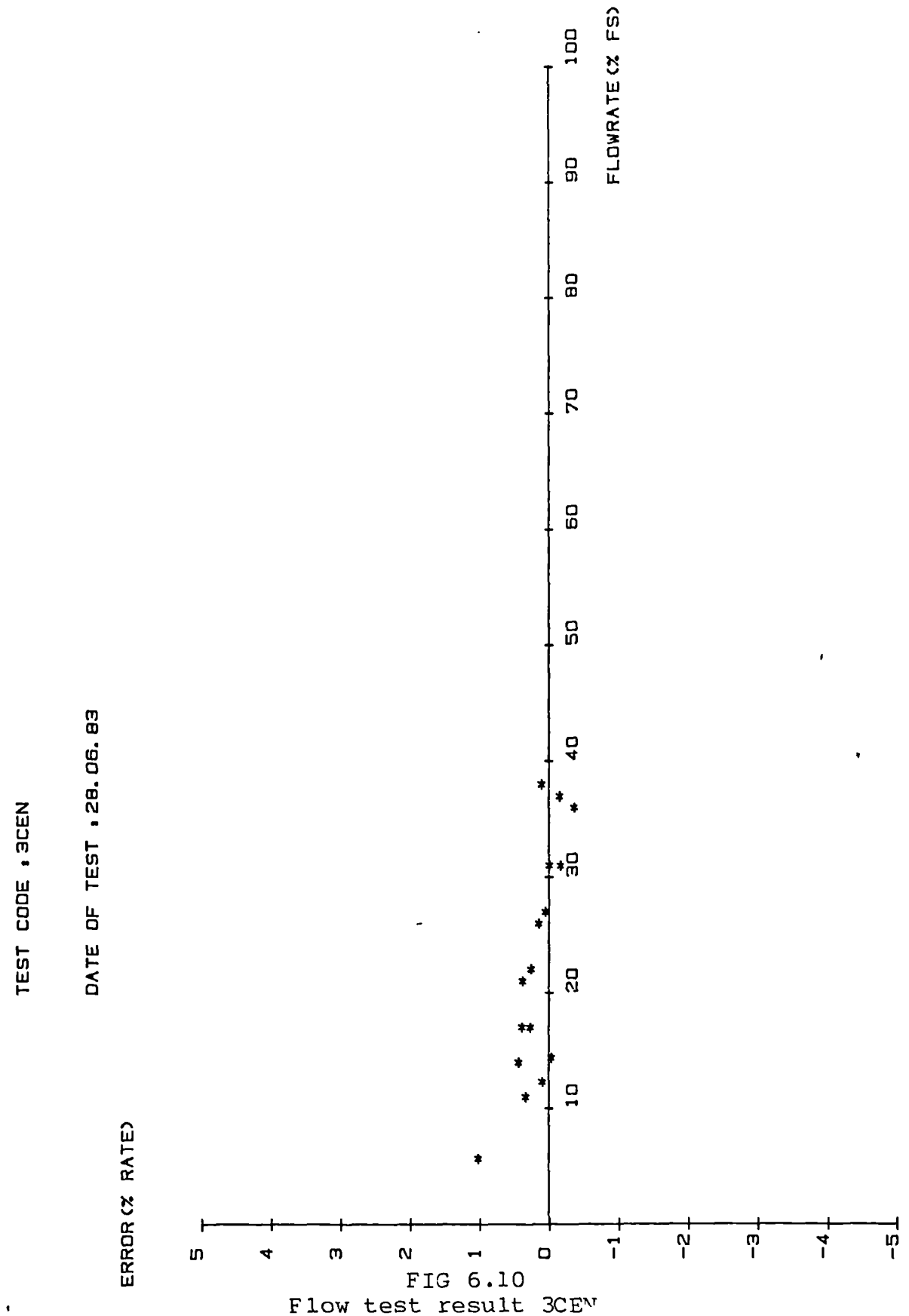

FIG 6.10
Flow test result 3CEN

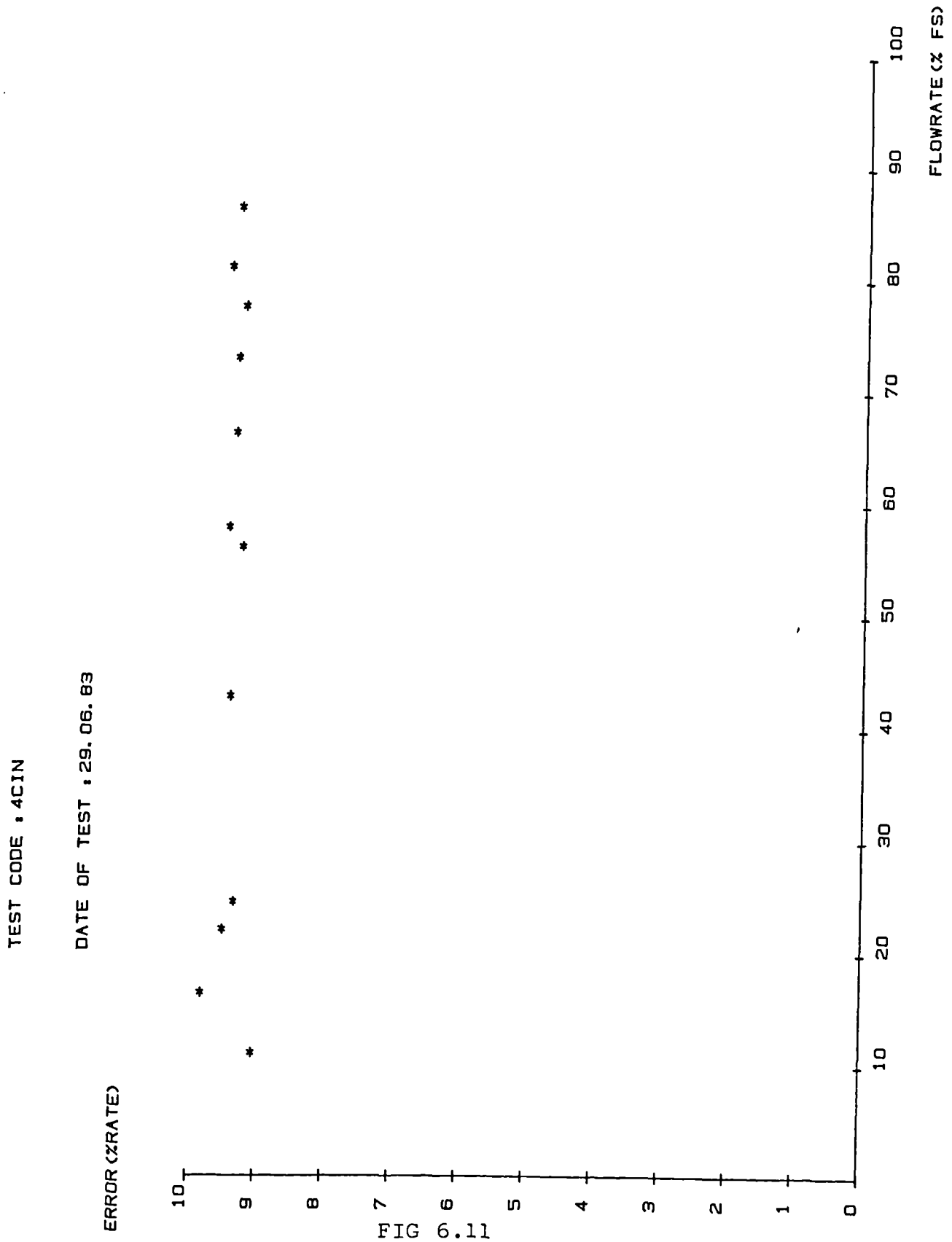

FIG 6.11
Flow test result 4CIN

of 10000 (set by the manufacturers for water based liquids) and since the flow was varied between Re numbers of $5x10^{-4}$ - 10^{-6} this will introduce a probable error of about 2%. Even taking this into account the errors are still substantial. It is believed that the system does not have temperature compensation but this effect should be very small (see errors in chapter 2).

For test 5 the rig was drained and the flowmeter removed. A half open gate value was inserted 4.5D upstream of the flowmeter in the vertical position (ie: 90° to the plane of the transducers). The transducers were remounted and the set up procedure was carried out. The zero was checked.

The results of testing the instrument are shown in figure 6.12 (5CIDV4.5) and show a reduction in error compared to the straight pipe run. Allowing for the incorrect setting of the Re value the errors would appear to be of the order of 4% - 5%, with an apparent decrease with flowrate. The scatter or repeatability appears to be contained in a band of approximately 1%.

The results of carrying out the test under external calibration conditions (without resetting flow at top end of range) are shown in figure 6.13, 6CEDV4.5. The results shows a similar reduction in overall error and a similar decease with flowrate. However the scatter now appears to be larger at approximately 1.5% at the lower end of the range.

The rig was again drained and the half open gate value was inserted 2.5 diameters upstream of the flowmeter in the vertical position. The flowmeter was cleaned and replaced on the pipework. Results of testing the instrument under these conditions are shown in figure 6.14 (7CEDV2.5) for the external calibration position. The instrument would now appear to have a highly non linear characteristic.

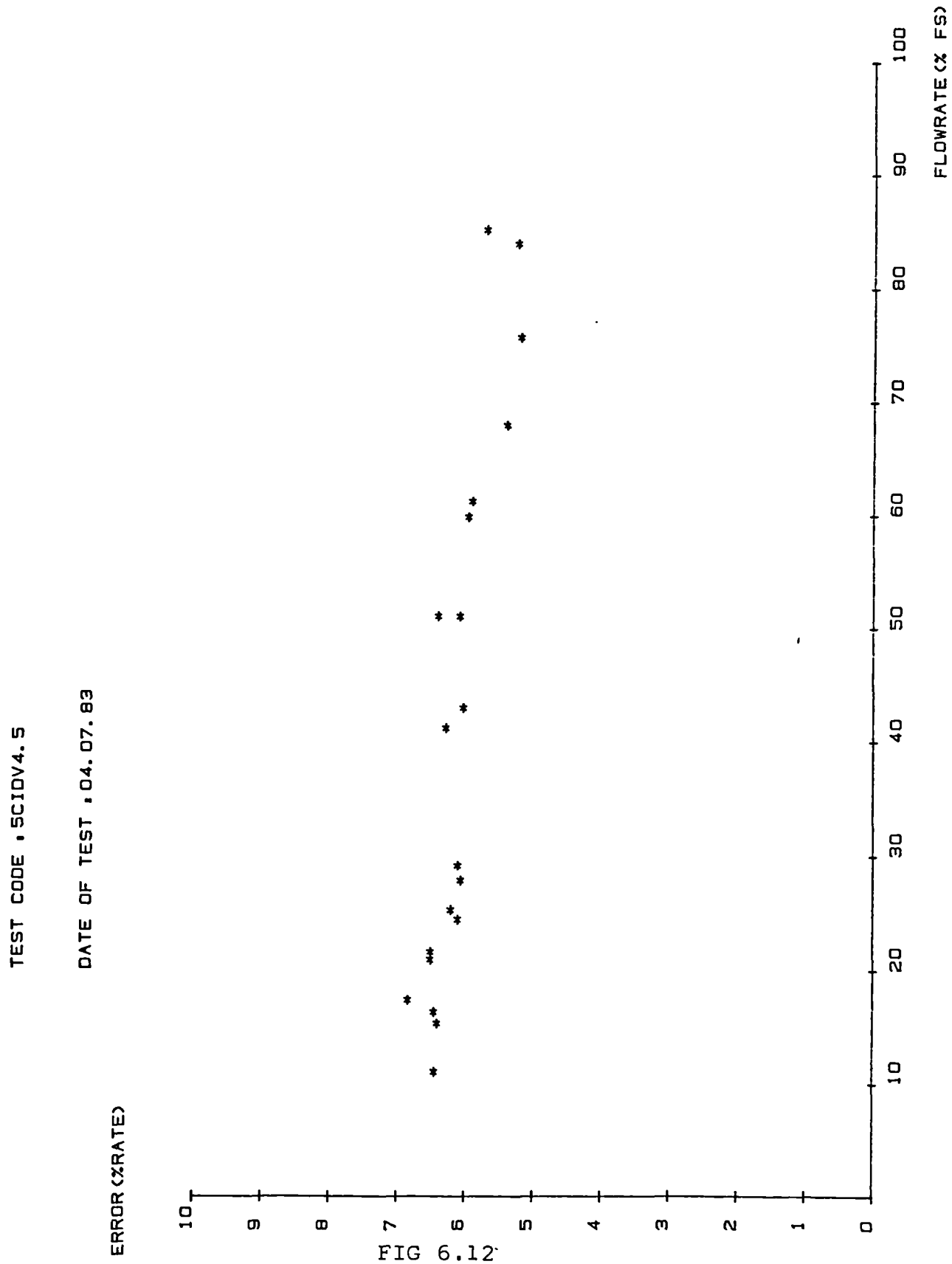

FIG 6.12
Flow test result 5CIDV 4.5

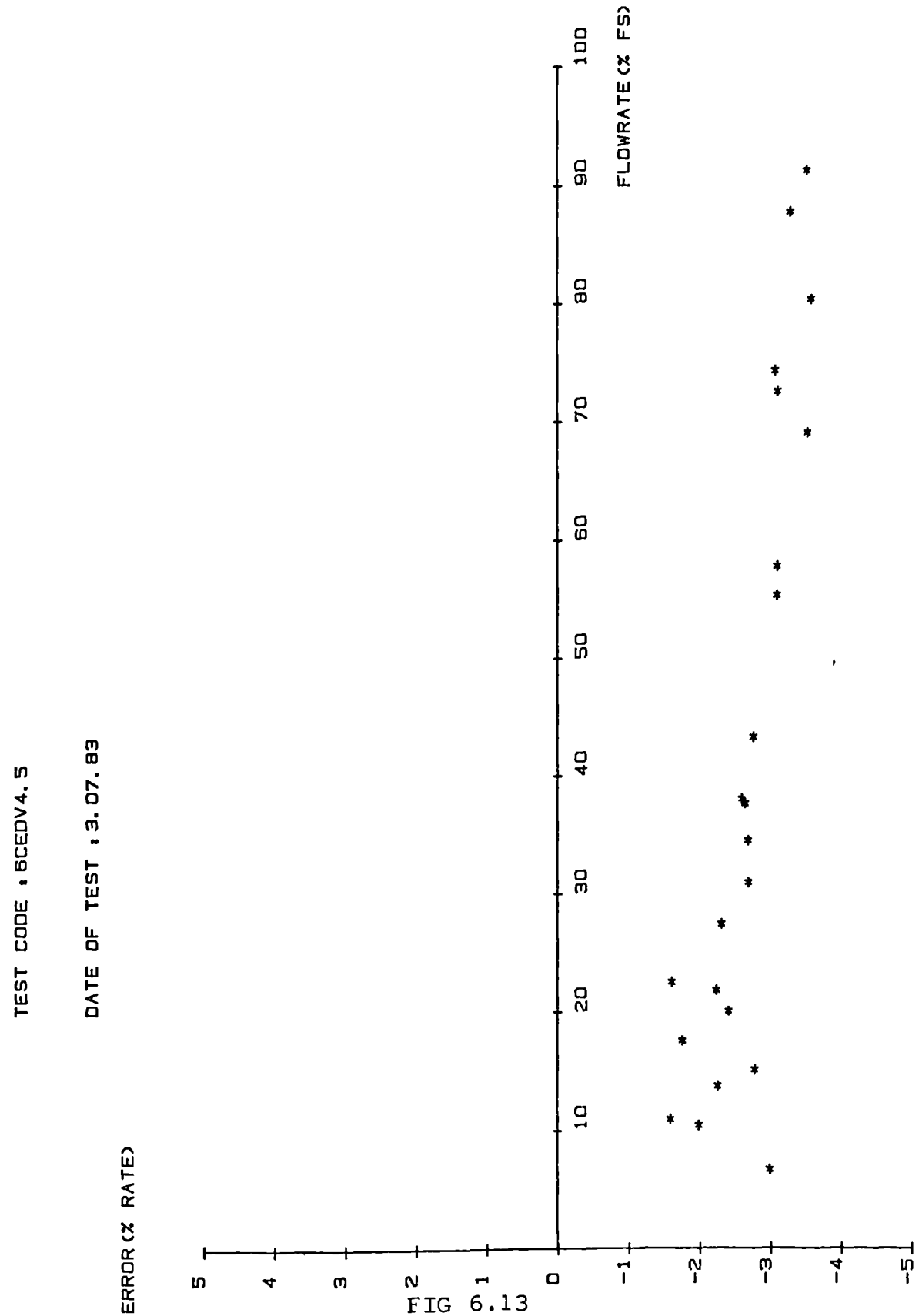

FIG 6.13
Flow test result 6CEDV4.5

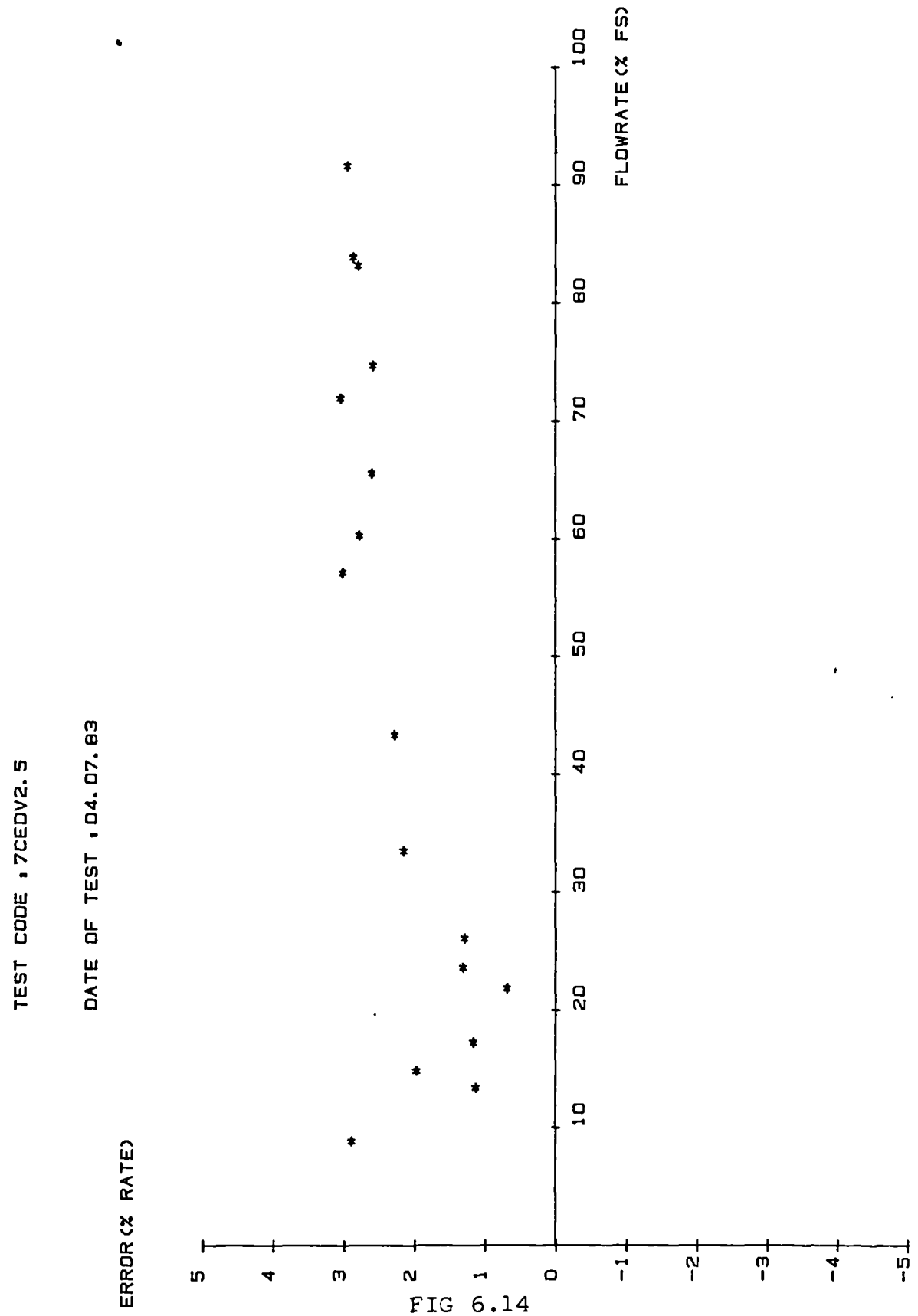

FIG 6.14
Flow test result 7CEDV2.5

Figures 6.15, (8CIDV2.5) is the same test as test 7 but under internal calibration conditions. As with the external calibration test (test 7) the error has reversed from what it was in the previous tests and has now gone more positive. The scatter of the results now is much wider at low flowrates.

Test 9 (figure 6.16, 9CIDH2.5) is a test with the gate valve, half open, in the horizontal position. For this test the flowmeter was removed, the rig drained, valve inserted and the flowmeter re-set on the pipe. The normal procedure was carried out and the zero was checked.

The results of this test show a rapid decrease in the error and a settling at a value of approximately 2% for most of the range 20%-90%. Over this range the scatter would appear to be very small.

The difficulty in predicting the flow profile after a valve does not allow more than speculative comment about the results. It is interesting, however, to compare test 9 and test 8 which are tests for the same disturbance but in a different alignment. In test 8 the generated profile could be imagined as cutting across the ultrasonic beam whereas the profile in test 9 could be considered to be in line with the beam.

In summary it can be said that under well developed flow conditions (ie: a straight run) the instrument has what would appear to be a systematic offset of about 9.5%. This value of offset is difficult to understand since information about the pipework had been previously supplied. The error in the nominal diameter is only of the order of 1%, and the temperature change ($\approx 6^{\circ}c$) is unlikely to produce an error of more than 1%. A possible source of error is that brought about by using a low value of Reynolds number (equivalent to 10^4) but this was set by the manufacturer for water based liquids. Since the range of flow is up to $Re=10^6$ this source of error could possibly add -2% at the top of the flowrange, ie: choosing a low value of Reynolds number for compensation purposes should overcompensate and bring down the error -

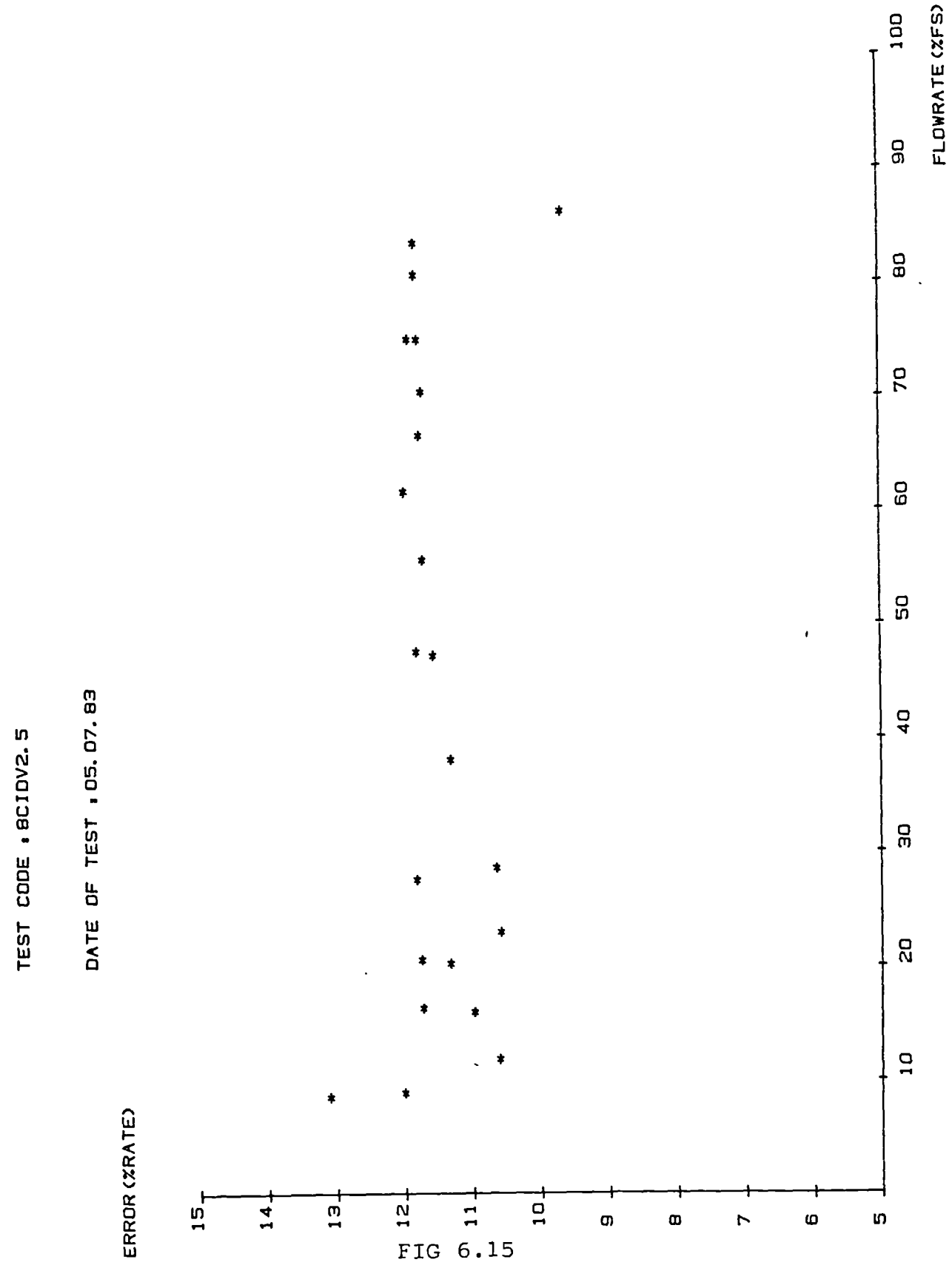

FIG 6.15
Flow test result 8CIDV2.5

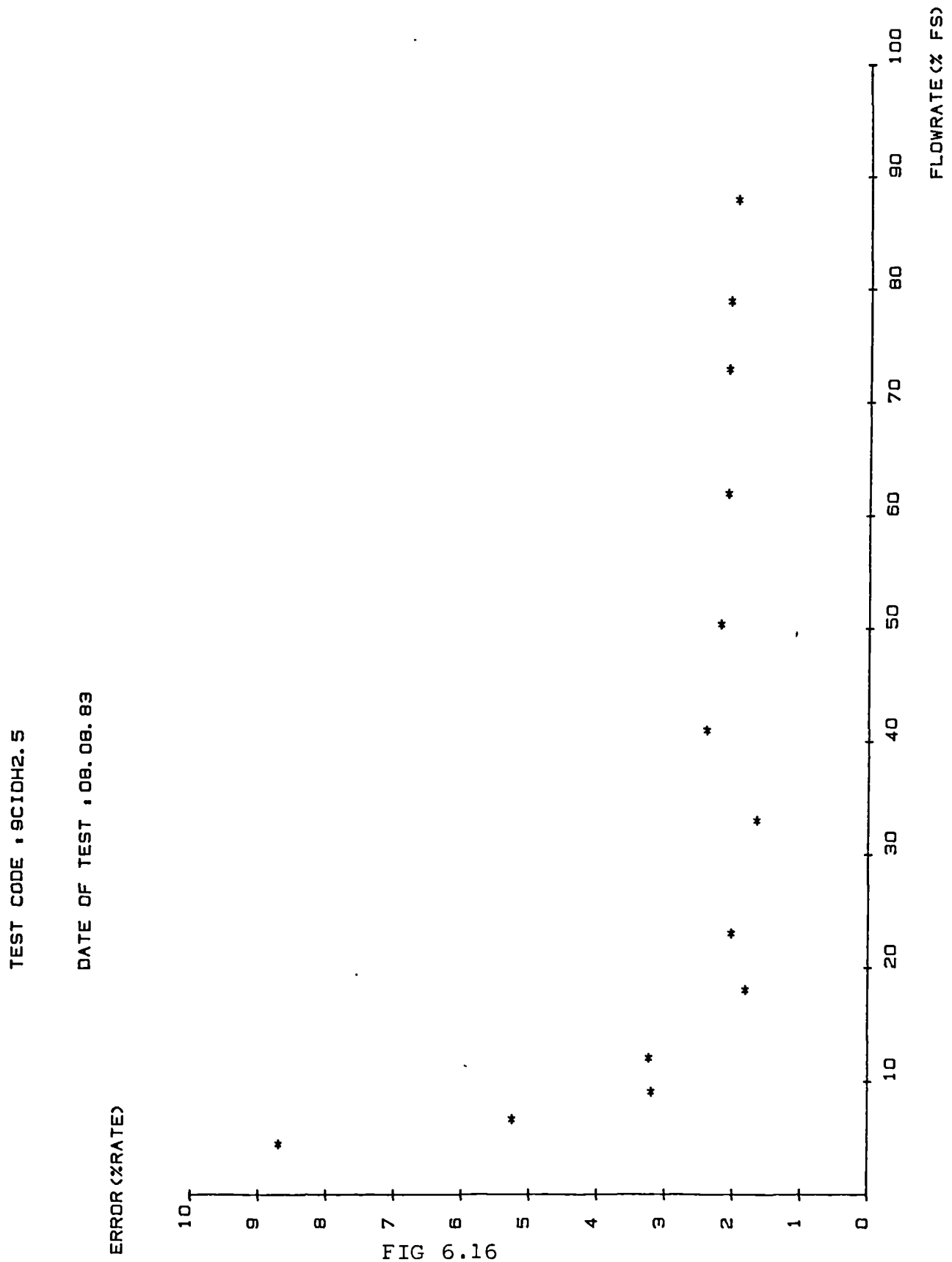

FIG 6.16
Flow test result 9CIDH2.5

if it is used as a constant over the full range. However, the instrument may consider the value as a range indicator and iterate the measured flow to produce a correction. This was not tested experimentally.

The error in the measurement of C must now be given a value. If the temperature range is considered to be approximately $6^{o}C$ then this would correspond to approximately 18m/s down from 1482m/s (value of C at $20^{o}C$ - Kaye and Laby) or about 1.2%. If the system was programmed with a value at $20^{o}C$ then the error in Q would be only of the order of 1%.

Added all together, the errors do not indicate the large systematic error. It is likely therefore that incorrect data has been programmed into the flowmeter. It should be noted that if the systematic error is removed the instrument has a very good repeatability band right down to 0.5m/s.

It is difficult to explain the spool piece instruments characteristic. Because the meter's range has been factory set it would seem reasonable for a compensation to be included (if a constant) at mid way of the range. This would then only add approximately + 1/2% over the full decade (0.5m/s $\approx$ 5m/s) and alter slightly the general slope of the characteristic.

6.3 Functional testing of the prototype instrument

The electronic section of the prototype instrument was assembled on a section of blockboard and mounted in a cupboard near the test rig. The test rig was the same rig as described in section 6.2.1. and shown in figures 6.17 and 6.18 is the transducer arrangement used in the flow tests The section of stainless steel pipe was flanged and fitted into the rig. A pair of parallel tracks were made to fit the pipe section. These tracks were made so that the transducer blocks were aligned across the diametrical chord and the tracks had a pair of screws and a

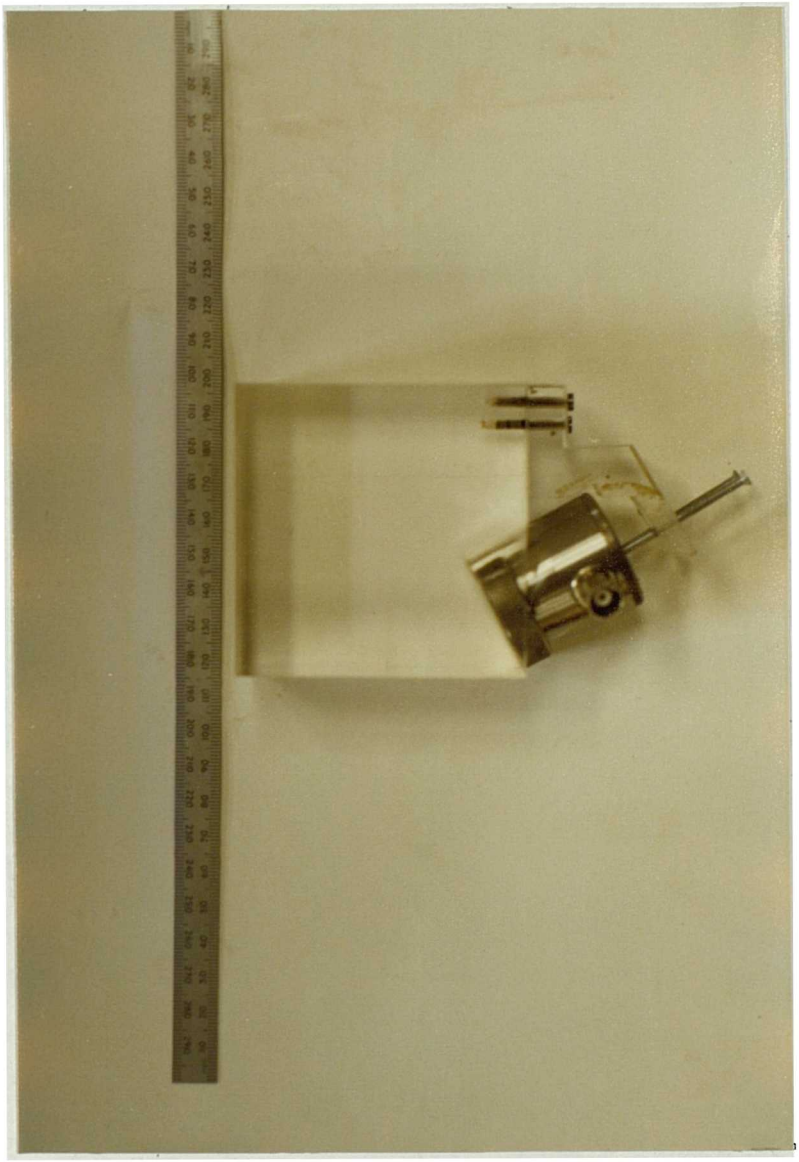

FIG 6.17
The transducer blocks used in the flow tests

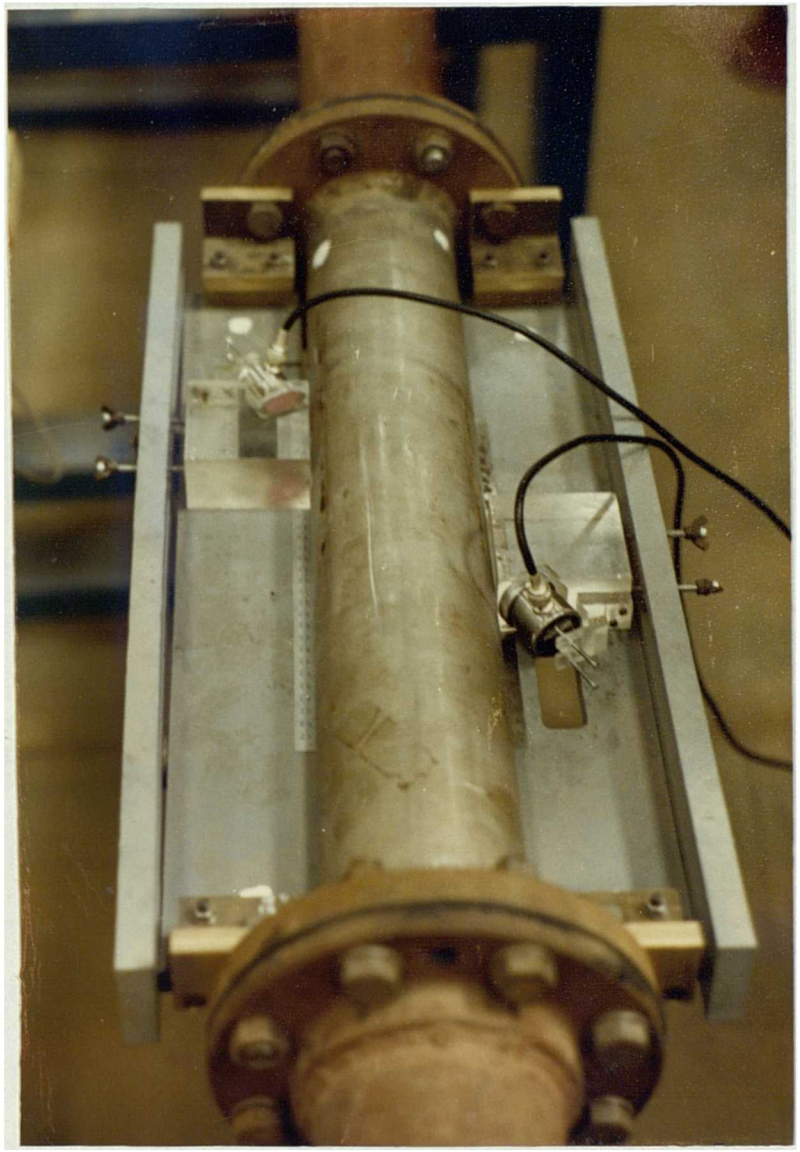

FIG 6.13
The transducer arrangement for flow testing

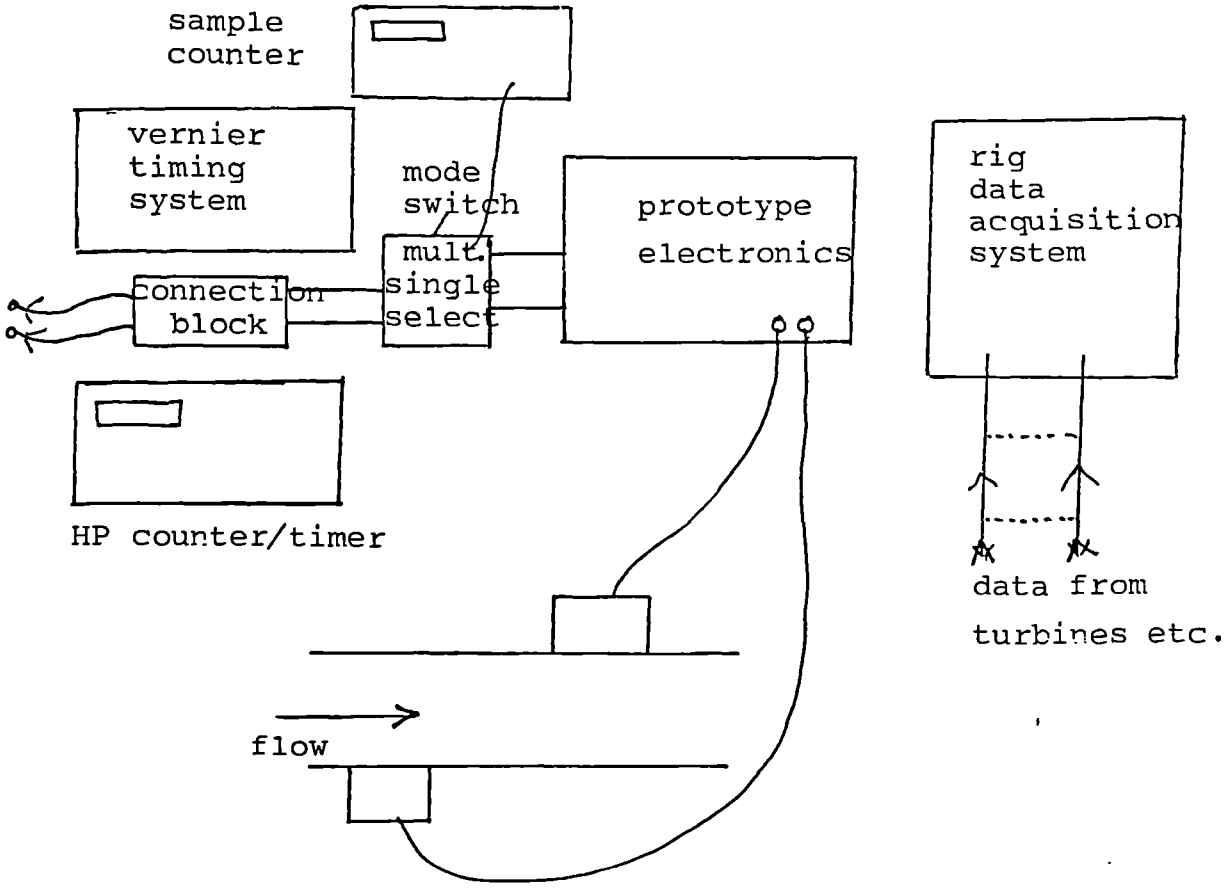

FIG 6.19
Experiment to flow test the prototype instrument

pressure plate to allow the block to be pressed against the pipe section. The transducers were connected to the prototype instrument by two, two metre lengths of coaxial cable.

The two turbines were recalibrated before being fitted into the rig and the calibrations were found to be,

Kent: $y = 4600.3 + 0.01325\ X$

Fisher: $y = 8004.7 - 0.01112\ X$

with the maximum uncertainties of

Kent: ± .26%

Fisher: ± .2%

and overall uncertainties of a flowrate measurement, taking into account the data acquisition system of,

Kent: ± .29%

Fisher: ± .26%

It can be observed that only one line has been fitted to the data with a consequent increase in overall uncertainty.

These values of meter factors were programmed into a master program that controls the data acquisition from the rig.

The prototype instrument was set up as described in chapter 5 and functionally tested. The HP counter/timer was set up nearby the instrument and throughout the flow and zero testing of the instrument the same cables and condition of triggering etc, were used for measurement purposes.

A connection block was designed such that the incoming pulses (from the receiver/processor) could be routed to either the HP counter/timer or the vernier timing system. A small length of coaxial cable was inserted into the fast oscillator limb to provide a zero offset. This meant that the system would only operate in one direction and thus would eliminate the need to change cables for the HP counter/timer, since the HP counter/timer is an unidirectional instrument. Equal lengths of cable were used throughout to eliminate differential delays.

The system was tested on a functional basis and found to work satisfactorily. Figure 6.19, now shows the experimental set up.

The prototype instrument can be used in two modes

(i) on a single shot basis

(ii) on a multiple shot (averaging) basis

On a single shot basis a pair of pulses (separated by Δt) is allowed through the selector to the oscillators. The oscillators run until detection at which point they are stopped and a count is observed in the counters, on the LED's. The count is in binary form.

A reset button has been installed on the connection block and this effectively loads both counters with zeros. Resetting the selector allows another pair of pulses through.

In the multiple mode of operation the selector is set for many pulses and for every pair allowed through a pulse is sent to a counter which counts up the number of samples.

In this mode of operation, however, the detector stops the oscillators between samples but the counters are not cleared. The counters thus accumulate n counts (n is the number of samples). In this mode of operation the stop switch on the selector is used to stop the system

operation and this is manually switched when the count in the first counter is nearly full (ie: all LED's alight). In between each sample a detector reset signal is derived from the master generator.

The problem that arises in this mode of operation is the capacity of the counters, which is $2^8 = 256$. This is not sufficient for good averaging. It was necessary, when operating in multiple mode to join the two prototype counters (using $\overline{RC}$ to clock) to form a 16 bit counter (max count now 65k) and to use the HP counter/timer in totaliser mode.

6.3.1 The procedure adopted for testing

The procedure adopted in the testing of the prototype instrument was as follows:

(i) Visual check of rig and instrument with all equipment being switched on and allowed to warm up.

(ii) The master generator was set to 60Hz (60 samples per second are thus obtained) and the received signal on both amplifiers was set to be 2v peak to peak on the maximum cycle amplitude.' For all tests a threshold level of approximately 55mV was set, (ie: 55mA across 100Ω). The zero crossing following the threshold level was taken as the reference marker (the negative going zero of the maximum cycle amplitude).

(iii) The zero offset as given by the vernier system was taken. This entailed connecting the vernier system to the connection block and setting the system into multiple mode operation until the counters filled up, and the system was stopped. The binary count was recorded in hexadecimal format (Ny) and the totaliser count was recorded off the HP counter/time (Nr). The sample number count was also taken (count). The entire system was reset.

(iv) The zero offset as given by the HP counter/timer was taken. This was achieved by connecting the HP counter/timer to the connection block and setting the system into multiple mode operation. The controls for the HP counter/timer were set for time interval mode (A → B) and 1000 samples were taken. The mean and standard deviation were recorded.

(v) The temperature in the rig was recorded over an average of 100 readings. This was achieved by using the rig temperature sensor and a master program to access and process the data.

(vi) The measurement of T1, T2 and the calculation of δt was undertaken. This was carried out by setting the HP gate time to 662 mS which provided measurement accuracy to the order of 10^{-13} seconds but rounded off to 10^{-12} seconds (picosecond level). The period could thus be measured to 3 decimal places. The measurement was taken using the same cable and triggering settings every time (whether the 1MΩ input or 50Ω input into the HP counter/timer was used it only affected the 10^{-12} seconds position displayed).

(vii) The prototype instrument was tested over the full flowrange. This entailed a down-up-down set of flowrates (approximately 20 readings) or vice versa . The master program was run to access the rig data and when the flow had established itself at a particular flowrate a block of 3 rig readings were taken and as many prototye instrument readings as possible were taken. This was achieved, in multiple mode operation, by allowing the counters to fill up and stopping the system, as described for the zero readings. The information was recorded and the system reset. If time permitted another reading was taken.

Each set of readings were taken and used independently. This was felt to be a measure of the repeatability of the system.

(viii) The flow was stopped and the system was allowed to settle. The vernier and HP zeroes were recorded (as previously described).

(ix) The oscillator periods T1 and T2 and the calculated δt were recorded, once again as previously described.

6.3.2 Evaluation of constants used in calculating flowrate.

Because Q is simply related to V through $\frac{\pi}{4}(D-2d)^2$, where (D-2d) is the internal diameter of the pipe section and because it is a simple matter to measure (D-2d), it was decided to work in flowrates of velocities v in m/s. Thus the turbine output, in m^3/hr can be referred to the ultrasonic instrument, by a correction using $\frac{\pi}{4}(D-2d)^2$ where (D-2d) refers to the ultrasonic instruments pipe section. Clearly the error in Q from incorrect knowledge of (D-2d) will now not enter into the results, but in any case could, in general, only be estimated.

A careful examination of the pipe section has shown the pipe to be slightly eccentric and careful measurement of (D-2d) provides the minimum and maximum values. An average value, then, was taken as (D-2d) = .10064.

The equation relating the velocity to the time difference Δt is

$$V = \frac{CC_p \sqrt{1-\left(\frac{c}{C_p}\sin\alpha\right)^2}}{2(D-2d)\sin\alpha}\Delta t$$

so that the constants required are C, Cp and α. The value of α was measured to be 62.5°.

6.3.2.1 Measurement of Cp

The blocks designed specifically for the rig were cut from a different piece of perspex from that used for the blocks on the zero test rig. It was necessary therefore to measure Cp and this was carried out by using the prototype instrument, HP counter/timer and the test box.

The two blocks and the test box were cleaned and relubricated with couplant. One block was inserted into the box and pressed against the face to exclude air. The transducer was positioned outside the box. A measurement of the time taken for the pulse to strike the end of the block and return was recorded. For this time the HP counter/timer was used in time interval mode and 1000 samples were averaged.

The second block was pressed against the first so that air was excluded from the interface. A second reading was taken as before (n=1000). The results of the test are given in table 6.2 from which it can be seen that Cp = 2756.7m/s.

Table 6.2
Relating to the measurement of Cp

Time to first reflection	58.339×10^{-6}	second
Time to second reflection	114.400×10^{-6}	second
Dimension of second block	.07727	metres
Cp	2756.7	m/s
Temperature	16°	centigrade

6.3.2.2 Measurement of C

In a similar manner to that described for the calculation of Cp, a calculation of C can be made using the brass plates to provide the reflection surfaces. This being so the results of this experiment are given in table 6.3.

Table 6.3

Relating to the measurement of C

Time to first reflection	78.346×10^{-6}	seconds
Time to second relfection	253.947^{-6}	seconds
Path length	.258	meters
Temperature	15.7°	centigrade
C	1469.2	m/s

As a check on the value of C the coefficient of temperature is given as 3.09m/s and therefore the value of C at 20°C would be 1469.2 + (4.3x3.09) = 1482.5 approximately and this compares favourably with previous values.

The temperature of the test rig cannot be controlled to much better than ± 3°C and since the range of temperature is likely to be 14°-20°C it was decided to use the value of C at 20°C and note that there would be an error.

6.3.2.3 Calculation of constant K.

In the equation

$$\nu = K\Delta t$$

the value for K is calculated to be 20110709 where the values are:

(D-2d)	=	.10064	m
C	=	1481.7	m/s
Cp	=	2756.7	m/s
α	=	62.5	°

6.3.3 Analysis of results.

The data obtained from the flow tests is:

for the prototype instrument:	Ny,1	count in counter (slow)
and HP counter	$N_{R'2}$	count in counter (fast)
	Count	No of samples
	T1	Period of slow oscillator
	T2	Period of fast oscillator
	δt	difference in periods (T1-T2)

and

for the test rig:	Vtruk	velocity calculated from the Kent turbine
	Vtruf	velocity calculated from the Fisher turbine
	temp	temperature of fluid

The procedure adopted when analysing the results is:

(i) The hexadecimal count (Ny) is converted to a decimal value. N_R is directly in decimal format from the Hp counter/timer.

(ii) Ny and N_R are divided by count to yield an average value.

(iii) The value of Δt is calculated from:

$$\Delta t = |N_y - N_R| T2 + (Ny-1)\delta t$$

where Ny and N_R are the average values and T2 and δt have their normal meanings.

(iv) The velocity is calculated from:

$$Velcalc = K \Delta t = 20110709 \Delta t$$

(v) If Reynolds number correction is employed then the equation used for correction is:

$$V_{fac} = 1.12 - 0.011 \, Log_{10} \, R_e$$

where

$$R_e = \frac{\rho v d}{\eta} = 10^6 v \text{ for water}$$

ρ = density

v = velocity

d = diameter of pipe

η = Kinematic viscosity

The value of velcalc previously found is used in above to provide a new value for V of

$$V_{corr} = \frac{Velcalc}{1{\cdot}12 - 0{\cdot}011 \log_{10} Re}$$

(vi) the values of velcalc (or corrected velcalc) and Vtruk are used to calculate the linear regression of velcalc on Vtruk. The values for zero flow are excluded from the regression analysis.

(vii) the new values of velocity calculated according to the line fit of (vi) are compared with the calculated velocities such that an error can be expressed as a percentage of rate (or full scale).

$$\%\ \text{error}_{(\text{rate})} = \frac{\text{Velcalc} - \text{Vel line}}{\text{Vel line}} \times 100$$

or

$$\%\ \text{error}_{(\text{FS})} = \frac{\text{Velcalc} - \text{Vel line}}{10} \times 100$$

(viii) The resulting errors, as a percent of rate, are plotted against percent of full scale flowrate and yield a scatter diagram.

Three programs were written to process and plot the data. They were:

Prog. Datasave: (Basic program, BBC machine).
This program saves all the raw data and converts the hexadecimal to decimal.

Prog. Dataproc: (Basic program, BBC machine).
This program accesses the raw data and produces a printout of the results as calculated according to (ii) - (vii) above.

Prog. US plot (Basic program, Horizon machine). This program plots the error and flowrate as percentages.

6.4 Flowtesting the prototype instrument

6.4.1 Flow tests

The prototype instrument was set up as described in section 6.3, Functional testing. The transducers were mounted on the track and were adjusted to provide maximum signal response. The transducers were then clamped in this position.

The instruments were switched on and allowed time to warm up. It will be recalled, that in the specification for the instrument, it was decided to pursue as part of the objective, a single shot device. For this reason the first test was designed to show the capability of the instrument when operated in this mode.

In accordance with the procedures of testing and analysing the results as given in sections 6.3.1 and 6.3.3, the graph of error against flowrate is given in figure 6.20 for 10 single shots at each of sixteen different flowrates. It can be seen that the majority of samples produce errors which are within a +5% band and this is the level of turbulence one would expect.

If the ten results are averaged then the resulting graph is as shown in figure 6.21. This set of results has a straight line fit of

$$y = .068 + 1.0014 \quad Vtruk$$

with a regression coefficient of $r = .9997$ (for R_e corrected flow).

A repeatability test was conducted at this position to show the spread of averaged results at two particular flow rates. The plot of this is shown in figure 6.22 and shows that the repeatability would appear to be of the order of +1/2%.

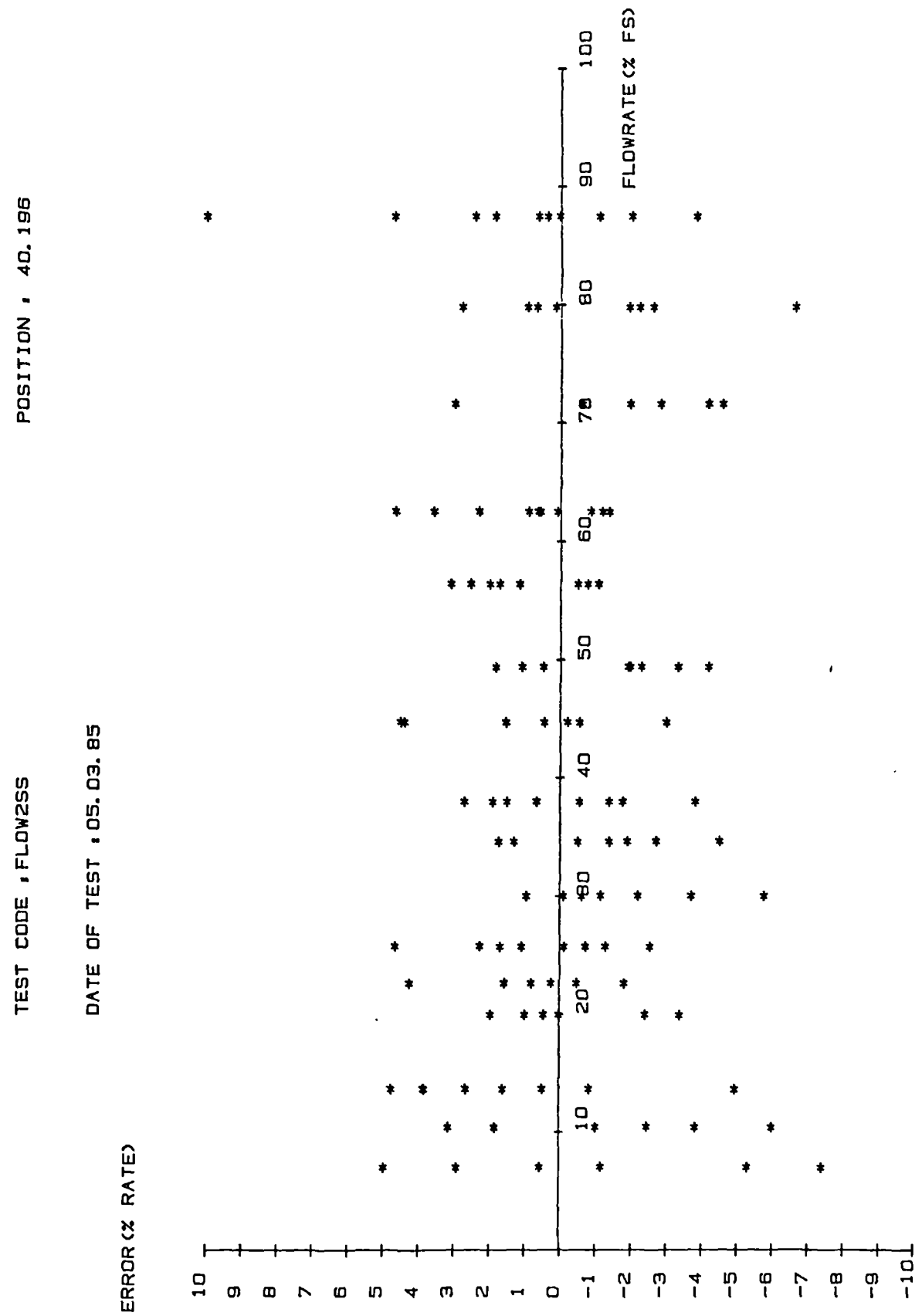

FIG 6.20
Prototype flow test result-single shot mode

After these preliminary tests a plan of testing was produced. This plan consisted, essentially, of calibrating the instrument at four different positions and with clamping and reclamping. The tests were conducted over a one month period and were coded Flow 4 to Flow 13.

For each test the transducers were completely removed from the pipe. The transducers and the pipework were cleaned and the transducers were replaced and their position was recorded. There were two exceptions to this procedure.

Flow 5 was a repeat calibration of flow 4 but halfway through the test the transducers were accidently dislodged from the pipe. This did not significantly affect the calibration.

Flow 10 was a repeatability test under the same conditions as Flow 9 (ie: not removed and reclamped).

Two typical scatter diagrams are given in figures 6.23 and 6.24 for Flow 9 and Flow 12 respectively. It should be noted that two sets of diagrams exist coded by P or PR which signifies no Reynolds number correction (P) and Reynolds number correction (PR).

It can be seen that the errors over the full range (approximately .5m/s - 9.5m/s, a turn down of 20:1) are within ±1% of rate.

Figure 6.25 shows a repeatability test on run Flow 10 where two flowrates were held constant and measurements using the prototype instrument were made. It can be seen that the repeatability is very high in this case at approximately 1/2%. At each flowrate (20%FS and 83% FS Flowrate) approximately 10 readings were taken.

The maximum signal response was found to be at position 1 which had a separation distance between transducers of .147 metres. The separation distance for other positions is given below in table 6.4.

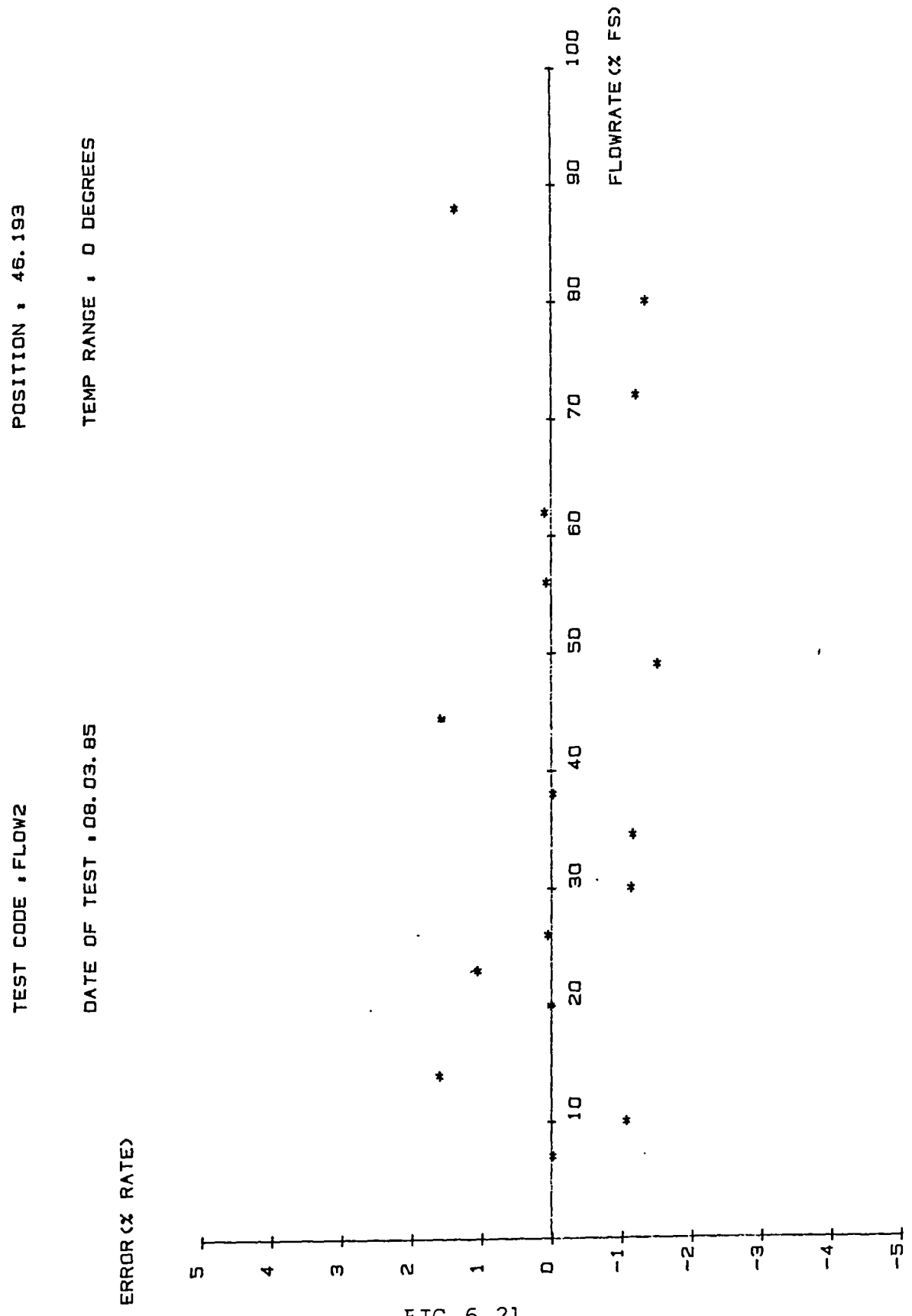

FIG 6.21
Prototype flow test result-average over 10 samples

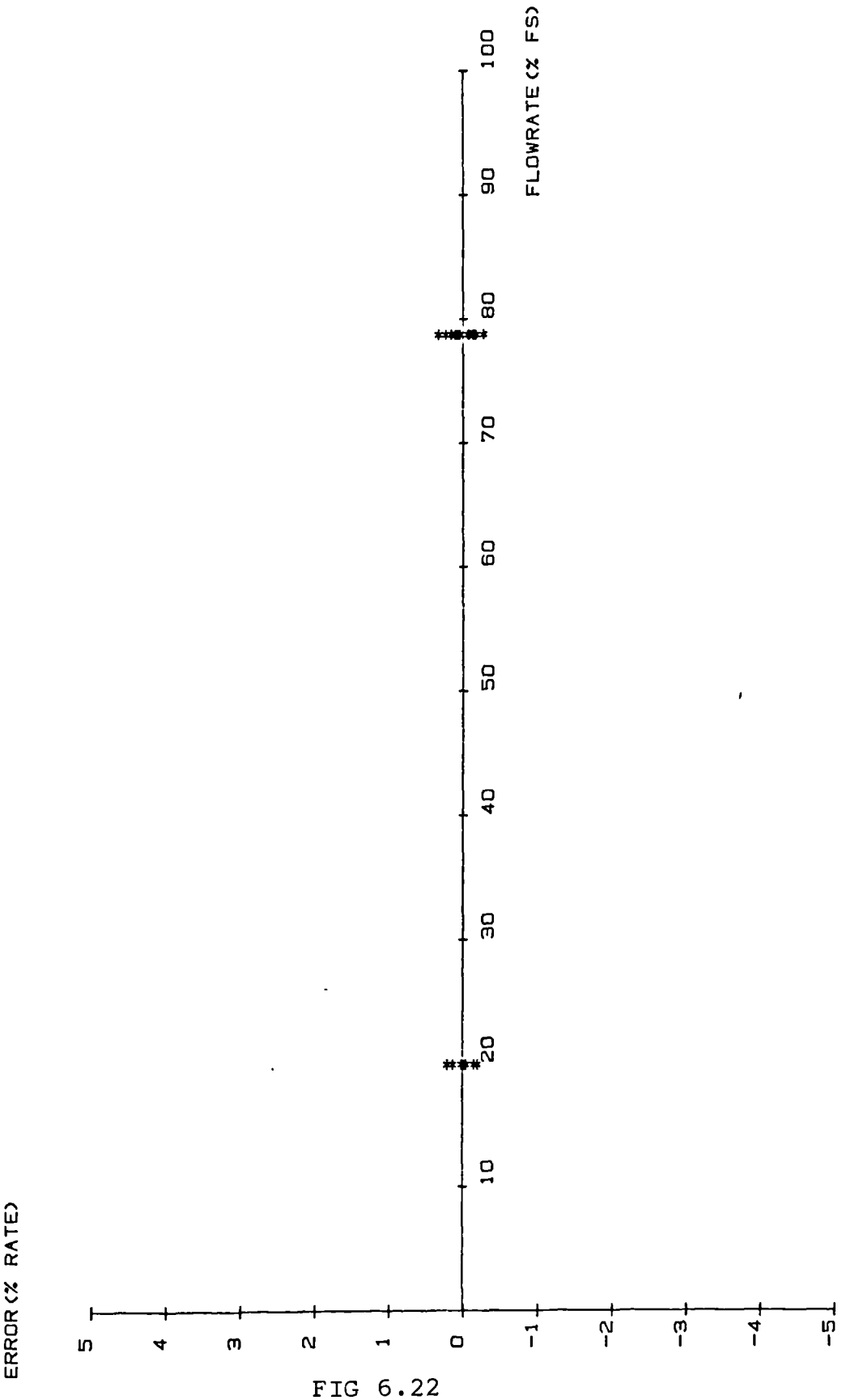

FIG 6.22
Prototype flow test result-repeatability

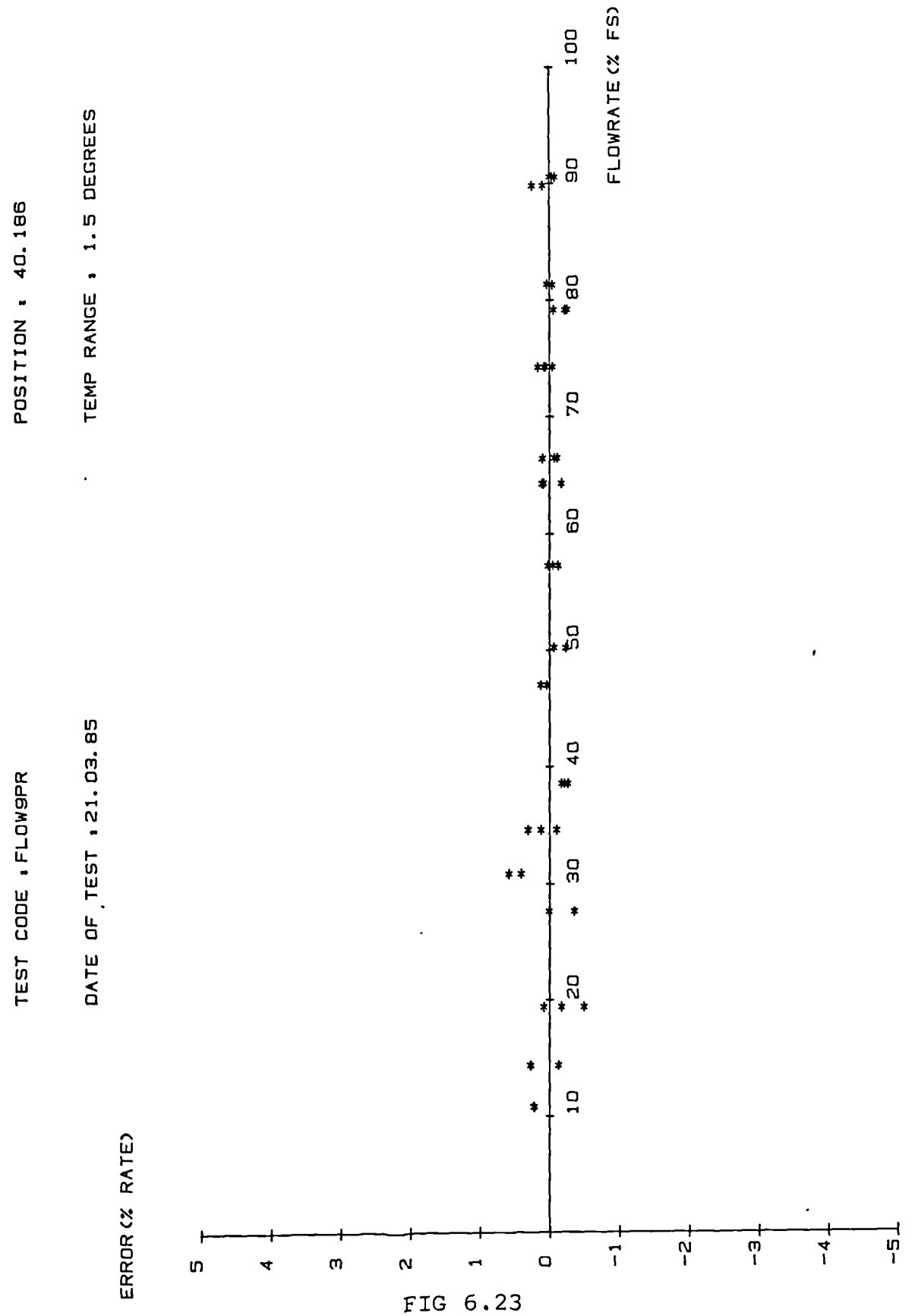

FIG 6.23
Prototype flow test result-run FLOW 9PR

Table 6.4
Position and separation distance between transducers

Position	Separation distance
2	.136 m
3	.146 m
4	.156 m

The results of running the tests and fitting the straight lines to data are summarised in table 6.5. The values of T1 and T2 and δt used in the analysis are those given under start conditions in table 6.5.

In addition to the above positions two further extreme positions were tried. However in order to obtain a received signal of approximately 2 volts peak to peak, it would have been necessary to increase the voltage for firing above a safety limit. The positions, therefore, were deemed unsuitable for test purposes.

6.4.2 Zero tests

It was decided to test the system under new compound conditions to ascertain if the compound had a setting time that would affect the zero offset. The rig was allowed to run and come to a stable temperature, this was approximately 18°C. Over the experiment the temperature did not change by more than +1/2%.

The transducer was lubricated with the compound and attached to the pipe in position 4. The zero was calculated using the result provided by the vernier system. The experiment was conducted over 1 1/2 hours, the approximate time of a calibration run.

Table 6.5
Summary of results

RUN	DATE	POS	TEST	TEMPERATURE MIN °C	MAX	EQUATION OF LINE FIT		
FLOW 2	08.03.85	1	SINGLE SHOT / AVERAGE	15.6	17.4			
FLOW 3	15.03.85	1	REPEATABILITY	14.7	15.7			
FLOW 4	15.03.85	1	CALIBRATION	16.0	17.8	=.085	+.9996	VTRUK
FLOW 5	15.03.85	1	CALIBRATION	17.8	19.6	=.0824	+.997	VTRUK
FLOW 6	15.03.85	1	RECLAMP CALIBRATION	19.1	20.5	=.079	+.997	VTRUK
FLOW 7	21.03.85	2	CALIBRATION	16.1	17.4	=.116	+.9965	VTRUK
FLOW 8	21.03.85	2	RECLAMP CALIBRATION	16.0	19.0	=.096	+1.003	VTRUK
FLOW 9	21.03.85	3	CALIBRATION	19.2	20.7	=.109	+.9915	VTRUK
FLOW10	22.03.85	3	REPEATABILITY	16.0	18.3			
FLOW11	22.03.85	3	RECLAMP CALIBRATION	18.3	20.4	=.117	+.9928	VTRUK
FLOW12	28.03.85	4	CALIBRATION	17.8	18.9	=.0954	+1.00129	VTRUK
FLOW13	28.03.85	4	RECLAMP	19.0	20.0	=.1045	+.998	VTRUK

Table 6.5 cont'd

Summary of results

RUN	REGRESSION COEFF	BEFORE RUN			AFTER RUN		
		T1	δt	T2	T1	δt	T2
FLOW 2		26.885	.827	26.058	26.904	.81	26.094
FLOW 3		26.824	.729	26.095	26.821	.727	26.094
FLOW 4	.999984	26.827	.728	26.099	26.827	.718	26.109
FLOW 5	.999954	26.830	.730	26.10	26.871	.730	26.141
FLOW 6	.999988	26.871	.730	26.141	26.829	.721	26.108
FLOW 7	.999991	26.812	.739	26.073	26.822	.716	26.106
FLOW 8	.999992	26.822	.716	26.106	26.830	.724	26.106
FLOW 9	.999995	26.822	.716	26.106	26.832	.720	26.112
FLOW10		26.887	.746	26.141	26.889	.738	26.151
FLOW11	.9999964	26.900	.737	26.163	26.836	.710	26.126
FLOW12	.99998	26.917	.717	26.20	26.963	.736	26.227
FLOW13	.999994	26.899	.726	26.173	26.885	.720	26.165

The result of this test is displayed on figure 6.26 and shows no appreciable drift in the zero as a function of settling time.

During the complete testing of the instrument zero readings were taken before and after the calibration run and at random intervals. The readings were taken within a short time of each other on the HP counter/timer and on the vernier system.

The results of these tests are given in figures 6.27 to 6.30. Each figure corresponds to a day of testing and the corresponding time at which the zero value was taken.

From all figures it can be seen that the vernier timing system is tracked almost identically by the HP counter/timer (whose accuracy specification is within ± 2.2 nS of true value).

For the random times when the zero was checked it fell within the range 5.1 nS - 6.16 nS for the vernier system and within 7.3 - 7.8 nS for the HP counter/timer, and these zeroes take into account no warm up period at all.

The offset as calculated using the measured zero yields the results shown in Table 6.6, where they are compared with the zero produced by the line fit.

If an average value of zero, under normal conditions is assumed to be 5.5 nS then a resulting value of velocity offset is .1106 m/s. This results in a worst case error for Flow 6 where the disagreement is the largest of all the tests.

Figure 6.31 is a graph showing the effect of zero offset (measured) against clamping/reclamping of the transducers in different positions. The graph shows the zero readings before and after the calibration runs. The overall shift in the zero would appear to be less than .5 nS.

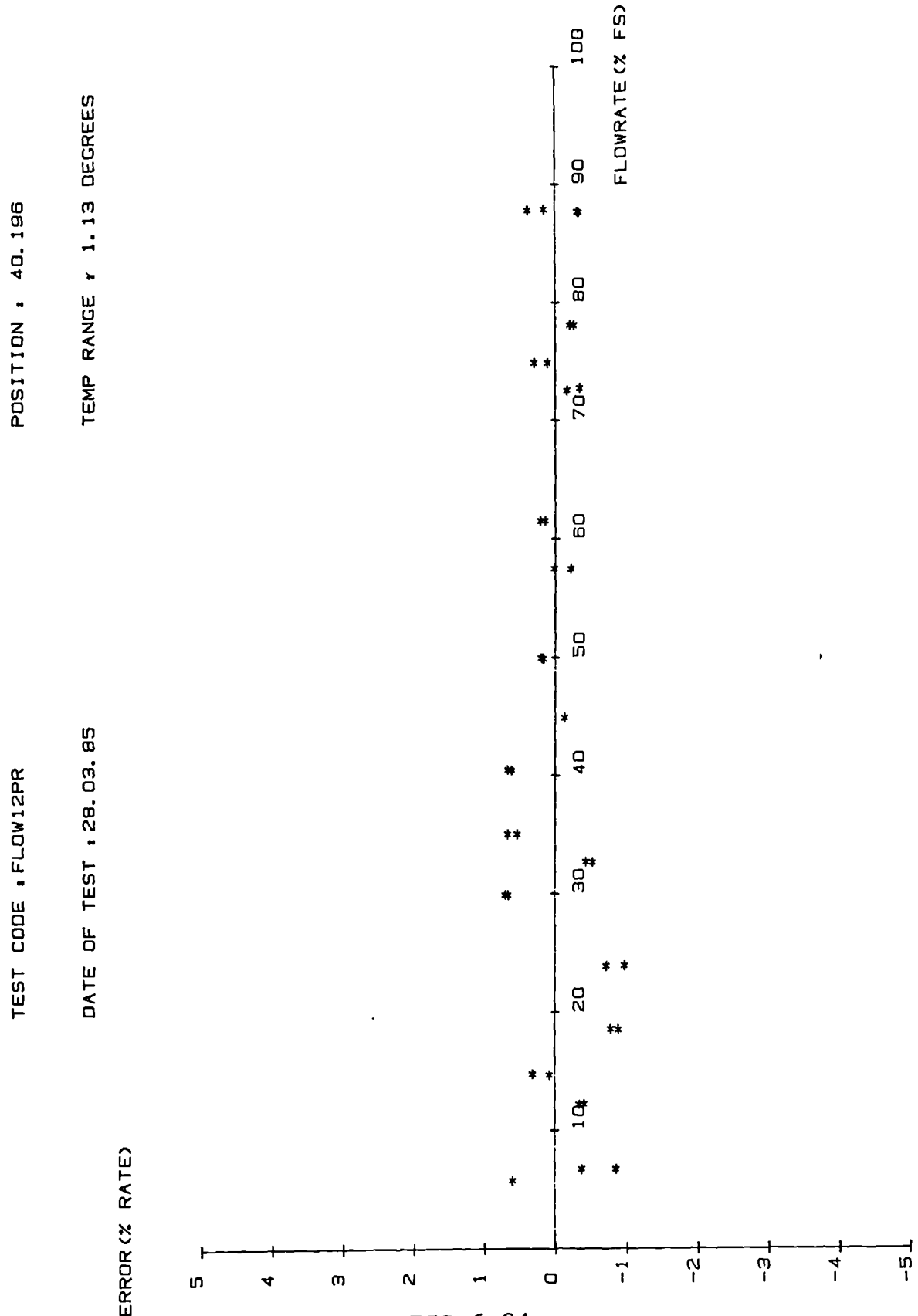

FIG 6.24
Prototype flow test result-run FLOW 12PR

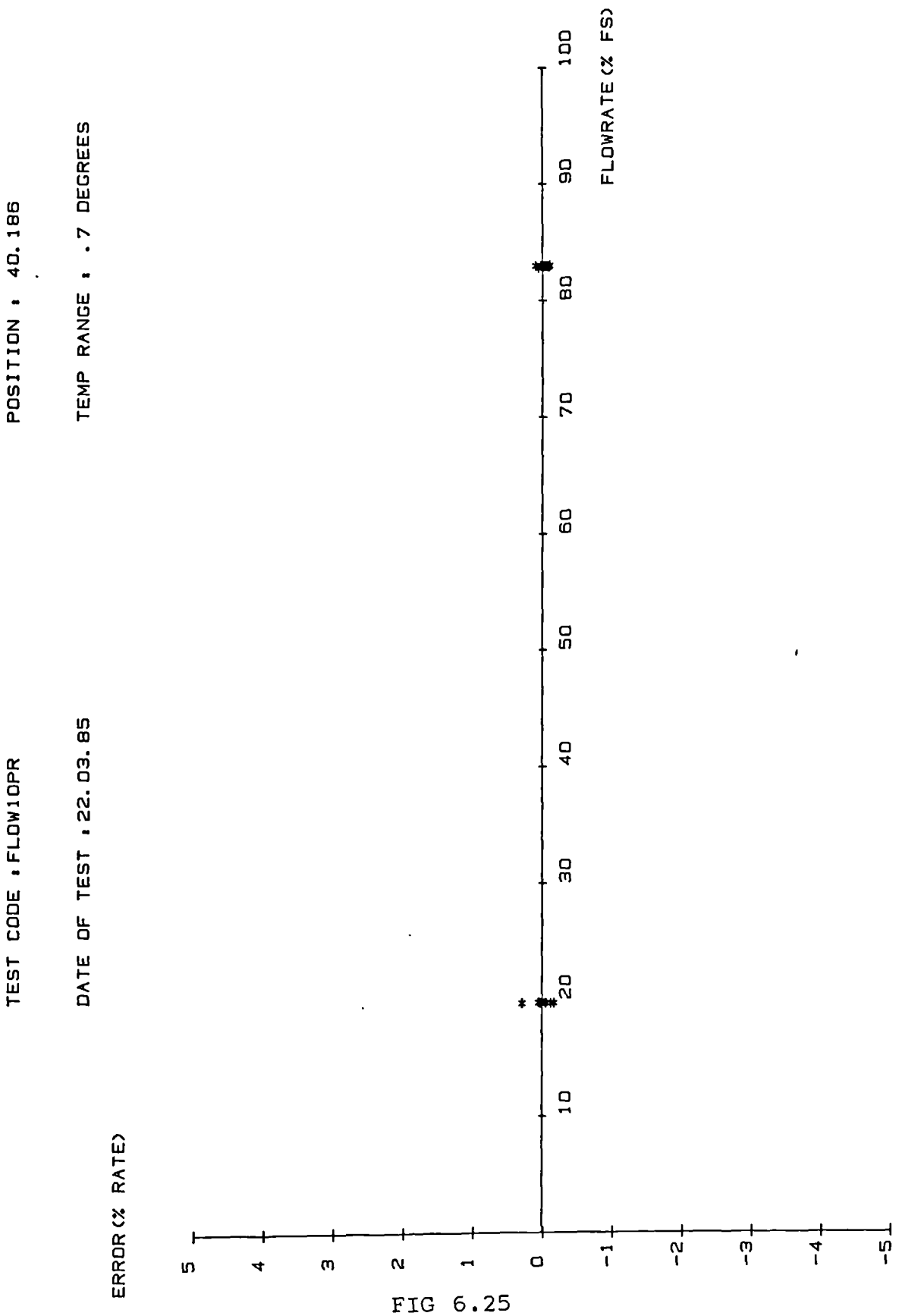

FIG 6.25
Prototype flow test result-repeatability

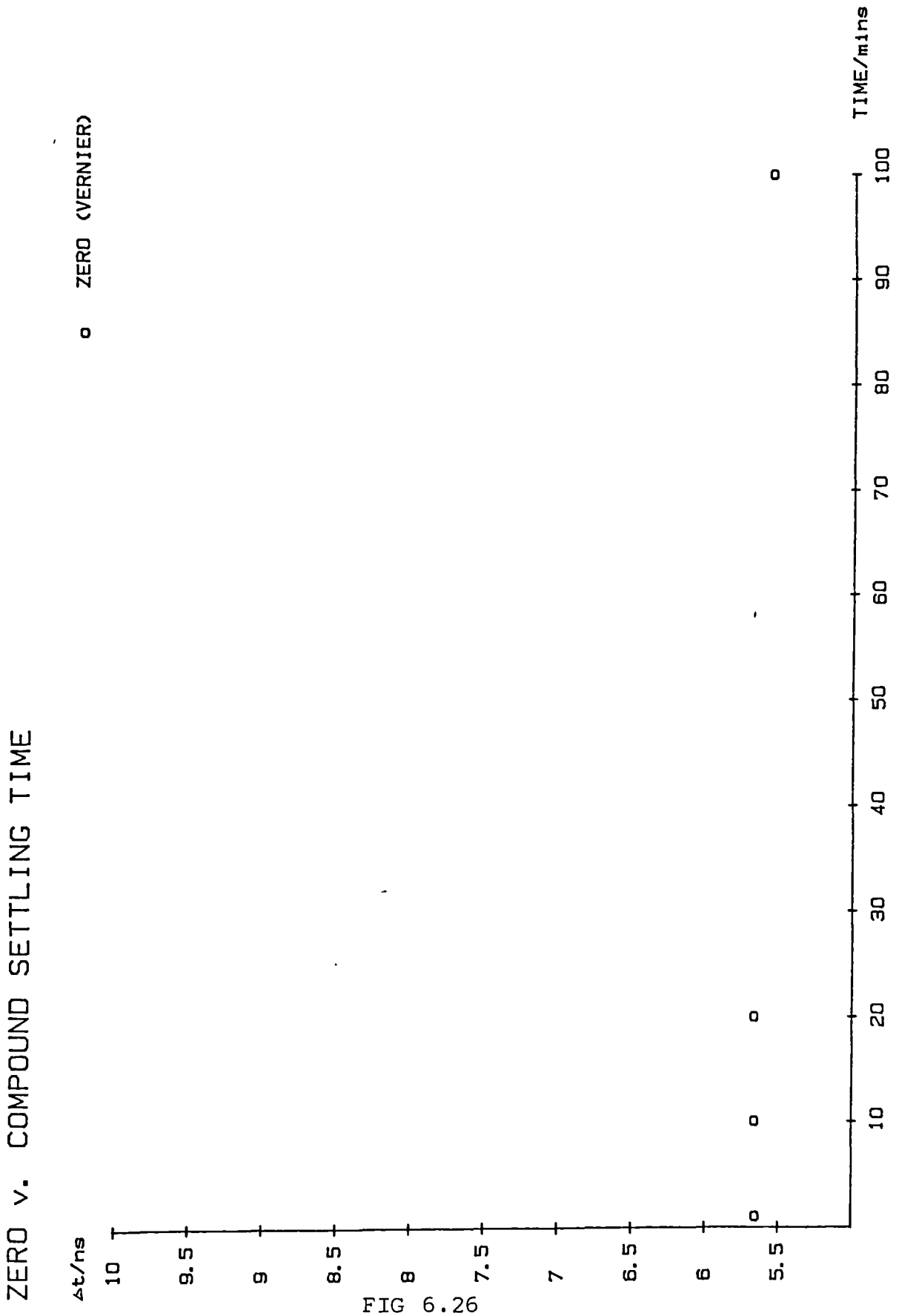

FIG 6.26
Plot of zero offset v. compound settling time

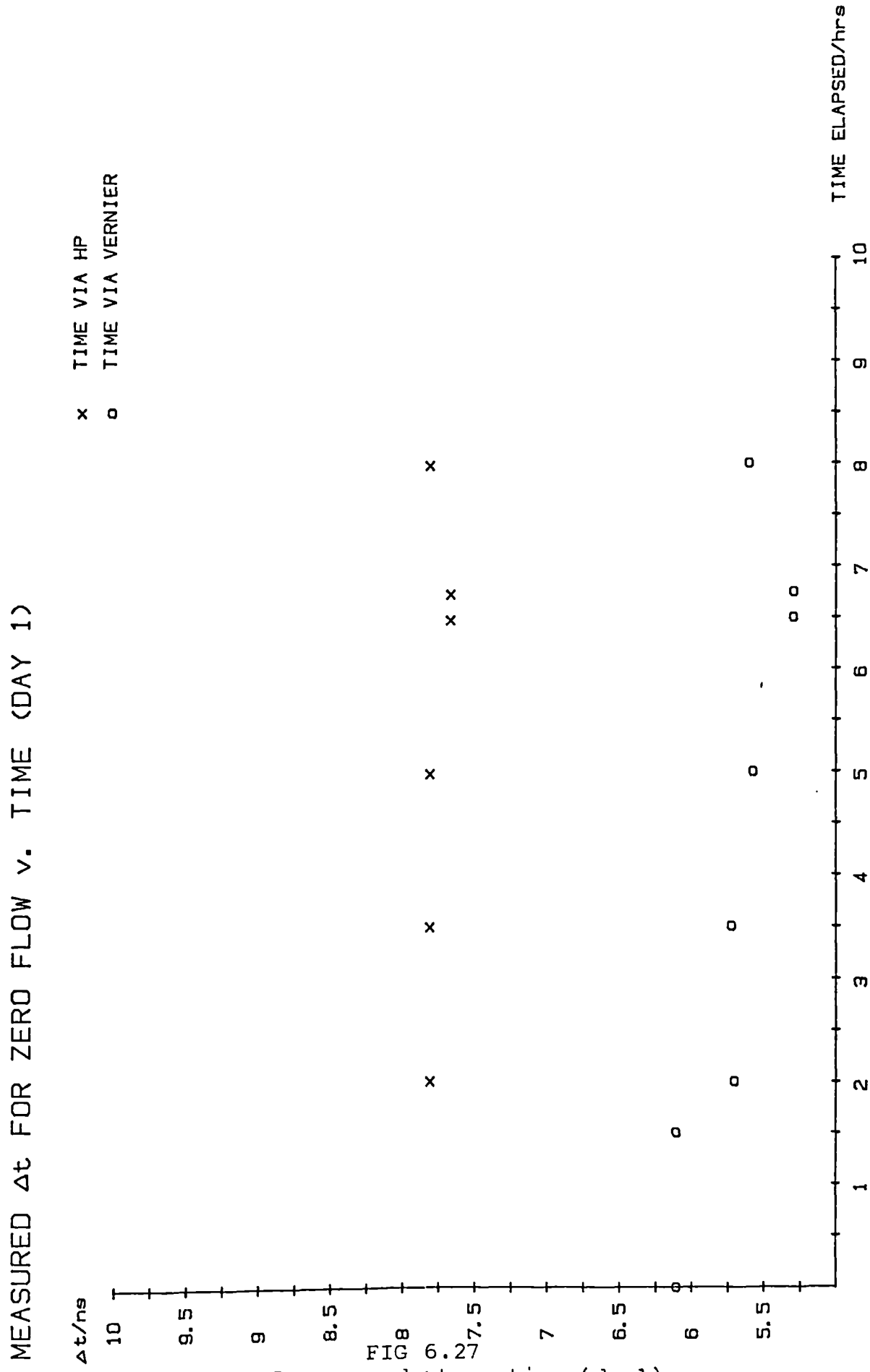

FIG 6.27
Plot of measured Δt v. time (day1)

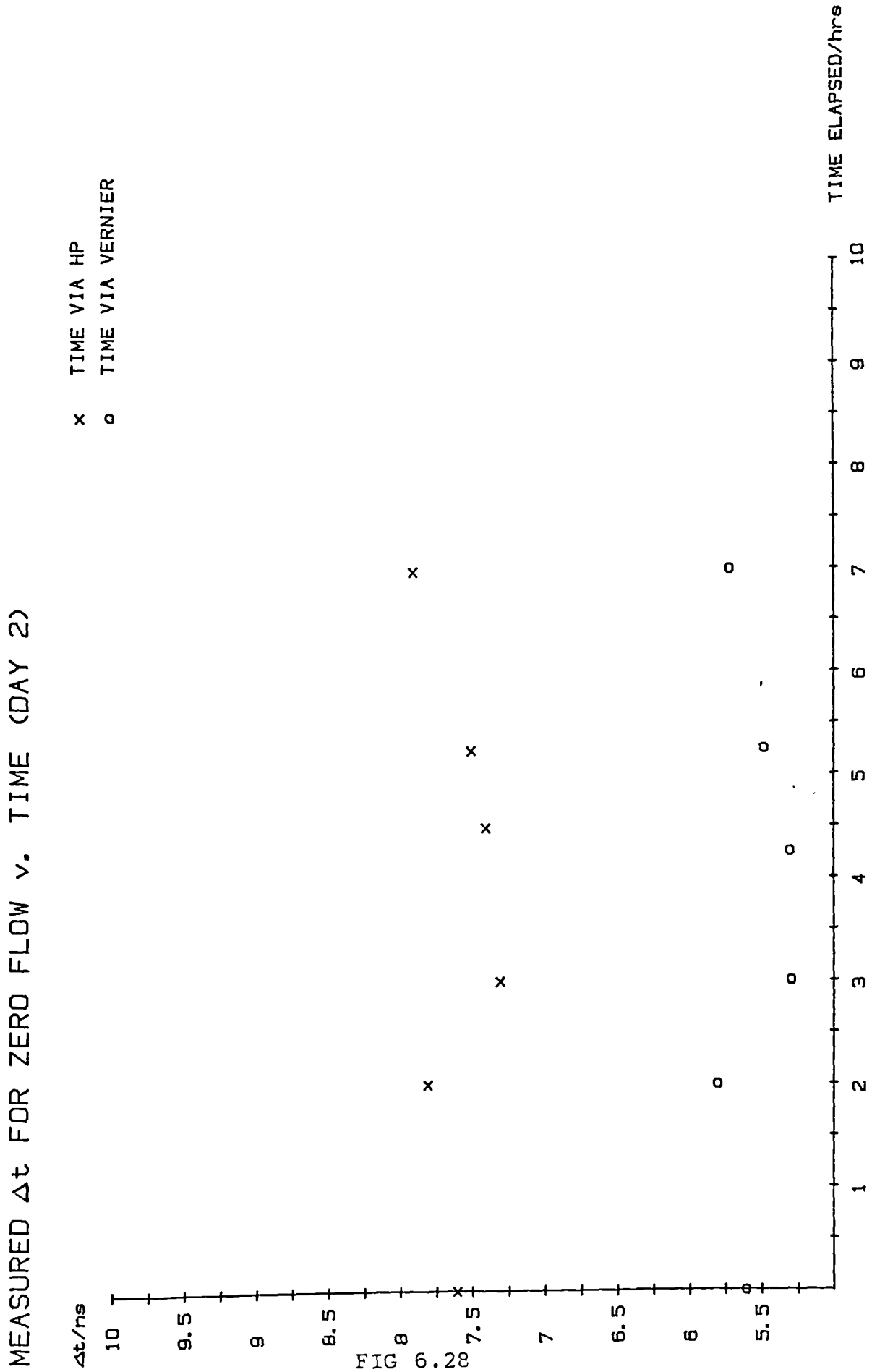

FIG 6.28
Plot of measured Δt v. time (day2)

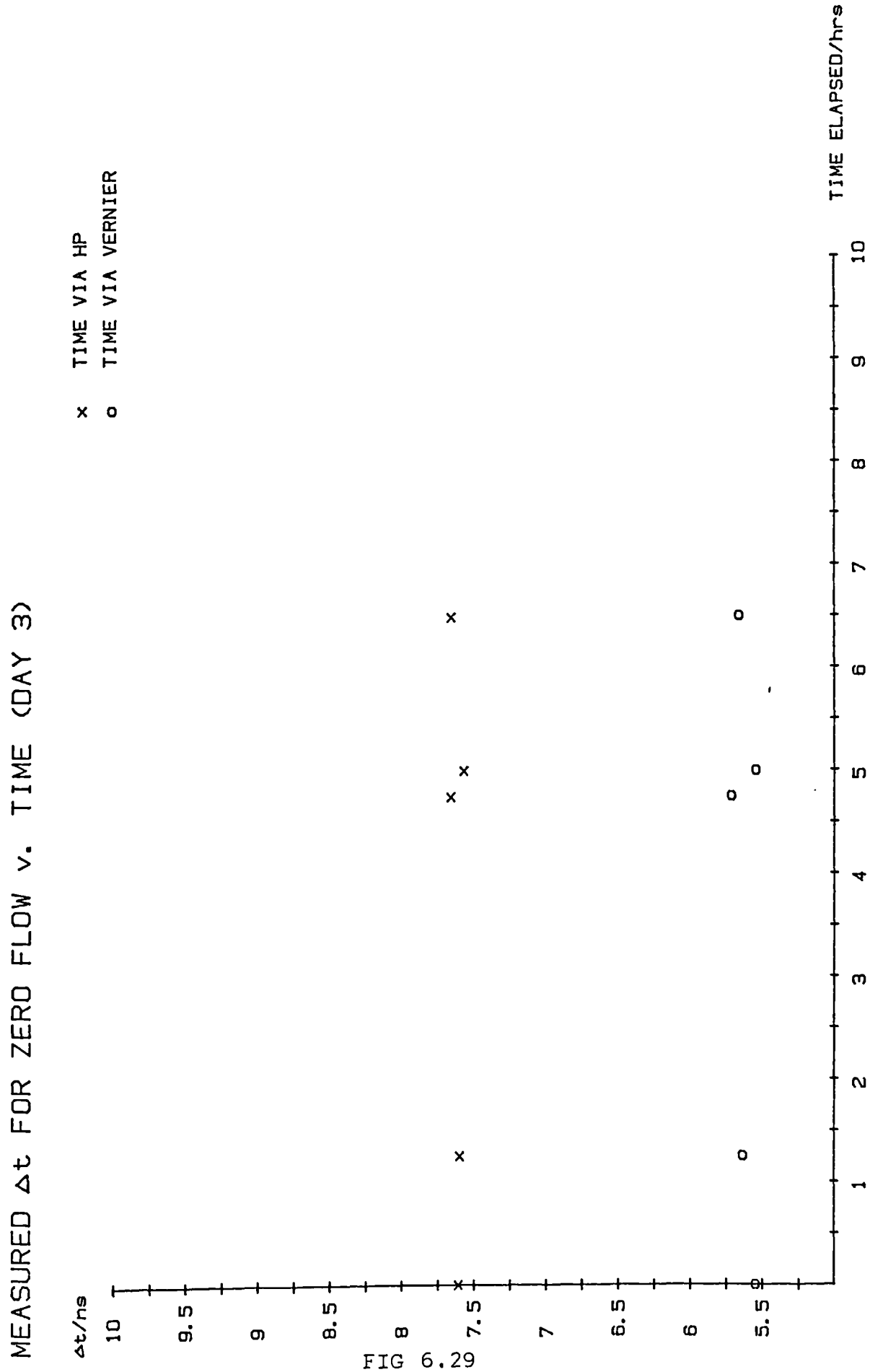

FIG 6.29
Plot of measured Δt v. time (day3)

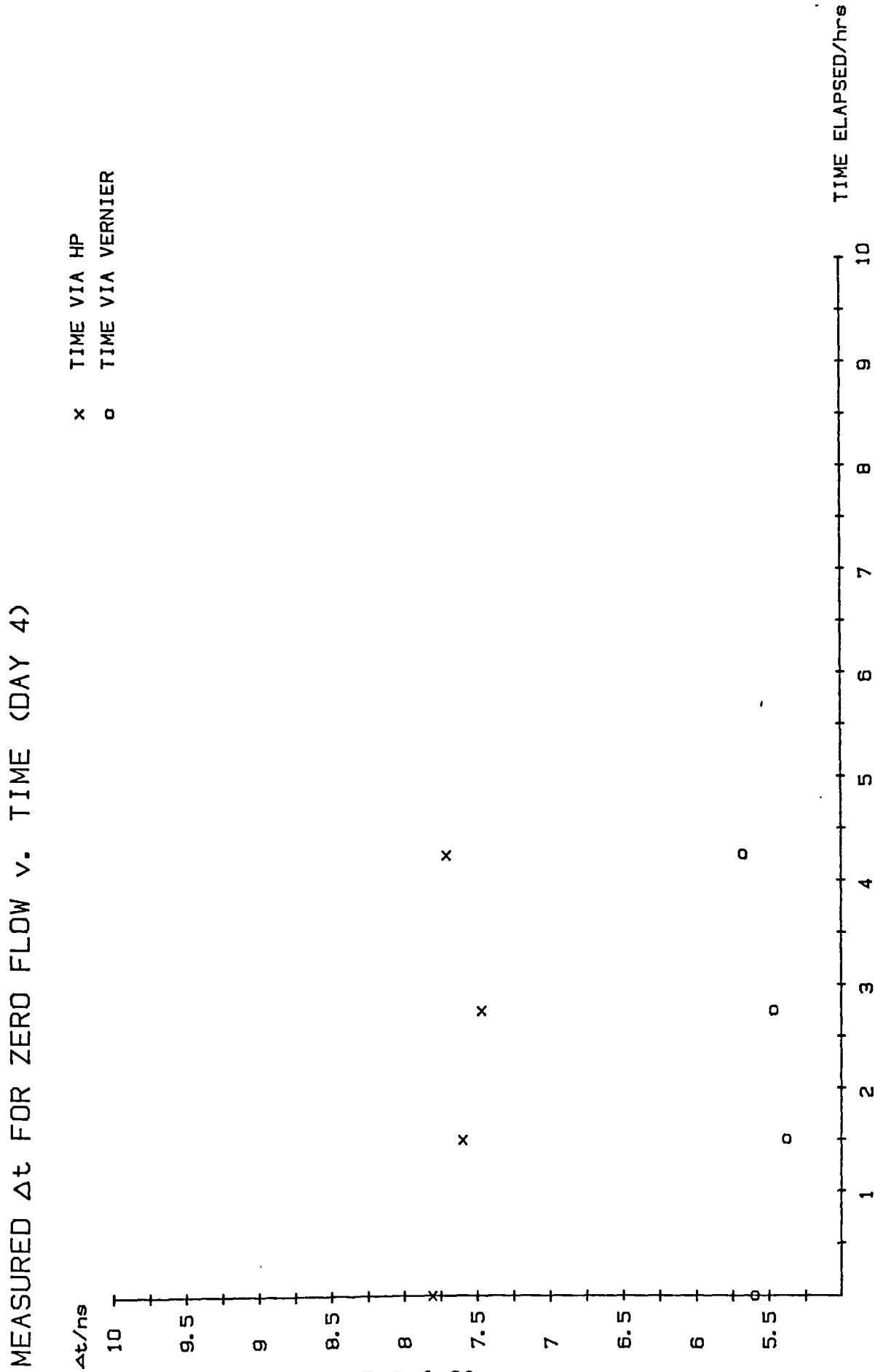

FIG 6.30
Plot of measured Δt v. time (day4)

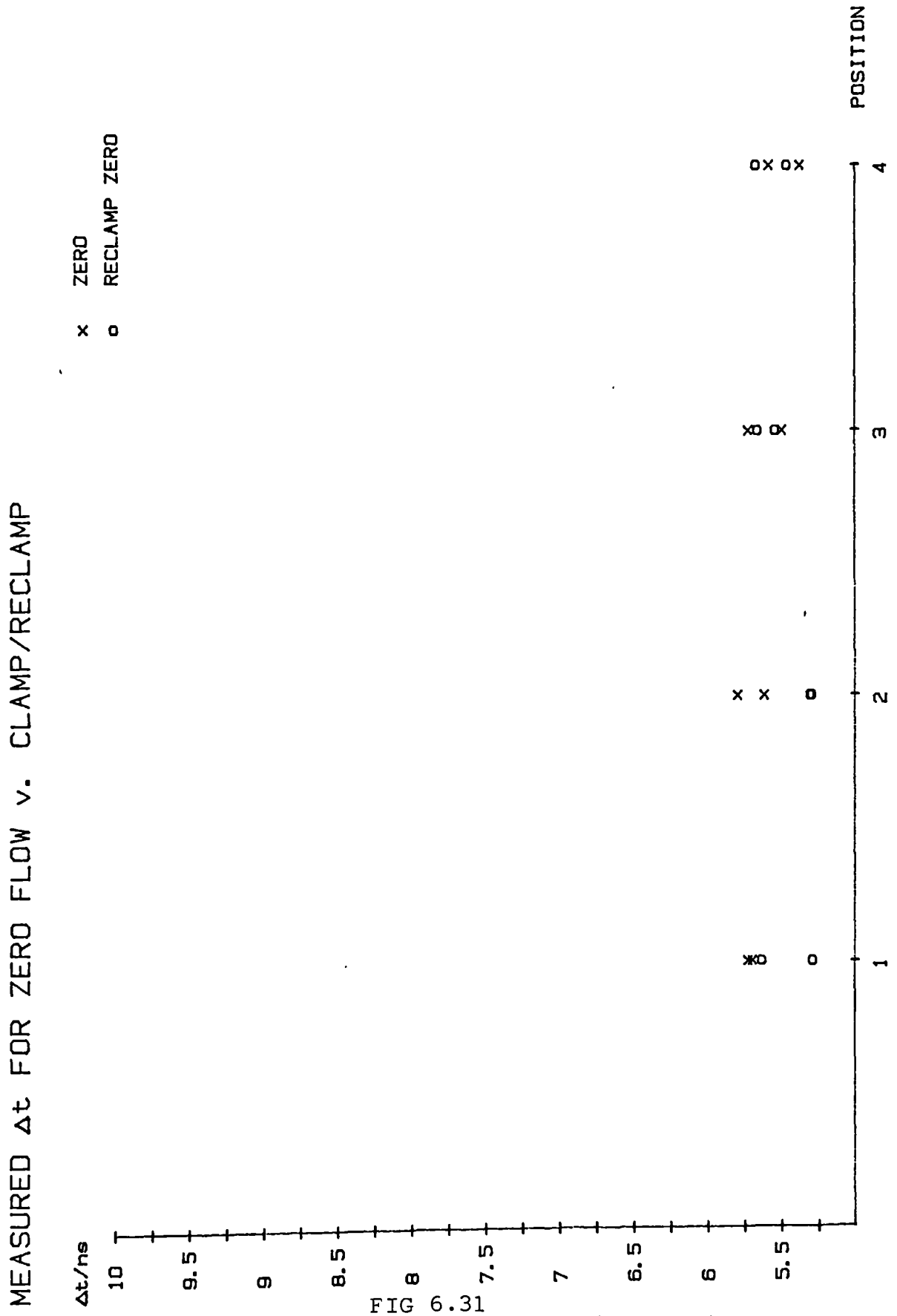

FIG 6.31
Plot of measured Δt v. clamping/reclamping

Table 6.6
Zero measurements

Run	Zero measured nS by HP(nS)	by Vernier (nS)	Calculated Offset(vernier)m/s	Line fit Offset m/s
Flow 4	7.87	5.69	.114	.085
Flow 5	7.75	5.58	.112	.0824
Flow 6	7.66	5.29	.106	.079
Flow 7	7.61	5.61	.113	.116
Flow 8	7.32	5.29	.106	.096
Flow 9	7.49	5.48	.11	.109
Flow 11	7.55	5.54	.111	.117
Flow 12	7.81	5.59	.112	.0954
Flow 13	7.46	5.42	.109	.1045

6.5 Measurement of C from outside of the pipe

The principle behind the measurement of C from outside of the pipe, was explained in chapter 2 and essentially consisted of following the wavefront from one transducer to the next and measuring the time taken.

The equation then relating the parameters was

$$C = \frac{1}{\sqrt{\left\{\left[(T-T_2) - \frac{L_T}{C_p}\sin\alpha + \left(\frac{L_C+L_D}{C_p}\right)\right]\frac{1}{D-2d}\right\}^2 + \frac{\sin^2\alpha}{C_p^2}}}$$

where

α	=	the angle in the block
Cp	=	the speed of sound in the wedge material
L_C, L_D	=	the distances travelled in the wedge by the wavefront
(D-2d)	=	the internal diameter
T	=	the time taken to travel the pipe
T_2	=	the time taken to travel between the blocks
L_T	=	distance between transducer planes

Careful measurement of α, Cp, L_C, L_D and D-2d was made and these values were found to be:

α	=	62.5°
Cp	=	2757 m/s
(D-2d)	=	.10064 m
L_C, L_D	=	.0346 m

The remaining requirement was, therefore, the measurement of T and T2 and L_T.

A set of parallel tracks were designed to fit the pipe section used for testing and these tracks allowed easy positioning of the transducers across the diametrical chord. There was a screw/pressure plate

arrangement to ensure good contact. A pair of high quality steel rules were attached to the pipe. This arrangement allowed precise positioning of the transducers.

The blocks were carefully fitted onto the tracks and positioned. The electronics were connected and the HP counter/timer was employed to measure the time, instead of the vernier system. (Certainly the vernier system could be used, probably in a normal counting mode,ie: as an oscillator of 26 nS period with on/off control).

A test was conducted on four positions which were each separated by .01m. The value of C was calculated and found to be consistent but incorrect. The test was repeated with the same result.

A large part of the reason for the discrepancy lies in the fact that the waveform is different for the two cases of blocks together and blocks across the pipe. These waveforms are shown sketched in figure 6.32

It can be seen that the time beteen the start of the waveform and the zero crossing taken is longer in the case of the transducers on the pipe than for the transducer blocks face to face.

The cycle to cycle variation is also a factor in the discrepancy in the calculation of C particularly the starting point.

A particular problem with the present design of prototype instrument is the feed through (from firing) which is still present, albeit in reduced form, when the blocks are placed face to face. This feed through interferes with the received signal and makes it difficult to estimate precisely the start of the signal.

However, this problem is not felt to be a severe one and would probably not be necessary in a commercial instrument (see discussion of results).

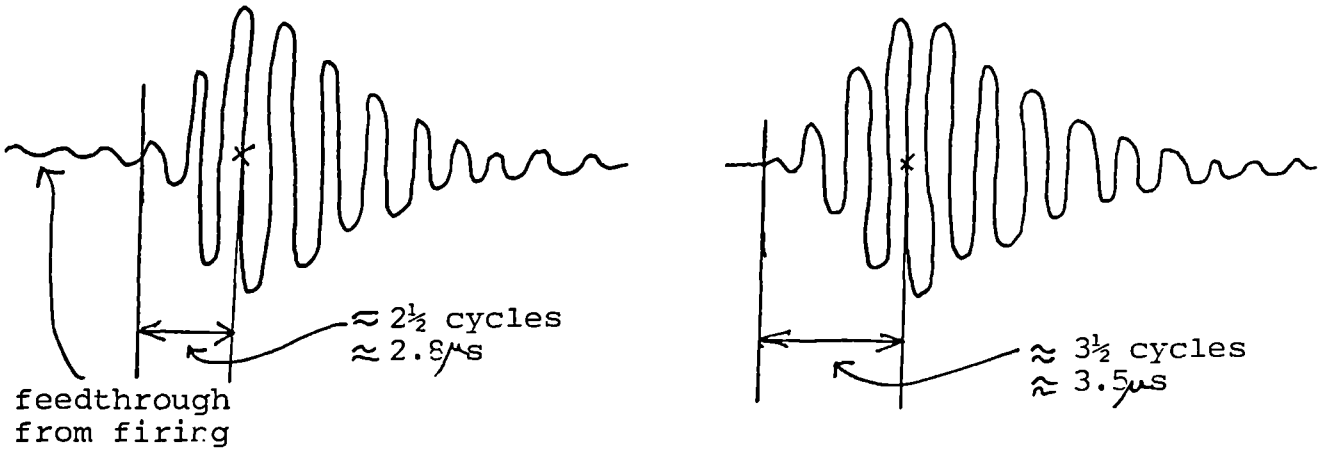

(a) (b)

FIG 6.32
Signal response (a) through perspex blocks (b) across pipework

To obtain the true time, therefore, the measured T and T2 require a small value to be subtracted which is not the same for both. In the case under consideration the time to be subtracted was viewed on an oscilloscope and was found to be:

for the blocks face to face (T2) = 2.8×10^{-6} seconds
for the blocks across pipe (T) = 3.5×10^{-6} seconds

The values for T, T2 and the calculation of C are shown in tabular form in table 6.7. The fluid temperature was approximately 18°c (thus C≈ 1476m/s).

Table 6.7
Relating to the estimation of C

Measured T (nS)	T2 (nS)	Corrected T (nS)	T2 (nS)	Distance L_T (m)	Calculated C m/s
104.46	27.82	100.96	25.02	.126	1466.24
107.65	27.82	104.15	25.02	.136	1466.8
110.96	27.82	107.46	25.02	.146	1464.9
114.183	27.82	110.683	25.02	.156	1464.8

It was noticed that the positioning of the blocks was critical and this can be seen clearly from the time change per mm moved, which is approximately 3.2×10^{-7} seconds.

A further experiment was carried out to measure C in the test box and this was found to be 1475.6 m/s.

6.6 Discussion of results

All scatter diagrams show an error band overall (repeatability band) of approximately +1.5% (of rate) over the full range tested (5% - 95% FS flowrate approximately a 20:1 turndown). The exception to this is Flow 4 which has a 2% band characteristic.

The instrument would appear to be linear to within 1.5% and highly repeatable ($\approx$ 1/2%) at any particular flowrate over the above range.

There are other sources of errors to consider to produce a final value of overall error or, a specification for the instrument, for the limited range of temperature, under which testing took place.

The first error to consider is the constant value of K used in the equation.

$$v = K\Delta t$$

This constant value assumes that C and Cp do not vary with temperature. However the tests were conducted over an approximate temperature range of 6°C. If one assumes that the change in Cp over 6°C is negligible the error in K brought about by a change in C can be shown to be

$$\frac{dK}{K} = \left[- \frac{C^2 \sin^2\alpha}{C_p^2 \left(1 - \left(\frac{C}{C_p}\sin\alpha\right)^2\right)} + 1 \right] \frac{dC}{C}$$

and for a 1°C change in C this reduces to

$$\frac{dK}{K} = .14\%/^{\circ}C$$

and therefore over a $6^{o}C$ change the change in K would be .84%. This error affects the calibration of the instrument.

Now consider the change in the calibration of the instrument. Over the full range of positions this is 1.1% (calibration slope of Flow 8 - Flow 9), but over the same position is only .65% (clamp and reclamp calibration of Flow 7 and Flow 8).

By far the biggest source of error would appear to come from the instability of the zero. This error is significant at low flows but not at the high flowrates.

The smallest offset is .079 m/s of Flow 6 and if the zero value is taken at .11 m/s the difference is .031 m/s. This would then correspond to a 3% error at the 1 m/s flowrate.

If a value of zero offset was chosen in between the minimum and maximum offsets of all regression lines, the error would reduce to +1.9% (choosing offsets .079 m/s flow 7 and .117 m/2 Flow 11).

For an individual position the maximum change in offset would be .02 m/s for position 2. This would then correspond to +1% (at 1 m/s) if the average value was chosen.

A final error source not discussed in these results is that from incorrect measurement of the bore (D-2d). This particular error is common to all clamp-on flowmeters and is difficult to estimate.

Therefore the error bands (or specification) for the prototype instrument would appear to be made up as follows:

in the worst case:

(1)	(2)	(3)
±1.5%	±.55%	±1.9% + errors from (D-2d)
		=± 3.95 % + errors from (D-2d)

and in the best case:

±1.5%	±.32%	±1% + errors from (D-2d)
		=± 2.82% + errors from (D-2d)

where (1) = error of scatter
(2) = calibration change error (incorporating the effects of temp.)
(3) = offset error at the 1 m/s level of flowrate.

If an error figure is used for (D-2d), say 1% then a 2% error needs to be added to the above figures for the prediction of Q since there is a direct value (ie: a 1% error in (D-2d) = 1% error in Q) and a value of 1% from incorrect measurement of C, resulting from the error in (D-2d).

Let us now compare the prototype instrument with the commercial instrument tested.

Common to both instruments (when the commercial instrument is in external mode) there is no error associated with the (D-2d) measurement. This was explained previously.

The scatter displayed by both instruments would appear to be of approximately the same magnitude at $\pm$1.5%. Both instruments exhibiting larger errors at the lower flowrates.

Both instruments were tested over approximately the same range of temperature and the errors associated with temperature and calibration for the prototype instrument could probably be equated to the 1% repeatability (with respect to clamping/reclamping) of the commercial instrument.

The remaining error is then due to the instability of the zero. For the commercial instrument it was observed, under all conditions, that the zero was highly stable at +1 LPM about zero. This would suggest that the instrument was measuring flowrates (in a 100mm pipe) of $+2 \times 10^{-3}$ m/s at no flow. It would appear therefore that the electronics and associated instability was $+0.1 \times 10^{-9}$ seconds. This figure is a factor of 5 times better than that of the prototype instrument.

However, the prototype instrument would appear to be the better of the two when the commercial instrument is used under its own internal calibration. The commercial instrument produces a systematic offset of approximately 9.5% and even if a 1% allowance was made for incorrect bore size (D-2d) the error would only reduce to approximately 7.5% of $\dot{Q}$. The worst case error for the prototype even with the zero instability was $\pm$3.95%.

The errors from the velocity profile disturbance tests would be approximately the same for all single beam systems and because no tests were conducted with the prototype instrument a comparison cannot be made. However, it is clear that a disturbance can seriously affect the performance of the single beam instrument.

It is unfortunate that the instruments cannot be tested over a range that extends to very low flowrates, or over a significant temperature range. It is believed that the commercial instrument has no facility for measuring and tracking C or flow profile effects (through R_e), whereas the prototype instrument has this facility.

Now consider the difficulty encountered when measuring C from outside of the pipe. In chapter 2 the analysis did not calculate the effect of a change in L_T. However, it can be shown that:

$$\frac{dC}{dL_T} = \frac{\sin\alpha \left((T-T_2) - \frac{L_T}{C_p}\sin\alpha + (L_c+L_D)\frac{1}{D-2d}\right)}{C_p(D-2d)\sqrt{\left\{\left[(T-T_2) - \frac{L_T}{C_p}\sin\alpha + \frac{L_c+L_D}{C_p}\right]\frac{1}{D-2d}\right\}^2 + \frac{\sin^2\alpha}{C_p^2}}^3}$$

and thus inserting typical values,

$$\frac{dC}{C} = .42\% / \text{mm of } L_T$$

and this corresponds to 6.2 m/s in water. It is thus obvious that a change in L_T has a significant effect on the calculation of C.

It is now clear why the precise positioning of the blocks is important.

A thorough investigation of the transducer and block arrangement showed, that, because the transducer is mounted on the block and only secured by screws, there was a slight amount of slip but that this was probably insufficient to account for the error in C.

A more probable reason is the misalignment of the blocks face to face and the difficulty encountered in holding them in position while measuring the time T_2.

Since the error in the C measurement is only 10 m/s (or approximately 1.5mm) the three above causes could well add up to produce this error.

In a commercial instrument, it is unlikely that this problem would arise. Firstly the transducers would be encapsulated and not prone to slippage. Secondly the geometry of the system would be well marked on each block. Thirdly, a mechanical jig could be constructed to hold the blocks together correctly aligned.

Most importantly the instrument could be partly calibrated and T_2 accurately known (at a precise temperature) and stored in a memory location. The task of computing C would then essentially reduce to a good design of jig for the pipework to produce accurate positioning.

Since the main part of T_2 is made up of time in the block, a low temperature coefficient material should be used. The other part τ of T_2, the electronic delay, would be small and hence changes in τ are also likewise, small.

However, there is excellent agreement between the results for all positions and this suggests that the theory is applicable over a wide band of separation distances.

The excellent agreement between results also shows that the relative movement between the transducers is not a particular problem, but that the initial setting up is. It would be expected, therefore, that the tracking of C with temperature should not present a problem provided the electronic unit is temperature compensated.

The main problem, therefore, would appear to be the construction of a precise mechanical jig. If this could be constructed to within 1 mm accuracy, then the error in measurement of C would be 6 m/s or less than 1/2%. The main error would then undoubtedly come from the incorrect measurement of the bore (D-2d) under well defined profile conditions.

CHAPTER 7 CONCLUSIONS AND SUGGESTIONS FOR FURTHER WORK

7.1 Introduction

A clamp-on ultrasonic flowmeter has been designed, built and tested and has been found to perform favourably over a flowrange of 0.6m/s - 10m/s (a 16:1 turndown) within an accuracy of $\pm$ 4% of rate. The instrument uses proprietary electronics, transducers and materials and is consequently inexpensive. It is reliable and highly repeatable and offers exceptional speed of response from its single-shot capability. It would thus seem suitable for difficult flows where it is not required to average a large number of readings. The instrument has been shown to be bidirectional. The instrument uses a novel timing system and makes full use of Lamb mode transmission phenomena. The instrument has been flow tested on a typical pipe section (stainless steel, 100mm pipe) with one fluid (water), however static testing on other pipe sections and theoretical development show that the instrument is applicable to a wide range of pipe sections and fluids.

The instrument has some advantages and some limitations and these together with suggestions for further work and improvements to the design will now be reviewed.

7.2 Advantage of the prototype instrument over the commercial instrument tested.

The commercial clamp-on instrument tested by the author is marketed for a specific size (overall diameter and wall thickness) and material, and for different pipes a new set of transducers and a scaling card must be purchased. Thus for a selection of pipework the cost of a complete range of accessories is prohibitive. An alternative approach to the covering of all pipe sections is therefore sought and it is hoped that the theoretical development of the transmission model and the discussions on the transducer design will lead to a single unit capable of encompasssing a majority selection of typical industrial pipes.

It is worthwhile to make a distinction here between a portable general purpose instrument and a specialised application (or applications) as in a flow measurement consultancy role or for particularly difficult industrial situations. In the latter cases a selection of transducers and blocks could be carried to meet the likely requirements.

7.3 Velocity profile averaging

Common to all single beam ultrasonic flowmeter systems is the error associated with the velocity profile and unless the profile is well known (say from a section of sufficient upstream and downstream straight pipe) a significant error can exist and this has been discussed in the thesis. In fact the errors arising from velocity profile effects and incorrect values of C (speed of sound in the fluid) probably account for a significant proportion of the error observed in the testing of the commerical instruments.

It has been shown that an offset dual beam system reduces the error due to profile effects and certainly for an insertion flowmeter, this principles is utilised. It is not known to the author if a similar system exists for a clamp-on flowmeter, but experimental work in the laboratory has shown this to be a possibility. In an experiment one transducer was placed on the pipe along the axis and then rotated so that the beam traversed the flow along a non-diametrical chord. The reflection was observed on the other transducer. This method offers the twin advantage of a longer path length in the fluid (relaxing the timing requirement) and of the beam interrogating more of the flow profile. Clearly this is an area worthy of further investigation. A stage further may well be the rotation of the transducers through 90^{o}, the beam thus traversing the fluid across the flow. This may then be a turbulence measurement system, which interrogates a transverse component of flow.

7.4 Transducer design

7.4.1 Excitation of Lamb waves

It has been mentioned earlier that the system has only been tested (under flow conditions) on one pipe, with one fluid. It has been shown, on the static rig, that a thicker walled vessel (100mm steel pipe) would be acceptable as a flow tube and further tests in these areas (on the static and flow rigs) are thus required. The flow tests should concentrate more on pipe sections and on flowrates below 1m/s and compensation for C and for velocity profile should be carried out in real time using an onboard microprocessor. Static testing will be discussed a little later.

Using the stainless steel section it has been shown that it is possible to transmit sound at an angle greater than the second critical angle and that this effect is due to the incident wave being coincident with the So or Ao modes, these modes being the widest of all Lamb modes. Furthermore it has been shown that for maximum transmission one should aim to intersect a Lamb mode since maximum transmission provides a higher signal/noise ratio. It has been shown that if the frequency thickness product is too large then the Ao and So models coalesce until transmission is no longer possible and the modes approach the Rayleigh velocity of waves on a half space. It is then necessary to consider intersecting another mode, at an angle less than the critical angle, and hence reducing the angle in the fluid. It may be worthwhile, then, to consider the factors under control and one of these is frequency. However altering the frequency means that a trade off has to be made since a lower frequency has associated divergence losses and a higher frequency has increased attenuation losses. Alternatively, one may consider that to correctly intersect a mode, an adjustment be made to the angle, and although it has been shown that a rotating mechanism is possible, it is prudent to design the transducer system without interfaces, if at all possible.

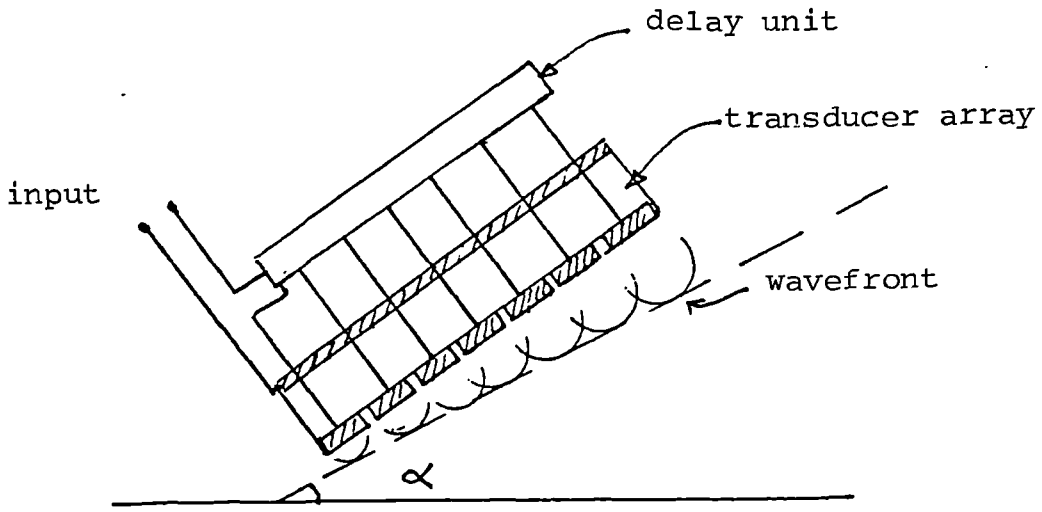

FIG 7.1
The piezoelectric transducer array

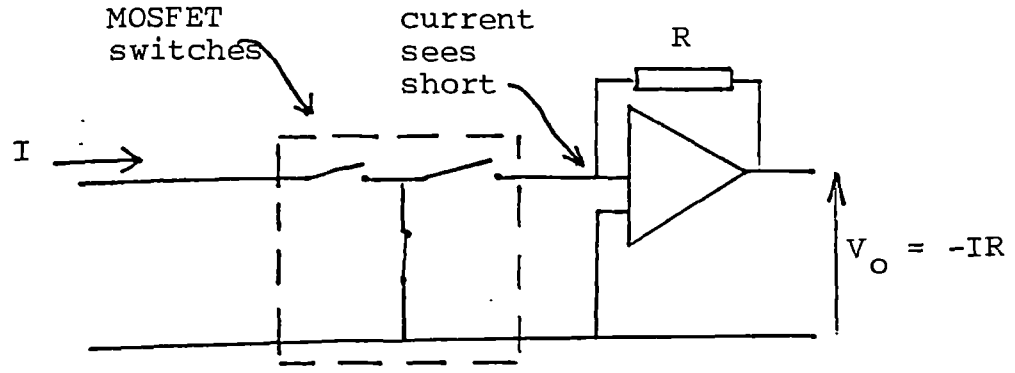

FIG 7.2
Current to voltage converter

One therefore searches for the right design and a solution may be to use a fluid enclosed in a thin membrane sack so that the transducer angle can be rotated and pushed against the sack and the total fixture then pushed against the pipe wall. The sack would then take the form of the transducer and wall. A similar 'dry' contact approach is known in the field of non-destructive testing.

An alternative approach may be considered such as that used in sonar applications. In this case a piezoelectric disc is manufactured as shown in Figure 7.1 and forms with the electronic delays a multiplexed array. Control of the delay allows each individual section to produce a (delayed) wavefront. A simple Huygens wavelet construction shows that a plane wave can be generated at any angle by simply altering the delay between firing. Similarly a delay is required when recombining the signal.

Both of the above transducer arrangements will allow correct angular positioning so as to intersect a mode and obtain maximum transmission. In addition the sonar approach will allow a beam to be generated within the block for measurement of C purposes, to be discussed shortly. All initialisation (set-up) procedures will be eased by stored algorithms in a microprocessor based system.

It has been shown in this thesis that the choice of transducer block material is important, particularly for applications above the critical angle. This can be readily seen by reconsidering that the incident wave length must match a Lamb mode wavelength so that $C_{LAMB} = \frac{Cp}{\sin\theta}$ where C_{LAMB} is the velocity of the Lamb mode, Cp is the velocity in the block and θ is the angle the transducer beam makes the normal. Clearly to excite the Ao or So mode where $C_{LAMB} < C_S < C_L$ then for $\sin\theta = 1$ $C_{LAMB} = Cp$ and this is the limiting case. Perspex although fulfilling the necessary conditions (Cp=2700m/s, $C_{LAMB} \approx$ 2950 m/S for s/steel) has very high attenuation and an alternative material should be considered. A suggested material is Polypenco, a plastic with low attenuation characteristics but similar speed characteristics to perspex. Further

characterisation of the material is necessary to ensure its viability, and reference should be made to its characteristics with respect to temperature particularly $\frac{\partial C_p}{\partial temp}$.

7.4.2 Temperature compensation

It has been shown that tracking of C (the speed of sound in the fluid) is essential for an accurate flowmeter and a method has been proposed and has been experimentally verified. It has been shown that the transducer block temperature coefficient is of importance in predicting C and that if it could be monitored, then C could be tracked to within 1/2%. One way of measuring the block's temperature is to insert a temperature probe. A more elegant solution is to provide a known pathlength in the block and monitor any change in the timing along the path, this then being related to temperature. The path method can be easily applied to the 'sack' or sonar transducer approach.

7.4.3 Mechanical setting

An added complication with the transducer arrangements is the need for precise mechanical positioning. An assortment of ideas by other authors has been put forward and one appealing method is to use the transducers on the same side of the pipe thus making use of the reflection off the far wall. Many designs can be envisaged such as a curved shoe with a channel for the transducers etc. The advantages of this type of system are precisely known distances and larger path lengths for timing.

7.4.4. Acoustic short circuiting

Common to many transducer arrangements and discussed in the literature is the acoustic short circuiting of the signal, i.e: sound travelling around the pipe and being picked up by the receiving transducer. This has not been a problem with the present prototype flowmeter. Suggested methods of alleviating the problem have been put forward by others. An acoustic break has been proposed and for some applications

it would appear that the natural acoustic break offered by the flange/gasket arrangement of rigs could be used to advantage.

Taking all factors into account, a trade-off will have to be made with respect to a particular design and will have to take into account the particular market sectors, at which the instrument is aimed. If the instrument is to be used in a consultancy role then it may be feasible to select options according to the application. Much work is required in this area to ensure that the designs are viable.

7.5 Design of Electronic circuits

7.5.1 Microprocessor control

Turning now to the electronic aspects of the flowmeter, it can be seen that it will be necessary to include some form of electronic intelligence and an obvious choice is a microprocessor based system. Work is presently in progress to incorporate a processor and all equipment (present design plus necessary additional circuits - to be discussed shortly) onto a single board. However, a rough outline of the expected functions of the processor can be sketched. These functions will include routines which will cover the control and synchronisation functions, (presently hardwired), the system calculations (Δt v, Q), compensation for velocity profile effects and changes in C, and a routine to operate the system as a Vernier or as a normal counting system (with a clock of approximately 40MHz. A further routine will be written to cover the set up of the instrument and this routine will be based on the results of the transmission model. It is envisaged that in this routine a look up table for typical industrial pipesections and their corresponding transmission, dispersion curves will be stored. The processor will then estimate from input data (e.g: pipe O/D (known)), fluid (often known), pipe I/D (approximately known), material (often known), approximate peak locations of transmission and transducer separation and will then, with user adjustment (i.e: moving and rotating the transducers) sweep through

regions of angles and positions to locate the optimum position. The instrument would then operate in its normal mode. The prototype instrument is limited at present since it requires manual operation and additions to the circuitry will be required to extend the range of the instrument and allow automatic operation.

7.5.2 Zero stability

The instrument is shown to exhibit larger errors at low flowrates (less than $\approx$ 1M/S) and this has been attributed to electronic drifts in the system. A solution to this problem would appear to be the use of reciprocal action. It will be recalled that the reciprocity theorem states that if a linear system is excited by a voltage and its output short circuit current is measured then that waveform will be identical to that produced with the same voltage applied to the output terminals and the short circuit current measured on the input terminals. In the present system the same voltage is applied to the transducers; (apart from the voltage drop across the isolating diodes, and it is the difference in the voltage drop that is important, this is negligible at the operating point). The simplest improvement to the present system would be the inclusion of a current to voltage circuit as shown in figure 7.2. In this case the switch would be a Tee network of MOSFET transistors with r_{ds} on=0.1Ω) and an operational amplifier of sufficient bandwidth (10-15MHz). The gain of the system would be unity. The added bonus to this system is that no signal is lost on protection resistances as in the prototype instrument at present. This would then mean an improved signal/noise ratio for the same gain.

7.5.3 Processing of the received signal

Additional circuitry is required to adapt the received pulse amplitude and form to processing. It has been discussed in the thesis that the pulse form changes shape and it will be necessary to study further the mechanisms that produce the pulse shape. It may well be that the instrument has to be operated within a limited range of situations. It is likely, therefore, that circuitry will be required to

automatically control the level of the pulse and to set the threshold detector level. Initial investigations in this area suggest that the two circuits may have to be linked. It can be conceived that a percentage of signals may be required to set up the gain and threshold adjustments on a regular basis.

Consider firstly the automatic gaining of the system. The assumption is made that since both transducers are fired at once the volume of fluid is effectively static (this is reasonable since over a time of approximate 100μS the fluid volume will have moved 0.1mm per m/s) and in which case the received pulse forms will be almost identical. In this case provided both pulses are amplified to approximately the same level the differential effect in the timing, brought about by slope changes will be negligible. A suggested circuit is shown in figure 7.3(a) and consists of a peak detector feeding a MOSFET transistor as a variable resistance. The MOSET draws virtually no current and the main requirements will be for a low loss capacitor, low leakage diode and low bias current op-amp.

In this circuit the peak level is stored on the capacitor and is as shown in Figure 7.3 (b). Provided the form of the pulse is known then it could also be used in another MOSFET transistor as a level on the comparator threshold circuit. This part of the design clearly requires more work in the typical pulse forms to be encountered and once again will be part of a general trade off. Both theoretical and experimental development must be carried out.

The receiving and processing circuit in general requires more attention and consideration of increased output from the preamplifier (presently 2V) to around 5V (thus increased dv/dt characteristics) is required; (the level being dependant on the differential limits of the comparator chosen). Additionally, faster comparators can be employed such as the AD9685, the delay through this device being of the order of 2.2nS and the offset $\pm$ 5mV.

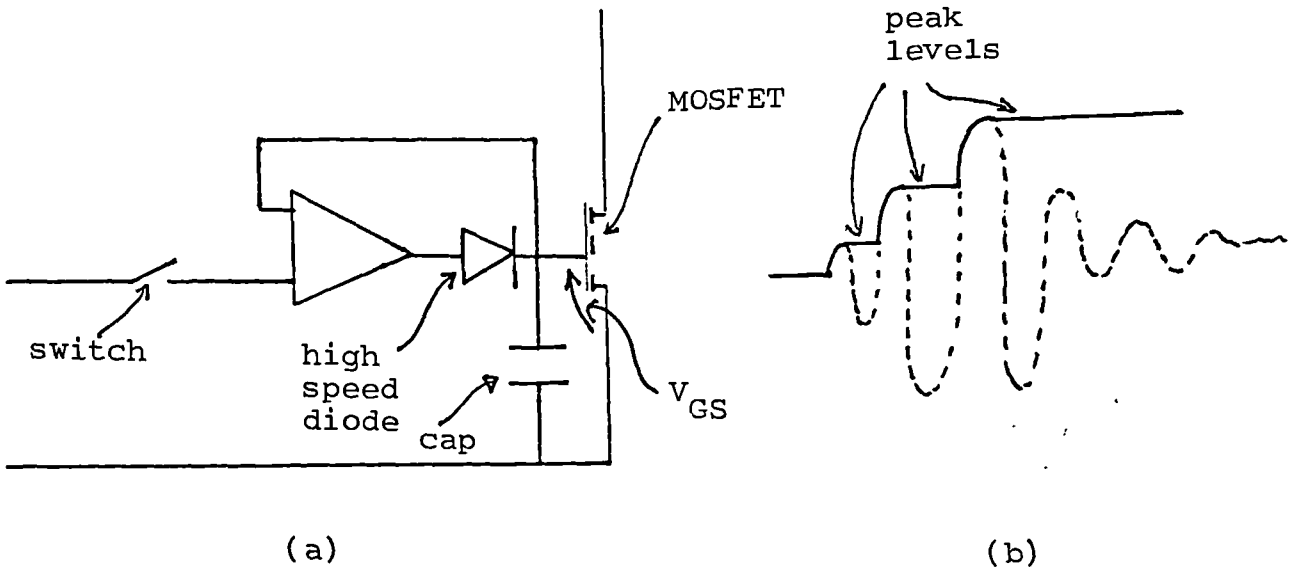

FIG 7.3
Peak detector (a) circuit (b) voltage across capacitor

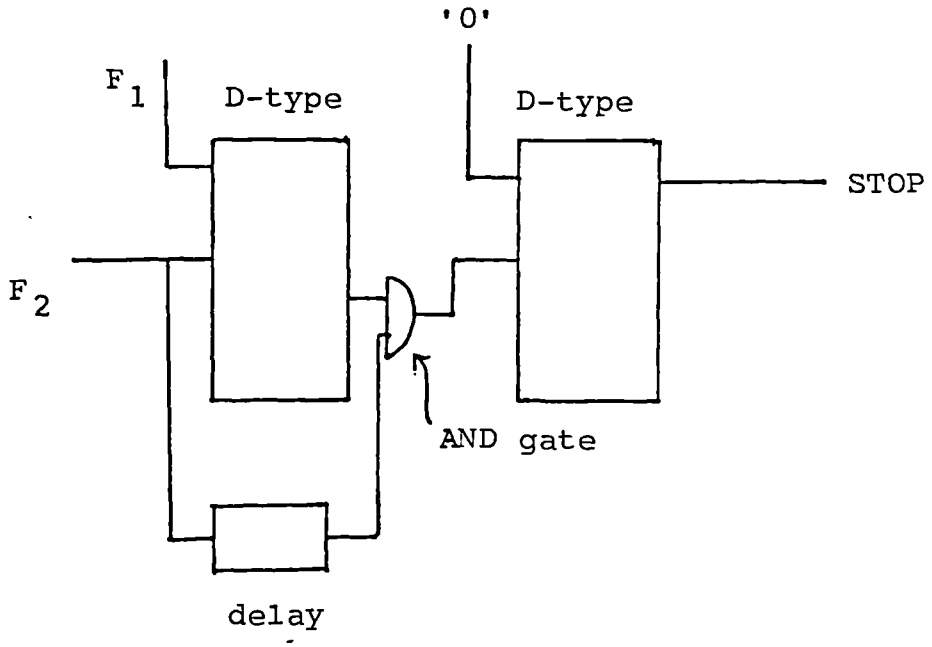

FIG 7.4
Circuit modification to reduce probability of detector 'failure'

The present circuit used for selecting single or multiple pulse pairs will be removed and gating of the strobe signal will be employed instead. This will then remove an extra circuit from the main signal path. The receiving and processing circuitry will be tested independantly.

7.5.4 The firing circuitry

The firing circuit in the prototype system is limited to approximately 30 volts and this is because the reaction of the transducer produces an additional voltage which when added to the firing voltage is near to the breakdown of the device (70v). If a voltage level in excess of 30 volts is required, and this may be necessary for very thick walled sections, then a review of this part of the circuit will be required. In its present form, however the circuit operates very successfully. A further interesting possibility is to use the system to fire multiple bursts and it is hoped to investigate this in the near future.

It is more efficient to match the transducer to the source at the frequency of operation, this will be achieved by using a transformer and will be incorporated in the next prototype instrument.' An objective, of less priority, is the complete design of a transducer for the flowmeter. This will entail reviewing the theory of transduction, constructing transducer (and thus identifying practical difficulties) and consideration of the models developed in this thesis. In the meantime it has been shown that suitable commerical transducers exist and perform satisfactorily.

7.5.5 The Timing System

The Vernier timing system has been shown to be successful, but requires further exhaustive testing under better environmental and experimental conditions. The need for a longer time delay unit is clearly seen but the system has been shown to be highly repeatable and monotonic over the limited range tested (approximately 300nS). Estimation of

the system resolution is difficult but has been conservatively set at 2nS. Improved traceable standards and further experimental testing will be required to set the accuracy level.

Control of the frequency of the oscillators is easily achieved by capacitively loading the gates. Improvements to the design of the oscillators may be required to cover for the worst case contingencies in terms of propagation delays, but these are minor. The starting arrangement should be reviewed and the starting circuit redesigned so as to eliminate the dependance on propagation delays. It has been shown that the systems may have a variable start up phase if the start pulse is longer than an allowable maximum.

It has been shown that δt (the difference in periods) can vary and can thus introduce an error. Although over a short period the error is small, the ageing effect of the electronics are likely to increase this. It is therefore necessary to include some on board monitor in any future model to measure the periods and the difference in periods. One possible way would be to have a crystal controlled oscillator with predictable ageing characteristics as a time reference and use this for gating the oscillator pulses. A possible better way of using the timing system, which has not been used in the experimental work, may be to keep the oscillators running and to just switch off prior to a timing. It has been shown, however, that there is no serious drift in δt over several hours. Further testing of the characteristics of the timing system with respect to temperature and time is therefore required.

The use of a D-type flip-flop as a detector has been shown to be successful but has associated with it a metastable state. This is shown to be caused by time signals arriving from different time frames. It will be necessary to include a circuit as shown in figure 7.4 to allow for failure of the flip-flop If the circuit is employed it has been shown that the chances are less than 1 in 10^{12} of failure. A consequent change in the calculation for Δt is necessary since this circuit would allow through two (or more) pulses after coincidence.

Using the above circuit it may be possible to utilise the output of the flip-flop as a measure of δt and this has been discussed in the thesis.

7.6 Transmission of sound through the pipewall

It is concluded that, although rough agreement between the theoretical and experimental models has been shown for the transmission of sound through plates and that the mechanism for the transmission of sound has been explained the models (both theoretical and experimental) require further development. The theoretical models chosen assume plates of infinite extent enclosed by two half spaces and excited by a source at infinity. The models have been analysed for continuous sinusoidal operation and they are thus suitable for any single frequency. Because the flowmeter operates with finite transducers and in a pulse mode of operation a study of transient bounded beams upon plates is, therefore, required and this will then need to be extended to curved plates and finally to a complete model of a pipe section. It will be essential to include attenuation and viscoelastic effects into the model and this complete work will be of a long term nature.

The results produced on the computer model were not quite in agreement with those found in experiments, an apparent shift of $3\text{-}5^{\circ}$ being noted. However the number of peaks observed were generally in agreement but their shape in the experimental model (wider and more rounded) did not compare too well with the theoretical (narrower and sharp). The lack of sharpness of the peaks is probably due to viscoelastic effects ignored in the computer model whilst the width is probably due in part to the exlcusion of viscoelastic effects but also other processes such as near field effects causing varying pressures along the plate. The divergence of the beam, is also likely to play an effect since the angles at the edges are now different from the optimum angle. Coupled with this work will be other designs of transducer systems such as the 'comb' approach. This is a transducer design that has a comb like structure and excites the normal component of the Lamb wave, (the spacing of the teeth correspond to the wavelength of the particular mode under consideration.

Further work in this area is therefore required and will consist of experimental work (ensuring the wall is insonified in the far field and from a parallel beam), and theoretical work which will include the introduction of complex sound velocities and their respective absorption coefficients.

The experimental procedure adopted for the transmission tests will be reviewed and a new design of transducer will be considered so that interfaces can be eliminated. The section of pipe will be extended and absorptive material will be fitted to both ends of the pipe to absorb internal reflections. The material parameters of the block, pipe and fluid will be accurately measured and used in the computer model and the model step size will be reduced from 0.5^{o} steps to initially 0.05^{o} steps. It is hoped to report on this work in the near future.

Further work is required in the understanding of Lamb waves and in particular their decay rates, which are known to be different for different modes. It has been shown that the stainless steel pipe section (thin walled) has a unique peak (in the axial direction) for a particular angular region. However the mild steel (thick walled) pipe section has several useable peaks and the collection of sound has been thus, more difficult. In the stainless steel case a larger volume of sound collected meant a better signal/noise ratio and this factor will be important, along with a selected mode, in the choice of system to be employed. Another area of interest is the effect of flanges etc on the propagating wave and this will need further investigation.

ACKNOWLEDGEMENT

I would like to express my sincere thanks for the help and support of my supervisor John Hemp. He not only taught me a great deal but provided constant encouragement and advice, as a colleague and as a friend.

I am indebted to John Heritage of CIT for further mathematical support and to Mike Sanderson of Salford University for his help in the overall electronic design. For help with specific electronic aspects I am grateful to Keith Bowdler of CIT.

I would like to thank Jane Heritage, Esther Hayes, Saul Nasse and Mike Smart for practical help with flowmeter calibration and computational work.

For helping with the constructional aspects of the project I acknowledge the help of John Parker and Dave Wallace.

I would like to thank Schlumberger for the loan of equipment and Mike Lock of CIT for the loan of equipment and for his advice. I would like also to thank Tom Wallace of Balteau Sonatest for helpful discussions.

For the use of facilities and for support I acknowledge with thanks Professor R. Baker and SERC.

For the patience to convert my handwriting for this document, many thanks to Sarah Weatherley and Tracey Harris.

Finally, without doubt I could not have attempted this project without the love and understanding of my family. Many thanks to Jackie, Damian and Stefanie.

LIST OF REFERENCES

(1)	LYNNWORTH, L.	Eight types of ultrasonic flowmeters Trans. Inst. M.C. Vol 3, No. 4 1981
(2)	LYNNWORTH, L.	Ultrasonic flowmeters in Physical Acoustics XIV ed. Mason & Thurston Academic Press 1979
(3)	SANDERSON, M.L. & HEMP, J.	Ultrasonic flowmeters - A review of the State of the Art Int. Conf. on Advances in Flow Measurement Techniques BHRA publishers, September 1981
(4)	McSHANE, J.L.	Ultrasonic Flowmeters in Flow Measurement and Control in Science and Industry 1974
(5)	RUTTEN, O.	Patent No. 520484 (German) September, 1928
(6)	DEL GROSSO, V.A & SPURLOCK, E.M.	The Feasibility of using wholly external ultrasonics to measure fluid flow within thick walled metal pipes. Naval Research Laboratory report no. 4967 November 1957 (USA)
(7)	FARRAL, W.R.	Design Considerations for Ultrasonic Flowmeters IRE Trans. on Medical Elections Vol 6, Part 4, 1959

(8)	FISCHBACHER, R.E.	Ultrasonic Flowmeter design. Control Vol 5, Part 43, 1962
(9)	LYNNWORTH, L	Generation and Propagation of pulses in single path contrapropagating flowmeters Trans. Inst. MC Vol 4, No. 1, March 1982
(10)	BAKER, R.C. & THOMPSON, E.J.	A two beam ultrasonic phase-shift flowmeter Conf. on fluid flow measurement in the mud 70's April 19 5, NEL Scotland
(11)	WESTINGHOUSE	Patent No.3940985, March 1976
(12)	ERICKSON, G.P. & GRABER, J.C.	Ultrasonic flowmeters Measurement and Control October 1983
(13)	LYNNWORTH, L.	Patent No. 3906791 (USA) September 1975
(14)	DROST, C.J.	Vessel diameter-independant volume flow measurements using ultrasound. Proc. San Diego Bio. Med. Symp. February 1978
(15)	LECHNER, H	Ultrasonic flow metering based on transit time differentials which are insensitive to flow profile J.A.S.A. 74 (3) September 1983
(16)	POTZICK, J. & ROBERTSON, B.	Patent No. 4445389 May, 1984

(17)	POTZICK, J.	Performance evaluation of the NBS long-wave acoustic flowmeter Rev. Sci. Inst. 55 (7), July 1984
(18)	ROBERTSON, B.	Flow and temperature profile independence of flow measurements using long acoustic waves Trans. ASME, Vol 106, March 1984
(19)	POTZICK, J.E. & ROBERTSON, B.	Long wave acoustic flowmeter. Instrument Society of America, Vol 22, No. 3 1983
(20)	LYNNWORTH, L.	Clamp-on ultrasonic flowmeters, limitations and remedies Inst. Technology, September 1975
(21)	BAUMOEL, J.	Patent No. 4373401 February, 1983
(22)	SANDERSON, M.L.,	Electromagnetic and Ultrasonic Flowmeters Short Course Notes - DFEI - Cranfield Inst. of Tech. December 1984
(23)	KALINOSKI, R.W. & VIGNOS, J.H.	Patent No. 4195517 April 1980
(24)	HEMP, J.	Theory of Transit Time Ultrasonic Flowmeters J. of Sound and Vibration 84(1) 1982
(25)	BRUMER, R.F.	Theoretical and Experimental Assessment of uncertainties in non-intrusive, ultrasonic flow measurement. NBS special publication 484. Proc. of Symp. on flow in open channels and closed conducts February 1977

(26)	SCHMIDT, T.R.	Clamp-on Ultrasonic Flowmeters - Application considerations and field test results. Inst. Soc. of AM. Conf. October 1980
(27)	PEDERSEN, N.E. & LYNNWORTH, L	Non-intrusive Dynamic Flowmeter IEEE Ultras. Symp. Proc. November 1973
(28)	DELL, T.G. & ERICKSON, G.	Ultrasonic flowmeters monitor taps for leaks Oil & Gas Journal August 1981
(29)	MUNK, W.D.	Ultrasonic flowmeter - a new approach to gas measurement Pipeline Industry April 1983
(30)	PEDERSEN etal	A new ultrasonic flowmeter for the gas industry Proc. Flow. Meas. Symp. NBS Spec. pub. February 1977
(31)	BATTYE etal	The design of a refrigerated hydrocarbon metering system of unprecedented size Inst. Conf. in Advances in Flowmeasurement techniques BHRA publishers, September 1981
(32)	LYNNWORTH, L. & PERDERSEN, N.E.	Ultrasonic mass flowmeter system Proc. 1972, IEEE Ultras. Symp. October 1972
(33)	RAYLEIGH	On the free vibrations of an infinite plate of homogeneous isotropic elastic matter Proc. of London Mthematical Society 20, 1899

(34) LAMB, H.
On waves in elastic plate
Proc. of Royal Society A93, 1917

(35) GRAFF, K.
Wave motion in elastic solids
Oxford University Press 1975

(36) SHERWOOD
Propagation in an infinite elastic plate
J.A.S.A. Vol 30, No. 10, October 1958

(37) LYON
Response of an elastic plate to a localised driving force
J.A.S.A. Vol 27, No. 2 March 1955

(38) MADIGOSKY & FIORITO
Modal resonance analysis of acoustic transmission and reflection lossess in viscoelastic plates
J.A.S.A. 65(5), May 1979

(39) VIKTOROV
Rayleigh and Lamb Waves
Ultrasonic Technology
Plenum Press 1967

(40) PITTS, PLONA & MAYER
Theoretical Similarities of Rayleigh and Lamb Models of Vibration
J.A.S.A, Vol 60, No. 2, August 1976

(41) PLONA
Effects of Lamb waves on ultrasonic bounded beam propagation
PhD thesis, Georgetown University, May 1975

(42) FREEDMAN
On the overlapping resonances concept of acoustic transmission through elastic plates I examination of properties
J. Sound & Vibration 82(2), 1982

(43)	SCHOCH	The Transmission of sound through plates Acustica 2, No. 1, 1952
(44)	CREMER	Acustica 7, 1942
(45)	GOTZ	Acustica 8, 1943
(46)	REISSNER	Helvetica Physica Acta 11, 1938
(47)	BREKHOVSKIKH	Waves in Layered media, New York Academic Press 1960
(48)	PLONA, PITTS & MAYER	Ultrasonic bounded beam reflection and transmission effects at a liquid/plate/liquid interface J.A.S.A. Vol 59, No. 6, June 1976
(49)	PLONA, BEHRAVESH & MAYER	Rayleigh and Lamb waves at liquid solid boundaries Ultrasonics July 1975
(50)	FREEDMAN & SWINERD	Internal field of an insonified elastic plate J.S.V. 68(4), 1980
(51)	SWINERD & FREEDMAN	Displacement field of an insonified thick elastic plate J.S.V. 70(2), 1980
(52)	FIORITO & UBERALL	Resonance theory of acoustic reflection and transmission through a fluid layer J.A.S.A. 65(1), January 1979
(53)	FIORITO, MADIGOSKY & UBERALL	Resonance theory of acoustic waves interacting with an elastic-plate J.A.S.A. 66(6), Decemeber 1979

(54)	FREEDMAN	On the overlapping resonances concept of acoustic transmission through plates II numerical examples and physical implications. J.S.V. 82(2), 1982
(55)	FREEDMAN & SWINERD	Internal and external fields of insonified plates along Lamb mode branchs of zero order. J.S.V. 83(4), 1982
(56)	DEIGHTON etal	Mode conversion of Rayleigh and Lamb waves to ompression waves at a metal-liquid interface. Ultrasonics November 1981
(57)	GILLESPIE etal	A new ultrasonic technique for the measurement of liquid level Ultrasonics January 1982
(58)	WATKINS etal	The attenuation of Lamb waves in the presence of a fluid Ultrasonics November 1982
(59)	BOGY & GRADCEWSKI	Reflection coefficient for plane waves in a fluid incident on a layered elastic half space. J.A. Mech. Vol 50, June 1983
(60)	BOGY & GRADCEWSKI	On the plane wave reflection coefficient and non-specular reflection of bounded beams for layered half spaces underwater. J.A.S.A. 74(2), August 1983
(61)	SIZMUR, M. FOND & BRAMPTON, J.R.	Recent advances in counting techniques Electronic Technology Vol 12, September, 1978

(62)	DRISCOLL, J.W.	Avoiding compromise in counter/timers Electronic Engineering October 1979
(63)	MILLER, L.	Counter Evolution Microwave Journal April 1983
(64)	HEWLETT PACKARD APPLICATION NOTE 200	Fundamentals of the electronics counters July 1978
(65)	HEWLETT PACKARD APPLICATION NOTE 52-2	Time keeping and frequency calibration August 1979
(66)	HEWLETT PACKARD APPLICATION NOTE 200-1	Fundamentals microwave frequency counters Octobe 1977
(67)	PORAT	Review of sub-nanosecond time-interval measurements Trans. Nucl. Science Vol 20, No. 5, 1973
(68)	SWAPP, M.	Time to digital convertor resolves picoseconds in time interval measurements. Motorola Tech. Dev. Vol 2, January 1982
(69)	TURKO, B.	A picosecond resolution time digitiser for laser ranging IEEE trans. on nucl. Sci. Vol NS 25, No. 1 February 1978
(70)	BUNN, T.L. etal	Design and operation of 12.5 nS multichannel scaler Rev. Sci. Inst. 55(11) November 1984

(71)	DHAWAN, S.	Time measurement with a multiphase clock IEEE trans. nucl. Sci, Vol NS-30, February 1983
(72)	LEGRELE & LUGOL	A one nanosecond resolution time to digital convertor IEEE trans. on Nucl. Sci, Vol NS-30 No. 1 February 1983
(73)	HUDOR, A.M.	Fast electronics for time of flight measurement Rev. Sci. Instrum. 52(6) June 1981
(74)	REINMULLER, M.	An automatic controlled timing unit for a time of flight mass spectrometer J. Phys. E. Sci. Instruments Vol 16, 1983
(75)	EVGRAFOV & KARTSENOV	A wide range start-stop time internal digitiser. Pribory i Telenika Eksperimenta, No. 2, March 1982
(76)	VORONOV etal	Time delay measuring circuit for a wave pulse used in acoustic measurements. Instrum anbd Meas. Tech, U.S.A. No. 1-2 January 1980
(77)	HEWLETT PACKARD APPLICATION NOTE 162-1	Time interval averaging
(78)	HEWLETT PACKARD APPLICTION NOTE 200-3	Fundamentals of time interval measurements
(79)	DENIYANCHUK etal	A fast time-interval digitiser Pribory i Tekruka Eksperimenta No. 2 March, 1983

(80)	KOVRIGIN, E.I. etal	High speed device for time interval measurement Tansk Institute of Automated Control Systems and Radio Electronics March-April, 1979
(81)	KINDLMANN, P.J. & SUNDERKAND, J	Phase stabilised Vernier chronotron Rev. of Sci. Instrum. Vol 37, No. 4 April 1966.
(82)	KAHANE etal	Fringe counting device for laser wavelength measurements Rev. Sci. Instrum 54(9) September 1983
(83)	BARTON & KING	Two Vernier time-interval digitisers Nucl. Ins. & Methods 97(1971)
(84)	BOWMAN & WHITEHEAD	A picosecond timing system IEEE trans. on Instr. & Measurement Vol 26, No. 2, June 1977
(85)	KARPOV	Vernier methods of measuring time intervals Meas. Tech. (USA) Vol 23, No. 9, September 1980
(86)	BOWMAN & WHITEHEAD	Detection System for a digital picosecond event timer Jounal of Physics E, Vol 9, 1976
(87)	STOLL. P.A.	How to avoid synchronisation problems VLSI design, November/December 1982
(88)	CHANEY, T.J. etal	Beware the synchroniser IEEE Comput. Soc. Conf. Compcon 72

(89) VEENDRICK, H.J.M. The behaviour of flip-flops used as synchronisers and prediction of their failure rate.
IEEE Jnl. of Solid State Circuits Vol SS-15 No. 2 April 1980

(90) FROST, H.M. Electromagnetic-ultrasound transducers: principles practice and applications In Physical Acoustics XIV ed. Mason & Thurston
Academic Press 1979

(91) SACHSE, W. & HSU, N. Ultrasonic transducers for materials testing and their characterisation.
In Physical Acoustics XIV ed. Mason and Thurston
Academic Press 1979

(92) SILICE et QUARTZ Manufacturers handbook

(93) EDO WESTERN Manufacturers handbook

(94) FILICYNSKI, L. Transients and the equivalent electrical circuit of the piezoeletric transducer
Acustica Vol 10. 1960

(95) REDWOOD, M. Transient performance of a piezoelectric transducer
J.A.S.A. Vol 33, No. 4, April 1961

(96) REDWOOD, M. A study of wave forms with generation and detection of short ultrasonic pulses
Appl. Mat. Res. April 1963

(97) REDWOOD, M. — Experiments with the electrical analog of a piezoelectric transducer
J.A.S.A. Vol 36, No. 10, October, 1964

(98) REDWOOD, M. — Determination of the parameters of a piezelectric transducer from the decay of resonant vibrations.
J.A.S.A. Vol 34, No. 7, July 1962

(99) MASON, W.P. — Electromechanical Transducers and wave filters
D. van Nostrand Company 1948

(100) STUEZER, O.M. — Multiple reflections in a free piezoelectric plate
J.A.S.A. Vol 42, No. 2, 1967

(101) STUEZER, O.M. — Impulse response measurement technique for piezoelectric transducer arrangements
IEEE trans. on sonics and ultrasonics Vol SU-15 No. 1, January 1968

(102) ZHANG, H.L. etal — Complete solutions of the transient behaviour of a transmitting thickness mode piezoelectric transducer and their physical interpretations.
J.A.S.A. 74 (4) October, 1983

(103) IEEE STANDARD ON PIEZO-ELECTRICITY — IEEE transactions on sonics and ultra-sonics Vol SU-31, No. 2, March 1984

(104) PIEZOELECTRIC CERMICS — Phillips application handbook Mullard 1974.

(105) HAYWARD etal — A systems model of the thickness mode, piezoelectric transducer
J.A.S.A. 76(2) August 1984

(106) HAYWARD, G. — A systems feedback representation of piezelectric transducer operational impedence
Ultrasonics July 1984

(107) CHALLISS, R. & HARRISON, J.A. — Rapid solutions to the transient response of piezoelectric elements by z-transform technique
J.A.S.A. 74 (6), December, 1983

(108) HAYWARD, G. & JACKSON, M. — Discrete-time modelling of the thickness mode piezoelectric transducer
IEEE trans-on-sonics and ultrasonics Vol SU-31 No. 3 May, 1984

(109) MARTIN, R. & SIGELMANN, R.A. — Force and electrical Thevenin equivalent circuits and simulations for thickness mode piezoelectric transducers
J.A.S.A. Vol 58, No. 2, August 1975

(110) SIGELMANN, R.A. & CAPRIHAN, A. — Design method for ultrasound transducers using experimental data and computers
J.A.S.A. Vol 62, NO. 6 December 1977

(111) LOW, G.C. & JONES, R.V. — Design and construction of short pulse ultrasonic probes for non-destructive testing
Ultrasonics March 1984

(112) SAYERS, C.M. & TAIT C.E. Ultrasonic properties of transducer backings
Ultrasonics March 1984

(113) FOSTER, F.S. & HUNT, J.W. The design and characterisation of short pulse ultrasound transducers Ultrasonics May 1978

(114) BELLEVAL, J.F. & LECURU, D. Improvement of ultrasonic transducers by using a multilayer front face Office National D'etudes et de recherches Aerospatiales T.P. No. 1978-114

(115) SUNG, K.M. Piezoelectric multilayer transducers for ultrasonic pulse compression
Ultrasonics March 1984

(116) BUI etal Experimental broadband ultrasonic transducers using PVf2 piezoelectric film Electroncis letters 5 Aug. 1976 Vol 12, No. 16

(117) LAKESTANI, F. etal Broadening the bandwidth of piezoelectric transducers by means of transmission lines
Ultrasonics July 1975

(118) WINTER, T.G. etal On driving a transducer to produce pulses shorter than the natural period of the transducer
Ultrasonics May 1975

(119) BROWN, A.F. & WEIGHT, J.P. Generation and reception of wideband ultrasound
Ultrasonics July 1974

(120) SMITH, W.M.R. & AWOJOBI, A.O. Factors in the design of ultrasonic probes
Ultrasonics January 1979

(121) KERVEL, S.J.H. van & THIJSSEN, J.M. A calculation scheme for the optimum design of ultrasonic transducers
Ultrasonics May 1983

(122) SILK, M.G. An extended model of the ultrasonic transducer
J. Phys. E. Sci. Instrum. Vol 16, 1983

(123) HALL, K.G. Performance and quality control of ultrasonic probes
British Journal of NDT March 1983

(124) BOND, L.J. & PUNJANI, M. Review of some recent advances in quantitative ultrasonic NDT
IEEE Proc. Vol 131, PEA No.4 June 1984

(125) KRAUTKRAMER Ultrasonic testing of materials
Springer-Verlag 2nd Ed. 1977

(126) WEIGHT, J.P. Ultrasonic beam structures in fluid media
J.A.S.A. 76(4) October 1984

(127) WALTON, A.P.T.B. & CHIVERS, R.C. The piezoelectric hydrophone for ultrasonic output assessment

(128) CHIVERS, R.C. & AINDOW Preliminary measuremetns of ultrasonic phase distributions
Acoustics letters Vol 4, No. 6, 1980

(129) LEWIN, P.A. & CHIVERS, R.C. Two miniture ceramic ultrasonic probes
J. Phys. E. Sci. Instrum. Vol 14, 1981

(130) LONGHURST, S.J. Broadband equalisation for ultrasonic transducers
MSC Thesis Cranfield Institute of Tech. September 1984

(131) OKYENE, J.G. & COUSIN, A.J. The design of high voltage SCR pulse generator for ultrasonic pulse echo applications
Ultrasonics March 1979

(132) REIN, H.M. & ZAHN, M. Subnanosecond-pulse generator with variable pulse width using avalanche transistors
Electronics letters Vol 11, No. 1, 9 January 1975

(133) KAYE & LABY Tables of physical and chemical constants
Longmans Publishers, London 1966

(134) KRITZ, J An ultrasonic flowmeter for liquids
Proc. ISA 10, No. 1-55-16-3, 1955

(135) TEXAS INSTRUMENTS Application note B215

(136) SPENDEL, K. D. Electromagnetic and ultrasonic flowmeters short course notes,
DFEI, Cranfield Institute of Technologies

(137) SPENDEL, K. D. Report 81/RCB/49 - Classified

(138) GOULT etal Computational methods in Linear Algebra
Thornes Publishers, London 1974

(139) HERITAGE, J. E. Part of a programme of ultrasonic flowmeter tests
Sponsored by the National Engineering Laboratory 1985